Freshwater Input Influence on Sea Surface Temperature Mean State and Variability in the Southeastern Tropical Atlantic

Dissertation

in fulfillment of the requirements for the degree of Dr. rer. nat.

of the Faculty of Mathematics and Natural Sciences at Kiel University

submitted by **Léo Costa Aroucha**

Kiel, July 2025

GEOMAR

C A U
Christian-Albrechts-Universität zu Kiel
Mathematisch-Naturwissenschaftliche Fakultät

The work was made possible with the support of a scholarship from the German Academic Exchange Service (DAAD).

First referee: Prof. Dr. Joke Lübbecke

Second referee: Prof. Dr. Arne Biastoch

Day of Disputation: 05/09/2025

Approved for Publication: 05/09/2025

Abstract

The Southeastern Tropical Atlantic (SETA) is an eastern boundary upwelling region and one of the most productive marine ecosystems in the world, characterized by the convergence of warm tropical waters from the north and cool subtropical waters from the south. The temperature front resulting from this convergence is the so-called Angola-Benguela Front (ABF). The ABF meridional migration is decisive for sea surface temperature (SST) changes off Angola, and plays a major role in determining seasonal and interannual SST variability in the region. SST interannual variability within the SETA is dominated by Benguela Niños (Ninãs), which are extreme warm (cold) events that usually peak from March to May. These acute events can have severe consequences for local communities due to their impact on rainfall, flooding, and fisheries. This thesis highlights the role of the previously overlooked mechanism of freshwater input, mainly from the Congo River, for both the SST mean-state and interannual variability in the SETA. To achieve this, a diverse array of datasets is utilized, including satellite measurements, ship-based in-situ observations, reanalysis products, and model simulation outputs.

Comparing high-resolution model simulations with and without a land-to-ocean runoff, it is shown that the presence of low salinity waters from the Congo discharge increases the mean state SST in the SETA coastal fringe by about 0.3ºC on average and by up to 0.9ºC from south of the Congo River mouth to the ABF. North of the River mouth up to about 4ºS, this input significantly reduces the mean state SST by more than 1ºC. This impact of river discharge on SST is linked to a halosteric effect, which modifies the sea surface height gradient and alters geostrophic currents, producing a southward (northward) coastal geostrophic flow, with an onshore (offshore) geostrophic component, hence, generating advective warming (cooling) and downwelling (upwelling) to the south (north) of the Congo River mouth. It also then contributes to pushing the ABF further south.

In addition, from both observations and reanalysis products, it is observed that anomalous freshwater input, mainly from the Congo River, can boost Benguela Niño/Niña events by altering the water column's stratification and vertical temperature gradient, consequently changing the turbulent heat loss magnitude. Anomalously high (low) salinity waters within the SETA are linked to the occurrence of positive (negative) Indian Ocean Dipole events via precipitation over the Congo basin and enhanced (reduced) river discharge, acting to amplify warm (cold) extreme events in the region through changes in turbulent heat fluxes, which is of great importance for local SSTs. From *in-situ* measurements of microstructure shear, dissipation rates of turbulent kinetic energy, and subsequently turbulent heat fluxes were estimated within the SETA coastal region. Low salinity waters during the warm 1995 Benguela Niño generated nearly 3 times less turbulent mixing when compared to the turbulent heat loss during the cold, high-salinity, 1997 Benguela Niña event. Salt advection variability, i.e. one of the dominant terms in the local mixed-layer salt balance, and its relation to wind stress variations and coastal dynamics, was shown to be crucial for the changes in the subsurface mixing term during these events.

Overall, the thesis draws attention to the impacts of the up-until-now unnoticed mechanism of freshwater input on SSTs and coastal ocean surface dynamics in the SETA. These results are crucial for the southwestern African coastal countries and local communities since the region sustains large marine ecosystems and highly productive fisheries, vital for socio-economic stability and food security. It also challenges the scientific community's understanding of these mechanisms in the projected climate change scenario of continuously increasing land-to-ocean discharge.

Zusammenfassung

Der südöstliche tropische Atlantik (SETA) ist eine Region mit Auftriebsgebiet am östlichen Rand und ist eines der produktivsten marinen Ökosysteme der Welt, das durch die Konvergenz von warmem tropischen Wasser aus dem Norden und kühlem subtropischen Wasser aus dem Süden charakterisiert ist. Die aus dieser Konvergenz resultierende Temperaturfront ist die sogenannte Angola-Benguela-Front (ABF). Die meridionale Verlagerung der ABF ist entscheidend für Veränderungen der Meeresoberflächentemperatur (SST) vor Angola und spielt eine maßgebliche Rolle für die saisonale und interannuelle SST-Variabilität in der Region. Die interannuelle SST-Variabilität innerhalb des SETA wird von Benguela-Niños (Niñas) dominiert, bei denen es sich um extreme Warm- (Kalt-)Ereignisse handelt, die üblicherweise zwischen März und Mai ihren Höhepunkt erreichen. Diese extremen Ereignisse können aufgrund ihrer Auswirkungen auf Niederschläge, Überschwemmungen und Fischerei schwerwiegende Folgen für die lokale Bevölkerung haben. Diese Arbeit befasst sich mit der Rolle des bisher vernachlässigten Mechanismus, der den Süßwassereintrags – vor allem aus dem Kongo – mit sowohl der mittleren SST als auch der interannuellen Variabilität im SETA verbindet. Dafür wird eine Vielzahl von Datensätzen genutzt, darunter Satellitenmessungen, schiffsgestützte In-situ-Beobachtungen, Reanalyseprodukte und Modellsimulationsergebnisse.

Der Vergleich von hochauflösenden Modellsimulationen mit und ohne Frischwasserabfluss vom Land in den Ozean zeigt, dass das Vorhandensein von Wasser mit niedrigem Salzgehalt aus dem Kongo-Abfluss die mittlere SST im küstennahen Bereich im SETA im Mittel um etwa 0,3°C und südlich der Mündung des Kongo bis zur ABF um bis zu 0,9°C erhöht. Nördlich der Kongo-Flussmündung bis etwa 4°S verringert dieser Eintrag die mittlere SST um mehr als 1°C. Diese Auswirkung des Flusseintrags auf die SST steht im Zusammenhang mit dem halosterischen Effekt, der den Meeresspiegelgradienten verändert und geostrophische Strömungen modifiziert, indem eine südwärts (nordwärts) gerichtete küstennahe geostrophische Strömung mit einer landwärtigen (seewärtigen) geostrophischen Komponente erzeugt wird, was zu advektiver Erwärmung (Abkühlung) und Absinken (Aufsteigen) südlich (nördlich) der Kongo-Flussmündung führt. Dies trägt auch zu einer Verlagerung der ABF nach Süden bei.

Darüber hinaus wird anhand von Beobachtungsdaten und Reanalyseprodukten festgestellt, dass anomaler Süßwassereintrag, hauptsächlich aus dem Kongo, Benguela-Niño/Niña-Ereignisse verstärken kann, indem er die Schichtung der Wassersäule und den vertikalen Temperaturgradienten verändert und dadurch die Stärke des turbulenten Wärmeverlusts beeinflusst. Anomal salzreiches (salzarmes) Wasser im SETA ist mit dem Auftreten positiver (negativer) Indischer-Ozean-Dipol-Ereignisse verbunden, die durch Niederschlag über dem Kongo-Becken und verstärke (verminderte) Abflussmenge ausgelöst werden und die warmen (kalten) Extremereignisse in der Region durch Veränderungen der turbulenten Wärmeflüsse verstärken, was von großer Bedeutung für die lokale SST ist. Anhand von In-situ-Messungen der Mikrostrukturscherung wurden die Dissipationsraten der turbulenten kinetischen Energie und anschließend die turbulenten Wärmeflüsse in der küstennahen Region im SETA abgeschätzt. Salzarmes Wasser führte während des

warmen Benguela-Niños 1995 zu fast dreimal geringerer turbulenter Durchmischung verglichen mit dem turbulenten Wärmeverlust während des kalten, salzreichen Benguela-Niña-Ereignisses 1997. Die Variabilität der Salzadvektion – einer der dominierenden Terme in der lokalen Salzbilanz der Vermischungsschicht – und deren Beziehung zu Änderungen in der Windschubspannung und Küstendynamik erweisen sich als entscheidend für die Veränderungen des Vermischungsterms unterhalb der Meeresoberfläche während dieser Ereignisse.

Insgesamt lenkt die Arbeit die Aufmerksamkeit auf die Auswirkungen des bisher unbeachteten Mechanismus, der den Süßwassereintrag mit der SST und der küstennahen Oberflächendynamik im SETA verbindet. Diese Ergebnisse sind von großer Bedeutung für die südwestafrikanischen Küstenländer und die lokale Bevölkerung, da die Region große marine Ökosysteme und sehr produktive Fischereien beherbergt, die für sozioökonomische Stabilität und Ernährungssicherheit entscheidend sind. Zudem wird das Verständnis dieser Mechanismen hinterfragt in Hinblick auf Klimawandelszenarios, die einen zunehmenden Süßwasserabfluss vom Land in den Ozean prognostizieren.

Table of Contents

List of Figures

List of Tables

Chapter 1

Introduction

Tropical oceans are key drivers of global climate variability and predictability across a wide range of time scales. They are crucial in redistributing the excess heat stored from the strong solar radiation, to which the tropics are subjected, to higher latitudes. The regional contrast of absorbed solar radiation drives the heat transport via both oceanic and atmospheric dynamics. Additionally, ocean-atmosphere processes and feedbacks within these regions are directly associated with local weather variations and global climate shifts. The most vital oceanic parameter to understand these mechanisms is Sea Surface Temperature (SST), which influences not only heat, gas, momentum, and moisture fluxes between ocean and atmosphere, but also affects atmospheric pressure fields, wind direction, wind curl, and intensity.

A good example of SST changes' impacts on a global scale is the El Nino Southern Oscillation (ENSO), which is the dominant mode of interannual climate variability (Philander, 1990), characterized by years of extremely anomalous SST in the Central to Eastern Equatorial Pacific Ocean, influencing the climate around the world (e.g. Alizadeh, 2024; Cai et al., 2020; Bove et al., 1998; Ropelewski & Halpert, 1987). Similarly, El Niño-like events have been described in the Southeastern Tropical Atlantic (SETA) restricted to the region off Angola, the so-called Benguela Niños/Niñas (Shannon et al., 1986). These events of anomalous SST in the SETA can impact both the marine ecosystem and rainfall along the Southwestern African coast (e.g. Lutz et al., 2015; Rouault et al., 2003; Boyer, 2001; Gammelsrød et al., 1998). The SETA is an eastern boundary upwelling region characterized by high biological productivity. It sustains rich marine ecosystems and fisheries, playing a key role in socio-economics and food security of southwestern African coastal countries (FAO, 2022; Kirkman et al., 2016; Jarre et al., 2015; Sowman and Cardoso, 2010).

This tropical region has a high freshwater influx from the presence of the Congo River mouth at 6ºS, and from minor rivers further south, being also influenced by precipitation from the Intertropical Convergence Zone (ITCZ). The Congo River, which is the second-largest river system in the world, dominates by far the freshwater input in the SETA, with a mean flow rate of about 40 000 m^3 s^{-1} (Dai and Trenberth, 2002; Campbell, 2005). It has long been shown that freshwater input can impact surface ocean temperatures (e.g. Vialard & Delecluse, 1998; Zhang & Busalacchi, 2009; Mignot et al., 2012; Hernandez et al., 2016; Echols & Riser, 2020; Gévaudan et al., 2021; Ma et al., 2023). Even though some studies attempted to understand the effect on SST of this high freshwater input in the SETA (Sena Martins & Stammer, 2022; White & Toumi, 2014; Materia et al., 2012), the importance of this forcing for the overall SST mean state and variability within this region remains partially unexplored and not fully elucidated.

The focus of this thesis is to disentangle and quantify the impact of the freshwater input on both the mean state and variability of SST in the SETA. For this, a wide range of datasets is used in the analysis, including in-situ measurements, satellite observations, reanalysis products, and model simulations. In this

chapter, the mean state, seasonality, and interannual variability of SST within the SETA are introduced in section 1.1, while the mechanisms by which a freshwater input could impact ocean temperatures at the surface are presented in section 1.2. Section 1.3 is dedicated to the motivation, goals, and outline of this thesis.

1.1 Southeastern Tropical Atlantic

1.1.1 Mean State

The Southeastern Tropical Atlantic (SETA) is situated on the west coast of Africa, in the Southern Hemisphere, a region encompassing the Tropical Angolan Upwelling System (TAUS), from 6ºS to 17ºS, and the Benguela Upwelling System (BUS) south of the Angola-Benguela Front (ABF, Figure 1.1a) (Körner et al., 2024), which is one of the most productive marine ecosystems in the world (Bakun et al., 2015). The SETA depicts a strong meridional SST gradient, characterized by the confluence of warm tropical waters from the north with cold subtropical waters from the south, which marks the position of the ABF (Figure 1.1a). The coastal southward transport of tropical waters is done by the Angola Current (AC), which has its core situated at around 50m depth and an estimated mean transport of 0.32±0.05 Sv (1 Sv = 10^6 m^3 s^{-1}) at 11ºS (Tchipalanga et al., 2018; Kopte et al., 2017). The AC is influenced by the southward propagation of Coastally Trapped Waves (CTWs), which originates at the equator (Bachèlery et al., 2016; Kopte et al., 2017; Tchipalanga et al., 2018) and connects the equatorial Atlantic to the two upwelling regions (i.e. TAUS and BUS). This current is a continuation of the Gabon-Congo Undercurrent (GCUC), which is supplied by remnants of the Equatorial Undercurrent (EUC) and the equator extension of both Guiana Current and Guiana Undercurrent (Brandt et al., 2024). On the other hand, the Benguela Coastal Current (BCC) (Figure 1.1a), i.e. the coastal branch of the Benguela Current (BC), flows north/northwestward, bringing cold subtropical waters to the ABF (Siegfried et al., 2019). The BC is the wind-driven eastern boundary current part of the South Atlantic subtropical gyre (Peterson & Stramma, 1991).

The sea surface salinity (SSS) within the SETA is characterized by low-salinity waters at its northernmost part (Figure 1.1b), mainly due to the freshwater input dominated by the Congo River outflow at 6ºS (Houdengnoto et al., 2021). Precipitation also plays a role in these low-salinity waters, especially in austral summer, when the ITCZ is located south of the equator. The meridional SSS pattern is created by the low-salinity waters in the north, followed by a salinity maximum until around 17ºS, where south of it the SSS declines again (Figure 1.1b). In terms of wind, the SETA is subject to southeasterly/southerly winds, driven by the South Atlantic Anticyclone (SAA) (Figure 1.1b). Strong winds prevail in the BUS until around 17ºS, generating an offshore Ekman transport favoring coastal upwelling within the BUS, and start to weaken at the Angolan coast, north of the ABF. A remarkable zonal wind gradient is also observed within the SETA, especially at the BUS, with offshore winds weaker than at the coast. This zonal wind gradient creates a quasi-permanent cyclonic wind stress curl, which also contributes to the upwelling via Ekman pumping (Figure 1.1c). Additionally, the cyclonic wind stress curl supports the southward advection of tropical waters via the AC, and modulates the AC core position and strength (Fennel et al., 2012; Junker et al., 2015; Tchipalanga et al., 2018).

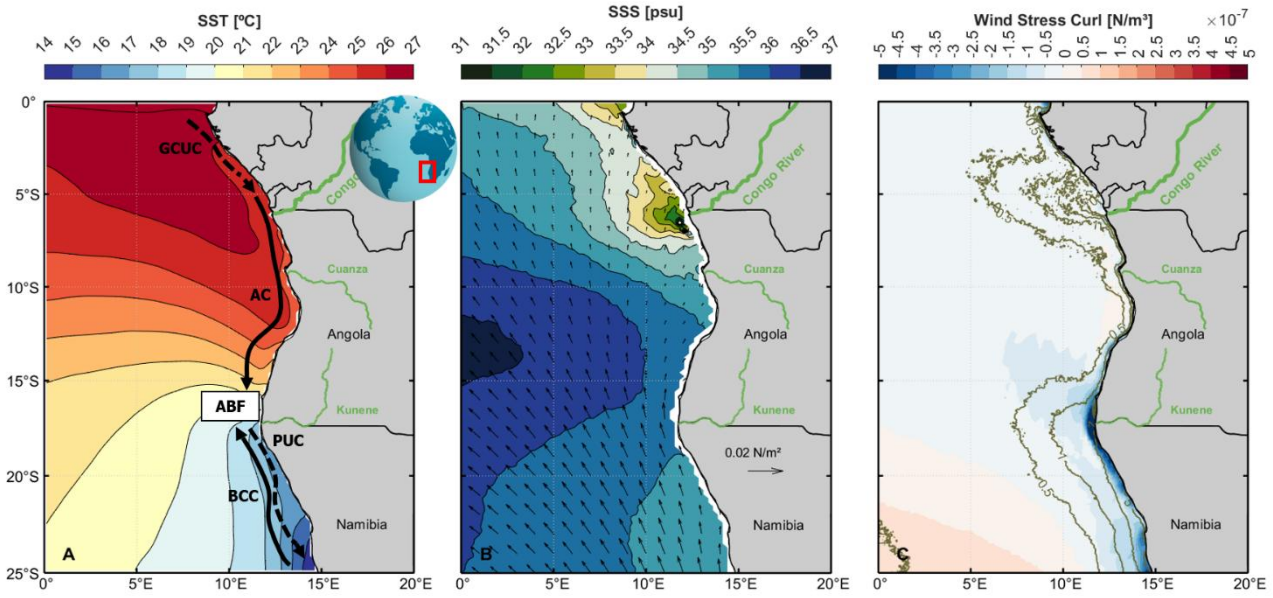

Figure 1.1. Mean background conditions for the Southeastern Tropical Atlantic. SST (ºC, contours) and schematic of coastal circulation superimposed (a), SSS (psu, contours) and wind stress (N m^{-2}, arrows) (b), and wind stress curl (N m^{-3}, shading) and chlorophyll concentration (mg m^{-3}, contours) (c). SST from OISST, 1982-2022, SSS from GLORYS12, 1993-2019, wind stress and curl from ERA5, 1993-2019, and primary productivity from Global Ocean Colour, 1997-2020. Solid (dashed) arrows in (a) indicate surface (subsurface) currents. GCUC: Gabon-Congo Undercurrent, AC: Angola Current, BCC: Benguela Coastal Current, PUC: Poleward Undercurrent, ABF: Angola-Benguela Front.

Due to the upwelling of nutrient-rich waters to the surface, the BUS is described as a high-productivity coastal system. South of 17ºS, the high chlorophyll concentration is located exactly where the cyclonic wind stress curl dominates (Figure 1.1c), corresponding to the upwelling region. Concomitantly, the high productivity at TAUS, north of 17ºS, is not wind-driven. Instead, it is determined by the combined effect of a CTW propagation and tidal mixing on the shelf break (Körner et al., 2024). Finally, Congo River plume is also responsible for bringing nutrients to offshore regions, such as iron (Fe) and silica (Si), influencing phytoplankton communities and consequently productivity levels north of TAUS (Figure 1.1) (Hatin et al., 2017; Vieira et al., 2020). These highly productive locations support fisheries and marine ecosystems of great economic importance for African countries (FAO, 2022; Kirkman et al., 2016; Sowman and Cardoso, 2010). Overall, the freshwater input, propagating waves, and coastal circulation in the SETA are also subject to strong seasonality. These seasonal differences will be detailed in the next section.

1.1.2 Seasonality

The SETA undergoes pronounced seasonal cycles (Brandt et al., 2023), with the warmest SSTs observed in February-March-April (FMA), and the coolest in July-August-September (JAS). In BUS, SST seasonality is driven by the weakening (strengthening) of the southerly winds during FMA (JAS), which shifts upwelling intensities and consequently SST's during the year, and are associated to seasonal variations in the position of the SAA (Brandt et al., 2023; Veitch et al., 2009). Conversely, within TAUS, these seasonal SST changes are unrelated to wind shifts, since the winds are relatively weak throughout the whole year (Brandt et al., 2023). Instead, they are connected to the propagation of equatorially forced Kelvin Waves (EKWs) that, when reaching the west African coast, partially transfer their energy to generate southward propagating CTWs (Clarke, 1983). The signature of such waves can be seen from the seasonal cycle of sea surface height

(SSH) (Figure 1.2a), and their propagation impacts the SST seasonality by moving the thermocline upward or downward (Rouault, 2012; Ostrowski et al., 2009). Downwelling (upwelling) waves are associated with an increase (decrease) in SSH, downward (upward) movement of the thermocline, and warmer (cooler) SSTs. CTWs in TAUS, however, present a semi-annual cycle, with the occurrence of two upwelling (peaking in July and December), and two downwelling (peaking in February and October) waves during a year (Figure 1.2a) (Polo et al., 2008; Ostrowski et al., 2009; Rouault, 2012; Tchipalanga et al., 2018), and their propagation alone cannot explain either the annual cycle observed in SSTs or the zonal SST gradient from the coast to offshore (Brandt et al., 2023; Körner et al., 2023). Indeed, surface heat fluxes and turbulent mixing have also been pointed to controlling SST seasonal changes in this region (Körner et al., 2023; Scannell & McPhaden, 2018).

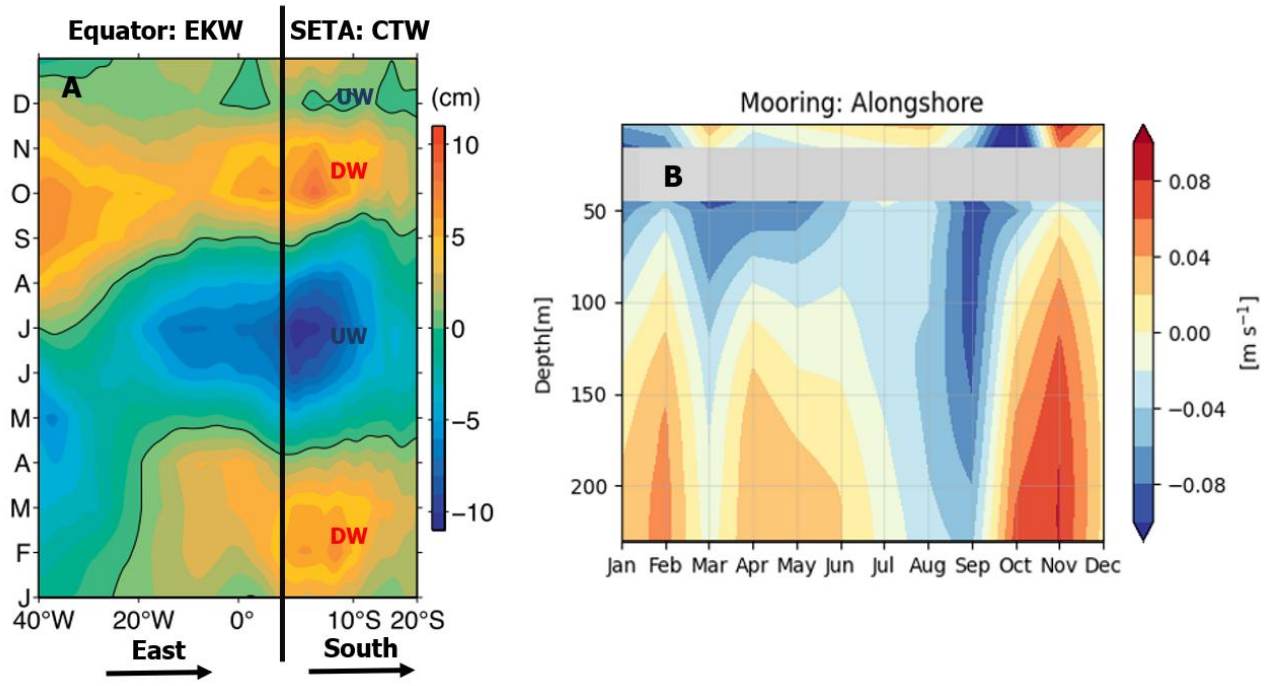

Figure 1.2. (a) Hovmöller diagram of the mean annual cycle of SSH anomaly showing the propagation of upwelling (UW, blue) and downwelling (DW, red) Kelvin waves (EKW) from west to east along the equator, and coastally trapped waves (CTW) propagating southward along the eastern boundary. The vertical black line separates the region of eastward propagation along the equator to the left and the region of southward propagation along the coast to the right. Adapted from Tchipalanga et al. (2018). (b) Alongshore current velocity mean annual cycle (rotated by -34º with respect to true north) recorded by the moored ADCP located at 10º50'S, 13º00'E combined to surface velocities from GLOBCURRENT.

Additionally, the passage of CTWs is closely linked to the seasonal variability of the AC (Kopte et al., 2018; Tchipalanga et al., 2018; Bachèlery et al., 2016a) (Figure 1.2b). Indeed, the observed reduced (enhanced) poleward flow agrees well with the passage of upwelling (downwelling) CTWs (Tchipalanga et al., 2018; Kopte et al., 2017; Rouault, 2012; Ostrowski et al., 2009), with southward maximum velocities occurring in February-March and September-October (Figure 1.2). The seasonality of the AC also controls the freshwater input in TAUS via meridional advection, and consequently the SSS seasonal cycle within TAUS (Brandt et al., 2023; Awo et al., 2022) (Figure 1.3).

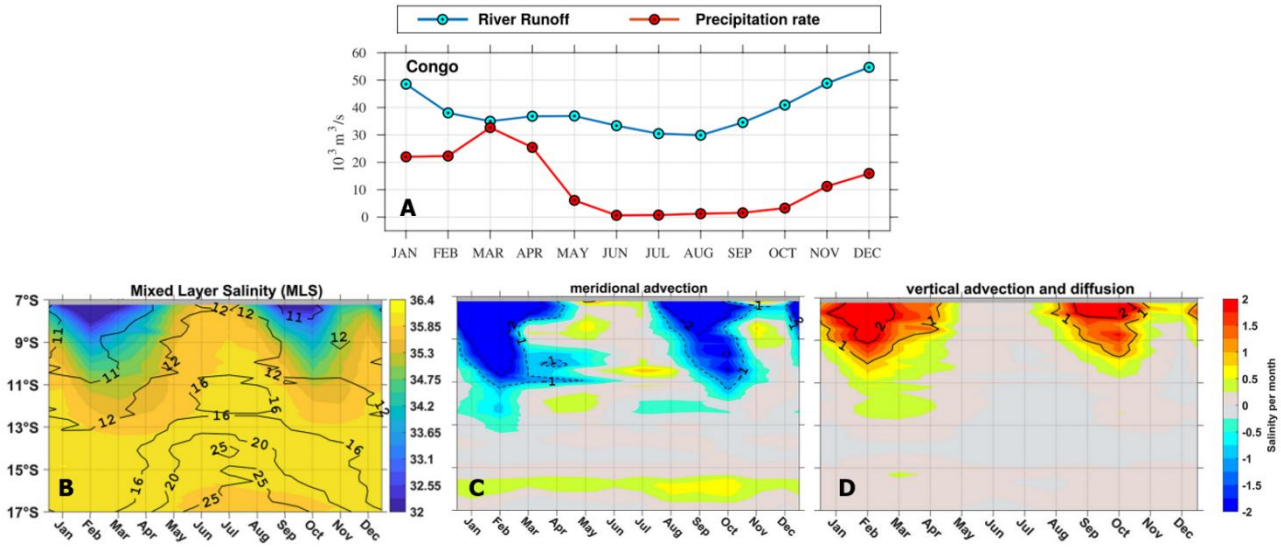

Figure 1.3. (a) Seasonal cycle of precipitation rate (red curve; m^3s^{-1}) and Congo runoff (blue curve; m^3s^{-1}) integrated over the Congo mouth (5ºE-13ºS, 3ºS-9ºS). From Houdengnoto et al. (2021). (b) Hovmöller diagram of seasonal cycle of Mixed Layer Salinity (MLS, shading) and mixed layer depth (MLD, in m), averaged for 1º off the coast. (c) Same as (b) but for meridional salt advection. (d) same as (b) but for the sum of vertical advection and diffusion. (b,c,d) adapted from Awo et al. (2022).

Freshwater input in the region is dominated by the Congo River, with a maximum discharge of above 50 $m^3 s^{-1}$ in December-January (Figure 1.3a) (Martins & Stammer, 2022; Houdengnoto et al., 2021). From January to April, due to the southernmost position of the ITCZ in austral summer/autumn (Munzimi et al., 2019; Sori et al., 2017), the precipitation over the Congo mouth region also strongly contributes to increasing the freshwater input in these months, even though the magnitude is still smaller compared to the Congo discharge (Figure 1.3a). This freshwater then reduces the SSS around 6ºS and is transported southward alongshore the west coast of Africa via the AC, with lower SSS at TAUS peaking in phase with the strengthening of the AC (Awo et al., 2022). Climatologically, the southernmost position of these low SSS waters from the Congo plume is around 12ºS-13ºS in February-March. This transport leads to a shoaling of the mixed layer (Figure 1.3) and consequently stronger stratification of low SSS waters above a maximum subsurface salinity in the region, which then favours the subsurface advection and turbulent mixing, creating an upward salt flux that counteracts the surface freshening (Brandt et al., 2023; Awo et al., 2022). Bearing in mind the importance of the changes in propagating waves, coastal currents, and winds to the overall picture of the SETA, the impacts of such changes on the SST interannual variability, mainly by triggering extreme warm and cold events off Angola, as well the overlooked freshwater input variability as a possible forcing mechanism for such events, are explored in the next section.

1.1.3 Interannual Variability

SST interannual variability in the SETA is strongest off Angola in a region termed Angola-Benguela Area (ABA, 8ºE to coast, 10ºS-20ºS) (Figure 1.4) (Lübbecke et al., 2010; Florenchie et al., 2003, 2004). This region is used for defining the Benguela Niño and Niña events, which are extreme coastal episodes of anomalously warm and cold SSTs, respectively (e.g. Imbol Koungue et al., 2019; Florenchie et al., 2003; Shannon et al., 1986). These events modulate the SST variability on interannual timescales in the region, and

they usually peak from March to May (Figure 1.4b), when SSTs in the region are climatologically higher (Brandt et al., 2023; Imbol Koungue et al., 2019; Lübbecke et al., 2010). Such extreme events impact marine ecosystems and fisheries in the region (Blamey et al., 2015; Boyer & Hampton, 2001; Gammelsrød et al., 1998), as well as modulate the upward supply of nutrients (Bachèlery et al., 2016b), also having consequences for rainfall and flooding in coastal Africa (Koseki & Imbol Koungue, 2020; Lutz et al., 2015; Hansingo & Reason, 2009; Rouault et al., 2003). This year-to-year variability is mainly forced remotely, via the eastward propagation of EKWs, generated by strong wind anomalies in the western equatorial Atlantic, that propagate southward as CTWs when reaching the African coast (Figure 1.4). These waves vertically displace the thermocline, affecting the local stratification, alongshore currents, and biogeochemical conditions (Imbol Koungue et al., 2017; Bachèlery et al., 2016b; Rouault, 2012). It has been shown that 70% and 50% of SSH and SST interannual variability in the ABA, respectively, are remotely forced via wave propagation (Bachèlery et al., 2020). Local forcing, however, can also trigger such acute SST anomalies, especially due to local wind variability, associated with changes in position and strength of the SAA (Illig et al., 2020; Lübbecke et al., 2019; Richter et al., 2010; Polo et al., 2008; Hu & Huang, 2007) (Figure 1.5). These local wind changes modulate the intensity of upwelling, the surface heat fluxes, and the structure of the coastal currents, impacting the meridional transport of warm tropical waters during Benguela Niño events (Lübbecke et al., 2019; Junker et al., 2015; Fennel et al., 2012). In some years, both local and remote forcing mechanisms played an important role in triggering such extreme episodes (e.g. Imbol Koungue et al., 2021). However, in the last decades, local forcing seems to play an increasingly important role in starting these events (Prigent et al., 2020). Therefore, improving the understanding of how local dynamics can affect Benguela Niños and Niñas becomes of great importance.

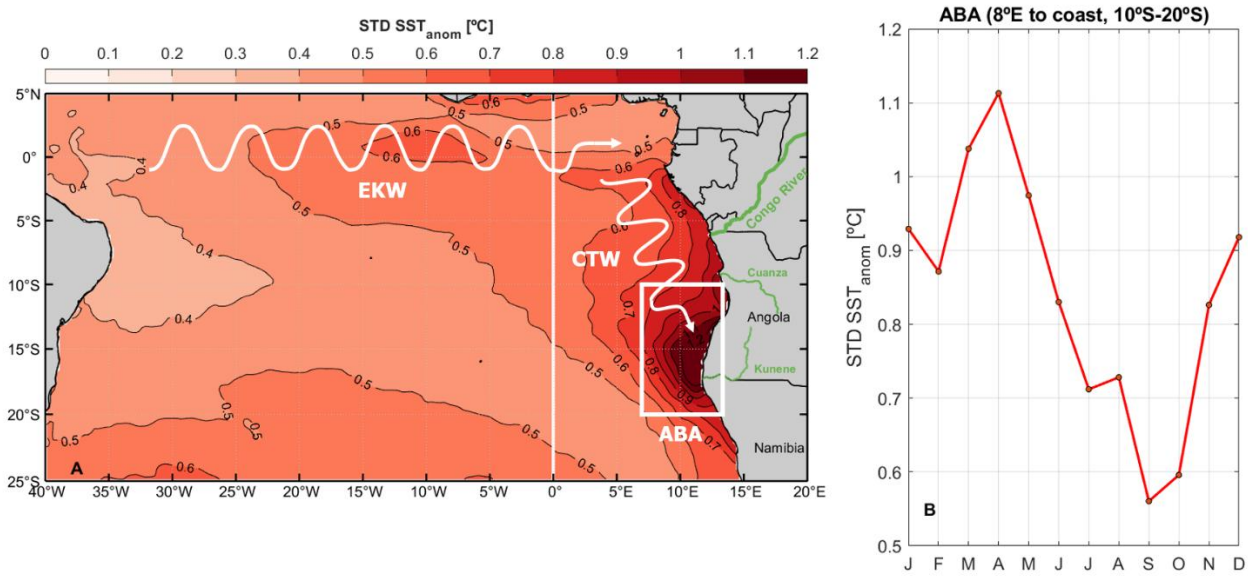

Figure 1.4. (a) SST anomalies standard deviation. White curved lines represent a schematic of propagating waves. White line at 0ºE separates the SETA from the Tropical South Atlantic. EKW: Equatorial Kelvin Wave; CTW: Coastally Trapped Wave; ABA: Angola-Benguela Area, 8ºE to coast, 10ºS-20ºS. (b) Standard deviation of ABA-averaged SST anomalies as a function of calendar month. SST data from OISST (1982-2022).

Lübbecke et al. (2019) showed that the 2016 warm event predominantly resulted from the combination of local processes related to the weakening of the southerly winds. These local mechanisms are

shown in Figure 1.5. Additionally, the authors considered, for the first time, a possible impact of increased freshwater input from both an anomalously high Congo River discharge and extreme precipitation in amplifying such warm events, by increasing stratification and reducing mixing of surface and subsurface waters. In fact, anomalous shifts in SSS have been observed during such extreme events (e.g. Gammelsrød et al., 1998), with negative anomalies of SSS reaching as far as 18ºS. Recently, Sena Martins & Stammer (2022) showed via satellite data years of low SSS waters intrusion into the ABA, also reaching around 16ºS. Even though they could not find a significant correlation between river discharge and the occurrence of extreme events, they evidenced a strong influence of this freshwater input in increasing the stratification within the region of highest SST variability (Sena Martins & Stammer, 2022). Still, the effect of freshwater input and SSS changes in forcing Benguela Niño and Niña events remains an overlooked mechanism

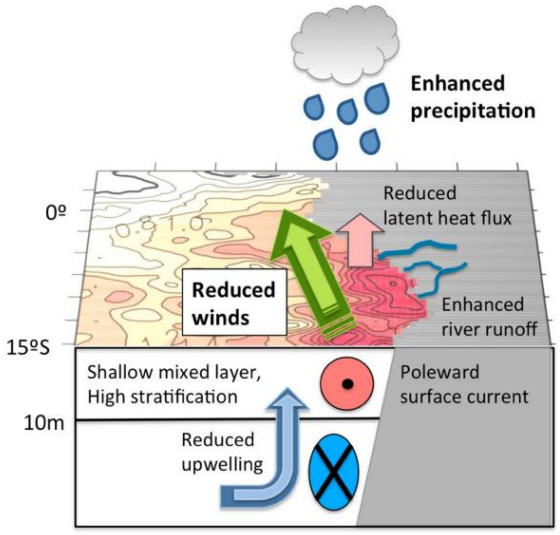

Figure 1.5. Schematic summarizing the processes that contributed to the warm event in early 2016. From Lübbecke et al. (2019).

Finally, interbasin interactions between Benguela Niño events and other climate variability modes remain poorly documented and are not yet fully understood in the existing literature. It has been shown that ENSO exerts influence on southern BUS with an 8-month lag by shifting the position of the SAA and consequently generating anomalous winds that lead to changes in upwelling intensity (Rouault & Tomety, 2022; Blamey et al., 2015; Tim et al., 2015). During an El Niño, anomalously weak upwelling favorable winds are observed, contributing to warming the southern BUS, while in a La Ninã, stronger-than-normal southeasterly winds cool the southern BUS SSTs. Effects of ENSO at northern BUS are weaker and oppose the ones in the southern BUS, with El Niño contributing to cooling northern BUS (Rouault & Tomety, 2022). In addition, Atlantic and Benguela Niño events present a strong correlation, with Benguela Niños tending to precede equatorial events by 1-3 months. This relation is also explained by changes in the SAA, emphasizing the role of local forcing in the phenology of such coastal mode of variability (Illig et al., 2020; Lübbecke et al., 2010; Polo et al., 2008; Hu & Huang, 2007). However, there is still debate whether Atlantic and Benguela Niños should be treated separately or as one variability mode, since their variabilities are strongly connected via remote forcing of propagating EKWs and CTWs (e.g. Bachèlery et al., 2020; Imbol Koungue et al., 2017, 2019; Lübbecke et al., 2010). Furthermore, Indian Ocean Dipole (IOD) related convection over Africa has

been shown to weaken Atlantic equatorial winds, and thereby trigger Atlantic Niño episodes (Fan et al., 2023; Zhang & Han, 2021), at the same time that the IOD relates to SSS variability in the SETA via the Congo basin hydrology (Jarugula & McPhaden, 2023). Further research is needed to explore the connections between ENSO, IOD, and Atlantic/Benguela Niño events, as these interactions may contribute to improved predictability of extreme Atlantic climate events.

1.2 Effects of Freshwater Input

Freshwater input into the ocean and the consequent changes in SSS have been extensively demonstrated to impact oceanic SST (e.g. Gévaudan et al., 2021; Echols & Riser, 2020; Balaguru et al., 2012a; Foltz & McPhaden, 2009; Zhang & Busalacchi, 2009). This impact is often associated with the generation of barrier layers (BL) between a density-stratified mixed layer (ML) and a temperature-stratified isothermal layer (IL), which reduces the vertical mixing of subsurface cooler waters with the warm waters at the surface, hence increasing SST (e.g. Balaguru et al., 2012a; Foltz & McPhaden, 2009). However, BL generation and ML shoaling can also generate cooling signatures in SST (Echols & Riser, 2020; Behara & Vinayachandran, 2016). At the same time, freshwater lenses can modify geostrophic flows due to changes in SSH and pressure gradients via the halosteric effect (Alory et al., 2021; Durand et al., 2019), which could, consequently, affect surface heat advection and SSTs. In this section, the two main mechanisms (i.e. halosteric effect and BL generation) by which a freshwater input can impact SST are detailed. Here, the focus is mostly on the plume-related processes, since the freshwater input in this region is dominated by the Congo discharge (see Section 1.1.2).

1.2.1 River Plumes, Pressure Gradients and Coastal Dynamics

Freshwater discharge from rivers carries more than one-third of the precipitation over land into the ocean (Trenberth et al., 2007), with approximately 40% of the freshwater entering the oceans being transported by the world's ten largest rivers (Dagg et al., 2004). They concentrate large freshwater input into the ocean through narrow outlets along the coast, exerting a profound influence on coastal and shelf regions via substantial interactions between river-borne low-salinity waters and oceanic high-salinity ones (Horner-Devine et al., 2015). River plumes are multiscale flow structures, generated by the flow of buoyant river water into the coastal ocean, and spanning a range of sizes and shapes, which depends mostly on the rate of discharge, tidal amplitude, coastline, bathymetry, ambient currents, wind stress and Earth’s rotation (Horner-Devine et al., 2015; Hopkins et al., 2013).

The Congo River plume can be classified as a surface-advected plume, with the lighter water spreading over the salty ocean, not influenced by bottom stress, and being deflected by the Coriolis force, generating an anticyclonic cyclostrophic plume (Yankovsky & Chapman, 1997; Fong & Geyer, 2002). It extends between 400 and 1000km northwestward (from September to January) and southwestward (from January to April), with its spreading determined by changes in wind stress, wind-driven currents, freshwater discharge, and coastal currents (Houdengnoto et al., 2021; Hopkins et al., 2013). Denamiel et al. (2013) and Vic et al. (2014) argue that this dominant northwestward spreading is primarily related to the unique

geomorphology of the Congo estuary. Once offshore, the plume salinity gradually increases mainly due to vertical turbulent salinity fluxes, which mix the surface low-density waters with salty subsurface waters, and is considered to be dominant over horizontal turbulent fluxes (Horner-Devine et al., 2015).

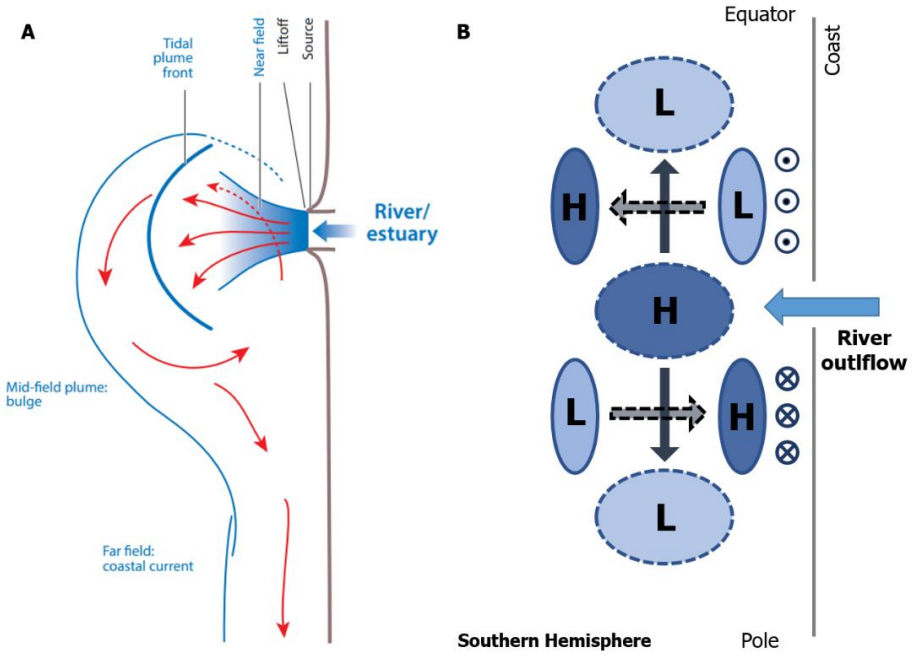

Figure 1.6. (a) Schematic representation of the prototypical large-scale plume comprising all dynamical regions. Adapted from Horner-Devine et al. (2015). (b) Pressure gradients and balance of geostrophic currents at the coast subjected to a river outflow. H: high-pressure area; L: low-pressure area. Dashed (solid) contours represent primary (secondary) pressure systems and associated geostrophic currents. Both schematics attempt to depict a theoretical scenario for the Congo River plume. In the Southern Hemisphere, the flow is deflected to the left by the Coriolis effect.

The Congo River plume can also be classified by its morphology as a prototypical large-scale plume, which is characterized by a relatively high discharge and narrow mouth, with its dynamics strongly influenced by the Coriolis effect (Horner-Devine et al., 2015) (Figure 1.6a). This type of plume evolves a freshwater bulge in the vicinity of the river mouth, an anticyclonic circulation around this bulge, and a coastal current extension in the direction of the propagating CTWs (i.e. southward, in this case) (Figure 1.6a) (Chao, 1988; Fong & Geyer, 2002; Horner-Devine et al., 2015). The bulge is a continuously growing subtidal feature, which accumulates 25% to 75% of the river's freshwater discharge, and reduces the transport of freshwater away from the river mouth region into the coastal current (Fong & Geyer 2002; Horner-Devine et al., 2015). Horner-Devine et al. (2015) divided a prototypical large-scale plume in different fields (Figure 1.6a): the liftoff point, where the upper layer of the plume loses contact with the bottom and becomes surface-advected; the near-field, where the river momentum still exceeds the plume buoyancy; the mid-field, where the inflowing river waters transits from the inertial near-field forces into a geostrophic or wind-dominated plume, and the momentum balance is dominated by Coriolis force, centripetal acceleration, and pressure gradients; and a far field region, where the initial momentum from the river discharge is lost and the plume dynamics are mainly driven by Earth's rotation, buoyancy and wind stress. If winds and local currents are not strong enough to force the plume offshore, a geostrophic coastal current propagating in the direction of a CTW is generated on the far-field plume (Horner-Devine et al., 2015) (Figure 1.6a). Overall, an alongshore wind,

associated with an offshore Ekman transport flow, weakens these alongshore currents and transport (Fong & Geyer, 2001).

The existence of the plume bulge and its associated anticyclonic circulation and coastal alongshore transport imply a freshwater input effect in triggering this geostrophic balance. Geostrophic balance describes a steady state when the horizontal current velocity is only governed by the balance between the pressure gradient and the Coriolis force (i.e. geostrophic flow), and, by neglecting friction effects in the momentum equation, the geostrophic balance equations read (Stewart, 2008):

$$u_g = -\frac{1}{f\rho}\frac{\partial \mathrm{p}}{\partial \mathrm{y}} \quad (1.1)$$

$$v_g = \frac{1}{f\rho}\frac{\partial \mathrm{p}}{\partial \mathrm{x}} \quad (1.2)$$

where u_g and v_g are the zonal and meridional geostrophic flows, respectively, f is the Coriolis parameter, ρ is a reference density, and p is the pressure. Since the Coriolis parameter is only dependent on the latitudinal position, the riverine input could only affect such currents by changing the horizontal pressure gradients. Indeed, the outflow from rivers creates a light and fresh parcel of water surrounded by salty oceanic water. The low density associated with this freshwater leads to a volume expansion of the water column, increasing the sea level (Durand et al., 2019). This expansion due to salinity changes is known as the halosteric effect.

The halosteric effect involves changes in SSH and pressure gradients. The river plume bulge represents a high-pressure area of increased SSH and reduced SSS. This higher SSH creates a primary meridional pressure gradient from the bulge to both north and south (Figure 1.6b). By adding the Coriolis effect, which deflects the flow to the left in the Southern Hemisphere, a primary zonal geostrophic flow balances the meridional pressure gradient, with an onshore (offshore) flow south (north) of the plume's bulge, leading to coastal downwelling (upwelling) (Figure 1.6b). Further, the generated zonal flow produces secondary zonal pressure gradients that, in turn, are balanced by a secondary northward (southward) alongshore geostrophic flow, north (south) of the bulge (Figure 1.6b). Both upwelling and downwelling processes, as well as the generated meridional alongshore geostrophic flows, could impact SSTs by moving colder and warmers waters to the surface or subsurface, respectively, and by bringing different temperature waters to north and south, especially in a region with a strong alongshore meridional temperature gradient such as the SETA (Figure 1.1a).

Additionally, river discharge waters do not necessarily have the same temperature as the ambient ocean water. Hence, one might argue the existence of a river-plume related thermosteric effect, adding to the halosteric one. However, the magnitude of such small temperature differences' effects on density is very small when compared to the large salinity shifts influencing the density fields (Durand et al., 2019). Furthermore, river outflows also involve a mass contribution to the overall SSH change. Nevertheless, it has been shown that this mass contribution is significant for changing SSH on a global scale, but not regionally, where the halosteric effect is believed to be more important (Durand et al., 2019).

Fong & Geyer (2002) pointed out that lateral pressure gradients related to salinity changes at river plumes can induce surface geostrophic flows projecting at the coast. Similarly, Alory et al (2021) and Topé et al. (2023) demonstrated an additional onshore geostrophic flow generated by the Niger River in Gulf of Guinea, discussing as well the possibility of such effect next to other river plumes. For the Congo River specifically, White & Toumi (2014) observed an annual southward coastal SST increase from 6ºS due to the river's presence, mentioning that this SST warming could be caused by changes in surface coastal currents. To comprehend if this mechanism is actually true for the Congo's case is fundamental to understanding the mean-state SST in the SETA, especially considering the future projections of amplified river discharges in the warming scenario (Müller et al., 2024; Aloysius and Saiers, 2017).

1.2.2 Mixed Layer and Barrier Layers

Freshwater input affects ocean stratification and can therefore significantly impact SST. Oceanic waters are far from being uniform and homogeneous fluids. The different characteristics in these waters shape the global ocean picture. Oceans are vertically stratified, separating layers of lower-density waters at the surface above layers of increasing density with depth. In most regions, the density structure is defined by the vertical temperature structure (Talley et al., 2011; Stewart, 2008). The surface layers are usually warmer and less dense than at subsurface due to the increased solar heat and incoming radiation. This is the case especially in the tropical region, where the incidence of solar heating is even stronger. However, salinity changes at the surface also control density shifts, impacting the vertical ocean stratification, especially in regions with high freshwater input, either from rivers or precipitation (e.g. de Boyer Montégut et al., 2007). Overall, understanding stratification changes in the ocean column is crucial, since they can modulate the vertical exchange of heat, oxygen, carbon, and nutrients, influencing biological productivity and fisheries (Li et al., 2020; Llort et al., 2019; DeVries et al., 2017; Keeling et al., 2010). Throughout this thesis, the focus is on the stratification changes and their impacts within the top layers of the ocean. The upper boundary ocean layer, connecting the ocean's surface with the atmosphere, is the so-called mixed layer (ML).

The ML is characterized by being the upper layer of the ocean, presenting well-mixed waters with temperature, salinity, and density nearly vertically uniform embedded in the surface layer, and ranging from the ocean's surface to the ML base, where the almost absent vertical density gradient starts to surge (Figure 1.7a). Mixing within the ML results mainly from atmospheric wind forcing, via interaction between the wind stress and the oceans' surface, where friction from this interaction generates turbulence and mixes the upper ocean layer (e.g. Talley et al., 2011; Stewart, 2008). Changes in water buoyancy can also induce mixing within the ML, resulting from changes in latent heat fluxes and evaporation, which increase the surface layer density (e.g. Talley et al., 2011; Stewart, 2008). In general, MLs are shallower in tropical regions (i.e. 5m – 40m deep or even shallower) due to the increased solar radiation and heat transfer into the ocean, which generates stronger vertical temperature gradients (e.g. de Boyer Montégut et al., 2004). However, defining the mixed-layer depth (MLD) is quite challenging and can be done by a variety of approaches (Holte & Talley, 2009; de Boyer Montégut et al., 2004). For example, Holte & Talley (2009) developed a hybrid method to assess the most adequate MLD definitions applied to *in-situ* profiles of temperature and salinity, including

definitions based on density, salinity, or temperature thresholds and gradients, extreme values, and statistical fits within the vertical profiles. Most importantly, in regions subject to high freshwater input and SSS changes, applying a salt-density-based criterion (e.g. threshold of 0.125 kg/m^3 increase) is crucial for well-representing the ML (de Boyer Montégut et al., 2007). By using this criterion, the MLD can actually be separated from the isothermal layer depth (ILD) definition, and the impacts of this difference can be assessed (e.g. Saha et al., 2021; Gévaudan et al., 2021) (Figure 1.7). Here, the MLD is always defined based on the vertical density field, and the definition for each study is described in the respective chapter.

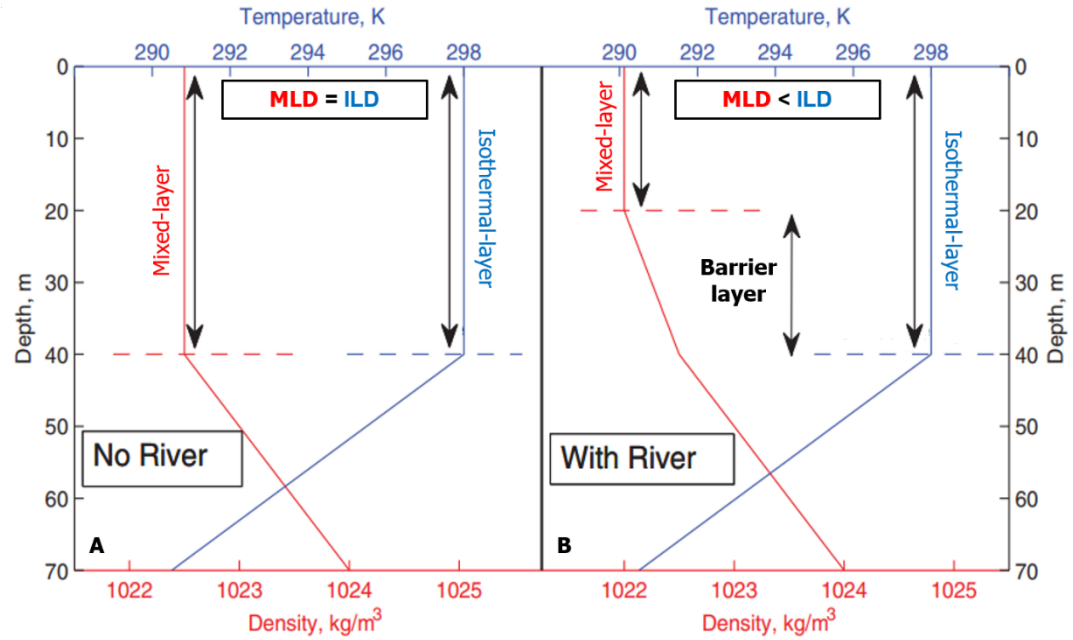

Figure 1.7. A schematic view of a river-induced barrier layers: the mixed layer (MLD) is shallowed, whilst the top of the isothermal layer (ILD) remains constant. If MLD = ILD, there is no barrier layer. Horizontal lines depict the bottom of the density and temperature mixed layers. Quantitative values and profile shapes are for illustration only. In this case, surface temperature does not change in (b) because here the net warming effect of barrier layer generation is zero (White & Toumi, 2014). Modified from White & Toumi (2014).

Similar to the MLD, the ILD is also the upper layer of the ocean characterized by uniform and homogeneous properties, with almost no vertical gradients in temperature. However, ILDs are defined solely based on a temperature criterion, not accounting for salt-density-related changes in the upper meters of the ocean. They mark the depth of the top of the thermocline (i.e. where ocean temperature starts to strongly decrease with depth), and are traditionally defined by the threshold of 0.2ºC decrease in the vertical temperature profile (e.g. de Boyer Montégut et al., 2004). In many regions of the ocean, especially in the subtropics – which are not usually subjected to strong SSS variability, ILD and MLD are the same, indicating a dominance of temperature over salinity in the density field (de Boyer Montégut et al., 2007) (Figure 1.7a). However, freshwater input from both river discharge and precipitation creates a shallower ML, constrained to density changes, that is situated within the ILD (Figure 1.7b). In such cases of the MLD, homogeneous in density, being shallower than the ILD, homogeneous in temperature, a barrier layer (BL) is created, increasing subsurface stratification, and acting as a barrier for the vertical mixing with the colder thermocline waters below (Figure 1.7b). The BL mechanisms is likely one of the most important by which salinity plays a direct role in air-sea interaction and coupling (Balaguru et al., 2012a). The difference between the MLD and the ILD is defined as the barrier layer thickness (BLT), i.e. BLT = ILD – MLD (Figure 1.7b).

The impact of freshwater input-induced BLs on SSTs in tropical regions has been extensively assessed in the last years in all ocean basins. BL generation and influence on SST variability have been linked to: the Amazon river discharge (Saha et al., 2021; Gévaudan et al., 2021; Balaguru et al., 2012a; de Boyer Montégut et al., 2007); the Congo river outflow (Sena Martins & Stammer, 2022; White & Toumi, 2014); several rivers and precipitation in the Bay of Bengal and Arabian Sea (Echols & Riser, 2020; Behara & Vinayachandran, 2016; Vinayachandran et al., 2015); the discharge of the Changjiang river in the East China Sea (Kako et al., 2016); the Niger river in Gulf of Guinea (Topé et al., 2023); and precipitation in the tropical North Atlantic within the ITCZ (Foltz & McPhaden, 2009). BL dynamics can also affect atmospheric responses, such as precipitation rates (e.g. Gévaudan et al., 2021; Vinayachandran et al., 2015; Balaguru et al., 2012a), and intensification of Tropical Cyclones (Balaguru et al., 2012b), as well as affect main SST variability modes such as the El Niño Southern Oscillation (ENSO) (Guan et al., 2025; Liu et al., 2022; Zheng & Zhang, 2012; Zhang & Busalacchi, 2009).

Freshwater input into the ocean triggers the formation of BL due to the freshening of the surface waters, then creating a shallow ML defined by the reduced density in the uppermost ocean layer (Figure 1.7). By reducing the vertical mixing of the surface layers with colder thermocline waters, at the same time that reduces the vertical temperature gradient between the ML and waters immediately below its base – since both water parcels are within the IL, BLs can contribute to warming the SSTs. Analysis of the BLT impacts on SSTs is usually performed via a mixed-layer heat budget, focusing on the vertical turbulent heat flux term. SST cooling (warming) is associated with stronger (weaker) vertical heat flux at the base of the ML when the BL is thin (thick) and the vertical temperature gradient at the ML base is strong (weak) (Saha et al., 2021; Gévaudan et al., 2021; Echols & Riser, 2020; Kako et al., 2016; Balaguru et al., 2012b; Foltz & McPhaden, 2009). In fact, turbulent fluxes calculation is proportional to stratification, given by the Brunt-Väisälä frequency (N^2), and to the vertical temperature gradient, both factors affected by the presence of a BL (see more on these equations in Chapter 5, Eq. 5.1). Recently, turbulent mixing is being pointed as an important factor in modulating Pacific SSTs and in the development of ENSO (Guan et al., 2025; Liu et al., 2025; Tozuka, 2025).

BLs and freshwater input are usually related to an SST warming. However, cooling effects are also associated with such processes. By isolating the ML from mixing below its base, BL generation can lead to a vertical temperature inversion, with surface layers being cooler than the waters immediately below the ML, especially in regions with very shallow MLDs (e.g. Echols & Riser, 2020; Kako et al., 2016; Vinayachandran et al. 2015). A thinner ML is more sensitive to atmospheric changes, predominantly during seasons of strong wind activity, and the freshwater contribution to shoaling such layers even more favors a strong interaction with surface winds, and as a consequence, to the increase in latent heat loss at the ocean's surface (Gévaudan et al., 2021; Behara & Vinayachandran, 2016). Additionally, very shallow MLs reduce the shortwave radiation (SWR) absorption within this layer, and the SWR is lost for depths below the ML base (Gévaudan et al., 2021; Echols & Riser, 2020; White & Toumi, 2014). The overall impact of BLs on SST variability is a balance between both warming and cooling effects presented above, also being subject to seasonality and

regional processes. Hence, the need to understand and evaluate such effects, particularly for each region, proves to be essential.

Within the SETA, freshwater input effects on SSS and SST, particularly from the Congo River discharge (CRD), have also been examined. Materia et al. (2012) correlated CRD to SST anomalies in the Gulf of Guinea, with long-lasting and strong anomalies in SSTs in the event of increased freshwater flow, while recently, Sena Martins & Stammer (2022) showed a strong increase in stratification linked to the CRD that could likely impact SSTs. Finally, White & Toumi (2014) performed a modelling study depicting that the Congo presence and its discharge led to an ML shoaling by up to 7m, creating BLs up to 6m thick at the river mouth. Concomitantly, they observed temperature inversions of up to 0.5K, with warmer waters below the ML (White & Toumi, 2014). The authors argue that the strong shoaling of the ML reduces the absorption of the solar SWR, which is no longer trapped within this layer. The cooling effect from the reduced SWR absorption balances the warming impact of the reduced vertical mixing from the BL generation (i.e, net flux change of 5.5 W/m^2 out of the ML at its base), hence the overall effect of the CRD on SST is not substantial (White & Toumi, 2014). Lastly, White & Toumi (2014) tested via sensitivity experiments the effects of doubling the CRD, and increasing the Congo River temperature by 3K. Their results showed no substantial differences by applying these constraints, suggesting that SST changes related to CRD are more dependent on environmental conditions (e.g., surface fluxes, wind stress, current velocities, background stratification) than on the river temperature or discharge rate (White & Toumi, 2014). The authors, however, focus their whole analysis on the region immediately at the Congo mouth, not extending the discussion to the upwelling region. The impact of the CRD and freshwater input in generating BLs and affecting SST off Angola and Namibia, and consequently the extreme Benguela Niño and Niña events, remains uncertain.

1.3 Motivations, Goals and Outline

1.3.1 Motivation and Goals

Freshwater input and variability have been shown to increase the mean state SST in other tropical regions, either via precipitation (Zhang and Busalacchi, 2009) or river discharges (Topé et al., 2023), and to impact geostrophic circulation in a tropical region (Alory et al., 2021). Also, a closer look into those mechanisms is crucial in view of the future scenario of amplified river runoff and changes in geostrophic flow in eastern boundary upwelling systems due to climate warming (Müller et al., 2024; Jing et al., 2023; Aloysius and Saiers, 2017).

Additionally, the Benguela Niños and Niñas underlying mechanisms, their forcings and impacts have been investigated in detail over the last years (e.g. Imbol Koungue & Brandt, 2021; Bachèlery et al., 2020; Imbol Koungue et al., 2019, 2017; Lübbecke et al., 2019; Rouault et al., 2018, 2007, 2003; Bachèlery et al., 2016a; Florenchie et al. 2003, 2004; Gammelsrød et al., 1998; Shannon et al., 1986). Even though these events are mainly forced remotely (~71%) (Bachèlery et al., 2020; Lübbecke et al., 2010), local forcing has been playing an increasingly important role in triggering these events in the last decades (Imbol Koungue et al., 2021; Lübbecke et al., 2019; Prigent et al., 2020; Richter et al., 2010). More recently, Lübbecke et al. (2019)

suggested freshwater input from precipitation and from the Congo River discharge as a possible new source and up-until-now unnoticed mechanism of local forcing that could amplify such events. This effect, however, remains poorly understood.

Furthermore, both climate and regional ocean model simulations struggle in well representing eastern boundary upwelling systems, which usually present a warm SST bias (e.g. Farneti et al., 2022; Small et al., 2024). The BUS, south of the SETA, is known to be even more difficult to simulate (Bonino et al., 2019; Kurian et al., 2021). Indeed, the strength of the Angola Current and the location of the ABF in the SETA are pointed out as key sources of such biases in general Earth system models (Koseki et al., 2018). Finally, even though the role of freshwater input in the SETA SST has been investigated, it has not been fully elucidated by both modelling and observational studies (Sena Martins & Stammer, 2022; Newinger and Toumi, 2015; White and Toumi, 2014; Materia et al., 2012).

Therefore, the comprehension of the mechanisms by which freshwater input influences the mean state and variability within the SETA is greatly important for both the socio-economics and ecosystem management within the local African communities, and for supporting the forecast of such extremes, assessing potential future changes, and contributing to improving ocean general circulation models. To do so, the following research questions will be addressed in this thesis:

- **Does the freshwater input in the SETA impact the mean-state SST? What are the mechanisms involved in this influence?**

- **What is the impact of the freshwater outflow on the SST variability within the SETA? Does it amplify or counteract the extreme warm and cold events in this region? Can this contribution be quantified?**

- **What are the mechanisms responsible for such an impact on SST variability?**

- **Do other ocean basins influence the freshwater input variability in the SETA? Can a connection be established between Benguela Niño and Niña events and SST variability modes from other oceans?**

1.3.2 Outline

Aiming to answer those questions, Chapter 2 details and discusses the different model simulations, the *in-situ* measurements and observational datasets, and the reanalysis products used in this work. Chapter 3 presents how the SST mean state and the regional coastal dynamics within the SETA are affected by the freshwater inflow, especially from the Congo River. For that, the focus is on two model simulations that only differ in the prescribed freshwater input: in one, this input is set to zero, in the other, a climatological discharge is prescribed. Then, the observed differences between the two experiments are compared, and the mechanism

responsible for such changes is discussed. In Chapter 4, the focus is on the most extreme Benguela Niño event in the satellite era, the 1995 Benguela Niño, to understand the mechanism by which freshwater input and anomalies of SSS can impact this mode of SST variability. Based mainly on reanalysis products, the importance of coastal current anomalies for the SSS variability off Angola, and therefore, for the freshwater input impact on these extreme events, is highlighted. Chapter 5 deepens the discussion by extending this analysis to other events, and further examining the extremely cold Benguela Niñas. Such impacts are quantified in terms of turbulent heat fluxes from subsurface to surface layers, exploring an extensive dataset obtained from different research cruises. Chapter 6 links the positive IOD event in 1994 to the 1995 Benguela Niño through a land and atmosphere bridge via the Congo River basin hydrology. A potential new source of prediction for Benguela Niños and Niñas and their amplification of extreme SSTs is statistically shown. Finally, Chapter 7 gives a summary of the research outcomes, answering the above-raised questions and discussing the perspectives and outlook of this work.

Chapter 2

Datasets

In this thesis, a broad range of datasets is used, exploring their advantages in each specific study and discussing the impact of their caveats on the observed results. To address the questions raised in Chapter 1, the first focus is on model simulations and experiments from a model configuration based on a state-of-the-art modelling framework (in Chapter 3). Further, reanalysis datasets and observations, such as satellite (in Chapters 4 and 6) and *in-situ* measurements from research cruises (in Chapter 5), are explored. Below, the importance and concerns regarding the scientific use of such different datasets are discussed, and details on the data utilized to achieve the obtained results are given.

2.1 Model simulations

Ocean modeling is a crucial instrument in understanding and predicting oceanic processes, having also significant implications for climate science, marine ecosystems, coastal management, disaster mitigation, and ocean policy and management. In addition, they are an increasingly valuable tool in interpreting what is seen from observations (Fox-Kemper et al., 2019). Further, ocean models can mimic observations with the advantage of increasing both spatial and temporal resolution, allowing the understanding, for example, of small and mesoscale processes and long-term ocean variability. Even though models can expand the reach of observations and contribute to the improvement of observational plans, they rely on the fidelity of their underlying parametrizations, assumptions, and uncertainties (Fox-Kemper et al., 2019).

Although ocean circulation models have evolved over the past decades (Fox-Kemper et al., 2019), challenges are long-lasting. A critical part of the overall Earth system modelling is understanding and well-representing the ocean circulation (Chassignet et al., 2019), since this circulation is crucial, for instance, in redistributing the thermal energy stored in the ocean system. Indeed, the oceanic equations of motion have long been known (e.g. Laplace et al., 1829; Navier, 1822; Stokes, 1845), along with the intricacies of seawater thermodynamics (IOC et al., 2010). The computational and storage requirements to discretize the equation of thermodynamics, however, are beyond the current computational capacity, even with the use of supercomputers (Fox-Kemper et al., 2019). Therefore, approximations and different model parametrizations are explored to improve the state-of-the-art ocean circulation models. Different mixing parametrization schemes, for example, are currently being tested to improve the representation of Tropical Atlantic mixing processes in such models (Bastin et al., 2025; Mrozowska et al., 2024). Hence, understanding the model limitations and caveats is crucial when analyzing model outputs.

One well-known and established issue in both climate and regional ocean model simulations in eastern boundary upwelling systems is the warm SST bias, with models overestimating the mean SSTs within these regions (e.g. Small et al., 2024; Farneti et al., 2022). Several processes were discussed as possible sources of these discrepancies, such as mixing representation, weak upwelling velocities and equatorward

surface flow, poor depiction of clouds, etc. (e.g. Bastin et al., 2025; Small et al., 2024; Bonino et al., 2019; Richter, 2015). Simulation of the BUS was pointed to be even more challenging to be performed, likely due to the encounter of significantly distinct water masses, the unique spatial structure of the wind field, its influence on the dynamics of these coastal waters, and the representation of the Angola Current (Kurian et al., 2021; Bonino et al., 2019; Koseki et al., 2018). Increasing spatial resolution for both the oceanic model and atmospheric forcing may somewhat alleviate the biases, since the use of higher resolution can better picture wind-related processes (Small et al., 2024; De La Vara et al., 2020).

Furthermore, the representation of SSS fields and freshwater runoff input into ocean models also poses a big challenge for the modelling community. Ocean salinity in coastal regions near river mouths is highly variable and associated with a strong vertical stratification, which adds complexity to a flawless representation by such models (Martins and Stammer, 2022; Nyadjro et al., 2022; Boutin et al., 2021). Additionally, salinity fields and their discrepancies to the observations are dependent on estimates of freshwater runoff, mainly from reanalysis, which are used as atmospheric forcing and traditionally have been very idealized (Chandanpurkar et al., 2022; Fox-Kemper et al., 2019). For the Congo River, specifically, the complexity of the Congo Basin hydrology and the lack of field observations were pointed out as the main reasons for such differences between the observed river discharges and those taken from reanalysis products (Chandanpurkar et al., 2022; Hua et al., 2019). One possible solution to improve such runoffs is the direct implementation of parametrizations for physical processes in estuarine box models (Verri et al., 2020; Sun et al., 2017).

Even though there are caveats and challenges in modelling the ocean system, they continue to further progress (Fox-Kemper et al., 2019). It is expected that a future increase in model resolution, the use of new parametrizations, and increasing coupling to other system models will improve the perspective of advanced ocean modelling. For instance, the specificity of river plumes, especially their associated strong density gradients, both vertically and horizontally, requires dedicated effort to work out novel turbulent closure models (Durand et al., 2019). The continuous use of the ocean observing systems is a crucial constraint for such improvements (Fox-Kemper et al., 2019). In the following, the ocean model, configuration, and experiments used in Chapter 3 of the present thesis are detailed.

2.1.1 INALT20 model experiments

A great advantage of using model experiments is the possibility of designing simulations to answer a specific scientific hypothesis. Here, to address the question of whether freshwater input might affect the SST mean-state within the SETA, the INALT20 model configuration (Schwarzkopf et al., 2019) was used. INALT20 is based on the Nucleus for European Modelling of the Ocean (NEMO) v3.6 ocean general circulation model, the state-of-the-art model framework (Madec and the NEMO team, 2016), and is part of the INALT family, which is a set of global ocean model configurations, initially developed to better understand the Agulhas Current system in a high spatial resolution (Figure 2.1). The INALT family configuration is the successor of the INALT01 high-resolution, which has been widely used to understand the

ocean-atmosphere dynamics associated with the Agulhas Currents, as well as impacts on the Atlantic (Malan et al., 2018; Rühs et al., 2017; Biastoch et al., 2015; Lübbecke et al., 2015; Durgadoo et al., 2013).

INALT20 consists of a regionally confined high-resolution grid (i.e. nest) combined with a global coarser grid (i.e. host, ORCA025, 1/4º horizontal resolution) (Barnier et al., 2006), via a two-way interaction, where both the host and the nest provide boundary conditions to each other. The high-resolution INALT20 (1/20º) covers the South Atlantic and the West Indian oceans (63°S – 10°N, 70°W – 70°E) (Figure 2.1), and has a vertical grid with 46 z levels, with 6m resolution at the surface to 250m in the deepest layers. This vertical resolution not only resolves the first baroclinic mode, therefore representing the major baroclinic currents (Stewart et al., 2017), but also has been shown as an appropriate choice for model configurations up to 1/20º resolution (e.g. Böning et al., 2016; Behrens et al., 2017).

Surface atmospheric (i.e. momentum, heat, and freshwater fluxes) and runoff forcing in INALT20 is done with the JRA55-do atmospheric reanalysis (Tsujino et al., 2018), which has been shown to improve model representation within the BUS and other eastern boundary upwelling systems, when compared to a coarser atmospheric forcing (Small et al., 2024; Prigent & Farneti, 2024), even though discrepancies in the runoff between JRA55-do and the measured discharge from river gauges have also been observed (Chandanpurkar et al., 2022). Additionally, enhanced vertical mixing over the upper 10m is applied, and SSS restoring is suppressed at locations where freshwater discharge enters the ocean (Schwarzkopf et al., 2019). Further details of the INALT family or the INALT20 configuration can be found in Schwarzkopf et al. (2019). Below, the model experiments here performed are detailed.

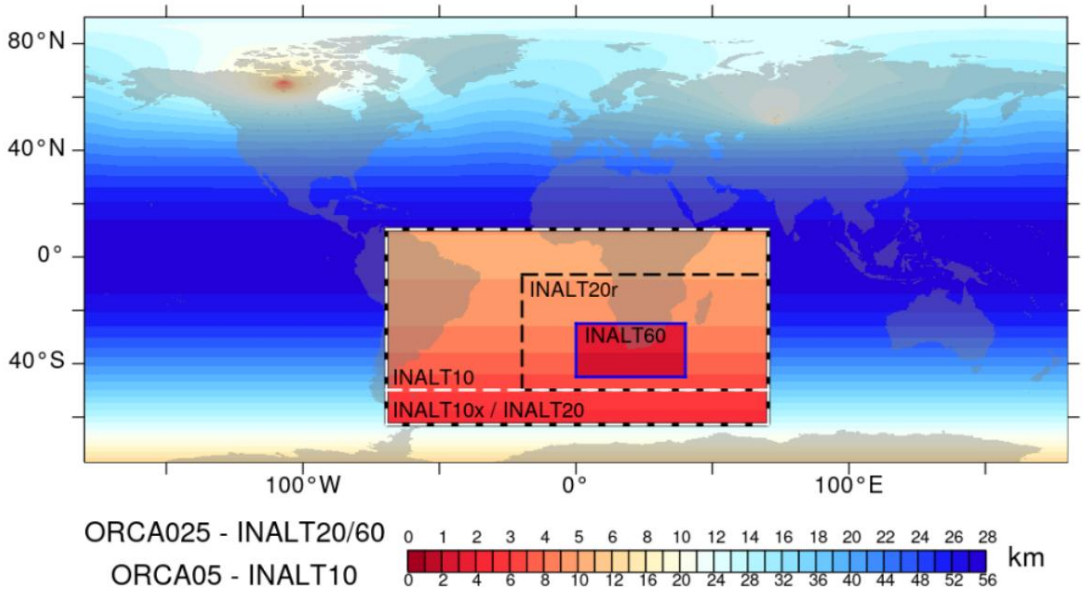

Figure 2.1. Grid sizes in the INALT family: shown is the zonal grid length (in km) for the global ORCA025 grid with the embedded INALT20 (outer black box), INALT20r (inner black box) and INALT60 (blue box) grids (upper scale), as well as for ORCA05 with the embedded INALT10x (white dashed box, same as INALT20) and INALT10 with its southern boundary shifted north (lower scale). From Schwarzkopf et al. (2019).

Three model experiments were developed by using the INALT20 configuration, which only differ in their prescribed river runoff. 5-daily averages as output data are analyzed for most of the variables, except for SSH and runoff, for which daily outputs are examined. The global SSH average at each location and time slice was removed to detrend the modelled SSH fields. The experiments are the following:

- CTRL: is the reference (control) simulation, with prescribed interannually varying daily runoff forcing from JRA55-do. This simulation is compared to observational datasets to ensure the INALT20 performance in representing the general characteristics of the SETA. This simulation has been described and utilized in recent works (e.g. Rühs et al., 2022; Schmidt et al., 2021; Biastoch et al., 2021). A 30-year-long spin-up integration initialized with temperature and salinity data from the World Ocean Atlas (WOA) (Huang et al., 2021; Levitus et al., 1998) precedes this hindcast simulation, which spans from 1958 to 2019.
- CLIMA: sensitivity experiment forced with a monthly climatological runoff also built from JRA55-do. Branch off from CTRL in the year 2000. For both CLIMA and CTRL, vertical mixing is enhanced where the land-to-ocean discharge occurs.
- NORIV: sensitivity experiment forced without any runoff forcing. Branch off from CTRL also in the year 2000.

The idea of performing three model simulations for the purpose of this study was to investigate not only how a climatological runoff forcing would impact the mean-state SST in the region, but also to check if the interannual variability of this land-to-ocean discharge would impact the SST variability within the SETA. By comparing CLIMA and CTRL to NORIV, one is able to observe how the ocean variables from the simulations with the presence of a climatological or interannually varying runoff differ from a situation in which the freshwater input would not exist. In the end, the focus of the model-based discussion is mostly on CLIMA and NORIV, and the consequent effects on the mean state SST, even though all three simulations were analyzed throughout the study (see Chapter 3 for more details). In the next section, the importance of using observational datasets is discussed, and the details of the datasets used in this thesis are presented.

2.2 Observational datasets

In-situ ocean measurements are fundamental to oceanographic research, providing direct information to understand the physical, chemical, biological, and geological phenomena within this dynamic environment. Unlike numerical ocean models, observations represent the "ground-truth" of the climate system, while also serving as benchmarks for model validation. Ocean observing systems have been developed in the last decades (e.g. Foltz et al., 2025; Hassoun et al., 2024), contributing to the observing, analyzing, and forecasting of the ocean across coastal and open oceans, from shallow to deep layers. They provide immense societal and scientific value by supplying the data required for such advancements. However, deficiencies as part of such systems are still observed, especially in near-coastal regions and subsurface oceans (Foltz et al., 2025). In addition, observational datasets are subject to uncertainties arising from instrumentation limitations, indirect measurement assumptions, and sparse sampling, which the latter leads to gaps in spatial and temporal resolution, and thus requires robust statistical approaches. The largest source of error in oceanographic understanding is likely the insufficient number of observations (Stewart, 2008). In the last decades, an effort

to overcome this lack of sampling has also been made by the use of satellite measurements, and reanalysis products (e.g. Lellouche et al., 2021; Hersbach et al., 2020; Reynolds et al., 2007). In Sections 2.2.1 and 2.2.2, details on the *in-situ* measurements and satellite products, respectively, used in the scope of this thesis are given. Reanalysis products are explored in Section 2.3.

2.2.1 *In-situ* measurements

Throughout this thesis, an extensive number of *in-situ* measurements, mainly from ship cruises, were utilized. Figure 2.2 depicts the location and the time-period at which the majority of these measurements were taken. The only data described in this section that was not collected by cruises is the Congo River discharge (CRD) data, taken from the Brazzaville-Kinshasha gauge station, situated 500km upstream of the River mouth and indicated by the green diamond in Figure 2.2a., which represents 98% of the total CRD (Alsdorf et al., 2016). River discharge rates are estimated either directly via Acoustic Doppler Current Profiles (ADCP) current meters, or via a combination of water level measurements and a rating curve, which relates water level to flow rate. Here, CRD estimates from 1947 to 2019 were used.

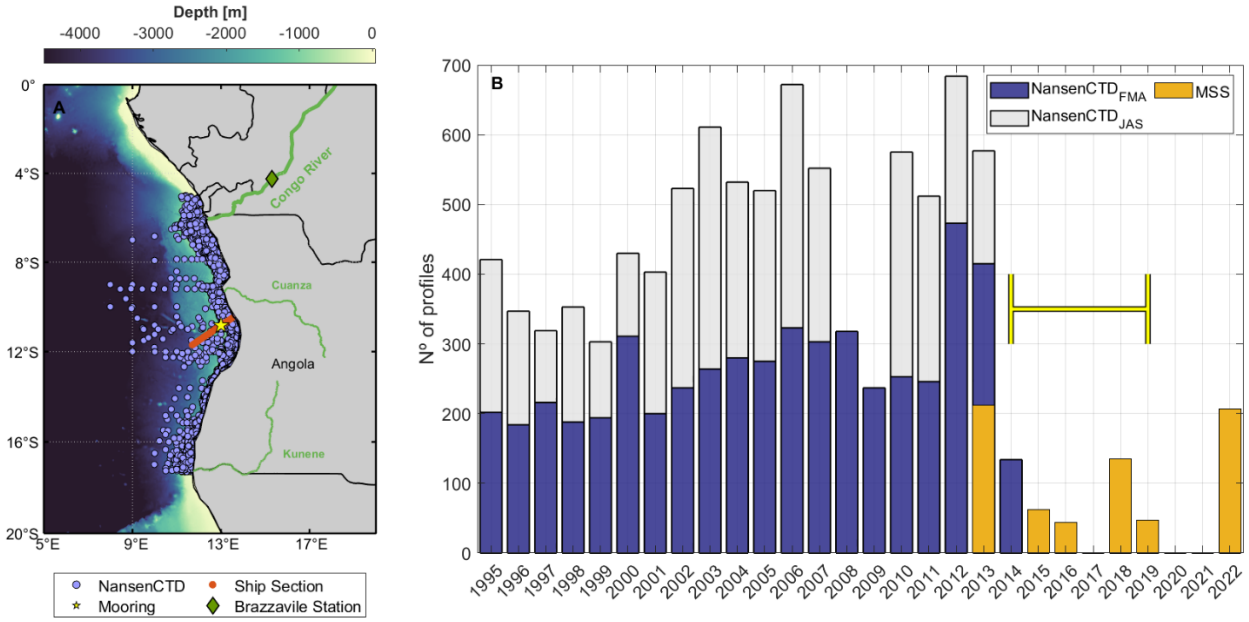

Figure 2.2. Summary of *in-situ* measurements used. (a) Location of Nansen Program's CTD profiles (purple circles), ship section with CTD and MSS profiles (orange circles), mooring (yellow star), and Congo discharge' Brazzaville station (green diamond). Shading is bathymetry from GEBCO. (b) Number of cruise profiles taken in each year. Blue (grey) bars are Nansen Program's CTD profiles during February-March-April (July-August-September). Orange bars are MSS profiles at ship's section, and yellow line indicates mooring's years here used.

The great majority of the hydrographic measurements used here were obtained from Conductivity-Temperature-Depth (CTD) profiles from the Nansen Programm of the Food and Agriculture Organization of the United Nations (FAO), where several research cruises were conducted on board the Research Vessel Dr. Fridtjof Nansen (Tchipalanga et al., 2018). This Programm marked the start of a new era in the Angolan coastal ocean monitoring, and from 1995 to 2014 covered the entire extent of the Angolan continental shelf (Tchipalanga et al., 2018) (Figure 2.2). More than 8000 profiles on Angolan coast were collected in these 20 years, with the surveys being carried out twice a year, once in FMA and once in JAS (Tchipalanga et al., 2018). Overall, CTD sensors can obtain information on temperature, conductivity, and pressure in the water

column. While they directly measure temperature, both conductivity and pressure measurements are converted to salinity and depth, respectively, via mathematical formulas. The location of the CTDs and the number of profiles per year and season are depicted in Figure 2.2.

Additionally, profiles from both CTD and Microstructure Sonds (MSS) obtained during 6 research cruise campaigns in the last decade were also explored here. Every campaign profiled the water column within the same ship section, depicted in Figure 2.2a. The MSS was equipped with 2-3 airfoils shear sensors, which measure the microstructure shear, and the profiles were obtained by a loosely free-falling tethered probe with a falling speed of 0.5-0.6 m/s (Körner et al., 2023). By assuming isotropy, the microstructure shear is then used to estimate turbulent kinetic energy (TKE). From TKE, eddy diffusivity is calculated, which is a crucial variable in estimating mixing processes and turbulent fluxes within the water column. The ship section from the different cruises were taken in: July 2013 (M098 cruise); October 2015 (M120); October 2016 (M131); June 2018 (M148), September 2019 (M158) and April 2022 (M181) (Figure 2.2b). Overall, 707 MSS profiles were obtained. Figure 2.2b also shows the number of MSS profiles for each year.

Finally, current velocity measurements were obtained from a mooring located off Angola at 13º00'E, 10º50'S (Kopte et al., 2017). The mooring is installed at the continental slope at about 1200m depth. At 500m on the mooring cable, an upward-looking 75-kHz Long Ranger ADCP is mounted to record flow velocities (especially the Angola Current) up to 45m below the sea surface. Flow velocities are estimated by analyzing the Doppler shift bounced back by the particles from the sound waves transmitted signal, i.e. the difference in frequency between the sound waves transmitted and received. With a vertical resolution of 16-m bin size, the mooring data is available since July 2013 to today (Imbol Koungue et al., 2024). However, only the measurements from 2013 to 2019 are used (period indicated by the yellow line in Figure 2.2b).

2.2.2 Satellite products

Remote sensing from satellites orbiting the Earth provides significantly more information than would be possible to obtain from the Earth's surface (Stewart, 2008), and they have been used to observe the ocean since the 1970s. In June 1978, the world's first oceanographic satellite was launched into orbit, the Seasat (Stewart, 1988), which strongly led to the improvement of techniques for evaluating the accuracy of remote ocean measurements and contributed to a better understanding of the system (Stewart, 1988). Since the late 1990s, more satellite datasets have become available, providing additional information to the ocean's perspective of supporting life abundance and regulating the climate (Reynolds et al., 2007). Different satellites equipped with various instruments can measure a broad range of variables at the ocean's surface, including SST, SSS, SSH (from which geostrophic velocities can be obtained), waves, chlorophyll concentration, wind, and other atmospheric components, such as precipitation. Such measurements allow an extensive global and spatial coverage of the surface of the ocean, and are also extensively combined with *in-situ* measurements or model outputs to create new datasets (Table 2.1).

SST can be obtained from satellite either via: spectroradiometers, which measure both the wavelength and amplitude of the light emitted from the surface of the oceans, land, and atmosphere; infrared radiometers, which evaluate the radiation reflected by oceans' surface; and microwave radiometers, which measures the

energy emitted at millimeter-to-centimeter wavelengths. Spectroradiometers are also used for chlorophyll concentration and sea-ice cover, for example, while microwaves are able to obtain information about atmospheric components, such as atmospheric water content and precipitation, as well as SSS. Rain rates are also taken from satellite scatterometers, a radar sensor that measures the scattering effect at Earth's surface, and are also used for wind-component products. Finally, wind speeds and SSH are also obtained from satellite altimeters, which calculate the time for a short electromagnetic pulse sent from the satellite to reach the surface and return.

During the last decade, a special focus on monitoring SSS has emerged (Boutin et al., 2021). Since 2010, three main satellite missions have been dedicated to observing SSS based on microwave radiometry (SMOS, Aquarius, and SMAP) (Boutin et al., 2021; Durand et al., 2019). The most recent Soil Moisture Active Passive (SMAP) satellite mission from NASA, with coastal measurements as close as 40km from the coast, allowed the scientific community to move forward to an unprecedented monitoring of global and coastal SSS (Boutin et al., 2021; Durand et al., 2019). The European Space Agency (ESA) funded program (Climate Change Initiative, CCI) combined these measurements, aiming to generate 16 years (2010-2025) of improved calibrated global SSS fields. Here, this dataset is explored from 2010-2020 (Table 2.1). Such advancements in estimating SSS fields are crucial in improving the performance of global ocean models and in refining the accuracy of reanalysis products, since salinity measurements, especially close to the coast and river mouths – with high uncertainty due to salinity variability and vertical gradients, are currently sparse both spatially and temporally (Jarugula et al., 2025; Nyadjro et al., 2022; Sena Martins & Stammer, 2022; Boutin et al., 2021).

Table 2.1. Datasets used and their sources. SST: sea surface temperature, SSS: sea surface salinity, T: temperature, S: salinity, E: evaporation, P: precipitation, LWR: Longwave radiation, SWR: Shortwave radiation, LHF: latent heat flux, SHF: sensible heat flux. U and V are the zonal and meridional current velocity components, respectively. U-wind and V-wind are the zonal and meridional wind components, respectively

Type	Product	Resolution	Time	Variables	Reference
Satellite	ESA-CCI	0.25 x 0.25	2010-2020	SSS	Boutin et al. (2021)
Satellite + In-situ	OI-SST	0.25 x 0.25	1982-2022	SST	Huang et al. (2021); Reynolds et al. (2007)
Satellite + In-situ	TAMSAT	0.0375 x 0.0375	1983-2020	P	University of Reading
Satellite + In-situ	GPCP	2.5 x 2.5	1979-2021	P	Adler et al. (2003)
Satellite + In-situ + Reanalysis	Near-surface velocities	0.25 x 0.25	1993-2022	U, V	Lumpkin & Garzoli (2011); Perez et al. (2019);
Satellite + Reanalysis	CCMP	0.25 x 0.25	1993-2019	U-wind, V-wind	Atlas et al. (2011); Mears et al. (2022)
Satellite + Reanalysis	GlobCurrent	0.25 x 0.25	1993-2022	U, V	Rio et al. (2014)
Reanalysis	GLORYS12	0.083 x 0.083	1993-2020	T, S, U, V	Lellouche et al. (2021)
Reanalysis	ERA5	0.25 x 0.25	1987-2021	LWR, SWR, LHF, SHF, U-wind, V-wind, E, P	Hersbach et al. (2020)

Table 2.1 gives details on the satellite and the combined datasets, as well as the reanalysis products, used throughout this thesis. A brief description of the products which include satellite measurements is here provided: The Daily Optimum Interpolation Sea Surface Temperature (OISST) incorporates observations from different platforms (satellites, ships, buoys and Argo floats) into a regular global grid, creating a spatially complete map of SST by interpolating these datasets; the Tropical Applications of Meteorology using SATellite data and ground-based observations (TAMSAT) merges satellite and gauge measurements to produce daily rainfall estimates for the African continent; similarly, the Global Precipitation Climatology Project (GPCP) integrates satellite measurements and gauge analysis over land to provide global monthly precipitation data; The Cross-Calibrated Multi-Platform (CCMP) combines wind retrievals from multiple types of satellites to a background reanalysis field from ERA5; the near-surface velocities product synthetizes geostrophic velocities from satellite altimetry, surface drifter velocities data and Ekman velocities from reanalysis winds, to provide global daily maps of 15m depth current velocities; finally, the GlobCurrent obtain the total velocity fields by combining satellite geostrophic surface currents to modelled Ekman currents at the surface and 15m depth from ERA5 wind stress. Further information on the reanalysis products is given in the next section.

2.3 Reanalysis products

Ocean reanalysis products are developed via a combination of numerical ocean modelling, processing observations from satellite and *in-situ* instruments, and data assimilation. They aim at providing the most accurate oceans' past state with a coherent and continuous four-dimensional grid (latitude, longitude, depth, time). These datasets have a wide application in both ocean and atmospheric sciences, being used to asses changes in observing systems, assimilation capabilities and forecast errors (Hersbach et al., 2020). Even though they are extremely valuable tools, reanalysis problems are also associated with systematic biases and uncertainties coming from the model simulations and the sparse observations (Lellouche et al., 2021; Hersbach et al., 2020). Temporal consistency and accuracy of the climate reanalysis products can be affected by the interaction between model biases and an evolving observing system (Hersbach et al., 2020).

The uncertainty and biases associated with reanalysis products have become less troublesome in the last decades, especially with the development of satellite altimetry in the 1990s and the rise of supercomputers, which allowed the development of models with higher resolution, introducing more of the ocean physics, and resolving the first Rossby radius of deformation (Barnier et al., 2006). The Argo network development since 2000 has made possible the correction of biases in the upper 2000m, for example. However, Lellouche et al. (2021) pointed out that the onset of the Argo could also introduce spurious ocean trends and variabilities, not necessarily associated with what is observed in reality. Another known issue within such reanalysis is the non-closure of energy budgets and their evolution over time, which needs to be better understood and might improve future products (Lellouche et al., 2021; Hersbach et al., 2020). Nevertheless, continuous observing systems are necessary for improving reanalysis datasets.

In this thesis, two reanalysis datasets (Table 2.1) are used: the atmospheric European Centre for Medium-Range Weather Forecasts (ECMWF) Reanalysis v5 (ERA5, Hersbach et al., 2020); and the Global

Ocean Eddy-resolving Reanalysis (GLORYS12, Lellouche et al., 2021). ERA5 is the fifth generation of the ECMWF atmospheric reanalysis of the global climate, providing global hourly estimates of a large number of atmospheric, land, and oceanic climate variables. The assimilation incorporates data from satellites, and *in-situ* observations from weather stations, moorings, ground-based radar, gauge measurements, etc. GLORYS12 has 50 vertical levels, is based on the ocean model Nucleus for European Modelling of the Ocean (NEMO), and has the atmospheric forcing from ERA5. Assimilated observations include satellite SST and altimetry, and *in-situ* temperature and salinity profiles. Only climatological monthly mean river runoff is incorporated into GLORYS12, however, the effects of interannual variations are included through data assimilation. It is available from 1993 to today, and data from 1993 to 2020 is used in the analysis. This ocean reanalysis was compared to the independent *in-situ* measurements from both the Nansen Program CTDs and the 13º00'E, 10º50'S mooring, showing a good performance in well representing the temperature, salinity, and current velocities in the coastal SETA (see more in Chapter 4). More details from these products is shown in Table 2.1.

Chapter 3

River discharge impacts coastal Southeastern Tropical Atlantic sea surface temperature and circulation: a model-based analysis

In this chapter, the impacts of the freshwater input, dominated by the Congo River discharge, on the mean state SST and coastal dynamics of the SETA are explored. The analysis is based on the INALT20 simulations, presented in Chapter 2. First, a comparison between the simulated fields from the INALT20 experiments with observational and reanalysis datasets is performed. Then, the observed differences between the experiments with and without a land-to-ocean runoff are discussed. Finally, the mechanism by which the River's presence affects the mean state SST, SSS, SSH, and current velocity patterns is highlighted.

The manuscript was published in *Ocean Science* in March 2025.

Citation: **Aroucha, L. C.,** Lübbecke, J. F., Brandt, P., Schwarzkopf, F. U., and Biastoch, A.: River discharge impacts coastal southeastern tropical Atlantic sea surface temperature and circulation: a model-based analysis, *Ocean Science*, 21, 661–678, https://doi.org/10.5194/os-21-661-2025, 2025

The candidate designed the original study, carried out all the analyses, produced all the figures, and authored the manuscript from the first draft to the final published version.

3.1 Abstract

The Southeastern Tropical Atlantic (SETA) coastal region sustains highly productive fisheries and marine ecosystems, thus having immeasurable socio-economic importance for southwestern African coastal countries. It is characterized by high sea surface temperature (SST) variability and significant freshwater input from land mainly due to Congo River discharge. In this study, using high-resolution ocean model sensitivity experiments, we show that the presence of low salinity waters from the river discharge increases the mean state SST in the SETA coastal fringe by about 0.26ºC on average and by up to 0.9ºC from south of the Congo River to the Angola-Benguela front (ABF). North of the Congo River up to about 4ºS, this input significantly reduces the mean state SST by more than 1ºC. We demonstrate that the impact of river discharge on SST is associated with a halosteric effect, which modifies the sea surface height gradient and alters geostrophic currents, producing a southward coastal geostrophic flow, with an onshore geostrophic component to the south of the Congo River. Hence, advective warming and downwelling are generated south of the river mouth. Furthermore, the southward advection generated by the low salinity waters pushes the ABF further south. Concomitantly north of the Congo's mouth, the sea surface height gradient generates a northward geostrophic coastal current with an offshore geostrophic component, which is associated with advective cooling and upwelling north of 6ºS. These results draw attention to the freshwater impact on SSTs and ocean surface dynamics, especially in the projected climate change scenario of continuously increasing land to ocean discharge.

3.2 Introduction

The Southeastern Tropical Atlantic (SETA, Fig. 3.1) is an eastern boundary upwelling region that features high biological productivity encompassing the tropical Angolan, and northern and southern Benguela upwelling systems (Jarre et al., 2015). This area sustains productive marine ecosystems and fisheries, with high socio-economic and food security importance for southwestern African coastal countries (FAO, 2020; Kirkman et al., 2016; Sowman and Cardoso, 2010). Within the SETA, the thermal Angola-Benguela front (ABF, Fig. 3.1a), which is characterized by the convergence of tropical warm waters from the north and cool subtropical waters from the south, is located at around 17ºS-18ºS, where the southward Angola Current (AC) encounters the northward Benguela Coastal Current (BCC) (Koseki et al., 2019). Due to the strong meridional sea surface temperature (SST) gradient in the ABF, its migration to the north and south is decisive for SST changes off Angola, and plays a major role in determining seasonal and interannual SST variability in the region (Lübbecke et al., 2010).

The source of riverine freshwater input in the SETA involves the outflow of three southwestern African coastal rivers (Fig. 3.1): the Congo River, with its mouth at 12.4ºE, 6.0ºS; the Cuanza River at 13.2ºE, 9.3ºS; and the Kunene River at 11.8ºE, 17.3ºS. The major input comes by far from the Congo River, which is the second largest river system in the world and has a mean flow rate of about 40.000 m^3s^{-1} (Dai and Trenberth, 2002; Campbell, 2005). The Congo River discharge (CRD) peaks during November-January, has a secondary maximum in April-May, and minima during March and August (Fig. 3.7). The discharge seasonality is governed by the precipitation over the Congo River basin which is mainly related to the movement of the

Intertropical Convergence Zone (ITCZ) (Sorí et al., 2017; Munzimi et al., 2019). The CRD is the greatest contributor to the sea surface salinity (SSS) mean state and variability in the eastern Tropical Atlantic (Martins and Stammer, 2022; Chao et al., 2015; Denamiel et al., 2013; Hopkins et al., 2013; Materia et al., 2012). Recently, both the CRD and the SSS in the area were linked to the occurrence of the Indian Ocean Dipole (IOD) with positive IOD events leading to increased moisture convergence over the Congo basin and subsequently enhanced CRD (Jarugula and McPhaden, 2023; McPhaden et al., 2024). The Congo River plume and the low SSS signal spread usually westward, driven mainly by zonal advection (Houndegnonto et al., 2021; Martins and Stammer, 2022). From February to April, however, the plume reaches its seasonal southernmost extension up to 12ºS, controlled by the meridional advection of the Angola Current (Kopte et al., 2017; Awo et al., 2022; Martins and Stammer, 2022). In some specific years, the low SSS signal can reach as far south as 18ºS (Aroucha et al., 2024; McPhaden et al., 2024; Gammelsrød et al., 1998).

River related low SSS has been associated with increased SST in the Eastern Tropical Atlantic. Materia et al. (2012) used observations to correlate freshwater discharge and SST increase in the Gulf of Guinea via mixed layer shoaling, while Martins and Stammer (2022) showed that the low SSS waters associated with CRD strongly increase stratification in the region. Moreover, it has been recently shown that freshwater input also contributes to boosting strong anomalously warm coastal events off the Angola coast, the so-called Benguela Niños (Shannon et al., 1986; Florenchie et al., 2004), via reduced turbulent heat loss due to increased stratification (Lübbecke et al., 2019; Aroucha et al., 2024). The intensification of these extreme coastal events through the CRD is also linked to the occurrence of IOD events (McPhaden et al., 2024). One of the main conditions for the low SSS influence on these events is that the freshwater plume from the CRD is advected to the Angolan-Namibian coasts, much further south than climatologically expected (Awo et al., 2022). These studies are based on the mechanism of the low salinity shoaling the mixed layer, which generates barrier layers between the density-stratified mixed layer and the temperature-stratified isothermal layer. The barrier layer presence weakens the vertical temperature gradient between the fresh mixed layer and the waters below it, reducing the impact of vertical mixing and turbulent heat loss, which then contributes to increasing SSTs.

On the other hand, the modelling study by White and Toumi (2014) did not find a substantial influence of the barrier layer generation on increasing the SST mean state off the Congo River mouth. By using different simulations with and without the river presence, the authors showed that although the CRD generates barrier layers up to 6m thick, the shoaling of the mixed layer is such that the penetration of the solar shortwave radiation is not trapped within this layer. Hence, the cooling effect from the reduced shortwave absorption exceeds the warming impact of the reduced vertical mixing (White and Toumi, 2014). However, their simulations showed a significant coastal warming impact from the CRD south of the river mouth (Fig. 5 in White and Toumi, 2014). At the same time, model simulations have shown that freshwater input and variability can indeed increase the mean state SST in other tropical regions. Zhang and Busalacchi (2009) pointed to the increase of positive SST anomalies due to amplified freshwater fluxes in the Tropical Pacific, while Topé et al. (2023) showed a similar effect in the Gulf of Guinea due to the presence of the Niger River. It has been demonstrated that the Niger River creates an additional onshore geostrophic flow in the Gulf of

Guinea to the west of the river mouth. However, changes in upwelling due to the Niger presence were not significant since the river-induced reduced MLD compensated for this onshore flow intensification (Alory et al., 2021). Additionally, recent climate projections have identified changes in the onshore geostrophic flow as a key factor controlling long-term trends in eastern boundary upwelling systems (Jing et al., 2023), highlighting the potential influence of the CRD on the future dynamics of the SETA upwelling system.

Overall, it is clear that river plumes affect not only the SST mean state but also its variability in tropical regions. For the SETA, specifically, they can amplify extreme warm events, impacting fisheries, marine ecosystems, and the socio-economics of African countries. Hence, it is crucial to better recognize the mechanisms by which freshwater input influences SST changes. This comprehension becomes even more important in view of future warming scenarios, which show amplified river runoff around the world (Müller et al., 2024; Aloysius and Saiers, 2017). In the present study, we aim to understand the impact of the freshwater input especially on the mean state SST, focusing on the SETA region. For this, we use three sensitive experiments from a nested ocean general circulation model: a control experiment with an interannual varying freshwater discharge from land to ocean (CTRL); a sensitivity experiment with a climatological freshwater runoff (CLIMA); and one with no runoff at all (NORIV). More details are given in Sect. 3.3.

This paper is organized as follows: in Sect. 3.3 we present the model configuration, the experiments, the datasets, and the methods for upwelling indices, advection term, and barrier layer calculation; in Sect. 3.4 we compare the model output against observational datasets, describe the differences between the experiments and the mechanisms responsible for these differences; in Sect. 3.5 we discuss our main findings and present concluding remarks.

3.3 Model, datasets and methods

3.3.1 INALT20

In this study we used the INALT20 model configuration (Schwarzkopf et al., 2019), which is based on the Nucleus for European Modelling of the Ocean (NEMO) v3.6 ocean general circulation model (Madec and the NEMO team, 2016). It consists of a high-resolution (1/20º) nest covering the South Atlantic and the West Indian oceans (70ºW – 70ºE, 63ºS – 10ºN, Fig. 2 in Schwarzkopf et al., 2019), embedded into the coarser resolution (1/4º) global host grid ORCA025 via a two-way nesting approach, allowing the host to provide boundary conditions to the nest as well as receiving information from the nest. INALT20 has a vertical grid consisting of 46 z-levels, with 6 m resolution near the surface and 14 levels in the upper 200 m. Although the uppermost level represents a 6 m thick layer with horizontal velocities, temperature and salinity defined at its centre (~3 m depth), we consider those as surface values. More details on INALT20 can be found in Schwarzkopf et al. (2019). The model is forced at the surface with momentum, heat and freshwater fluxes from the atmospheric product JRA55-do (Tsujino et al., 2018). It has been recently shown that the use of JRA55-do as the forcing product performs better in the Benguela upwelling region in comparison to other datasets (Small et al., 2024).

3.3.2 Model experiments

The study is based on three simulations that only differ in their prescribed river runoff. In the reference (control) simulation (CTRL) an interannually varying daily runoff forcing from JRA55-do (Tsujino et al., 2018) is applied. This simulation has been previously used and described also by Schmidt et al. (2021), Biastoch et al. (2021) (therein referred to as INALT20-JRA-long), and Rühs et al. (2022) (SIM_{JRA}). The sensitivity experiment CLIMA is forced with a monthly climatology of the years 2000 to 2019 built from the JRA55-do runoff. In the second sensitivity experiment (NORIV) no runoff forcing was applied. For CLIMA and CTRL, vertical mixing is enhanced where runoff enters the ocean. The hindcast simulation from 1958 to 2019 (CTRL) is preceded by a 30-year long spin-up integration initialized with temperature and salinity data from the World Ocean Atlas (WOA) (Huang et al., 2021; Levitus et al., 1998). CLIMA and NORIV branch off from CTRL in 2000, spanning from the period 2000-2018. We analyze 5 day-averaged output data, except for sea surface height (SSH) and freshwater runoff, for which daily outputs are used. Modelled SSH fields are detrended by removing the global average at each location and time slice.

3.3.3 Observational and reanalysis datasets

To assess the model performance in representing the mean state and variability of key variables, we compared CTRL outputs against a variety of datasets ranging from satellite and reanalysis products to in situ measurements. The datasets are described below. We used monthly averages of all these products for the time period from 2000-2018 to have a consistent comparison with the corresponding model output. Exceptions are mentioned below. Finally, all gridded datasets were interpolated onto the INALT20 1/20º spatial grid. Interannual variability is calculated as the monthly standard deviation of the variable anomalies.

A blend of satellite and in situ measurements of SST was obtained from the high-resolution National Oceanic and Atmospheric Administration (NOAA) Optimum Interpolation SST (OISST) (Huang et al., 2021; Reynolds et al., 2007). The data has ¼º spatial resolution and is available from 1981 to the present day at the National Center for Environmental Information.

For salinity, we took SSS v03.21 measurements from the European Space Agency Sea Surface Salinity Climate Change Initiative (ESACCI) (Boutin et al., 2021). It consists of composites of bias-corrected SSS from the satellite missions Soil Moisture and Ocean Salinity (SMOS, 2010-2019), NASA Aquarius (2012-2015), and Soil Moisture Active Passive (SMAP, 2015-present), with the data available from 2010 to 2018.

SST and SSS as well as zonal and meridional ocean velocities were obtained also from the GLORYS12 reanalysis product (Lellouche et al., 2021). It is based on the NEMO with atmospheric forcing by ERA-Interim and ERA5 with assimilated in situ profiles of temperature and salinity from the CORAv4.1 database. It has a 1/12º horizontal resolution and 50 vertical levels and covers the period from 1993 to the present. The product is distributed by the EU Copernicus Marine Service (CMEMS). Although GLORYS12 is forced by climatological river runoff, it has shown good performance in the SETA region in reproducing the temperature and salinity mean state and variability both at the surface and at depth (Aroucha et al., 2024).

To validate the freshwater input data from the model, we use CRD data at Kinshasha-Brazzaville Station, Republic of Congo from the ORE-HYBAM observatory. Daily values are available from 1947 to 2023.

Finally, we used current velocity measurements from 45m to 500m depth from a moored ADCP off Angola at 13ºE, 10º50'S, 77 km away from the coast (Kopte et al., 2017). The data is available from 2014 to 2021. Alongshore and cross-shore velocities were derived by rotating 34º anticlockwise from the north. To complement the mooring measurements at the surface, we obtained monthly total current velocities from the GLOBCURRENT dataset (Rio et al., 2014), which consists of zonal and meridional velocities at the surface and 15m depth from combined CMEMS satellite geostrophic currents and modelled Ekman currents. This dataset is available at 0.25º resolution from 1993-2022, and is also distributed by the CMEMS.

3.3.4 Mixed layer depth, isothermal layer depth, and barrier layer thickness definitions

The isothermal layer depth (ILD) is here defined by a 0.2ºC threshold referenced to the temperature value at 3m depth (first vertical level of the model), T_{3m}, while the mixed layer depth (MLD) is the depth at where the potential density (σ_0) referenced to its value at 3 m depth (σ_{3m}), is increased by an amount equivalent to a 0.2ºC temperature change at the local salinity ($\Delta\sigma_0$), as follows:

$$ILD = depth\ where\ [T = T_{3m} - 0.2ºC] \quad (3.1)$$

$$MLD = depth\ where\ [\sigma_0 = \sigma_{3m} + \Delta\sigma_0] \quad (3.2)$$

$$\Delta\sigma_0 = \sigma_0(T_{3m} - 0.2ºC, S_{3m}, P_0) - \sigma_0(T_{3m}, S_{3m}, P_0) \quad (3.3)$$

where S_{3m} and P_0 are salinity and pressure at 3m depth and the ocean surface, respectively. The barrier layer thickness (BLT) is the difference between the ILD and MLD: $BLT = ILD - MLD$. These fields were calculated based on 5-day-averaged temperature and salinity vertical profiles, and these definitions, which ensure that salinity changes at the surface are particularly considered for shoaling the mixed layer and generating barrier layers, have been extensively used during the last years (e.g. Aroucha et al., 2024; Gévaudan et al., 2021; Saha et al., 2021). In addition, the squared Brunt-Väisälä frequency (N^2) fields were obtained by averaging from surface to 50m depth the N^2 at each depth level calculated from the monthly temperature and salinity vertical profiles, since the MLD in this region is usually shallower than 50m (Körner et al., 2023; Aroucha et al., 2024).

3.3.5 Horizontal advection

To investigate whether SST differences between the simulations stem from changes in surface dynamics and consequently surface advection, we calculated the surface horizontal advection as:

$$Adv = -\boldsymbol{v} \cdot \nabla T \quad (3.4)$$

where $\boldsymbol{v}$ and ∇T are the 5-day-averaged surface horizontal current vector and temperature gradient, respectively. Advection was calculated individually for each experiment, where $\boldsymbol{v}$ and ∇T were both taken from the same experiment (e.g. $Adv_{CLIMA} = -\boldsymbol{v}_{CLIMA} \cdot \nabla T_{CLIMA}$). Values within 20km off the coast were neglected due to the large calculation errors close to the coast.

3.3.6 Upwelling indices

Following Alory et al. (2021) and Marchesiello and Estrade (2010), we define dynamical upwelling indices to evaluate the freshwater input impact on the competing effects of geostrophic flow and Ekman transport on coastal upwelling. The effect of convergence/divergence of the geostrophic flow at the coast on vertical velocities is described by the Geostrophic Coastal Upwelling Index (GCUI):

$$GCUI = \frac{-u_G \cdot MLD}{2L_u} \quad (3.5)$$

where L_u represents the cross-shore width where upwelling occurs, here defined as 50km (see Fig. 3.5), u_G is the cross-shore surface geostrophic current (defined below) averaged within the L_u and MLD is the mixed layer depth. Defining L_u as 50km fits to the width of the minimum cross-shore temperature gradient in this area, which is located at the shelf break (Körner et al., 2023), and is close to the Rossby radius of deformation in the region (Chelton et al., 1998).

The Ekman Coastal Upwelling Index (ECUI) is a function of L_u, the alongshore wind stress, τ_a, averaged within L_u, the water density, ρ, and the Coriolis parameter, f, and is defined as follows:

$$ECUI = \frac{-\tau_a}{\rho f L_u} \quad (3.6)$$

The ECUI represents the vertical velocities due to the convergence/divergence of the Ekman transport at the coast. Positive (negative) values of both GCUI and ECUI represent upward (downward) vertical velocities, indicating upwelling (downwelling). The total upwelling is represented by the sum of both indices.

The surface cross-shore (u_G) and alongshore (v_G) geostrophic currents were calculated from the sea surface height (SSH) fields based on the following equations:

$$v_G = \frac{g}{f} \frac{\partial SSH}{\partial x} \quad (3.7)$$

$$u_G = -\frac{g}{f} \frac{\partial SSH}{\partial y} \quad (3.8)$$

where g is the gravitational acceleration, here taken as 9.8 m/s^2 and f is the Coriolis parameter. Both the geostrophic currents and the upwelling indices were calculated based on 5-day data averages and by considering the alongshore wind stress, SSH, MLD and ρ individually for each model experiment.

3.4 Results

3.4.1 Model validation

Figure 3.1a shows the CTRL mean SST for 2000-2018 in the SETA compared to the mean SST for the same period for both OISST and GLORYS12. Overall, the SST spatial mean state from CTRL compares well to the mean SST of both products (Fig. 3.1a), although CTRL overestimates the SST in almost the whole SETA (Fig. 3.1b and 3.1c). The highest and most considerable biases are within the ABF and the coastal upwelling regions (i.e. from 15ºS to 30ºS). In CTRL, the ABF is located too far south, creating a warm bias at 17ºS – 18ºS of around 2.5ºC and 2.0ºC compared to OISST (Fig. 3.1b) and GLORYS12 (Fig. 3.1c), respectively. In the Benguela upwelling region (~19ºS – 30ºS), the coastal warm biases to both products are of similar spatial pattern and magnitude.

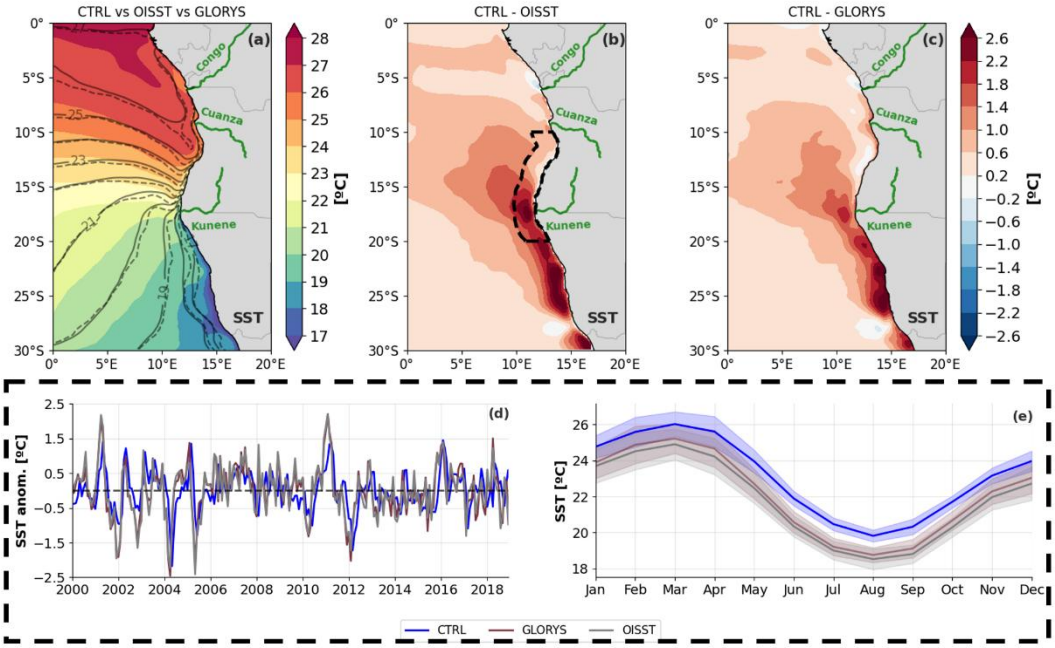

Figure 3.1. Comparison of simulated SST against observations and reanalysis. (a) Mean SST from CTRL (shading), OISST (solid contours), and GLORYS (dashed contours) averaged from 2000-2018. Contour interval is 1 ºC. (b) Difference between CTRL and OISST mean SST. Black dashed contour indicates coastal Angola-Benguela area (CABA, 10ºS–20ºS, 200km away from coast). (c) Difference between CTRL and GLORYS mean SST. (d) SST anomalies averaged for CABA shown for CTRL, in blue, and datasets (GLORYS in brown and OISST in grey). (e) Same as (d) but for the monthly climatologies. Shadings indicate monthly standard deviations.

In the coastal Angola-Benguela area (CABA;10ºS–20ºS, 200km away from coast), CTRL depicts well the SST anomalies as presented by the satellite and the reanalysis product (Fig. 3.1d), although they are underestimated in specific years – especially during Benguela Niño events (e.g. 2001 and 2011). In fact, the SST variability from CTRL is lower within the whole SETA region (Fig. 3.10a-c) relative to both products, mainly in the CABA and ABF regions. The highest SST variability in the model simulation is restricted to a thin coastal band, while the OISST and GLORYS12 highest variabilities are observed from 8ºE to the coast (Fig. 3.10a-c). Regarding the SST seasonality, CTRL nicely agrees with both OISST and GLORYS12 products (Fig. 3.1e). As previously mentioned, a warm bias is indeed present in the CABA, being stronger when compared to the satellite product than the reanalysis. It is noteworthy that for both CABA SST interannual variability and seasonality, there is no substantial difference between CTRL and CLIMA (blue

lines mostly overlap green lines in Fig. 3.8a-b). The reasons for this will be further discussed. However, in the seasonal climatologies, a constant offset of ~0.3ºC is observed between the simulations with (CTRL and CLIMA) and without freshwater input (NORIV) at the coastal Angola-Benguela region (Fig. 3.8b), already indicating that this input could create an SST mean state difference.

For the model validation with respect to SSS (Fig. 3.2) we focus on two different regions: the previously cited CABA region (where the highest SST variability is present in the SETA, i.e. the region where Benguela Niños occur); and the Congo River mouth area (CRMA, solid black contour in Fig. 3.2b, 2ºS–10ºS, 200km away from coast), which represents the area of major freshwater input to the SETA. Overall, the SSS mean state from CTRL compares well against both ESACCI and GLORYS12 products with the lowest salinity values present within the CRMA, as a response to the CRD. However, there are SSS biases when comparing CTRL to both products. North of 10ºS and compared to ESACCI, CTRL slightly overestimates the offshore SSS up to ~5ºS, while close to the coast it presents salinity values more than 1.0 lower than observed with satellites (Fig. 3.2b). North of 5ºS CTRL presents a fresh bias in relation to ESACCI, both at the coast and offshore (Fig. 3.2b). The fresh bias at the coast of CTRL compared to ESACCI occurs especially from October to May (Fig. 3.2g). On the other hand, when comparing the simulated SSS north of 10ºS to the GLORYS12 product, the model simulation shows mean coastal SSS values exceeding those of the reanalysis product by more than 1.5, while there is a fresh bias west of 12ºE (Fig. 3.2c). At the coast, CTRL presents higher SSS values than GLORYS12 mainly from June to September (Fig. 3.2g). Besides the observed differences, the SSS seasonal cycles at the CRMA are similar within the three products with the lowest (highest) salinity values coinciding with the season of highest (lowest) CRD – i.e. austral summer (winter) (Fig. 3.2g).

Regarding the CABA region, both ESACCI and GLORYS12 present similar SSS mean values and spatial patterns. When comparing these products to CTRL, we see a salty bias ranging from 0.1 to 0.7 from 10ºS extending further south (Fig. 3.2b, c). It is an indication that the CRD freshwater influence on the SSS in CTRL is restricted to further north than what is observed in satellite and reanalysis products. The difference is even higher from September to November (Fig. 3.2e). As a consequence, the CTRL output presents a higher (lower) SSS variability north (south) of 10ºS in comparison to both products (Fig. 3.10d-f). The CTRL SSS variability is especially weaker in the CABA (Fig. 3.2d and Fig. 3.10d-f) when compared to both reanalysis and satellite, which could partly explain the same area of weaker CTRL SST variability in comparison to the standard deviations of OISST and GLORYS SST's (Fig. 3.10a-c), since SSS has been shown to influence extreme warm events in the CABA (Lübbecke et al., 2019; Aroucha et al., 2024). Finally, it is important to highlight that CTRL and CLIMA, similarly to what was observed for SST, show very similar SSS anomalies and seasonal climatologies, especially in the CABA (Fig.3.9a-d, blue and green lines overlapping).

In terms of freshwater input, it is central to bear in mind that the model freshwater input considers not just the freshwater from the Congo River, but all freshwater input from land to the ocean, given by JRA55-do. To check how much of this input can be attributed to the CRD, we averaged the CTRL freshwater input for a coastal box at the Congo mouth and compared it to the discharge at the Kinshasha-Brazzaville station, which represents 98% of the total CRD (Alsdorf et al., 2016) (Fig. 3.7). In terms of magnitude, the seasonality

of both freshwater inputs is similar (Fig. 3.7e). The seasonal climatology of the CTRL input compares well with the in situ station especially from December to April, while from June to October it shows lower freshwater input into the ocean (Fig. 3.7e). Although the seasonality is well represented by CTRL, the interannual variability of the freshwater input is not as highly correlated to the Kinshasha-Brazzaville station (i.e. r = 0.46; Fig. 3.7d). Similar discrepancies were observed in the study by Chandanpurkar et al. (2022).

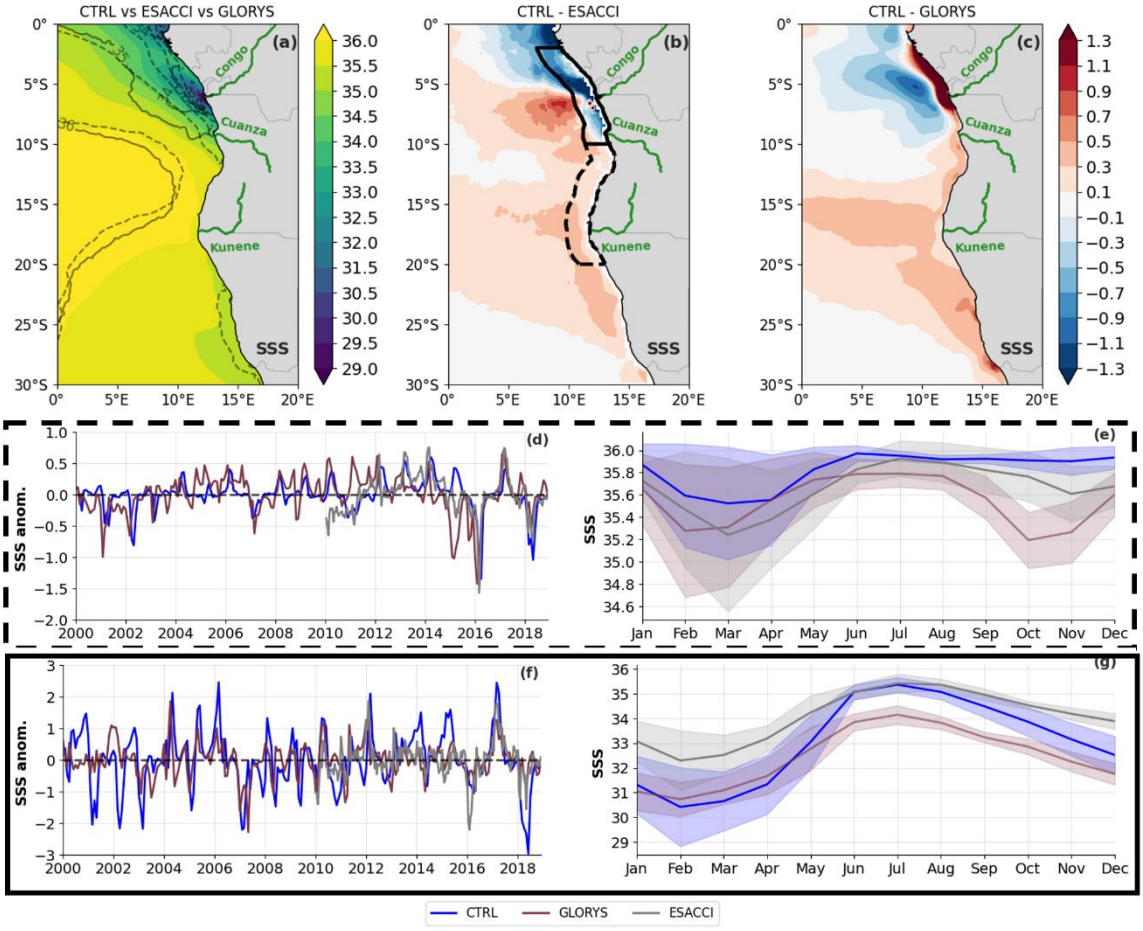

Figure 3.2. Comparison of simulated SSS against observations and reanalysis. (a) Mean SSS from CTRL (shading), ESACCI (solid contours), and GLORYS (dashed contours; contour interval is 1). Both CTRL and GLORYS averaged from 2000-2018, while ESACCI averaged from 2010-2018. (b) Difference between CTRL and ESACCI mean SSS from 2010-2018. Black dashed contour indicates coastal Angola-Benguela area (CABA, 10ºS – 20ºS, 200km away from coast). Black solid contour shows Congo River Mouth area (CRMA, 2ºS-10ºS, 200km away from coast). (c) Difference CTRL and GLORYS mean SSS from 2000-2018. (d) SSS anomalies averaged for CABA for the CTRL, in blue, and datasets (GLORYS in brown and ESACCI in grey). (e) Same as (d) but for the seasonal climatologies. Shadings indicate monthly standard deviations. (f) and (g) same as (d) and (e) but for CRMA.

Furthermore, the alongshore and cross-shore current velocities from CTRL were checked against the 11ºS mooring measurements taken in the CABA (Fig. 3.11). The mooring velocities were complemented at the surface with data from GLOBCURRENT (see Sect. 3.3.3). In general, the Angola Current is underestimated by CTRL throughout the year, especially from January to May (Angola Current core located around 30-70 m depth) (Fig. 3.11b, d). Further, the model presents a much stronger northward surface coastal jet than what is observed at the mooring position. Since advection plays a major role in the SSS distribution in the region, it is likely that a stronger (weaker) than observed northward (southward) current traps the low SSS further north in CTRL. This would explain the increased (reduced) SSS variability north (south) of 10ºS previously identified (Fig. 3.10d-f). It would also mean that the freshwater transport to south of 12ºS is nearly

absent in the model experiments. Still, at the surface, CTRL seems to well represent the seasonality of the GLOBCURRENT velocities at the mooring position, with a stronger southward (northward) current from January to February (March to August) and September to October (November to December) (Fig. 3.11b,d).

Overall, we believe that CTRL represents the major aspects of the mean state and seasonality of the variables discussed here. Moreover, the initial analysis of NORIV already points out the impact of freshwater input on both SST and SSS. Still, it seems that in the simulations no significant differences result from interannual vs. climatological land to ocean discharges, indicating an insignificant impact of the interannual freshwater input variability on the variables analyzed here. In the following, we will analyze the differences between the three experiments.

3.4.2 Impacts of freshwater input

3.4.2.1 Differences between the experiments

To understand whether the freshwater input into the ocean impacts the SST near the southwestern African coast, we first look at the mean SST differences between the three experiments (Fig. 3.12). The freshwater presence significantly affects the SST mean state in the coastal SETA region, regardless of using an interannual (CTRL) or climatological (CLIMA) runoff (Figs. 3.12a, b); similar SST differences between these two experiments with discharge and the one without (NORIV) are observed not only in terms of the spatial pattern but also in the magnitude of those differences. At the same time, no significant mean SST difference was observed between CTRL and CLIMA experiments (Fig. 3.12c), as also seen in Fig. 3.8a-b. Additionally, CTRL and CLIMA did not significantly differ in the mean SSS fields (Fig. 3.12f). Regarding SST variability, our experiments show no significant influence of freshwater input on monthly standard deviations of SST anomalies (Fig. 3.13). We thus conclude that the presence of a land to ocean discharge alone generates the observed SST differences, with no further impact of an interannual varying discharge. Hence, in the following, we will focus on the effects of the climatological freshwater runoff presence on the SST mean state in the SETA.

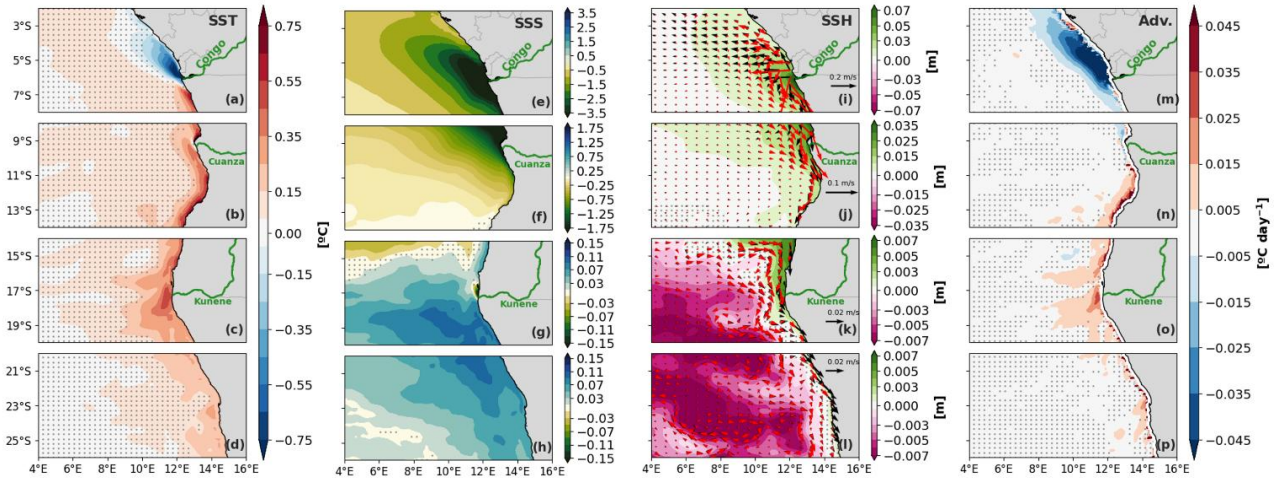

Figure 3.3. Differences between CLIMA and NORIV mean states (CLIMA-NORIV) for SST (a-d); SSS(e-h); SSH(i-l); Horizontal Advection (m-p). Stippled grey areas indicate where the difference is not significant in a 95% confidence level. Black (red) arrows from i-l depicts total (geostrophic) currents difference between experiments. Note that colorscales change for individual subplots for SSS and SSH.

Figure 3.3 depicts the mean state difference between CLIMA and NORIV for SST, SSS, SSH, ocean currents, and horizontal advection (Adv). The freshwater input significantly warms the southwestern Africa coastal fringe, south of the Congo River mouth. By including the discharge, the mean SST is increased by up to 0.9 ºC near the coast at about 13ºS, and 0.26 ºC on average in the CABA (Fig.3.3a-d). With freshwater input, strong warming is also observed at the Kunene River mouth (Fig. 3.3c). This pattern of positive SST differences is observed along the whole coast, from the Congo River mouth at ~6ºS extending to ~28ºS. Concomitantly, freshwater discharge generates a significant cooling north of the Congo River (i.e. decrease in SST of up to -1.9ºC at 6ºS), with a maximum of negative SST difference from ~6ºS to ~4ºS (Fig. 3.3a).

In order to understand this difference in SST, we investigate the dynamic effects of the river presence. A land to ocean discharge significantly reduces the SSS in the whole SETA up to ~15ºS (Fig. 3.3e-g). The magnitude of freshening is stronger at the Congo's mouth where differences reach -6 and decreases towards the south (note that colorscale limits change from Fig. 3.3e to Fig. 3.3g). Although different rivers flow into the Atlantic at the southwestern African coast, the discharge rate from the Congo River is by far the largest and completely dominates the SSS differences observed between the model simulations. Still, a lower magnitude SSS reduction is also observed at the Kunene River mouth (Fig.3.3g). The mean low SSS plume from the Congo River spreads towards the west-northwest, consistent with the main direction of the CRD dispersion shown in previous studies (Houndegnonto et al., 2021; Awo et al., 2022; Martins and Stammer, 2022). From 17ºS to the south, however, an overall increase in SSS is noted when including the discharge in the experiments. Even though the magnitude of the SSS increase is only ~5% of the SSS decrease further north, it is still significant (Fig. 3.3g-h). An SSS decrease due to the freshwater presence is accompanied by a similar pattern of increasing SSH (Fig. 3.3i-l). This inverse relation is a consequence of the halosteric effect in the water volume, i.e. an expansion (contraction) of a water volume via the density reduction (increase) owing to the lower (higher) salinities. The SSH increase patterns in the SETA coincide not only with the strong changes in SSS due to the CRD, but also with the regions at the coast, where the model's freshwater input into the ocean takes place (Fig. 3.7). Differences in SSH reach up to 7cm at the Congo's mouth (i.e. ~6ºS, Fig. 3.3i), and are ~10 times smaller at Kunene River mouth, although still significant (Fig. 3.3k).

As a consequence of the changes in SSH, the freshwater input changes the dynamics of the coastal SETA. The red (black) arrows depicted in Fig. 3.3i-l represent the difference between CLIMA and NORIV in the geostrophic (total) currents. By including the land to ocean discharge, a strong coastal southward jet is generated at the southwestern African coast from south of 6ºS. This current is mainly geostrophic and follows the SSH gradients to ~17ºS. South of this latitude the ageostrophic component is stronger, but geostrophy still seems to play a role in the southward current (Fig. 3.3l). In contrast, north of the Congo's mouth we observe a northwestward geostrophic current, also following the northernmost extension of the high SSH dome generated by the low SSS plume (Fig. 3.3i), flowing parallel to the coastline. Acting on the strong mean state meridional temperature gradient present in the region (Fig. 3.1a), these shifts in the surface coastal currents lead to changes in horizontal temperature advection. The differences in horizontal temperature advection (Fig. 3.3m-p) closely resemble those in SST (Fig. 3.3a-d). Except for the coastal stripe from 6ºS to 11ºS, freshwater-induced horizontal advection appears to be responsible for the increased coastal SST in CLIMA. The relative

effects of changes in surface currents and in the surface horizontal temperature gradients present in the area (Fig. 3.1a) will be investigated further in the next section.

Finally, by calculating the BLT and the squared Brunt-Väisälä frequency, N^2, we also assess the freshwater input impacts on the mean stratification and stability of the water column. BLT and N^2 differences among the experiments (Fig. 3.14) show extremely similar patterns to the ones observed in SSS (Fig. 3.3e-h), with a significant negative (positive) SSS difference implying a significant positive (negative) difference in both BLT and N^2 averaged from surface to 50m. It represents an increase in the water column stratification and a generation of barrier layers at the Congo plume via freshwater discharge in the SETA. As well as at the Congo River plume, a similar response to the freshening is observed at Kunene River mouth, but with smaller magnitude (i.e. BLT larger than 8m at 6ºS, and ~3m at 17ºS). Further, the barrier layer induced by a freshwater input does not fully correspond with the region of increased SST. It is expected that a combination of stronger stratification with a weaker vertical temperature gradient within the BLs could isolate the surface from the deeper water column layers, reducing the mixing and contributing to an SST increase. However, it has been shown that this might not always be the case in the SETA due to the counteracting effect of solar radiation penetrating through the very shallow mixed layer (White and Toumi, 2014). However, at the Kunene River mouth the pattern of lower SSS and thick barrier layer seems to boost the SST differences, creating an area of higher SST differences at 17ºS (Fig. 3.3c).

Overall, we find that including a freshwater discharge in the experiments leads to significant changes in the dynamic and thermodynamic mean state of the SETA. These effects are characterized by the CRD freshwater input reducing the SSS, followed by a halosteric increase in SSH, thereby generating poleward coastal currents south of the river mouth, and equatorward coastal currents north of it; advecting warmer waters to further south and cooler waters to the north of the Congo's mouth. Although the observed differences south of the area of the major Congo influence (i.e. south of 13ºS) are small when compared to the river's mouth region (i.e. ~6ºS), they are still significant. Albeit small, the change in the 2000-2018 mean state indicates that the effects presented above are constantly and continuously present. In fact, the isotherms' outcropping latitudes are shifted towards the south in CLIMA compared to NORIV (Fig. 3.14) as a consequence of this mean state change. Likely due to the constant southward coastal jet, the presence of a freshwater discharge moves the isotherm's position further south. Therefore, the position of the ABF, a front of strong temperature gradient, is also pushed towards the south in the experiment with the freshwater input present. This shift in the ABF location might have substantial impacts on the environmental conditions around this region, which will be further discussed in Sect. 3.5. In the following section, we detail the warming from advection in the CABA.

3.4.2.2 Advection warming the coastal Angola-Benguela area

In this section, we disentangle the cascade of events described in Sect. 3.4.2.1 by showing the role of the freshwater-induced dynamical change in increasing the SST at the southwestern African coast. Figure 3.4 statistically shows the SSH response to the SSS change, the horizontal advection response to the SSH change, and the SST response to the advection change, from the CRMA region to the CABA. Each point corresponds

to one of the 228 analyzed months, indicating significant correlations throughout the year, and representing mean state permanent responses.

The difference in SSH in the CRMA is strongly and inversely correlated to the SSS change in the same region ($r = -0.82$, $p < 0.05$, Fig. 3.4a), highlighting the crucial role of the halosteric effect in increasing the SSH at the Congo's mouth. At the same time, a positive and significant correlation is observed between a CRMA SSH change and the horizontal advection in the CABA (Fig. 3.4b). A 5cm increase in SSH implies a ~6 W/m^2 increase in horizontal temperature advection in the CABA. Finally, differences in both horizontal temperature advection and SST in the SETA coastal area are also positively and significantly correlated (Fig. 3.4c), indicating that the stronger advection in CLIMA leads to increased SST compared to NORIV.

To investigate if the causes of the horizontal temperature advection differences observed between the model experiments stem from changes in the surface currents or from shifts in the horizontal temperature gradients, we calculated the terms by only varying one of these parameters, and then compared the results. Figure 3.15a depicts total horizontal temperature advection differences [$(-\boldsymbol{v}_{CLIMA} \cdot \nabla T_{CLIMA})$ - $(-\boldsymbol{v}_{NORIV} \cdot \nabla T_{NORIV})$], similar to Fig. 3.3m-p; Fig. 3.15b shows the effect by only changing the temperature gradient (i.e. [$(-\boldsymbol{v}_{NORIV} \cdot \nabla T_{CLIMA})$ - $(-\boldsymbol{v}_{NORIV} \cdot \nabla T_{NORIV})$]); and Fig. 3.15c displays the influence related to changes only in the horizontal velocity (i.e. [$(-\boldsymbol{v}_{CLIMA} \cdot \nabla T_{NORIV})$ - $(-\boldsymbol{v}_{NORIV} \cdot \nabla T_{NORIV})$]). From Fig 3.15 we can see that by changing only the horizontal velocity in the calculation (Fig. 3.15c), we generate a spatial pattern and magnitude that mostly resembles the total advection difference (Fig. 3.15a). The dynamical effect on the advection term generates a similar warming (cooling) signal by the freshwater presence south (north) of the Congo's mouth (i.e. ~6ºS). The difference pattern resulting from only changing the current also depicts a stronger advection extending to ~28ºS, even though the mean state current change at this location is considerably weaker than the strength of this shift at around 6ºS (Fig. 3.3i). The maximum positive difference in Fig. 3.15c is located in the ABF region (i.e. 15ºS – 18ºS), supporting the argument that the stronger southward current created by the freshwater input from land pushes the ABF further to the south (Fig. 3.14).

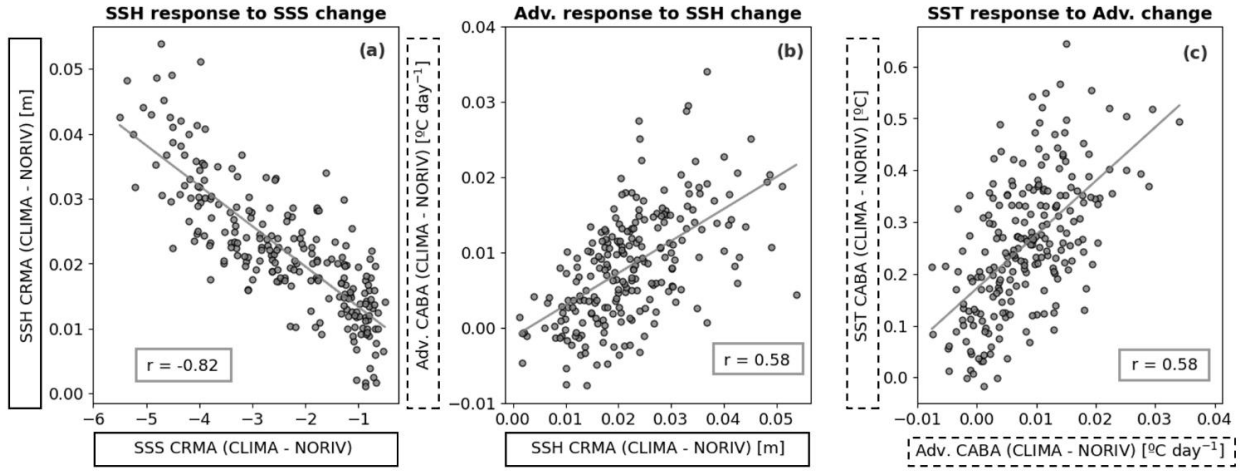

Figure 3.4. Ocean response to land to ocean discharge. (a) Linear regression of monthly SSS differences upon monthly SSH differences (CLIMA – NORIV) averaged for CRMA. (b) Linear regression of monthly SSH differences upon monthly advection differences (CLIMA – NORIV) averaged for CRMA and CABA, respectively. (c) Linear regression of monthly advection differences upon monthly SST differences (CLIMA – NORIV) averaged for CABA area. CRMA and CABA are defined in Fig. 3.2.

Finally, it is likely that, by changing the geostrophic dynamics at the southwestern African coast, a freshwater discharge can shift the surface waters distribution in the SETA. For instance, an increased southward transport in the CLIMA experiment implies that warmer and saltier tropical waters push cooler and fresher subtropical waters to further south with the freshwater input. This can be seen not only by the isotherm's outcropping position southward shift in Fig. 3.14 but also by the increase in SSS south of 17ºS (i.e. a region which is usually not reached by Congo River waters) (Fig. 3.3). Indeed, both temperature and salinity horizontal gradients present in the SETA (see Figs. 3.1a and 3.2a) are important to these southward shifts, however, the strongest differences between the experiments are only significant due to a dynamical change in the surface geostrophic currents. Besides the advective effects in the CABA, it is still unclear, however, from which mechanisms the freshwater input can generate the coastal warming from 6ºS to 11ºS. In addition, we wonder whether a shift in the surface geostrophic currents might also impact the local geostrophic upwelling. In Sect. 3.4.2.3 we attempt to answer these questions.

3.4.2.3 Changes in upwelling

In the previous sections, we have shown that the presence of a land to ocean freshwater discharge leads to an intensification of the surface geostrophic currents in the SETA dominantly in alongshore direction, especially close to the Congo River mouth. The strengthening of the geostrophic dynamics in this region by the freshwater input generates also cross-shore currents. Offshore geostrophic flows (Fig. 3.3i,j) favor coastal upwelling while onshore flows are related to downwelling. In fact, it has been recently shown that an additional onshore geostrophic flow is generated by the Niger River presence in the Gulf of Guinea to the west of the river mouth, even though no significant impact on upwelling was attributed to this onshore geostrophic flow (Alory et al., 2021). To investigate if this is also the case along the southwestern African coast, we calculate dynamical upwelling indices for the CLIMA and NORIV experiments.

Figure 3.5 shows the mean state differences between CLIMA and NORIV in the calculated upwelling indices. No changes between the experiments were found for ECUIs (Fig. 3.5b, green lines) along the southwestern African coast. This result was expected since both experiments are based on an ocean-only model with the same atmospheric wind forcing. Overall, the ECUI dominates the total upwelling intensity along the southwestern African coast, especially in the Benguela Upwelling system, south of 17ºS (Fig. 3.5b). In this area, the GCUI is much weaker and close to zero from ~28ºS to 23ºS. It is widely known that wind-driven upwelling dominates this eastern boundary system (e.g. Bordbar et al., 2021; Brandt et al., 2024; Fennel, 1999). North of 17ºS, ECUI still dominates but to a lesser extent. An onshore geostrophic flow counteracts the wind-driven upwelling from 17ºS to 6ºS (i.e. negative values for GCUI). It has been recently shown that at this location, in the Angolan upwelling system, upwelling and high productivity are not governed by the wind forcing, but were shown to be mixing-driven and related to the passage of coastally trapped waves (Brandt et al., 2024; Körner et al., 2024). Still, from 30ºS to 10ºS no large differences were observed between the upwelling indices from the different simulations.

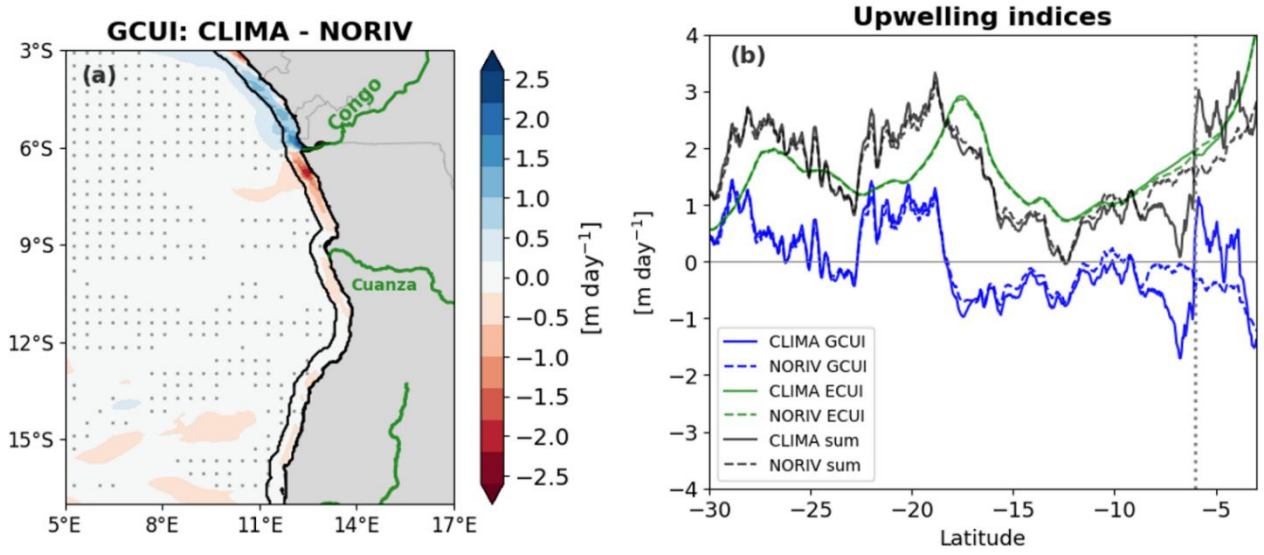

Figure 3.5. Freshwater input impact on upwelling. (a) Difference between CLIMA and NORIV for the mean Geostrophic Coastal Upwelling Index (GCUI). Coastal mask in (a) represents 50km away from coast, indicating the region where upwelling occurs (i.e. L_u, Eqs. 5, 6). (b) Mean upwelling indices averaged for coastal mask depicted in (a). Solid (dashed) lines indicate CLIMA (NORIV) indices. GCUI, ECUI and the sum of the indices are represented by blue, green and black lines, respectively. The pointed line in 6ºS indicates the position of Congo River mouth. Positive (negative) values in both (a) and (b) represent upwelling (downwelling).

However, from 10ºS to further north, and especially around the Congo river mouth, strong and significant differences in the GCUI are found between the experiments. From the NORIV experiment, the coastal geostrophic upwelling is nearly absent around the area of Congo River influence (Fig. 3.5b). On the other hand, by including land to ocean freshwater input, an offshore (onshore) geostrophic flow resulting from the low salinity water discharge generates coastal divergence (convergence) from 6ºS to 4ºS (8ºS to 6°S) (Fig. 3.5 a,b). The resulting upwelling (downwelling) corresponds to reduced (increased) SST in CLIMA, when compared to NORIV (Fig. 3.3a). Thus, the freshwater-induced downwelling might explain the warming signal from 6ºS to 10ºS, not explained by the strengthened coastal southward advection.

3.5 Conclusions and discussion

In this study, we have shown the effects and mechanisms of the freshwater input presence on the mean state SST in the southwestern African coastal region. To do that, we focused on comparing two model experiments: one with climatological freshwater discharge (CLIMA); and one without any discharge from land to ocean (NORIV). The processes are summarized in Fig. 3.6. Including a land to ocean freshwater discharge results in a strong reduction in SSS near the coast which generates a halosteric effect in the water column, increasing the SSH, and creating a geostrophic surface circulation. The halosteric SSH increase as a result of the CRD creates a primary alongshore SSH gradient that is in balance with a cross-shore geostrophic current, which, in turn, generates a secondary cross-shore SSH gradient (Fig. 3.6). While the primary alongshore gradient is associated with cross-shore geostrophic currents, upwelling north of the Congo River mouth, and downwelling south of it, the secondary gradient drives the alongshore geostrophic current related to the alongshore advection that reduces and increases the SST north and south of 6ºS, respectively (Fig. 3.6). While this advective signal can propagate southward (Fig. 3.6) due to the coastally trapped wave adjustment

and affect regions further south, in the north it must be limited to the region close to the Congo River mouth as there is no equatorward wave propagation. It is also in agreement with the fact that the SSH maximum is at the coast south of the river's mouth and moves away from the coast north of it (Fig. 3.3). In summary, the halosteric increase in SSH at the Congo's mouth produces a southward coastal geostrophic flow, with an onshore geostrophic component south of 6ºS. The generated southward coastal jet advects warmer waters further south, from ~10ºS to ~25ºS. Concomitantly, the onshore geostrophic components significantly reduce the upwelling from 6ºS to 10ºS. North of 6ºS the opposite occurs. The halosteric increase in SSH generates a northward geostrophic current at the coast which advects cooler waters to the north at the same time that the offshore component of this geostrophic flow is associated with a significant increase in upwelling from 6ºS to 4ºS. Hence, the climatological freshwater discharge simultaneously generated downwelling and advection that increases the mean state SST south of the River mouth; and upwelling and cooling from advection, reducing the SST mean state north of it. Furthermore, the southward advection likely pushes the Angola-Benguela front further south. Overall, it seems that changes in stratification did not play a major role in altering the surface temperatures, especially at the Congo River mouth. In the following, we will discuss the main findings and caveats of our study.

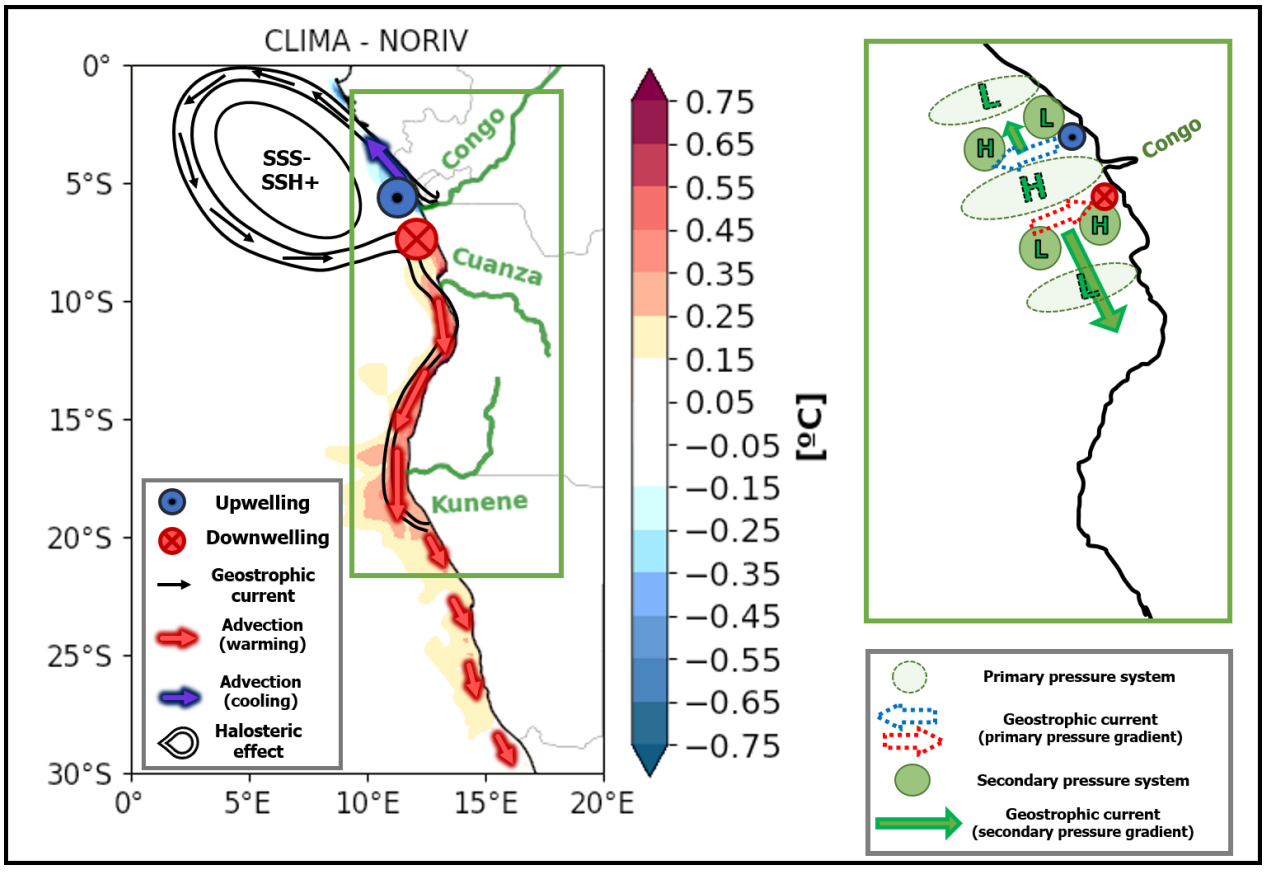

Figure 3.6. Schematic summarizing the processes related to the freshwater input effect on mean state SST at the southwestern African coast. Halosteric effect generating primary alongshore pressure gradient, producing cross-shore geostrophic currents associated with upwelling (downwelling) north (south) of the Congo's mouth, which creates a secondary cross-shore pressure gradient. The secondary gradient drives the alongshore flow responsible for the advection. This signal propagates southward due to coastally trapped wave adjustment, while in the north it is restricted to region close to river's mouth since there is no equatorward wave propagation. H (L) indicates high (low) pressure area.

The CTRL mean SST presented a warm bias when compared to satellite and reanalysis products. The warm SST bias is indeed an established and longstanding issue in both climate and regional ocean model simulations along the eastern boundary upwelling systems (e.g. Farneti et al., 2022; Small et al., 2024). Weak upwelling velocities and equatorward surface flow, poor representation of clouds, and model spatial resolution have been discussed as some of the causes of these errors (e.g. Richter, 2015; Bonino et al., 2019; Small et al., 2024). Within the SETA, the Benguela upwelling system appears to be even more challenging to simulate, likely due to the convergence of significantly distinct water masses, the unique spatial structure of the wind field, and its influence on the dynamics of these coastal waters (Bonino et al., 2019; Kurian et al., 2021). For instance, the ABF location and the strength of the Angola Current have been pointed out as major causes of warm biases in general circulation models (Koseki et al., 2018). At the same time, De La Vara et al. (2020) showed that the warm bias in the region is decreased by increasing the oceanic model resolution. Furthermore, Small et al. (2024) recently showed that using the higher resolution JRA55-do as atmospheric forcing in an ocean model also contributes to reducing the SST bias in the Benguela upwelling region, since it can better represent the alongshore winds and its associated downwind surface currents in comparison to the lower resolution CORE, even though a substantial bias relative to observations remains. Finally, the direct comparison between CTRL and the satellite product could present some caveats, since in this case, we are comparing measurements at different depths (satellite skin layer temperature vs 3m depth as 1st level from the model).

Simultaneously, there are also difficulties in well representing SSS fields, especially near the coast and close to river mouths, due to its high variability, strong vertical gradients, and low sampling rates in those regions (Boutin et al., 2021; Martins and Stammer, 2022; Nyadjro et al., 2022). However, both ESACCI and GLORYS12 products have been used and validated in the southwestern African coastal region against independent in situ measurements (Tchipalanga et al., 2018; Martins and Stammer, 2022; Aroucha et al., 2024). Overall, they seem to perform well, with the larger uncertainties located at the Congo mouth, as expected (Martins and Stammer, 2022). In this study, the highest differences between the model SSS and both the satellite and reanalysis products were also found in the SETA coastal region. As previously mentioned for temperature, the ESACCI satellite measurement of skin layer salinity can also likely differ from the 3m depth 1st level of CTRL, considered here as the surface. Further, in regions of strong vertical stratification such as river mouths, the depth level difference between products creates even larger SSS biases, as shown in the Gulf of Guinea by Nyadjro et al. (2022). Furthermore, the uncertainty of JRA55-do CRD is not well defined and might be substantial. Large discrepancies between this reanalysis forcing and the Brazzaville-Kinshasa gauge measurements have been attributed to the Congo Basin complex hydrology and the lack of field observations of climate variables in the region (Chandanpurkar et al., 2022; Hua et al., 2019). Hence, discrepancies between model and satellite SSS data within this region could be mainly related to the fidelity of these estimates (Chandanpurkar et al., 2022).

Additionally, the SSS variability in the coastal SETA is determined not only by freshwater input from the CRD, but also by the subsequent horizontal advection of the low SSS water by surface currents, with the river plume usually spreading west-northwestward, while some fractions of it being also advected southward

along the coast (Houndegnonto et al., 2021; Awo et al., 2022; Ngakala et al., 2023). This southward alongshore advection is subject to interannual variability mainly driven by the Angola Current and the propagation of coastally trapped waves (Awo et al., 2022; Martins and Stammer, 2022). Therefore, the SSS differences between the model simulation and the analyzed datasets are also likely explained by shifts in the freshwater input and more importantly by the surface circulation difference between the three products. In the latter case, the CTRL low SSS from the CRD is confined to further north (i.e. to ~10ºS) than what is observed for both ESACCI and GLORYS (Fig. 3.2).

Regarding SST variability, patterns of SST anomalies standard deviations from CTRL resemble those in observations (Fig. 3.2c). Besides the reduced amplitude for extreme events in CTRL, the interannual anomalies are overall well represented. The reason for the reduced SST variability in the model simulation remains uncertain (Fig. 3.10b-c). Recently, Prigent and Farneti (2024) showed that using JRA55-do atmospheric forcing improved the SST variability simulation in eastern boundary upwelling systems, including the CABA (see their Fig. 10), when compared to the use of CORE-II forcing. Hence, it is believed that the cause of the variability underestimation in our case is not in the atmospheric forcing. One possible explanation, as well as for SSS, could be a too weak southward current in CTRL. Similar to the SSS variability, extreme events of SST in the region are also forced by coastally trapped wave propagation and a southward advection mechanism related to equatorial and local dynamics, usually peaking in boreal spring (e.g. Aroucha et al., 2024; Bachèlery et al., 2020; Imbol Koungue et al., 2019; Rouault et al., 2007, 2018; Florenchie et al., 2004). Therefore, a weaker representation of the Angola Current might generate reduced SST anomalies during extreme events. In fact, Benguela Niños for which southward advection played an important forcing role, such as 2001 and 2011 (Rouault et al., 2007, 2018), were shown to have reduced SST anomalies in CTRL (Fig. 3.1c). At the same time, the January-May alongshore southward current is underestimated by the model in relation to the mooring measurements (Fig. 3.11). This fact also implies the reduced SSS variability in the CABA in CTRL, another likely reason for the underestimated CTRL SST variability, since low SSS waters have been linked to extreme positive SST events in the region (Aroucha et al., 2024; Lübbecke et al., 2019).

In this study, we focused on the climatological runoff impact on the SST mean state (i.e. CLIMA vs. NORIV), since no significant differences in the SST means were observed between the simulations with climatological vs. interannually varying runoff (i.e. CTRL vs. CLIMA, Fig. 3.12). This does not necessarily imply, however, that an interannually varying runoff does not influence the SST variability in the region. It has been recently shown through observational datasets that a freshwater input in the ABA could indeed boost extreme warm events in this area through increasing stratification and reducing vertical mixing (Aroucha et al., 2024; Lübbecke et al., 2019). For this, a combination of anomalously high CRD with stronger southward advection and the passage of a coastally trapped wave is required to bring the low SSS waters close to the ABF region (Martins and Stammer, 2022). In the 19 simulated years (2000-2018), however, the southernmost extension of a coastal SSS difference between CTRL and CLIMA was ~14ºS (-0.1 in December 2010, not shown), still too far north for the expected influence to take place. Hence, from the experiments analyzed here, not much can be said regarding CRD anomalies influencing SST variability in the ABA. Nevertheless,

relevant outcomes regarding the freshwater influence on the SST mean state in the SETA can be concluded from the present study.

During the last few years, modeling studies have been addressing the processes by which a freshwater discharge could impact SSTs. The main argument is that increasing the input of low salinity waters into the ocean would increase SSTs by strengthening the stratification and inhibiting the upwelling of cold waters (e.g. Topé et al., 2023; Zhang and Busalacchi, 2009). On the other hand, at the Congo River mouth, the work from White and Toumi (2014) pointed to no significant influence of an increased stratification by freshwater in warming the sea surface. Instead, they showed that the mixed layer shoaling due to the Congo discharge generated a considerable heat loss to beneath this thin layer, which then exceeded the reduced vertical mixing impact, even though barrier layers were formed (White and Toumi, 2014). In fact, this latter result agrees with what we found in this study. In spite of the significant barrier layer difference between CLIMA and NORIV at the river plume, the barrier layer generation area differs from the observed spatial warming pattern (solely concentrated at the coast, south of 6ºS). We hypothesize that this is due to the same argument presented by White and Toumi (2014); i.e. the surface heat loss due to the very shallow MLD at the river mouth. Additionally, their simulations demonstrated a significant coastal warming impact south of 6ºS (White and Toumi, 2014). Although the authors did not explore this further, they suggested that a change in ocean dynamics due to the river's presence is responsible for the observed coastal warming pattern. Here we dug into this mechanism, showing that indeed the coastal warming was a consequence of modified ocean dynamics via a change in geostrophic currents. Furthermore, we showed that those changes in SST are restricted to the coast since the geostrophic current strengthening reflects the location of the coastal freshwater input.

It is long known that river discharges can impact oceanic SSH (e.g., Meade and Emery, 1971; Piecuch et al., 2018; Chandanpurkar et al., 2022). To the best of our knowledge, however, this is the first study to report that a halosteric change in SSH and its gradients due to a freshwater discharge can impact the mean state coastal SST at an eastern boundary upwelling system, via a change in geostrophic currents, subsequently altered horizontal temperature advection, and upwelling. The lateral salinity-generated pressure gradient at river plumes can induce surface geostrophic flows projecting at the coast (Fong and Geyer, 2002). Alory et al. (2021) found an additional onshore geostrophic flow in the Gulf of Guinea due to the River Niger input, also pointing to the possibility of a similar effect next to other large river plumes. The authors, however, observed that, with the river presence, the MLD was reduced and compensated for the increase in the onshore geostrophic flow, not having an overall significant impact on the coastal geostrophic upwelling (Alory et al., 2021). Here we show that the Congo River can not only change the surface geostrophic flow, but also limit upwelling to the south of its estuary by this generated onshore geostrophic current, at the same time that it can induce upwelling north of the river plume via an offshore component of this geostrophic flow (Fig. 3.5), as the changes in the MLD are here less significant than the changes in the coastal current. This work highlights the importance of properly understanding the impact of high freshwater input in ocean mixing and stratification, as well as in the coastal dynamics. The results presented here might become even more relevant in the future when considering recent studies showing upwelling shifts at the southwestern African coast due

to wind-related geostrophic deviations in climate change scenarios (Ayissi et al., 2024; Jing et al., 2023). The role of geostrophic flows in eastern boundary upwelling systems mean state and long-term changes is more prominent in the Atlantic basin when compared to the Pacific (Jing et al., 2023). In addition, Jing et al. (2023) recall an ongoing discussion of the interaction between upwelling and other greenhouse warming-related processes (e.g. stratification, mesoscale activity) in these regions. As river runoffs are expected to be amplified in the future (Müller et al., 2024; Aloysius and Saiers, 2017), halosteric-related shifts in geostrophic flows can appear as an additional mechanism in this debate.

Furthermore, as we showed that the freshwater presence pushes the ABF southward, we wonder if the future runoff amplification could also contribute to the recently observed trend of warming off the Angolan coast, where fresher and warmer tropical waters are moving poleward due to an Angola Current intensification (Roch et al., 2021; Tomety et al., 2024). Finally, the mechanism shown here could also play a role in Benguela Niño events in this area. Most of the advective warming from the southward geostrophic current is located within the CABA where these events occur. Hence, in years of increased freshwater discharge, these warming events could be boosted by different mechanisms: the reduced vertical mixing via increased stratification (Aroucha et al., 2024), and the strengthening of the southward advection and downwelling due to the halosteric SSH increase, as shown in this work.

Open research. The data and scripts that support the findings of this study are available through GEOMAR at https://hdl.handle.net/20.500.12085/2b927bcd-afab-4bc6-ba97-634d09435daa (Aroucha and Schwarzkopf, 2024). Experiments identifiers are INALT20.L46-KFS10X (CTRL), INALT20.L46-KFS111 (CLIMA), and INALT20.L46-KFS106 (NORIV). Other datasets used in this work are publicly available under the following links: OISST (https://psl.noaa.gov/data/gridded/data.noaa.oisst.v2.highres.html); GLORYS12 (https://data.marine.copernicus.eu/product/GLOBAL_MULTIYEAR_PHY_001_030/download); ESACCI (https://data.ceda.ac.uk/neodc/esacci/sea_surface_salinity/data/v03.21/30days); Congo River discharge (https://hybam.obs-mip.fr/data/); Current velocities from mooring data (https://doi.org/10.1594/PANGAEA.870917; https://doi.pangaea.de/10.1594/PANGAEA.909911; https://doi.org/10.1594/PANGAEA.909913; https://doi.pangaea.de/10.1594/PANGAEA.939249; https://doi.org/10.1594/PANGAEA.962193); GLOCURRENT data (https://data.marine.copernicus.eu/product/MULTIOBS_GLO_PHY_MYNRT_015_003/download?dataset=cmems_obs_mob_glo_phy-cur_my_0.25deg_P1M-m_202311).

Acknowledgments. The authors declare that they have no conflict of interest. LCA acknowledges the German Academic Exchange Service (DAAD). The model integrations were enabled by the provision of computing resources on the high-performance computing system JUWELS at the Jülich Supercomputing Centre (JSC) in the framework of the Earth System Modelling Project (ESM) and at the North German Supercomputing Alliance (HLRN). We thank Klaus Getzlaff for his help with the model data archive, and the two anonymous reviewers and the editor for their helpful comments on the paper. This study was supported by the German

Academic Exchange Service (DAAD) via the Doctoral Research Grant 57552340, and by the Bundesministerium für Bildung und Forschung (grant no. 03F0795A (SPACES-II-BANINO) and 03F0796A (SPACES-II-CASISAC)). LCA and JFL took part in conceptualizing and outlining the paper. LCA wrote the first draft and produced the figures. FUS and AB developed and ran the sensitivity experiments. All authors contributed to the discussion of the results and the writing of the manuscript.

3.6 Supplementary Material

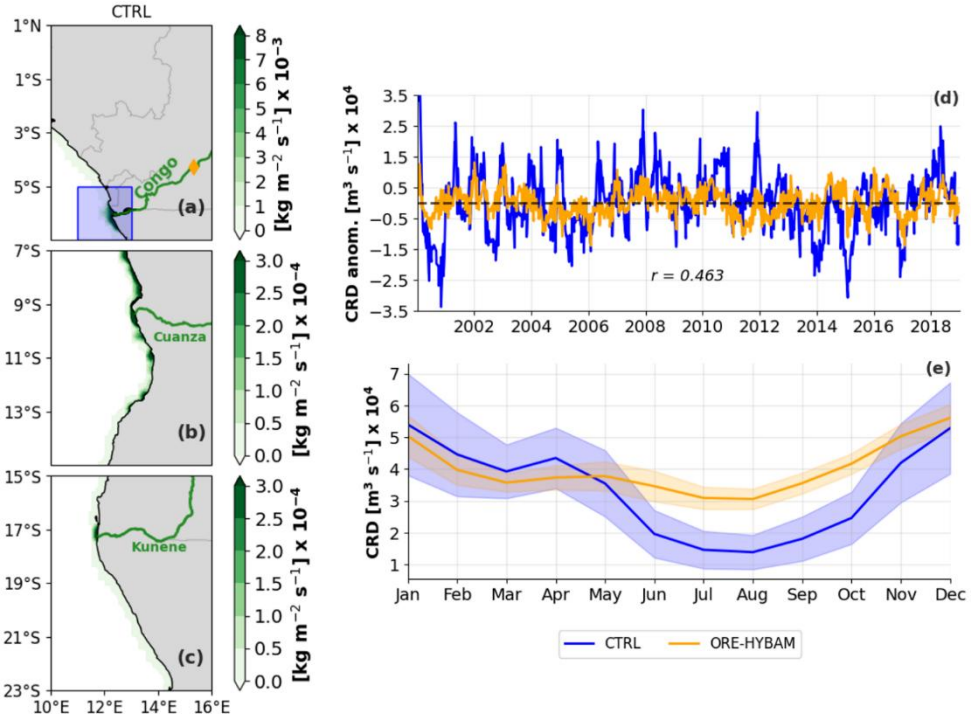

Figure 3.7. Freshwater input from CTRL (blue) vs Congo River discharge from Kinshasha-Brazzaville station (orange). (a) Freshwater input from CTRL run. Blue box (5ºS – 7ºS, 11ºE – 13ºE) in (a) represents the area where CTRL freshwater input was averaged. Orange diamond shows location of Kinshasha-Brazzaville station. (b) and (c) same as (a). Note that colorbar scales change from (a)-(b). (d) Daily anomalies of both box-averaged CTRL freshwater input and ORE-HYBAM river discharge. (e) Seasonal climatology from 2000-2018 of both products. Shading in (e) indicates monthly standard deviations.

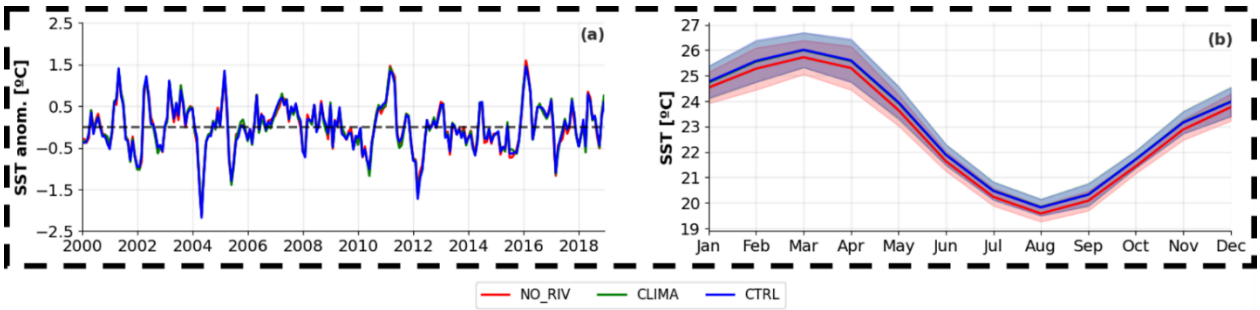

Figure 3.8. (a) SST anomalies averaged for CABA shown for the three model experiments (CLIMA in green, NORIV in red, CTRL in blue). (b) Same as (a) but for the monthly climatologies. Shadings indicate monthly standard deviations.

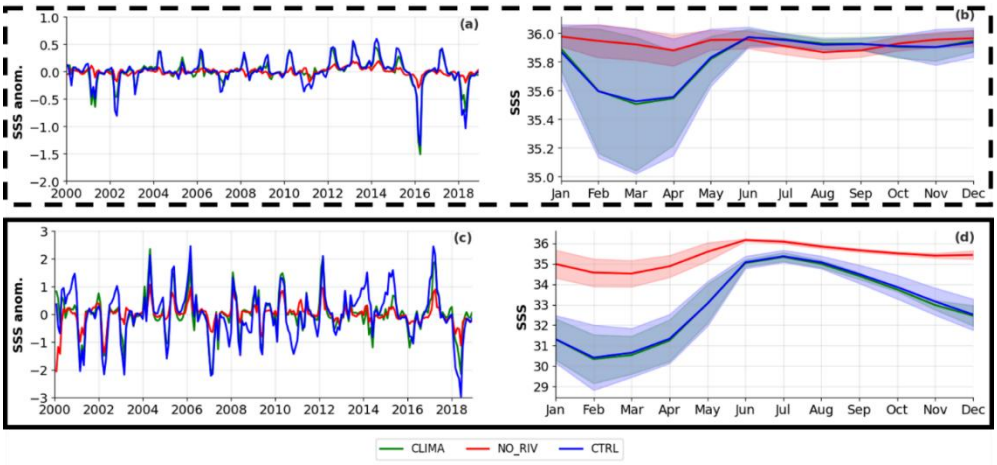

Figure 3.9. (a) SSS anomalies averaged for CABA for the three model experiments (CLIMA in green, NORIV in red, CTRL in blue). (b) Same as (a) but for the seasonal climatologies. Shadings indicate monthly standard deviations. (c) and (d) same as (a) and (b) but for CRMA.

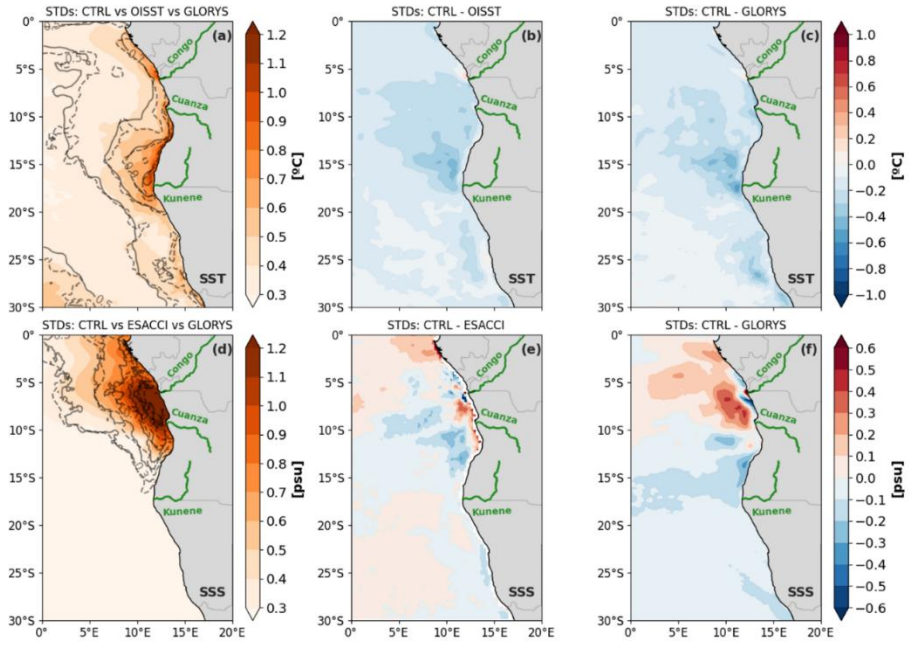

Figure 3.10. Comparison of simulated SST variability against observations and reanalysis. (a) Mean SST anomalies monthly standard deviation (STD) from CTRL (shading), OISST (solid contours), and GLORYS (dashed contours) from 2000-2018. (b) Mean difference in SST anomalies STD between CTRL and OISST. (c) Same as (b) but difference between CTRL and GLORYS12. (d) Same as (a) but for CTRL SSS anomalies STD, compared to ESACCI (solid contours, from 2010-2018) and GLORYS12 (dashed contours, 2000-2018). (e) Same as (b) but for ESACCI SSS and anomalies from 2010-2018 (f) Same as (c) but for SSS.

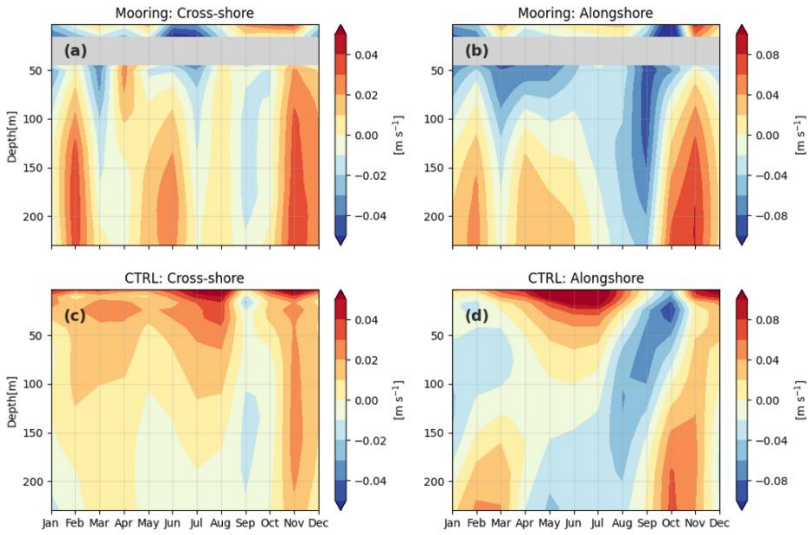

Figure 3.11. Cross-shore (a, c) and along-shore (b, d) current velocity climatology (rotated by -34º with respect to true north) recorded by the moored ADCP located at 10º50'S, 13º00'E combined to surface velocities from GLOBCURRENT (a, b); and taken from CTRL run (c, d) at nearest grid position from mooring location and -34º rotation. Climatologies were calculated over the period 2014 – 2018.

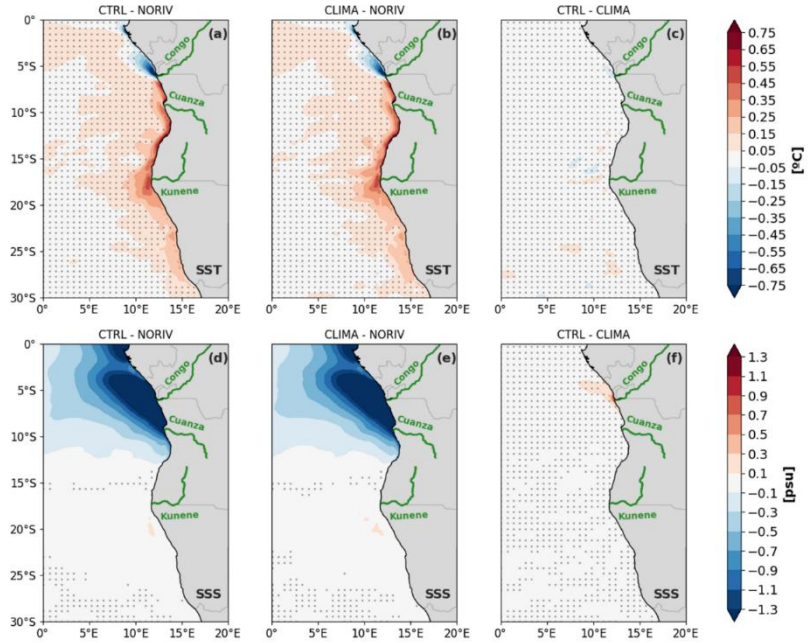

Figure 3.12. Mean state difference between runs. (a) Mean SST CTRL – Mean SST NORIV. (b) Mean SST CLIMA – Mean SST NORIV. (c) Mean SST CTRL – Mean SST CLIMA. (d), (e), (f) same as (a), (b), (c), respectively, but for SSS. Stippled grey areas indicate where difference is not significant in a 95% confidence level.

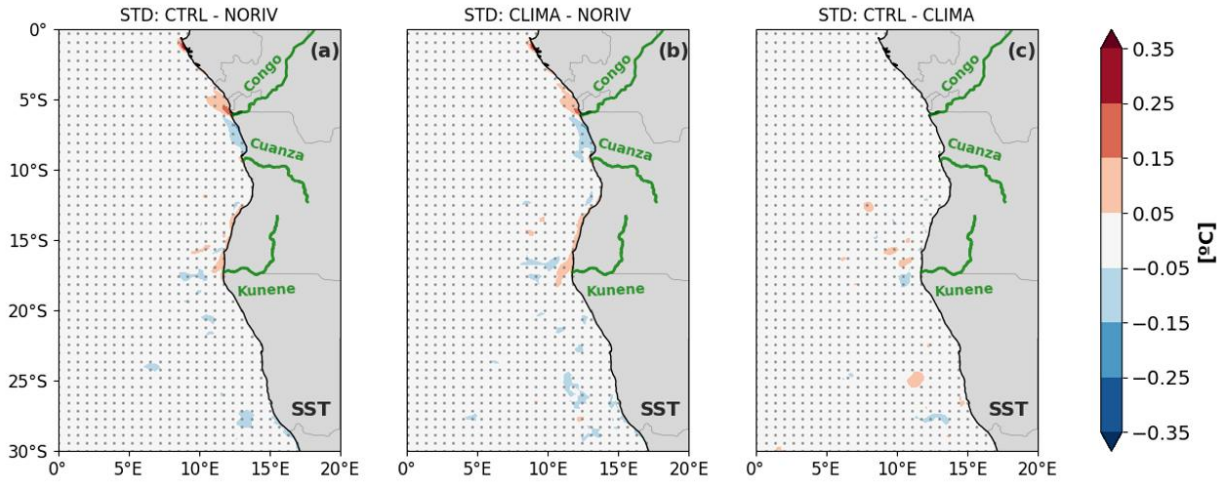

Figure 3.13. Monthly SST anomalies standard deviation (STD) mean difference between runs. (a) Mean SST anomalies STD CTRL – Mean SST anomalies STD NORIV (b) Mean SST anomalies STD CLIMA – Mean SST anomalies STD NORIV. (c) Mean SST anomalies STD CTRL – Mean SST anomalies STD CLIMA. Stippled grey areas indicate where difference is not significant in a 95% confidence level.

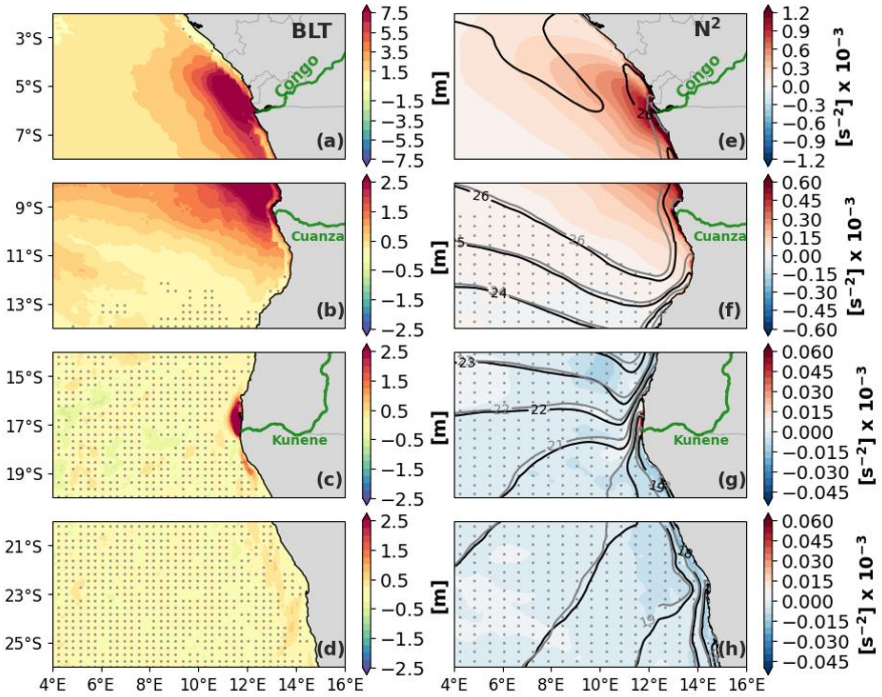

Figure 3.14. Difference between CLIMA and NORIV mean states (CLIMA-NORIV) for BLT (a-d); N^2 averaged from surface to 50m depth (e-h). Stippled grey areas indicate where difference is not significant in a 95% confidence level. Black (grey) lines from e-h depicts isotherms from CLIMA (NORIV) run. Note that colorscales change for a (e) in relation to b-d (f-h).

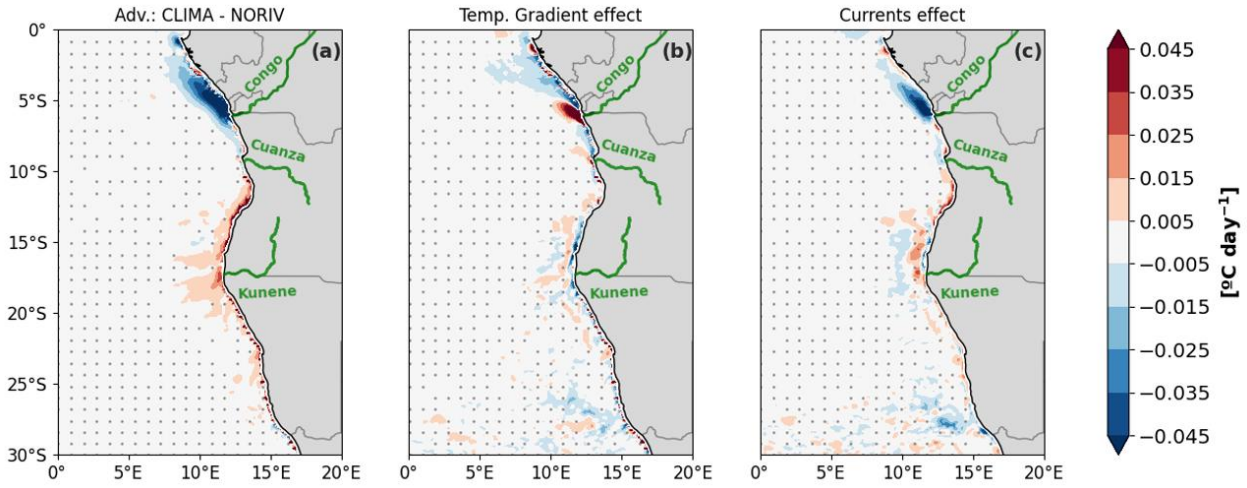

Figure 3.15. Difference between CLIMA and NORIV mean states (CLIMA-NORIV) for horizontal advection. In (a) both temperature gradient and horizontal currents are from the different runs; in (b) only temperature gradient is different (currents from CLIMA); in (c) only horizontal current is different (temperature gradient from CLIMA). Stippled grey areas indicate where difference is not significant in a 95% confidence level.

Chapter 4

The Influence of Freshwater Input on the Evolution of the 1995 Benguela Niño

In Chapter 3, it was shown that river discharge plays an important role in changing the SST mean state in the SETA. The exact role of such input to the dominant SST variability mode within this region, i.e. Benguela Niños, remains uncertain. To address this question, the satellite-era's most extreme warm event off Angola, the 1995 Benguela Niño, is explored in Chapter 4. Here, the up-until-now unnoticed effect of anomalous freshwater input acting as a local forcing during this event is analyzed. Based on the available reanalysis and satellite products, also including *in-situ* datasets obtained during several research cruises within this area, the chapter presents the first research work to ever focus and further discuss the negative SSS anomaly propagation to the Angola-Benguela area and its role in amplifying a Benguela Niño event, even though other papers have mentioned the possibility of this impact (e.g. Lübbecke et al., 2019). From now on, the focus of this thesis is to unravel the impacts of freshwater input on the SST variability in the Southeastern Tropical Atlantic.

The manuscript was published in *Journal of Geophysical Research: Oceans* in January 2024.

Citation: **Aroucha, L. C.**, Lübbecke, J. F., Körner, M., Imbol Koungue, R. A., & Awo, F. M.: The Influence of Freshwater Input on the Evolution of the 1995 Benguela Niño, *Journal of Geophysical Research: Oceans*, 129, e2023JC020241, https://doi.org/10.1029/2023JC020241, 2024.

The candidate designed the original study, carried out all the analyses, produced all the figures, except Figure 4.6, and authored the manuscript from the first draft to the final published version.

4.1 Abstract

Benguela Niño events are characterized by strong warm sea surface temperature (SST) anomalies off the Angolan and Namibian coasts. In 1995, the strongest event in the satellite era took place, impacting fish availability in both Angolan and Namibian waters. In this study, we use direct observations, satellite data, and reanalysis products to investigate the impact that the up-until-now unnoticed mechanism of freshwater input from Congo River discharge (CRD) and precipitation had on the evolution of the 1995 Benguela Niño. In the onset phase of the event, anomalous rainfall in November/December 1994 at around 6ºS, combined with a high CRD, generated a low salinity plume. The plume was advected into the Angola-Namibia region in the following February/March 1995 by an anomalously strong poleward surface current generated by the relaxation of the southerly winds and shifts in the coastal wind stress curl. The presence of this low surface salinity anomaly of about -2 psu increased ocean stability by generating barrier layers, thereby reducing the turbulent heat loss, since turbulent mixing acted on a weak vertical temperature gradient. A mixed layer heat budget analysis demonstrates that southward advection of Angolan waters drove the warming at the onset, while reduced mixing played the main role at the event's peak. We conclude that a freshwater input contributed to the SST increase in this exceptionally strong event and suggest that this input can influence the SST variability in Angola-Namibia waters through a combination of high CRD, precipitation, and the presence of a strong poleward surface current.

4.2 Plain Language Summary

Benguela Niño events are characterized by excessive warming of the sea surface temperature off the Angolan and Namibian coasts. One of the strongest-ever recorded warm events dates back to 1995, impacting fish availability in both Angolan and Namibian waters. In our research, we investigate if freshwater from rain and from the Congo River could have impacted the evolution of this 1995 Benguela Niño. In the event's early stage, high precipitation and river discharge generated a low salinity pool at the Congo River mouth, which in February/March 1995 was taken to the south by an exceptionally strong surface current, generated by changes in wind strength and direction at the African coast. This low sea surface salinity in a shallow layer in the upper meters of the ocean increased the ocean's stability. As the stabilized waters diminished the usual mixing from the depths below which cools down the surface waters, it contributed to an increase in warming in the surface layer of the ocean. We conclude that the warming of the surface waters in the region was indeed influenced by the combination of high precipitation and high Congo River discharge with a strong surface current towards the south.

4.3 Introduction

Benguela Niños are El Niño-like events in the southeastern tropical Atlantic Ocean (Fig. 4.1) characterized by strong warm anomalies, particularly off the Angolan coast (Shannon et al., 1986; Florenchie et al., 2004). These events modulate the sea surface temperature (SST) at interannual time scales in this region and usually peak in boreal spring, from March to May, when the SSTs in the region are climatologically high

(Brandt et al., 2023; Imbol Koungue et al., 2019; Lübbecke et al., 2010). At the same time, the Angola-Benguela front, i.e. a thermal front located usually at 17ºS due to the confluence of northern tropical warm waters and southern colder waters from the Benguela Current, is located furthest south (Lübbecke et al., 2010). During the strong warm event, positive SST anomalies can reach up to 3ºC in the Angola Benguela area (ABA, defined as 8ºS – 20ºS, 8ºE to the coast, Fig. 4.1) consequently impacting the biology and ocean-atmosphere processes at the southwestern African coast. In fact, it has been shown that these events not only influence marine ecosystems and fisheries in the region (Blamey et al., 2015; Binet et al., 2001; Boyer & Hampton, 2001; Gammelsrød et al., 1998), modulating the upward supply of nutrients (Bachèlery et al., 2016b) but have also consequences for rainfall and flooding in coastal Africa (Rouault et al., 2003; Hansingo & Reason, 2009; Lutz et al., 2015). Hence, understanding the development of these warm events is of great socioeconomic importance for local communities.

Benguela Niños have been shown to be triggered mainly remotely. The relaxation of the trade winds in the western equatorial Atlantic generates eastward propagating downwelling equatorial Kelvin waves followed by coastally trapped waves (CTWs) propagating southward when reaching the African coast (Florenchie et al. 2004; Lübbecke et al. 2010; Bachèlery et al. 2016a; Imbol Kounge et al. 2017; Rouault et al., 2018). The propagation of these CTWs is also responsible for controlling the variability and seasonality of the Angola Current (Bachèlery et al., 2016a; Kopte et al., 2017). The Angola Current is a geostrophic poleward undercurrent usually situated below the equatorward coastal jet (Fennel et al., 2012; Tchipalanga et al., 2018), restricted to the upper 120m of the water column and with its core at around 50m depth. (Tchipalanga et al., 2018; Kopte et al., 2017). This poleward current is situated closer to the sea surface seaward of the coastal jet (Fennel et al., 2012). The passage of a downwelling (upwelling) CTW in austral summer (winter) enhances (weakens) the Angola current (Tchipalanga et al., 2018), with the downwelling waves deepening the thermocline, resulting in a high SST anomaly. Bachèlery et al. (2020) showed that 71% of both Benguela Niños and Niñas (i.e. the counterpart of Benguela Niño events, where SST is anomalously cold in ABA) events are forced remotely at the equator.

Local forcing, however, also plays an important role in generating and modulating these coastal warm anomalies due to local wind fluctuations (Polo et al., 2008; Hu and Huang, 2007; Illig et al., 2020) in association with shifts in the position and strength of the South Atlantic Anticyclone (Richter et al., 2010) by modulating upwelling intensity and consequently SST at western coastal Africa. In addition, local wind forcing plays a major role in determining the structure and variability of the eastern boundary circulation in this area (Fennel et al., 2012; Junker et al., 2015), which are usually impacted by the southerly winds related to the atmospheric Benguela low-level coastal jet (Patricola & Chang, 2017). Imbol Koungue et al. (2021) showed that a combination of both local and remote forcing was important in triggering the 2019 Benguela Niño, and Lübbecke et al. (2019) suggested that local wind forcing in combination with anomalous high freshwater input into the ocean due to both local precipitation and Congo River discharge (CRD) impacted the generation of the 2016 warm event in the southeastern tropical Atlantic.

The role of freshwater input in the development of warm events is through the generation of barrier layers (Figs. 4.1b, c). The presence of barrier layers increases ocean stability and stratification, hence reducing

the mixing and entrainment of cool subsurface waters into the mixed layer, thereby leading to an SST increase. In fact, in the Pacific, it has long been shown that freshwater input can impact surface warming by the generation of these barrier layers associated with a decrease in entrainment cooling (Vialard & Delecluse 1998). For the eastern tropical Atlantic, Materia et al. (2012) showed the effect of Congo River freshwater discharge on warm events occurring in the Gulf of Guinea, while White and Toumi (2014) quantified the formation of barrier layer up to 6m thick in model simulations due to a mixed layer shoaling by the CRD. However, the role of freshwater input for SST variability in the southeastern tropical Atlantic has not been fully elucidated by modeling studies (White & Toumi, 2014). More recently, Sena Martins and Stammer (2022), despite not being able to find a significant correlation between the river plume patterns and the occurrence of a Benguela Niño, showed evidence for a strong influence of the CRD low-salinity layer in increasing stratification in the region

The 1995 Benguela Niño was the strongest event ever recorded in the satellite era (Imbol Koungue et al., 2019) evidencing SST anomalies averaged for February-March-April up to 3ºC in the region (Fig. 4.1a). It was first described by Gammelsrød et al. (1998) and was associated with high mortality and southward displacement of fish from Angolan to Namibian waters, also economically impacting these countries. The eastward propagation of an equatorial Kelvin wave followed by a southward CTW along the African coast was shown through forced ocean simulations at the onset of the event (Imbol Koungue et al., 2019), and was associated with a 0.73ºC increase in the peak of SST anomalies (Imbol Koungue & Brandt, 2021). On the other hand, no clear evidence of a Kelvin wave influence was detected from satellite observations, with the sea surface height anomalies appearing to be stationary and not propagating along the southwestern African coast (Richter et al., 2010). In fact, the role of remote forcing via the propagation of a Kelvin wave was not the most pronounced in the 1995 Benguela Niño in comparison with other warm event years (e.g. 1984, 2010/2011; see Fig. 6 from Imbol Koungue et al., 2019). More recently, Song et al. (2023) when simulating Benguela Niño/Niña events with a single-layer ocean linear model excluding the local forcings (e.g. precipitation and freshwater advection) did not find a clear energy route of equatorial waves (i.e. remote forcing) triggering the 1995 extreme warm event. The authors suggested that the coastal SST anomaly might have been forced locally for this year (Song et al., 2023). Finally, in Gammelsrød et al. (1998), Conductivity-Temperature-Depth (CTD) profiles identified the presence of a freshwater plume of low salinity at 18ºS in March 1995, much further south than climatologically expected (i.e. maximum southward displacement extending only to around 12ºS in February-March-April; Awo et al., 2022). At the same time, similar CTD profiles showed the occurrence of barrier layers at 9ºS (see Fig. 2b from Gammelsrød et al., 1998). Although Gammelsrød et al. (1998) associated the Benguela Niño event with these strong negative salinity anomalies on the Angolan coast, the study did not mention the barrier layers presence or possible impacts on this event. Overall, it seems that both remote and local forcing played a role in the generation of this event.

The aim of this paper is to evaluate the impact of the high freshwater input followed by the strong low salinity signal in the 1995 Benguela Niño event. We intend to depict and discuss an up-until-now unnoticed effect of the increased stratification through the presence of barrier layers in the strongest warm event ever recorded in the southeastern tropical Atlantic. We also use a mixed layer heat budget analysis to

discuss the oceanic and atmospheric processes responsible for the high SST signal. For that, we use satellite data and reanalysis products, comparing them to diverse in-situ measurements, including CTD profiles and sections from different cruises, and a mooring situated in the region. The paper is divided as follows: in section 4.4 we introduce the different datasets used and the methods for defining the barrier layer and the mixed layer heat budget terms. In section 4.5 we describe not only the processes that led to a high freshwater input in the ABA at the onset of the event, and the impacts of this input on the water column stratification, but also the different processes related to the heat budget terms that were responsible for the warming during the event. In section 4.6, we discuss the results and future perspectives, and end with concluding remarks.

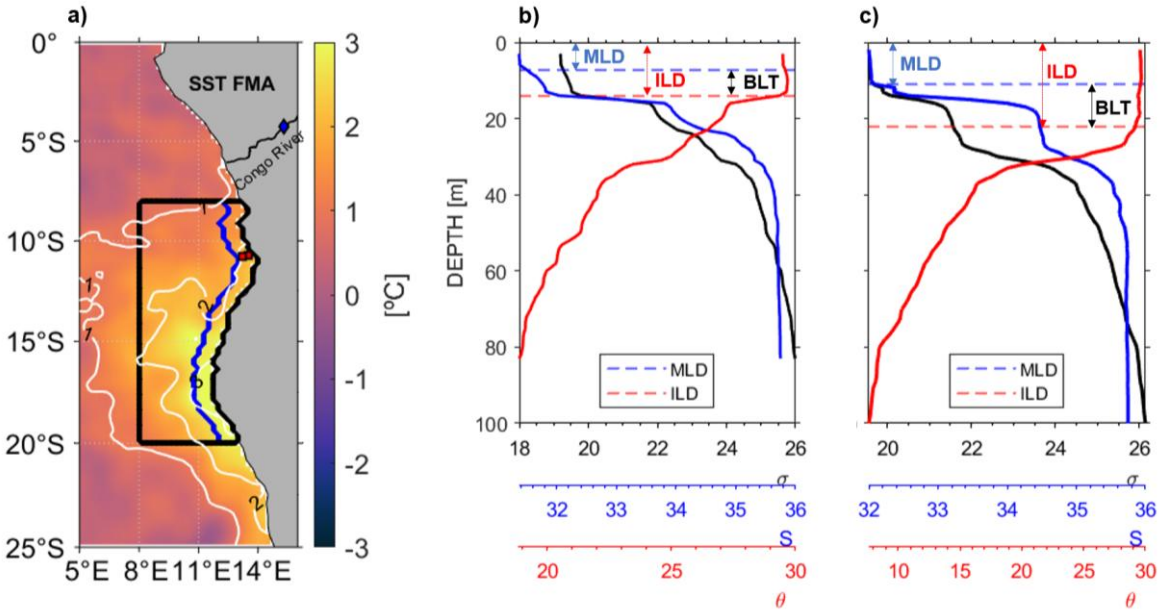

Figure 4.1. (a) Detrended monthly SST anomalies from OISST for February-March-April 1995. White contours are anomaly isotherms 1ºC apart from each other. Blue diamond represents Congo River Brazzaville station. Contours indicate ABA (8ºS – 20ºS, 8ºE to the coast, black) and coastal box 1 (8ºS – 20ºS, 1º away from the coast, blue). Red squares indicate the location of CTD profiles depicted in (b, c). CTD profiles from Nansen Programme (b) on 16th March 1995 at 10.74ºS and 13.5ºE and (c) on 27th March 1995 at 10.76ºS and 13.2ºE. Red, blue, and black solid lines in (b, c) represent potential temperature (θ), salinity (S), and density (σ) profiles, respectively. MLD = Mixed Layer Depth, ILD = Isothermal Layer Depth, BLT = Barrier Layer Thickness.

4.4 Data and Methods

4.4.1 Datasets

SST monthly averages were obtained from the high-resolution NOAA Optimum Interpolation SST (OISST), with 0.25º spatial resolution, which consists of a blend of satellite and in-situ measurements (Reynolds et al., 2007; Huang et al., 2021). OISST data is available at National Centers for Environmental Information (www.ncei.noaa.gov) from 1981 to the present day.

We use monthly averages of the 6-hourly wind vectors from the Cross-Calibrated Multi-Platform (CCMP) (Atlas et al., 2011; Mears et al., 2022). CCMP combines a background field from European Centre for Medium-Range Weather Forecasts (ECMWF) reanalysis 5 (ERA5, Herbach et al., 2020) with 10-m wind retrievals over the ocean from different types of satellites. CCMP data is available from 1993-2019, with a 0.25º x 0.25º spatial resolution, at the Remote Sensing Systems platform (www.remss.com). We calculate wind stress by applying the bulk formula $\vec{\tau} = \rho_a \, x \, c_D \, x \, \overrightarrow{u_{10}} \, x \, u_{10}$, with $\rho_a = 1.22$ kg m^{-3} and $c_D = 0.0013$.

Monthly surface heat fluxes, i.e. Shortwave Radiation (SWR), Longwave Radiation (LWR), Latent Heat Flux (LHF), and Sensible Heat Flux (SHF) were used from the ERA5 reanalysis (Hersbach et al., 2020). This data is available at 0.25º horizontal resolution from 1940 to present days and is distributed by the Copernicus Climate Change Service via https://cds.climate.copernicus.eu/.

Furthermore, for the freshwater input data, monthly Congo River discharge measurements were obtained from SO-HYBAM (http://www.ore-hybam.org/) at Brazzaville Station, Republic of Congo, available from 1947 to 2019. Monthly means of precipitation from merged satellite and surface rain gauge observations, with 2.5º x 2.5º spatial resolution, were taken from the Global Precipitation Climatology Project (GPCP) (Adler et al., 2003). Data is accessible from 1979 to 2020 at https://psl.noaa.gov.

Finally, monthly means of potential temperature, salinity, zonal and meridional currents from the Global Mercator Ocean Reanalysis product (GLORYS12) (Lellouche et al., 2021) were used in order to calculate the Mixed Layer Depth (MLD), Isothermal Layer Depth (ILD), and consequently Barrier Layer Thickness (BLT). The Brunt-Väisäla frequency (N^2) calculations were also based on this product as well as the Mixed Layer Heat Budget analysis described in section 4.4.2.2. The product has a 1/12º spatial resolution and 50 vertical levels, with 1m vertical resolution in the first levels, increasing with depth, and data available from 1993 – 2019. This dataset is distributed by the EU Copernicus Marine Service Information (http://marine.copernicus.eu/).

Since GLORYS12 and CCMP products are limited to the time period 1993 – 2019, only these 27 years were used for all above-cited datasets. Detrended anomalies for each dataset were calculated by removing within the same period monthly climatologies and trends from the data. In order to evaluate how well GLORYS12 represents the main processes occurring in ABA, in-situ measurements were compared to this reanalysis product. The assessment and validation of the GLORYS12 product against in-situ measurements are provided in Supporting Information Text S1. Text S1 also describes the observational datasets used to perform this analysis.

4.4.2 Methods

4.4.2.1 Barrier Layer Thickness

In this study, we define the Mixed Layer Depth (MLD) as the depth at which potential density (σ_Θ) is increased by $\Delta\sigma_\Theta$ relative to its own value at a reference depth, as follows (de Boyer Montégut et al., 2004; de Boyer Montégut et al., 2007; Mignot et al., 2012; White & Toumi, 2014; Gévaudan et al., 2021; Saha et al., 2021):

$$MLD: depth\ where\ \sigma_\Theta = \sigma_{rfd} + \Delta\sigma_\Theta \qquad (4.1)$$

$$\Delta\sigma_\Theta = \sigma_\Theta(T_{rfd} - 0.2ºC, S_{rfd}, P_0) - \sigma_\Theta(T_{rfd}, S_{rfd}, P_0) \qquad (4.2)$$

where *rfd* represents the surface level of the GLORYS12 reanalysis (i.e. ~0.5m) as the reference depth. $\Delta\sigma_\Theta$ represents the potential density change equivalent to a 0.2ºC temperature decrease at the local

salinity. P_0 is the pressure at the ocean surface, and T_{rfd} and S_{rfd} are respectively the temperature and salinity at the reference depth. At the same time, ILD is defined by a 0.2ºC threshold, where:

$$ILD: depth\ where\ T = T_{rfd} - 0.2ºC \qquad (4.3)$$

Finally, the Barrier Layer Thickness (BLT) definition is the difference between the ILD and the MLD:

$$BLT = ILD - MLD \qquad (4.4)$$

Additionally, for the identification of the stability and stratification of the water column within the 1995 event, the Brunt-Väisäla frequency N^2 was also obtained at each depth by using the same GLORYS12 product. Then, N^2 was averaged from the MLD until 50m, since the MLD in this region is climatologically shallower than 50m (not shown). Both anomalies of BLT and N^2 were calculated by removing the climatology within the 1993-2019 period.

4.4.2.2 Mixed Layer Heat Budget

In order to assess the processes driving the temperature change during the 1995 Benguela Niño, reanalysis, and satellite products were used to perform a mixed layer heat budget analysis. Here we use an approach similar to several previous papers (e.g. Stevenson & Niiler, 1983; Moisan & Niiler, 1998; Foltz et al., 2003, 2020; Echols and Riser, 2020; Körner et al., 2023). The equation used here is as follows:

$$\frac{\partial \mathrm{T}}{\partial \mathrm{t}} = -\boldsymbol{v}.\nabla \mathrm{T} + \frac{q_{net}}{\rho\ c_p\ h} + r \qquad (4.5)$$

where ∂t= 1 month; T = $\bar{T}_{ML}$, which is the temperature averaged for the mixed layer; $\boldsymbol{v}$ represents the horizontal currents averaged for the mixed layer h = MLD; ρ is the seawater density, taken here as 1025 kg/m^3; c_p is specific heat capacity taken as 4000 J/kg ºC. From left to right each term denotes respectively: Mixed layer temperature tendency, temperature horizontal advection within the mixed layer, net surface flux corrected for the SWR that penetrates into the mixed layer, and residual. The residual contains the terms not represented in the equation, such as turbulent heat loss (i.e. heat loss at the base of the mixed layer due to turbulent mixing), entrainment, and the vertical temperature velocity covariance (Körner et al. 2023; Hummels et al., 2014; Foltz et al. 2003). Actually, the temperature/velocity covariance is considerably smaller than the other contributions and is usually neglected in the ML heat budget analysis (Foltz et al., 2003; Hummels et al., 2014; Körner et al., 2023). In addition, the residual includes the contribution of processes unresolved by the spatial and temporal scales of the data used here, and the uncertainty arising from the data. The net surface heat flux term (q_{net}) consists of the sum of q_{abs}, LWR, LHF, and SHF, where q_{abs} represents the amount of shortwave radiation absorbed within the mixed layer. Here, q_{abs} is defined based on Foltz et al. (2020) where: $q_{abs} = SWR\ (1 - 0.47e^{-h/15})$, considering an albedo rate of 6% where h is the MLD in

meters. All heat fluxes used here were obtained from the ERA5 reanalysis dataset and interpolated into the GLORYS12 grid.

4.5 Results

4.5.1 Low-salinity plume propagation

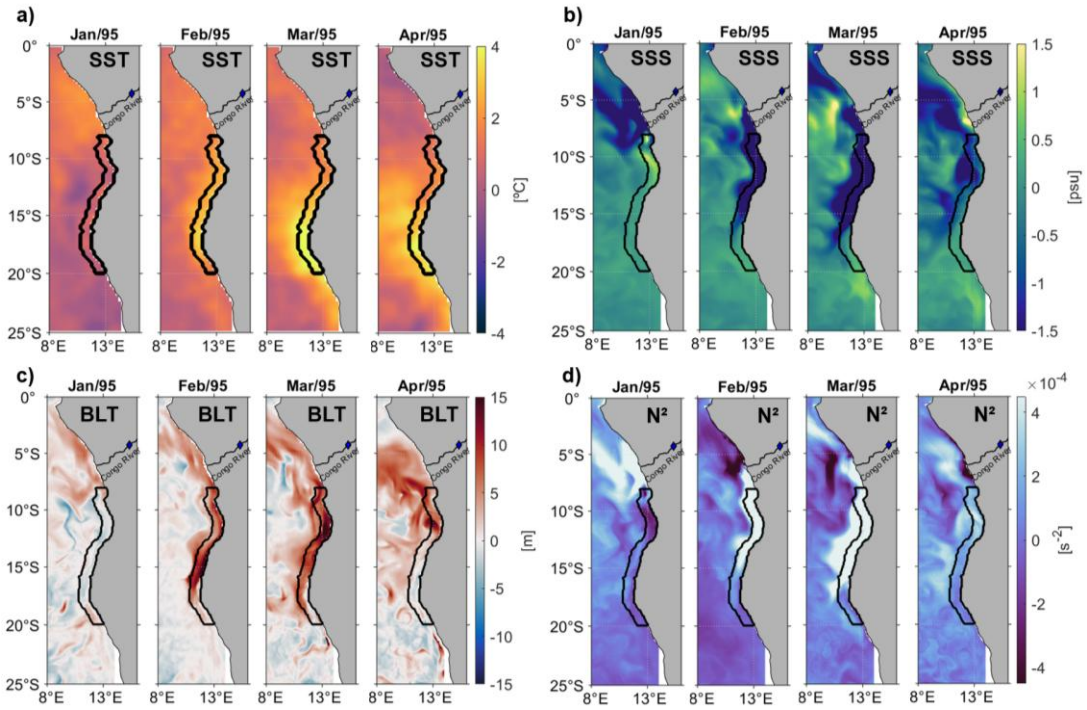

Figure 4.2. Detrended monthly anomalies from January to April 1995 for SST (a), SSS (b), BLT (c), N^2 (d). Black contours indicate coastal box 1 region (8ºS – 20ºS, 1º away from coast). Blue diamond represents Congo River Brazzaville station. SST from OISST. SSS from GLORYS12, BLT and N^2 calculated from GLORYS12 dataset.

The 1995 Benguela Niño event started to develop in February when positive SST anomalies of 2ºC averaged for the ABA coastal region (i.e. coastal box 1) were observed (Figs. 4.2a, 4.3a). The event peaked one month later, in March, when the ocean surface temperature was up to at least 4ºC warmer than climatology close to the Angola-Benguela front (Fig. 4.2a). One characteristic of this event was that the positive SST anomalies were not restricted to the ABA, but reached south of 20ºS extending also to the northern Namibian upwelling region around 23ºS (Fig. 4.2a, also Gammelsrød et al., 1998). In fact, a similar pattern was observed during the 2010/2011 Benguela Niño event, when the strong poleward subsurface Angola current advected warm waters as far as 25ºS (Rouault et al., 2018). In April, warmer waters remained in the region until the demise of the event in May. Concurrently, at the onset of the event in February 1995, a low-salinity plume with negative sea surface salinity (SSS) anomalies of up to -3 psu was present in the area, apparently advected poleward from the north (Fig. 4.2b). This poleward propagation of the low-salinity is consistent with the local current speed and will be addressed in section 4.5.2. At the peak of the event in March 1995, this freshwater plume was observed at around 18ºS, much further south than climatologically expected. In February and March, low-salinity waters in the region, mainly generated by the outflow of the Congo River (blue diamond in Fig. 4.2), are expected to have their maximum southward extension until 12ºS (Awo et al., 2022). The mean observed SSS anomaly for the coastal box 1 (8ºS – 20ºS, 1º wide band along the coast) was almost -2 psu at

the onset of the 1995 event in February, and remained strong in March (Fig. 4.3d). The freshwater influence was initially restricted to the coastal area off Angola, but expanded further offshore in March. In April, the low-salinity pattern started to vanish and the anomalies at the coastal box were within the limit of the standard deviation for this month (Figs 4.2b and 4.3d). Figures 4.3a and 4.3c show that both signals of low SSS and high SST anomalies from the coast to 1º degree offshore are the strongest ones detected for the analyzed period. Negative anomalies of SSS at the coast also peaked at the beginning of 2016 (Fig. 4.3c) during the 2016 warm event. Indeed, Lübbecke et al. (2019) showed that a high freshwater input into the region might also have influenced the SST warming during this event.

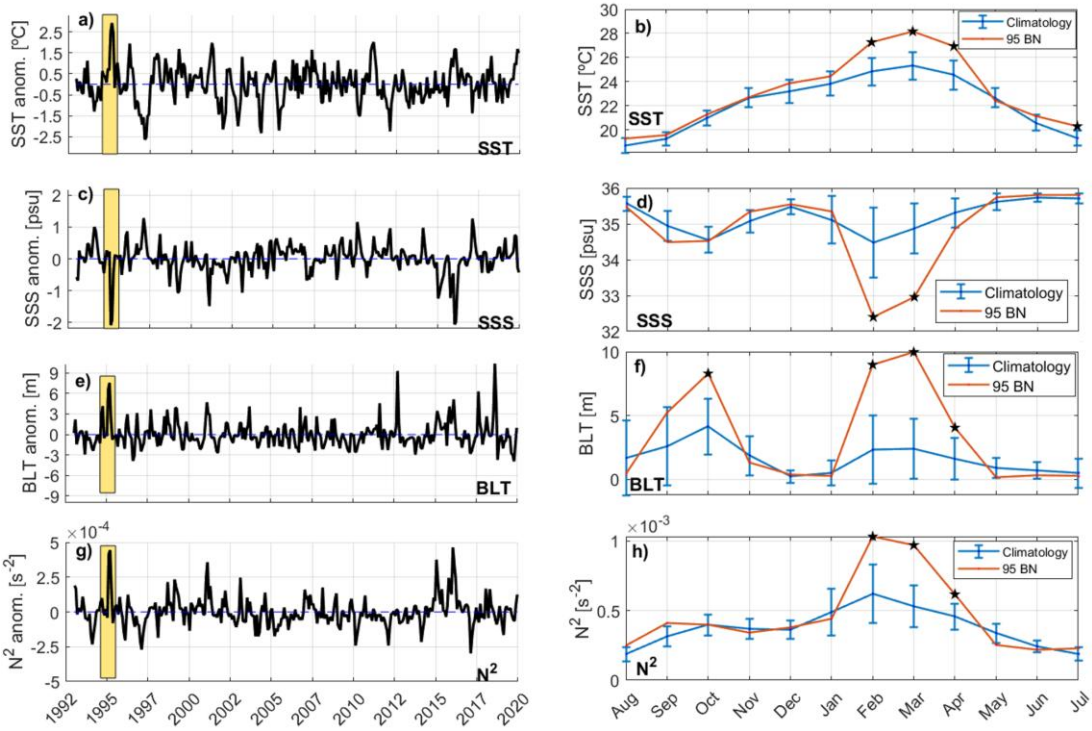

Figure 4.3. Detrended monthly anomalies of SST (a), SSS (c), BLT (e) and N^2 (g) averaged for coastal box 1 region (8ºS – 20ºS, 1º away from coast) from 1993-2019. Yellow shading indicates the period from August 1994 to July 1995. (b) SST climatology (shown from August to July, in blue) calculated over 1993-2019 and monthly values (in red) from August 1994 to July 1995 averaged in the coastal box 1. (d, f, h) same as (b) but for SSS, BLT, and N^2, respectively. Intervals in Figs. (b, d, f, h) depict monthly standard deviation. SST from OISST. SSS from GLORYS12, BLT, and N^2 calculated from GLORYS12 dataset. Black stars in (b), (d), (f) and (h) indicate significant differences from monthly climatologies of each respective month at a 90% confidence level according to the Student's *t* test.

Low surface salinities can lead to the formation of barrier layers and enhance the upper ocean stratification. Concomitant patterns of positive BLT and N^2 anomalies were observed close to the coast at the beginning of the event, reaching further south and spreading offshore in March (Figs. 4.2c and 4.2d). BLT anomalies of up to 15m indicate strong anomalous stratification of the water column, which is also reflected in its stability indicated by the Brünt-Väisäla frequency positive anomaly. The barrier layer presence could also be observed in the CTD profiles taken from the Nansen Programme in 1995 (Figs. 4.1b and 4.1c). The vertical profiles (Figs. 4.1b and 4.1c) show a significant change within 10 days, which is an indication of the importance of submonthly processes acting in the region (Goubanova et al., 2013; Bachèlery et al., 2016a). However, from the vertical profiles of temperature, salinity, and density (not shown) we can see that the presence of the barrier layer on the coast of Angola is persistent from the onset (February 1995) to the demise of the event (April 1995). High stratification was likewise observed during the 2016 warm event (Figs. 4.3e,

4.3g, and in Lübbecke et al., 2019). Freshwater input at the ocean surface creates a shallow mixed layer, where the most pronounced salinity and density gradients are located above the highest temperature gradient (Figs. 4.1b and 4.1c). The difference between the depth of these two gradients creates a more stratified water column, isolating the surface layer from the cooling from below induced by mixing and entrainment, which can favor surface warming.

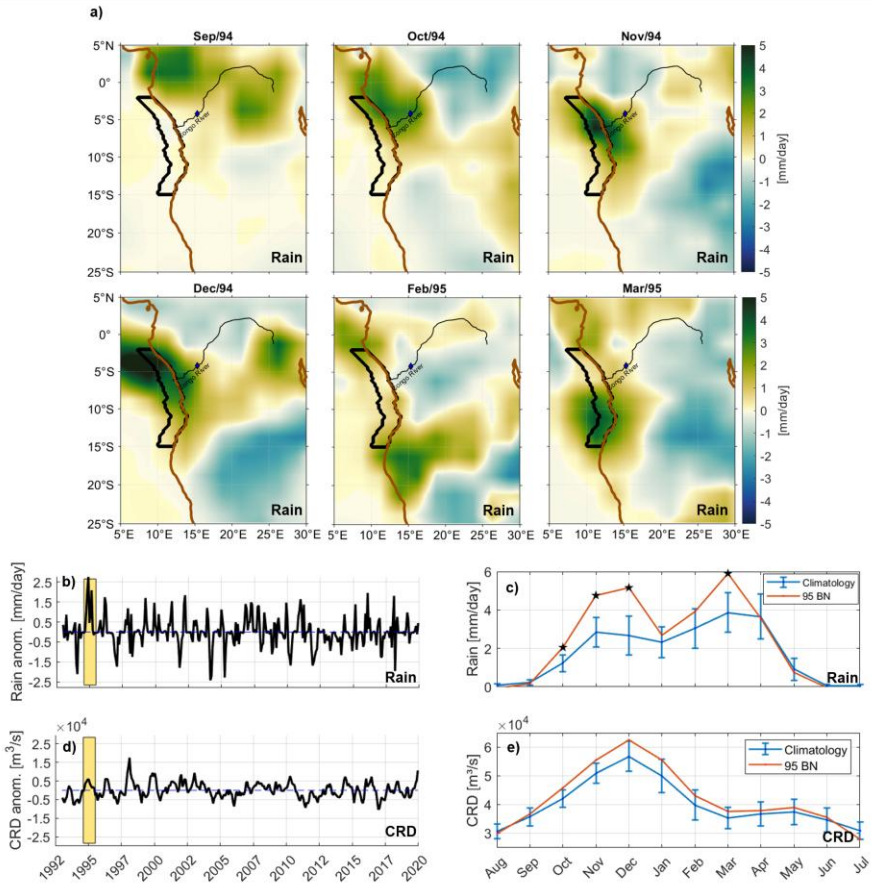

Figure 4.4. Detrended monthly anomalies from September 1994 to March 1995 for precipitation (a). Black thick contours indicate coastal box 2 region (2ºS – 15ºS, 2º away from coast). Brown contour denotes coastline. Blue diamond represents Congo River Brazzaville station. Detrended monthly anomalies of precipitation averaged for coastal box 2 region (b) and Congo River discharge (d) from 1993-2019. Yellow shading indicates the period from August 1994 to July 1995. (c) Precipitation climatology (shown from August to July, in blue) calculated from 1993-2019 and monthly values (in red) from August 1994 to July 1995 averaged in the coastal box 2. (e) same as (c) but for Congo River discharge. Intervals in Figs. (c, e) depict monthly standard deviation. Black stars in (c) and (e) indicate significant differences from monthly climatologies of each respective month at a 90% confidence level according to the Student's t test.

In order to understand the origin of the low salinity plume, we analyzed two possible sources of freshwater input in the region during the event. Precipitation anomalies of up to 5 mm/day were observed prior to the 1995 Benguela Niño event, in November/December 1994, in the proximities of the Congo River mouth around 5ºS, north of the ABA (Fig. 4.4a). The positive anomalies 2-3 months prior to the event were the strongest ones recorded in the time series and were high above the monthly climatological mean and standard deviation (Figs. 4.4b-c). This order of magnitude in precipitation anomalies was not seen in any other year during the 27 years analyzed period. Freshwater input averaged for the coastal box 2 region of around 3 mm/day higher than the climatology was also found in March 1995 (Figs. 4.4a, c). This could already be a response to the surface warming initiated in February 1995, which brings even more non-saline water to

the region via enhanced precipitation, indicating a positive feedback of freshwater input during the event. Regarding the CRD, the data indicate that only in December 1994 the river outflow was higher than climatologically expected, although the difference is not significant (Fig. 4.4e). It also reflects the increased precipitation over land, upstream in the Congo river, from September to November/1994 (Fig. 4.4a). The magnitude of the positive anomaly in the river discharge compared to other years was not exceptional (Fig. 4.4d). However, one can still observe that an anomalous freshwater input from the Congo was present in December 1994, 2 months prior to the onset of the 1995 Benguela Niño.

We conclude that both anomalously high precipitation and Congo River discharge 2-3 months prior to the onset of the 1995 Benguela Niño were main contributors as freshwater sources to the event. Both sources also contributed to the 2016 warm event (Lübbecke et al., 2019). Since the stronger precipitation anomalies in 1994/1995 were located close to the Congo River mouth, one can also conclude that the anomalously high freshwater input in ABA came from the north and was advected southward. However, indicating which freshwater source was the most significant in impacting the warming is beyond the scope of this study. Overall, it was shown that due to both an above-average precipitation and CRD, a freshwater plume was generated and could propagate southward towards the ABA, generating stability and stratification of the water column concomitant with the warm anomalies during the 1995 Benguela Niño. The processes and dynamics that allowed the southward freshwater propagation to occur will be discussed in the next section.

4.5.2 Role of Alongshore Current and Wind Forcing

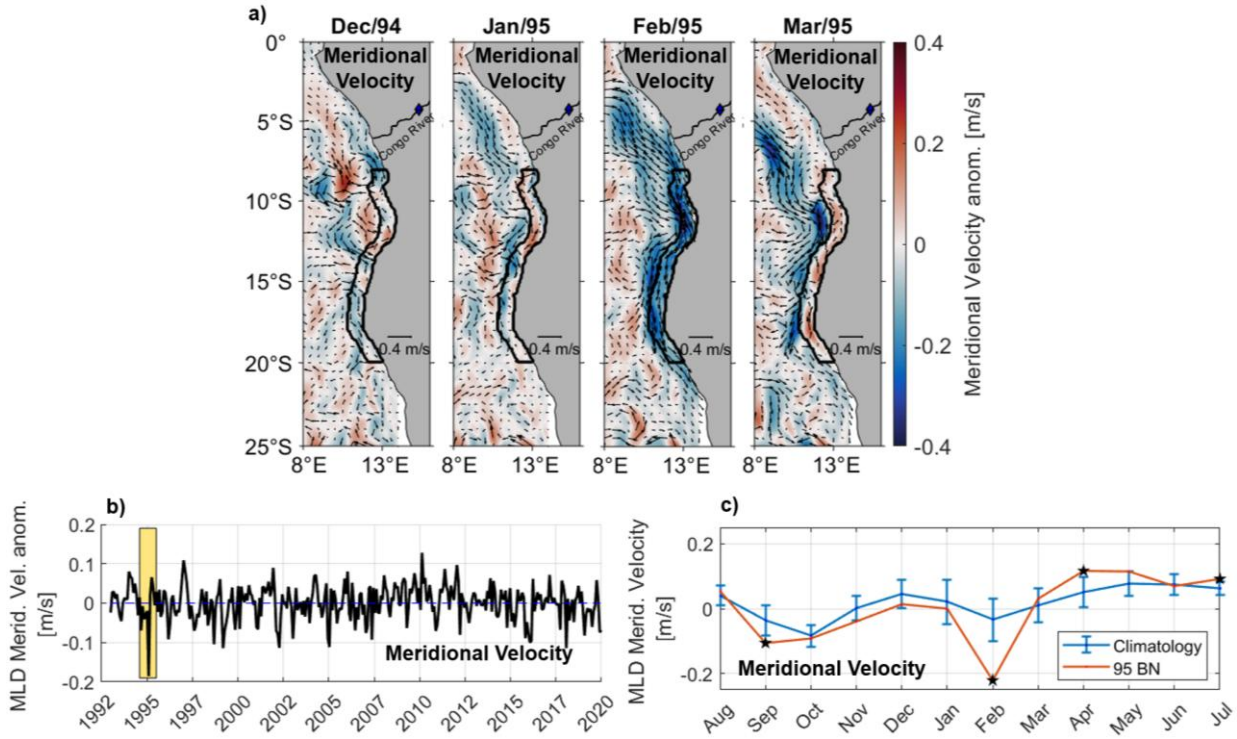

Figure 4.5. Detrended monthly anomalies from December 1994 to March 1995 for mixed layer meridional velocity (a). Arrows indicate the current anomaly direction. Black contours indicate coastal box 1 region. Blue diamond represents Congo River Brazzaville station. Detrended monthly anomalies of mixed layer meridional velocity averaged for coastal box 1 region from 1993-2019 (b). Yellow shading indicates the period from August 1994 to July 1995. Mixed layer meridional velocity climatology (shown from August to July, in blue) calculated from 1993-2019 and monthly values (in red) from August 1994 to July 1995 averaged in the coastal box 1 (c). Intervals in Fig. (c) depict monthly standard deviation. Black stars in (c) indicate significant differences from monthly climatologies of each respective month at a 90% confidence level according to the Student's t test.

In the southeastern tropical Atlantic, low-salinity waters, mainly from the CRD, and their southward propagation are usually restricted to 12ºS (Awo et al., 2022). However, as shown in the previous section, during the 1995 Benguela Niño the freshwater plume was advected further south in February and March, until around 18ºS. In order to investigate what might have caused this anomalous poleward transport during the warm event, we analyzed the mixed layer meridional current anomalies from the GLORYS reanalysis product. From January 1995, a southward current anomaly at around 3ºS and 2º offshore of the coast started to develop (Fig. 4.5a). In February 1995, this negative current anomaly was even stronger (i.e. about -0.4 m/s) and was shifted closer to the coast (Fig. 4.5a). In March 1995, the southward anomaly weakened and was again moving offshore. The really strong negative signal observed in February 1995 is even more clearly visible when averaging the current anomalies for the coastal box 1 (Figs. 4.5b and 4.5c). From the analyzed period, this month had by far the strongest southward current observed at the mixed layer. February 1995 was also the month with the fastest southward advection of the low salinity plume. The -1 psu signal at 10ºS in January 1995 to 18ºS in February 1995 (see Fig. 4.2b) propagated southward with a roughly estimated speed of about 0.37m/s. This estimate agrees in magnitude with the mixed layer current anomaly strength. In addition, the meridional velocity anomalies started to develop in December/January 1995 close to the Congo River mouth concomitantly with the strong precipitation observed in December in the same region.

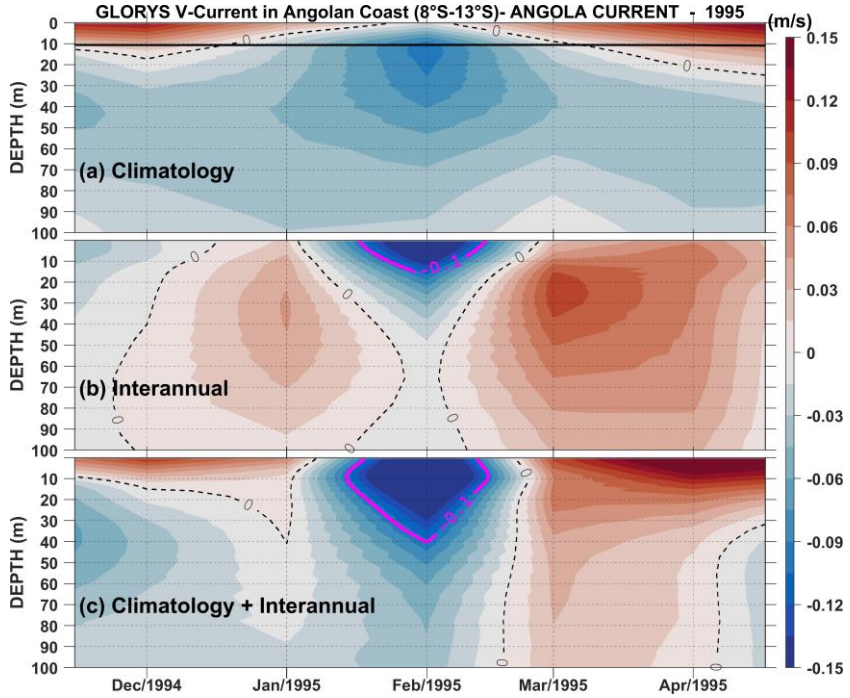

Figure 4.6. Depth-time Hovmöller diagram of climatology (calculated from 1993 to 2019, and shown between November and April) (a), monthly detrended anomalies (b), and absolute values (c) of coastal Angolan meridional current (v) averaged from 8ºS to 13ºS, 1º away from the coast (b, c) are shown from November 1994 to April 1995. The black line represents the density ocean mixed layer thickness obtained directly from GLORYS12 reanalysis, defined by sigma theta, and also averaged for the same area. Magenta contour depicts -0.1m/s isoline.

It is known that the Angola Current has its core at subsurface (Tchipalanga et al., 2018; Kopte et al., 2017). It might be argued that this current could not be driving the southward transport of the low-salinity signal in the 1995 Benguela Niño, since the freshwater input generated a very shallow mixed layer and hence a surface current would be needed to carry the low-salinity plume. This raises the question of the mechanism behind the southward transport of the freshwater plume.

In order to tackle this question, we analyzed both GLORYS12 velocities at depth and wind data from CCMP. From the vertical structure of the meridional current during the 1995 Benguela Niño (Fig. 4.6), we could see an anomalously strong surface poleward current at the coast. While the Angola Current core from the GLORYS12 reanalysis is climatologically situated at 10-20m depth in February (Fig. 4.6a), during February 1995, the strongest southward anomalies were found especially at the surface (Fig. 4.6b). Note that during this event, not only the position of this highest poleward velocities was lifted upward but also the current strength was higher. Both of these features can only be reached by strong shifts in the wind field in the same period since local wind stress and wind stress curl are the main drivers of the strengthening and uplifting of the Angola Current (Fennel et al., 2012; Tchipalanga et al., 2018).

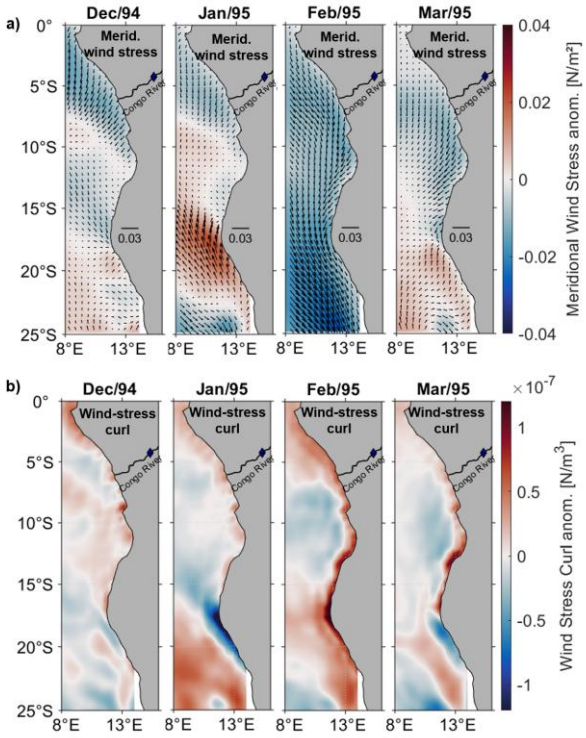

Figure 4.7. Detrended monthly meridional wind-stress anomalies (a) and wind-stress curl anomalies from December 1994 to March 1995 (b). Arrows indicate the direction of the wind stress anomaly. Blue diamond represents Congo River Brazzaville station. Positive values in (b) indicate weakening of the wind stress curl.

Overall, in the region, southerly winds that strengthen seaward are observed, leading to a negative (cyclonic) wind stress curl close to the coast (e.g. Lübbecke et al., 2019). However, during the 1995 event, we could observe changes in both wind stress and wind stress curl (Fig. 4.7). From December 1994 to January 1995, the meridional wind stress weakened (Fig. 4.7a) around 5ºS-7ºS, concomitant with the onset of the poleward current anomaly development (Fig. 4.5a). In February 1995, the wind stress was even weaker offshore, and the weakening extended to the whole region, exactly at the time when the poleward current anomaly was strongest. Concomitantly, a strong weakening (strengthening) of the wind stress curl, indicated by positive (negative) anomalies in Figure 4.7b, was observed throughout the African coast (offshore). These shifts in the curl were most pronounced in February 1995 from 7ºS to 13ºS, indicating stronger than normal winds at the coast in this latitudinal band. Consequently, reduced (enhanced) coastal (offshore) wind stress curl was generated. Fennel et al. (2012) showed that under this scenario, with a diminished wind stress curl at the coast, the equatorward coastal jet weakens and the undercurrent (i.e. the Angola Current) is able to

reach the surface, which explains the anomalously strong surface poleward current at the coast observed during the 1995 event.

4.5.3 Processes driving the warming

The combination of a high CRD and precipitation concomitant with the strong southward Angola Current and its uplifted core to the surface were shown to be the main drivers of the anomalous high freshwater input into the Angolan coast during the 1995 Benguela Niño. Now, we investigate what processes led to the surface warming by performing a mixed layer heat budget analysis (see section 4.4.2.2) for the coastal region off Angola during this anomalous event. We first describe the mechanisms responsible for the climatological heat budget, and then discuss the anomalies during the 1995 event.

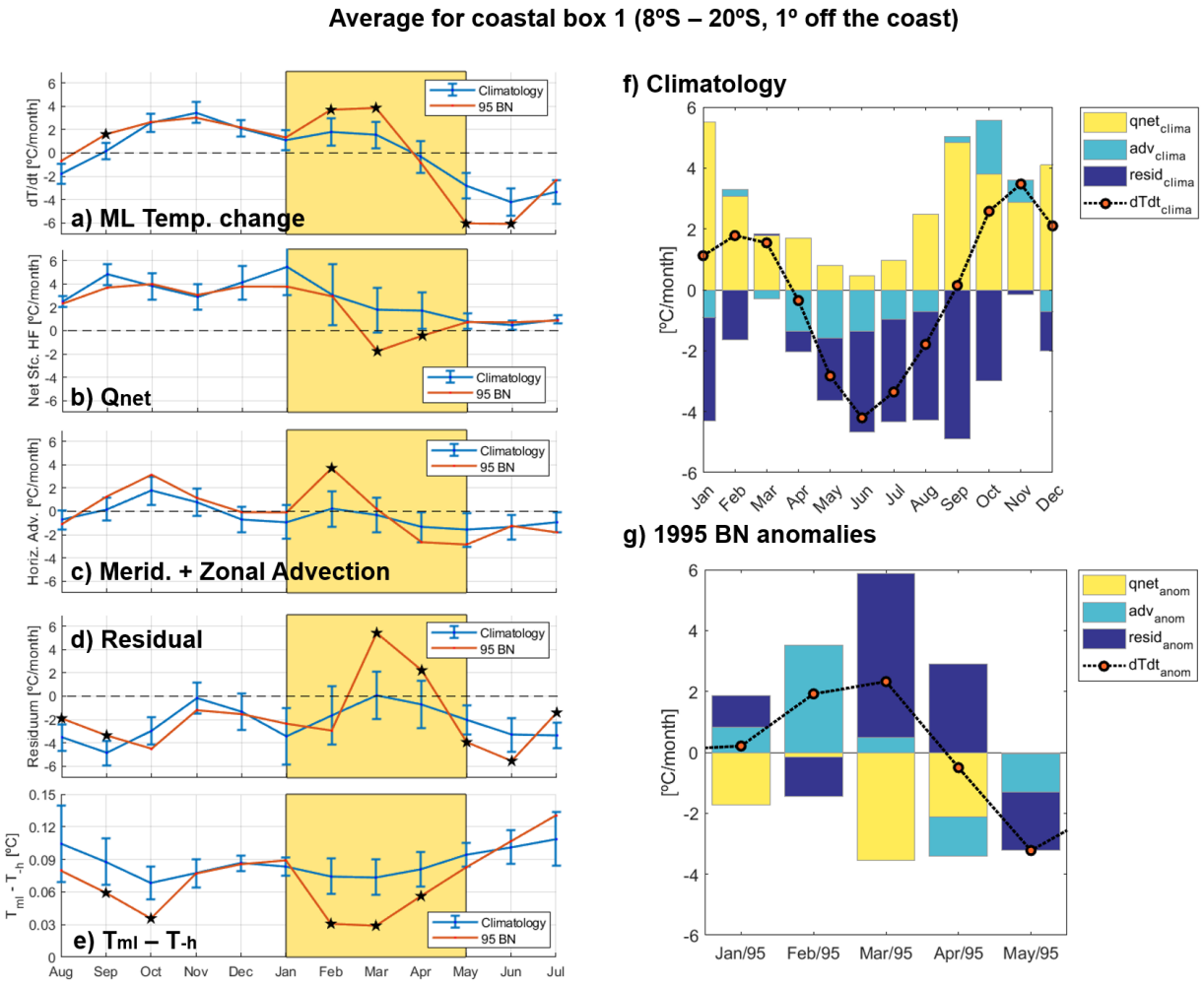

Figure 4.8. Monthly climatology (blue) of the terms from mixed layer heat budget equation averaged for coastal box 1 from 1993-2019 depicted from August to July for a) Temperature tendency; b) Net surface heat flux; c) Horizontal advection; d) Residual; e) Temperature gradient (i.e. difference between ML temperature and temperature at the base of ML). Intervals indicate monthly standard deviation. a-e) In red are monthly values from August 1994 to July 1995 of the parameters mentioned above, respectively. f) Climatological contribution of each calculated term for coastal box 1 mixed layer temperature between 1993-2019. g) Detrended monthly anomalies of the terms from mixed layer heat budget equation averaged for coastal box 1 from November 1994 to May 1995 coastal box. Black stars in (a-e) indicate significant differences from monthly climatologies of each respective month at a 90% confidence level according to the Student's *t* test. Yellow shading in (a-e) indicates the period from January to May 1995.

The monthly climatology of each term with its monthly standard deviation is shown in Figures 4.8a-e. Figure 4.8f depicts the contribution of each term to the climatological surface warming (positive) and

cooling (negative). As recently shown by Körner et al. (2023), the mixed layer heat content in this region is climatologically dominated by the surface heat fluxes and turbulent heat loss at the base of the mixed layer, here included in the residual term. The highest (lowest) temperatures are observed in austral summer (winter) when the net surface heat fluxes warming the ocean's upper layer are strongest (weakest) (Fig. 4.8f). In addition, the residual term is a cooling term throughout the year. Further, the mean horizontal advection plays a cooling role, especially during austral winter (Fig. 4.8f), when the Angola-Benguela front is located furthest north. Still, the temperature gradient and currents are stronger in the meridional direction suggesting that the meridional advection plays a more prominent role in this term than the zonal. In fact, the October peak in warming due to advection (Fig. 4.8f) is sustained by the southward Angola Current bringing warm equatorial waters further south (Körner et al., 2023).

Figure 4.8g depicts the anomalies of each term of the heat budget equation during the 1995 Benguela Niño, while Figures 4.8a-e show anomalies significantly different in relation to the monthly climatology (i.e. black stars). During the event's development and demise significant shifts in the ML temperature for the coastal area were observed at its onset in February, at its peak in March 1995, and at its demise in May 1995 (Fig. 4.8a). Within this period we can as well observe the reduced temperature gradient between the ML and its base (Fig. 4.8e). During February and March, for instance, the ML temperature gradient is almost 3 times weaker than climatologically. Hence, we focus on explaining the anomalies within these months (i.e. yellow shading in Figs. 4.8a-e). In February 1995, the advection term was the only contributor to the warming of the mixed layer off Angola, concomitant with the strong anomalous poleward surface current in this month (Fig. 4.5c), bringing warm waters further south. Even though the net heat flux average for the coastal box 1 indicates a net cooling during this month (Fig. 4.8g), from the spatial anomalies (Fig. 4.16b) we can see a positive anomaly from 8ºS to 13ºS, which might also have contributed to warming the waters further advected southward. In addition, positive residual anomalies are present at the coast during February (Fig. 4.16d), from the River mouth until 15ºS. The net residual cooling in February appears to be counteracting the advection warming, although the residual shift in this month is not significant (Fig. 4.8d). On the other hand, in March 1995 during the peak of the event, the advection term stood for only 8% of the sum of the anomalous warming terms at the coast off Angola (Fig. 4.8g), contributing mostly to the warming offshore of the box (Fig. 4.16c). The main contributor to warming up the mixed layer at the coastal region in March was by far the residual term (i.e. 92%, Fig. 4.8g). Noteworthy, the residual spatial positive anomalies during March agree well with the SSS and BLT anomalies up to 18ºS (Fig. 4.16 and Fig. 4.2b,c). The same is observed for the following April. The significantly reduced ML temperature gradient within these months indicates the location of the mixed layer base within the isothermal layer (Fig. 4.1b,c), which leads to reduced turbulent heat loss at the base of the ML, since the turbulent mixing acts on a weak vertical temperature gradient (White & Toumi, 2014). Consequently, strong positive residual anomalies are observed in March and April. In fact, turbulent heat loss, here included in the residual term, is a crucial mechanism in this region not only for the cooling especially near the coast but also for an upward salt flux, bringing the more saline subsurface water towards the surface (Awo et al., 2022; Körner et al., 2023). The high residual anomaly maintained the surface warming during March 1995, counteracting the surface cooling in the same month due to surface heat fluxes. This

damping term in the heat fluxes was mainly due to a significant latent heat loss in March 1995 (Figure 4.14). In April 1995 the high positive anomaly in the residual term (i.e. possibly related to the remaining stability due to the lower surface salinity during this month) was counteracted by surface heat fluxes and the northward advection of cool waters from the south, which contributed to the demise the event. The residual term will also be discussed in the next section.

Overall, when considering the mean interannual anomalies for each term (Fig. 4.15) we find that the 1995 Benguela Niño event stands out especially in terms of advection, residual, and ML temperature gradient anomalies. The advection anomaly in February 1995 was in fact the highest positive advection anomaly observed in the 27 years analyzed period (Fig. 4.15a). The advection term has acted as the main factor to initially warm the surface waters by bringing warmer equatorial waters to the ABA. The extremely strong poleward current might also have contributed to taking this warming further south than 20ºS. At the same time, one of the strongest residual anomalies was also seen during the 1995 event, together with the most negative anomaly in the ML temperature gradient for almost 3 decades (Fig. 4.15d-e). In fact, Figure 4.15e shows that this gradient was also extremely reduced during the 2016 warming event, which was also likely to have been influenced by an anomalous freshwater input (Lübbecke et al., 2019). Indeed, the ML temperature gradient anomaly time-series agrees quite well with both the N^2 and BLT anomaly time-series (i.e. r = -0.41, r = -0.53, respectively) as well as with the SSS anomalies (i.e. r = 0.48). Hence, our results suggest that the combination of the initial strong advection by the poleward current at the surface, and subsequently less turbulent mixing due to higher water column stability resulted in the strongest Benguela Niño event ever recorded in the satellite era.

4.6 Summary and Discussion

In this study, we described the strong 1995 Benguela Niño and investigated the role of anomalous freshwater input into the ABA (8ºS – 20ºS, 8ºE to the coast) during this event. We analyzed the impact of this low-salinity anomaly on the temperature change within the mixed layer at the onset of the warming, highlighting the importance of the dynamical mechanism that allowed the freshwater plume to be advected from north of Angola to the ABA.

The 1995 Benguela Niño developed in February 1995 and peaked in the following March with averaged SST anomalies of up to 2.5ºC in the ABA coastal region (8ºS – 20ºS, 1º away from the coast). Simultaneously, an anomalous low-salinity plume was present in the region, shoaling the mixed layer and generating higher water column stratification and stability due to barrier layer anomalies of up to 15m. A large barrier layer contributes to the surface warming by inhibiting the cooling from below due to entrainment and mixing. The strong freshwater input resulted from a combination of the anomalous high CRD and precipitation in the months prior to the event and was advected from around 2º-5ºS to 18ºS, much further south than climatologically expected (Awo et al., 2022). This low-salinity plume advection was only possible due to a concomitant surfacing and strengthening of the Angola Current, which occurred due to a weakening of the coastal wind stress curl and wind stress during the event, allowing the current core to be present at the

coast and to move from subsurface to the surface. This anomalous poleward transport partially explaining the intensity of the 1995 event was also suggested by Rouault (2012).

In addition to this, a CTW might also have played a role in strengthening the southward current. A previous study recorded the presence of an intraseasonal downwelling CTW in March 1995, 2 weeks before the peak of the event, with an amplitude of almost 3 cm (Imbol Koungue & Brandt, 2021). Furthermore, a much higher than usual Angola Current transport of 11 Sv from January to March 1995 was reported during the 1995 Benguela Niño (Mercier et al., 2003). Moreover, Sena Martins and Stammer (2022) recently stated that the causes of low-salinities anomalies spreading southward in this area were a higher CRD combined with the occurrence of the CTW between February and March. Hence, since the Angola Current variability is highly controlled by the passage of these waves (Bachèlery et al., 2016a; Kopte et al., 2017; Tchipalanga et al., 2018), we suggest that this CTW might also have contributed to the strong southward current transport. It appears that during the 1995 event, the combination of relaxed southerly winds offshore and the weakening of the wind stress curl at the coast, uplifting the Angola Current core to the surface, with the apparent presence of the CTW and an above climatology freshwater input in the region were the mechanisms that allowed low-salinity anomalies to reach the ABA.

The mixed layer heat budget analysis approach has been widely used to identify sources of surface warming in the tropical Atlantic, both from observational datasets (e.g. Foltz et al., 2003; Hummels et al., 2014; Foltz et al., 2020; Hummels et al., 2020; Körner et al., 2023), and reanalysis product (Ma et al., 2023). Our analysis showed that anomalous advection was responsible for the warming at the onset of the event, in February, while the residual term was the main contributor during the peak of the event in March. In this study, the residual term includes the effect of turbulent mixing, processes not represented by the temporal and spatial scale of the dataset here used, and errors of the other terms. The errors in this region are likely influenced by uncertainties arising from the SWR in the net surface heat fluxes (Körner et al., 2023) due to poor representation of shallow clouds (Huang et al., 2007). Additionally, sub-monthly variability within the Angolan coast (Goubanova et al., 2013; Bachèlery et al., 2016a) is likely to contribute to the residual term. However, the residual of the ML heat budget in this region can be assumed to be largely explained by the turbulent mixing at the base of the ML, especially in shallow regions close to the coast (Körner et al., 2023). The energy source of the turbulent mixing is the interaction of internal waves with the continental slope (Zeng et al., 2021). Zeng et al. (2021) find that the mixing is essentially more effective when stratification is weaker. The stratification in the ABA region is connected to freshwater fluxes, surface heat fluxes, and the passage of CTWs (Awo et al. 2022, Zeng et al., 2021; Körner et al., 2023). The freshwater plume present in coastal waters during the 1995 Benguela Niño influences turbulent mixing at the base of the mixed layer in two ways. Firstly, the available energy for mixing acts on a stronger stratification decreasing the eddy diffusivity (White & Toumi, 2014; Zeng et al. 2021, Körner et al. 2023). Secondly, in the presence of high freshwater input and the consequent barrier layer formation, the temperature gradient between the mixed layer and the water below it (i.e. $\bar{T}_{ML} - T_{-h}$) is close to zero (e.g. Echols & Riser, 2020), as the mixed layer base resides within the isothermal layer. Thus, the turbulent mixing acts on a weak vertical temperature gradient (White & Toumi, 2014). Hence, the anomalously high freshwater during early 1995 reduces the turbulent heat loss. The barrier

layer presence and higher water column stability impact were observed especially in March 1995. It is also likely that this impact remained important in April 1995 since an anomaly in the residual term was still high in this month. Overall, we showed that an anomalous freshwater input in the ABA can indeed significantly contribute to the surface warming during a Benguela Niño, and should also be taken into account as a local forcing for these events. We also observed that this influence strongly depends on the advection of the freshwater to the south and thus on shifts in the wind field.

The influence of freshwater input in the generation of barrier layers in the southeastern tropical Atlantic that increased ocean stratification and stability has been discussed in previous studies (Materia et al., 2012; White & Toumi, 2014; Lübbecke et al., 2019; Sena Martins & Stammer, 2022). Salinity shifts impacting surface warming in the tropical Atlantic via barrier layer formation and stratification have also been recently assessed (Gévaudan et al., 2021). There is, however, no consensus on the importance of barrier layers generating surface warming in the Equatorial and tropical Atlantic. While Pailler et al. (1999) and Foltz & McPhaden (2009) indicated strong warming related to barrier layers, Balaguru et al. (2012), Hernandez et al. (2016), and Gévaudan et al. (2021) found no significant relationship between these variables based on models. It was seen that salinity stratification can indeed play a major role in stabilizing surface layers of the ocean, leading to the upper-layer warming (Maes & O'Kane, 2014). However, it is hard to establish a direct correlation on interannual timescales also for the southeastern tropical Atlantic (White & Toumi, 2014; Sena Martins and Stammer, 2022), due to different processes affecting and changing the SST. When referring to Benguela Niños, it seems even more difficult, since the freshwater input does not seem to trigger these events, which are caused either remotely by the propagation of an equatorial Kelvin wave followed by a CTW at the African coast due to equatorial wind shifts, or by local atmospheric and wind changes (Florenchie et al., 2003; Richter et al., 2010; Rouault et al., 2018; Imbol Koungue et al., 2019). Still, such unique freshwater propagation as in this specific 1995 event indeed contributed to the surface warming.

In relation to Benguela Niñas, we believe that a lower freshwater input would not be an important factor in intensifying these cooling events. Climatologically, the low salinity plume is not usually spread over the whole ABA (Awo et al., 2022). Hence, in anomalous years of lower precipitation/river discharge, no significant change in the stratification off Angola would be observed. High freshwater input could, however, be a factor counteracting a cooling event. In these cases, the SST change during a Benguela Niña would be decreased, since the cooling event would be counteracted by the warming due to lower SSS and higher stratification. Still, this is very speculative and overall we believe that a freshwater input would not impact a Benguela Niña event the same way as it could do with the Benguela Niños.

Some open questions remain and should be approached in future studies. First, it is still unclear which mechanism is the most prominent driver in generating the negative salinity anomalies in ABA. We wonder if a high anomalous freshwater input would be enough to generate such anomalies, or if this freshwater plume presence in the Angolan-Nambian coast is only possible combined with a stronger Angola Current core at the surface. It is likely that in years of strong poleward Angola Current, freshwater especially from the CRD might be brought to the ABA. However, is it uncertain if solely the freshwater transport could generate stratification anomalies or if an anomalous freshwater input is also required. Further, White & Toumi (2014)

when evaluating the impact of the amount of freshwater input from the Congo River on the spatial distribution of SST, did not find any significant changes between the control and the double CRD simulations. They suggested that the location of temperature changes is more dependent on environmental conditions than on the magnitude of the freshwater input (White & Toumi, 2014). In addition, the most important freshwater source to generate such salinity anomalies could not be clearly distinguished in our study between an anomalous CRD or precipitation. Different model simulations and experiments with climatological and reference river runoff and precipitation, like the works from Zhang & Busalacchi (2009) and White & Toumi (2014) could provide these answers. Furthermore, besides the 1995 Benguela Niño and the 2016 warming event, we highlight that the freshwater might also impact other events (e.g. 2001 Benguela Niño) as shown by the time series anomalies in Figure 3. Thus, the general influence of the freshwater input on the SST variability in the southeastern tropical Atlantic is still not well defined. Still, we could conclude from the present analysis that the freshwater input into the ABA related to the strength of the Angola Current is an active local forcing player in the intensification of Benguela Niños.

Acknowledgments. This study was supported by: the German Academic Exchange Service (DAAD) Doctoral Research Grant (Number 57552340); the EU H2020 program under grant agreement 817578 (TRIATLAS project); and the German Research Foundation through grant no. 511812462 (IM 218/1-1). The received funding did not lead to any conflict of interest regarding the publication of this manuscript. The authors thank the captains, crews, scientists, and technicians involved in several research cruises in the Angola-Namibian waters who contributed to collecting data used in this study. We thank M. Dengler and R. Hummels for their helpful insights and discussion in part of the analysis for this research. We are also grateful to the two anonymous reviewers for their valuable comments and suggestions, which helped improve the quality of the present paper.

Open Research. All datasets and products used in this work are freely available in the following links: OISST (https://psl.noaa.gov/data/gridded/data.noaa.oisst.v2.highres.html); CCMP 6-hourly wind vectors (https://www.remss.com/measurements/ccmp/); ECMWF ERA5 surface heat flux (https://cds.climate.copernicus.eu/cdsapp#!/dataset/reanalysis-era5-single-levels-monthly-means?tab=form); The near-surface drifter-wind-altimetry synthesis can be accessed via: https://www.aoml.noaa.gov/ftp/phod/pub/lumpkin/decomp/; Congo River discharge was obtained from https://hybam.obs-mip.fr/data/; Precipitation from the GPCP product is available via https://psl.noaa.gov/data/gridded/data.gpcp.html; GLORYS12 product is available at https://data.marine.copernicus.eu/product/GLOBAL_MULTIYEAR_PHY_001_030/download; CTD profiles from the Nansen Programme are publicly available at https://doi.pangaea.de/10.1594/PANGAEA.886492; (Tchipalanga et al., 2018b). Flow velocities from mooring data at 11˚S are available at https://doi.pangaea.de/10.1594/PANGAEA.939249 (Hummels et al. 2021). CTD sections from previous cruises can be accessed via: M98 (2013; https://doi.pangaea.de/10.1594/PANGAEA.868640), Krahmann & Brandt, 2016); M120 (2015;

https://doi.pangaea.de/10.1594/PANGAEA.868654, Kopte & Dengler, 2016); M131 (2016; https://doi.pangaea.de/10.1594/PANGAEA.910994, Brandt et al., 2020); M148 (2018; https://doi.pangaea.de/10.1594/PANGAEA.928997, Dengler et al., 2021); M158 (2019; https://doi.org/10.1594/PANGAEA.952354, Brandt et al., 2022).

4.7 Supplementary Material

Introduction

Text S1 compares the GLORYS reanalysis product against *in-situ* measurements from CTD cruise sections, CTD profiles from Nansen Programme, mooring observations, and drogued drifters. Figure 4.9 indicates the location of in-situ measurements obtained from different cruises. Figures 4.10, 4.11, 4.12 and 4.13 show the GLORYS reanalysis product capacity in reproducing these observations (temperature, salinity, current velocity) taken at the locations indicated in Figure 4.9. Figures 4.14, 4.15, and 4.16 add to the discussion on the Mixed Layer Temperature Change, depicting respectively the climatological surface heat fluxes in comparison with the 1995 Benguela Niño event, and the interannual anomalies of each term of the Mixed Layer Heat Budget equation.

Text S1: Comparison of GLORYS reanalysis with *in-situ* measurements

In order to evaluate GLORYS capacity in reproducing the main processes occurring in ABA, in-situ measurements were compared to this reanalysis product. CTD sections of temperature and salinity at around 11ºS (Fig. 4.9) from five different cruises were compared to the daily GLORYS reanalysis (Fig. 4.10). The sections were taken from: 21-23 July 2013 (M098); 28-31 October 2015 (M120); 27-28 October 2016 (M131); 16-19 June 2018 (M148) and 23-24 September 2019 (M158). The GLORYS product was interpolated into a 1/100º grid and the same positions of the cruise sections were selected in the reanalysis product. The daily GLORYS was then averaged for the corresponding days of each cruise section. While the agreement is in general high, a discrepancy between the compared datasets was observed within the M131 section, taken in October 2016, with the reanalysis underestimating the salinity values in the upper 30m of the water column (Fig. 4.10). This is likely related to the fact that GLORYS12 uses a climatological CRD input which might overestimate (underestimate) salinity values in years of anomalously high (low) CRD. In fact, one of the highest negative anomalies recorded from 1993-2019 in the CRD (Fig.4.4d) was in September/October 2016 which could explain the difference observed between the M131 section and the reanalysis. Overall, the reanalysis product can quite well reproduce the observed temperature and salinity profiles for almost all sections (Fig. 4.10).

In addition, flow velocities were obtained from a moored current meter off Angola at 13º00'E, 10º50'S (Kopte et al., 2017). The mooring records current velocities up to 45m below the sea surface since July 2013 with an upward-looking 75-kHz Long Ranger acoustic Doppler current profiler (ADCP). The mooring location is indicated in Figure 4.9. The almost 10-year long dataset allows a climatological comparison of the velocities against the GLORYS reanalysis product currents (Fig. 4.11). The GLORYS grid

point nearest to the mooring position was selected and both zonal and meridional currents from the mooring and GLORYS product were rotated by -34º against the North in order to derive cross-shore and alongshore velocities regarding the orientation from the Angolan coast. In terms of magnitude, one can see that the alongshore component is much stronger than the cross-shore, being, therefore, more easily reproduced by GLORYS (Fig. 4.11). In addition, the upper 200m alternating poleward (Angola Current – AC) and equatorward flow (Kopte et al., 2017; Tchipalanga et al., 2018) could also be seen in both datasets, even though the mooring measurements are limited to below 45m. Signals of the two seasonal peaks (i.e. February-March and October) in the strength of the AC could as well be observed in the mooring data and in the reanalysis. One feature that GLORYS is not able to reproduce well is the equatorward flow between 100-300m from April to June. However, this might be irrelevant to this study since we are focusing mostly on the shallower currents, and in periods from January to March. Overall, the reanalysis product seems to reproduce quite well both cross-shore and alongshore currents, especially the latter, in terms of magnitude and seasonality.

Concomitantly, we used monthly averages of daily 15-m current, with 0.25º x 0.25º spatial resolution, consisting of estimates from a synthesis product of in-situ drogued drifter velocities measurements, satellite-derived Ekman velocities, and geostrophic velocities from sea level anomalies (Lumpkin & Garzoli, 2011; Perez et al., 2019). This dataset is available from 1993 to 2021. The mixed layer current speed from the GLORYS product (Fig. 4.5) also agrees well with the 15-m current measurements (Fig. 4.12) in terms of magnitude and current direction.

Finally, more than 8000 CTD profiles collected along the entire Angolan coast from the Nansen Programme (Tchipalanga et al., 2018) and taken between March 1995 and March 2014 were used to validate the GLORYS temperature and salinity datasets in the region. Each profile was limited to 230m depth and the GLORYS product was interpolated again into an even 1/100º horizontal grid, and later into an even 1 m depth vertical grid. Each CTD position was then selected for the reanalysis product and both datasets were compared (Fig. 4.13). The Taylor diagram shows good correlations between GLORYS and CTD profiles for both temperature (i.e. 0.96) and salinity (i.e. 0.68) and also close values for Root-Mean Squared Difference (RMSD) and Standard Deviations (Fig. 4.13). Therefore, through comparison with different in-situ measurements, we conclude that the GLORYS12 product provides a quite good representation of the temperature, salinity, and current velocities observed for the Angola-Benguela region.

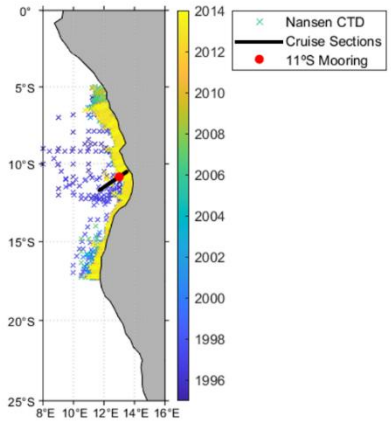

Figure 4.9. Location of CTD profiles, Cruises Sections, and 11ºS mooring.

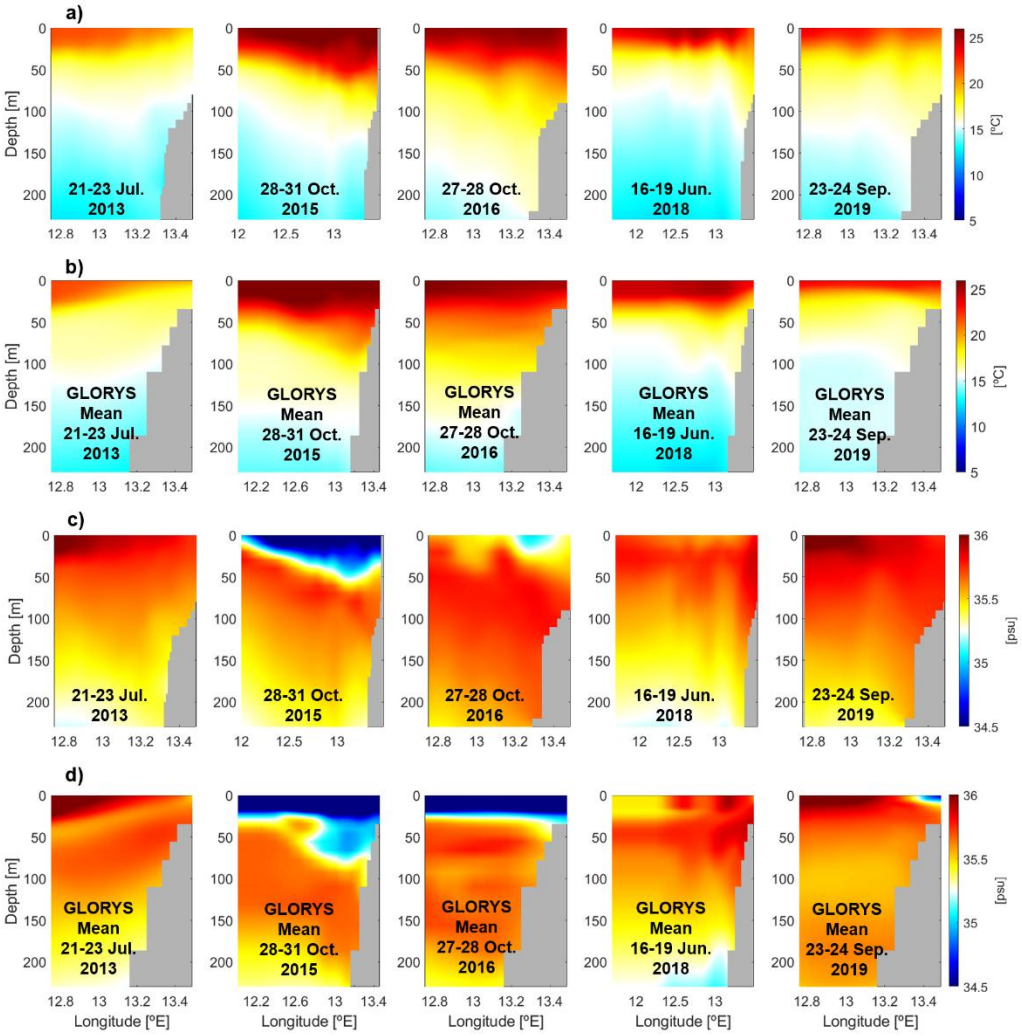

Figure 4.10. CTD sections from the 5 different cruises depicting temperature (a) and salinity (c) profiles, with their corresponding sections in interpolated GLORYS dataset for temperature (b) and salinity (d). GLORYS sections are taken as the average of the daily fields that match cruises sections dates.

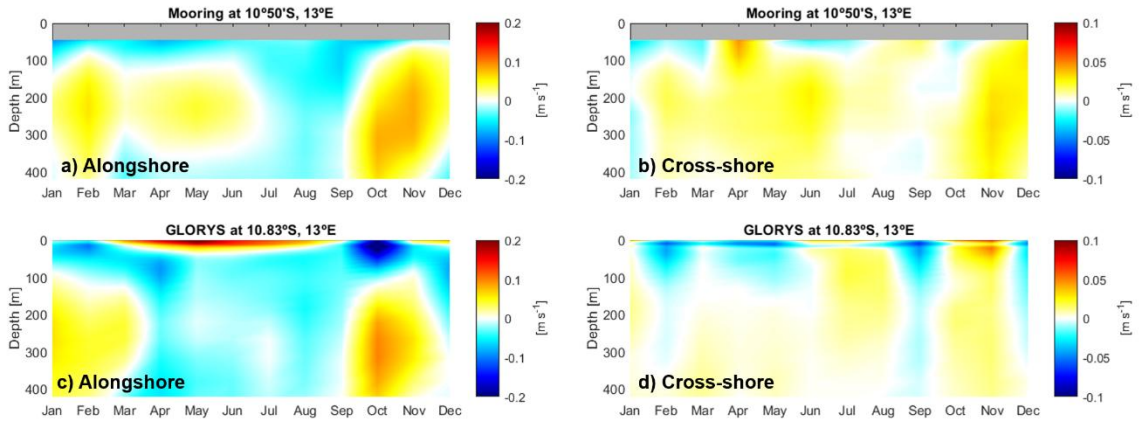

Figure 4.11. Alongshore (a, c) and Cross-shore (b, d) velocity climatology (rotated by -34º with respect to true north) recorded by the moored ADCP located at 10º50'S, 13º00'E (a, b) and the corresponding climatology taken from GLORYS dataset (c, d) at nearest grid position from mooring location and -34º rotation. Both climatologies were calculated over the period 2013 – 2019.

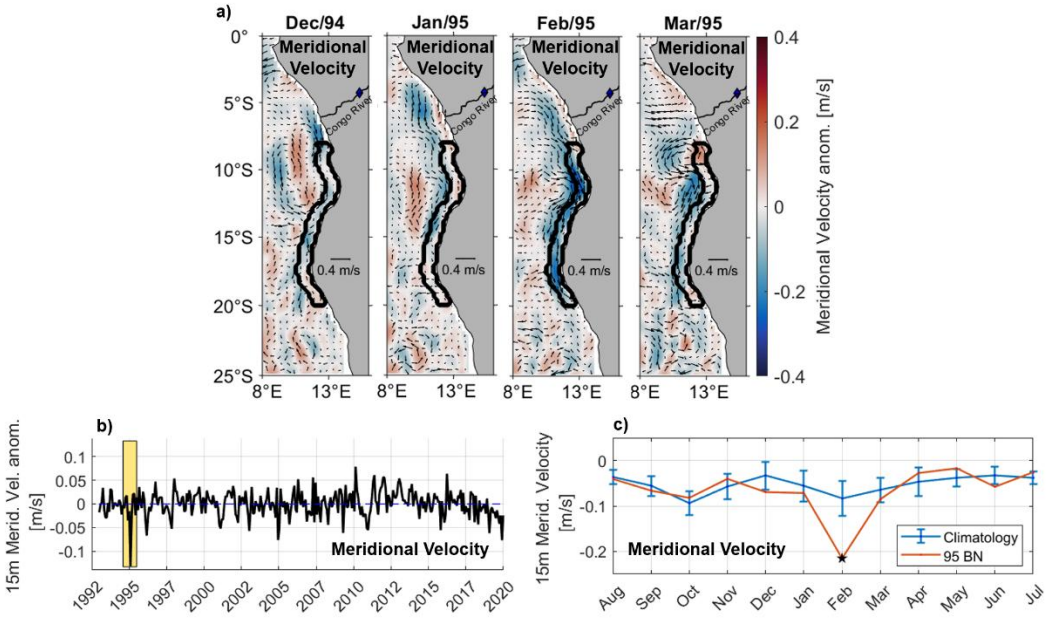

Figure 4.12. Detrended monthly anomalies from December 1994 to March 1995 for meridional velocity (a). Arrows indicate the current anomaly direction. Black contours indicate coastal box 1 region. Blue diamond represents Congo River Brazzaville station. Detrended monthly anomalies of meridional velocity averaged for coastal box 1 region from 1993-2019 (b). Yellow shading indicates the period from August 1994 to July 1995. Meridional velocity climatology (shown from August to July, in blue) calculated from 1993-2019 and monthly values (in red) from August 1994 to July 1995 averaged in the coastal box 1 (c). Intervals in Fig. (c) depict monthly standard deviation. Black stars in (c) indicate significant differences from monthly climatologies of each respective month at a 90% confidence level according to the Student's t test.

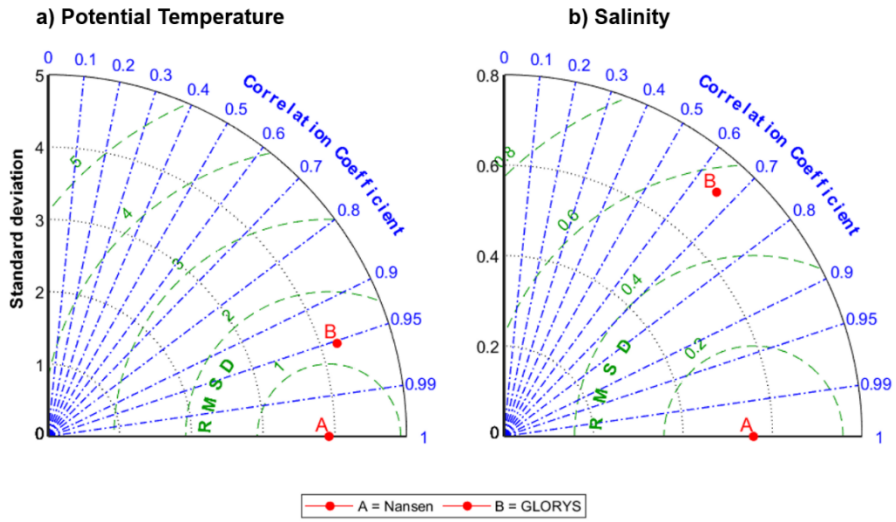

Figure 4.13. Taylor Diagram comparing reference as Nansen profiles (A) with GLORYS interpolated profiles (B) for Temperature (a) and Salinity (b) from 1995-2014.

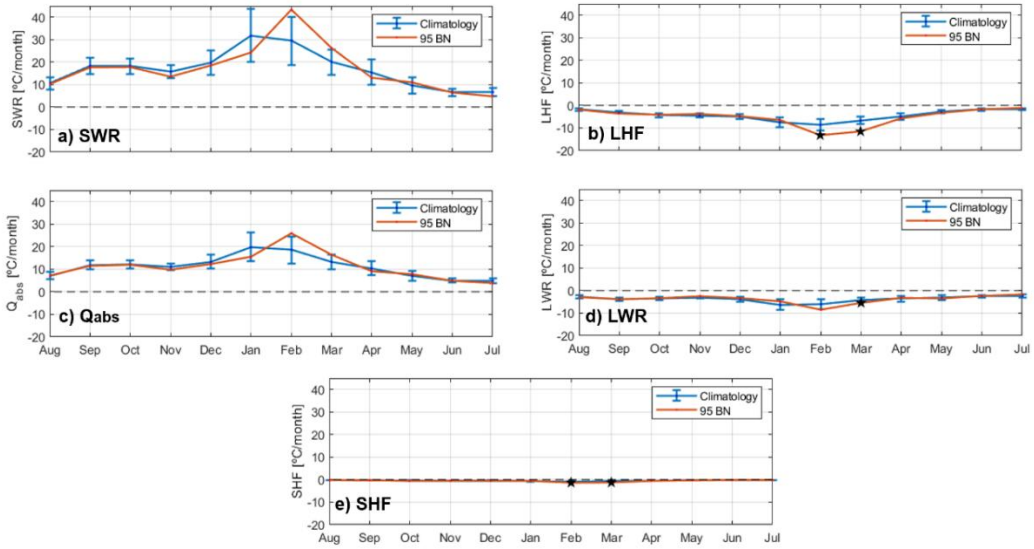

Figure 4.14. Monthly climatology (blue) of the terms from mixed layer heat budget equation averaged for coastal box 1 region (8ºS – 20ºS, 1º away from coast) from 1993-2019 depicted from August to July for a) Shortwave Radiation (SWR) b) Latent Heat Flux (LHF); c) SWR absorbed by the mixed layer (Qabs); d) Longwave Radiation (LWR); e) Sensible Heat Flux (SHF). Intervals indicate monthly standard deviation. a-e) In red are monthly values from August 1994 to July 1995 of the parameters mentioned above, respectively. Black stars indicate significant differences from monthly climatologies of each respective month at a 90% confidence level according to the Student's *t* test.

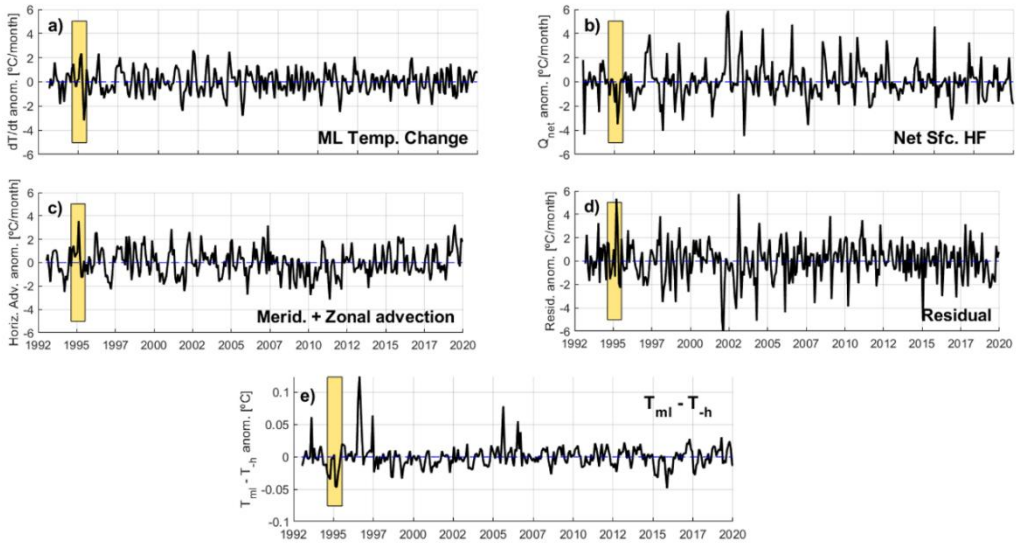

Figure 4.15. Detrended monthly anomalies (a - d) of the mixed layer heat budget equation terms averaged for coastal box 1 region (8ºS – 20ºS, 1º away from coast). Same for (e) but for mixed layer temperature vertical gradient. Anomalies are based on GLORYS12 and ERA5 datasets and calculated over the period 1993 – 2019.

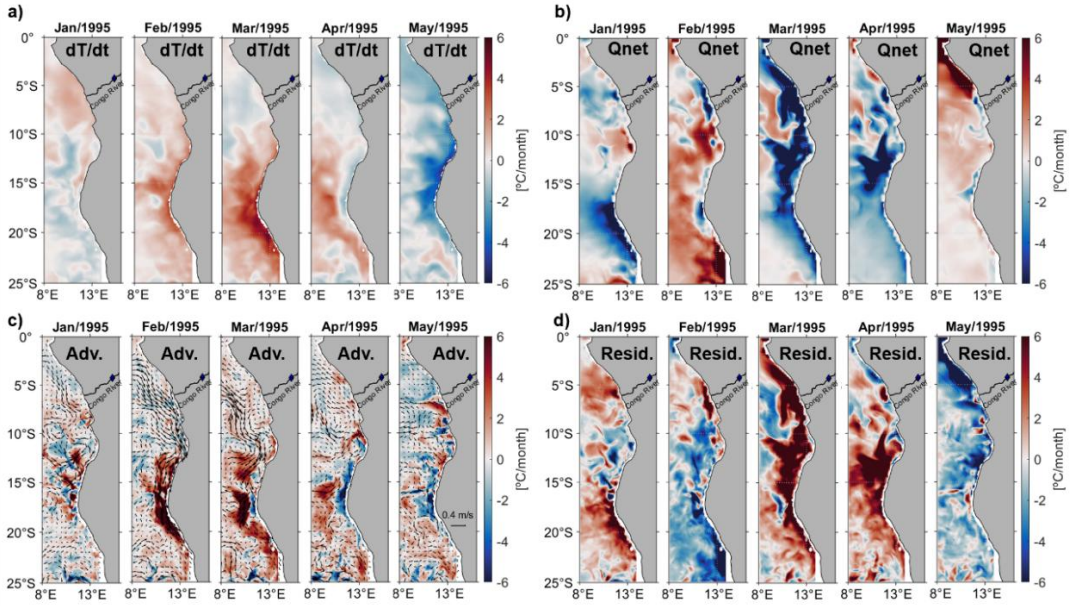

Figure 4.16. Detrended monthly anomalies from January to May 1995 for mixed layer heat budget terms. (a) temperature tendency, (b) net surface heat flux, (c) horizontal advection, (d) residual. Arrows in (c) indicate mixed layer currents anomaly. Blue diamond represents Congo River Brazzaville station. Anomalies are based on GLORYS12 and ERA5 datasets and calculated over the period 1993 – 2019.

Chapter 5

Turbulent Heat Flux Responses to Sea Surface Salinity Variability during Benguela Niños and Niñas

In Chapter 4 we showed that sea surface salinity changes can be associated with amplification of Benguela Niño events via reducing the vertical temperature gradient and increasing stratification. In Chapter 5, we extend this discussion to the extremely cold Benguela Niña events, quantifying in terms of turbulent heat fluxes the importance of the sea surface salinity variations and consequently the upper ocean stratification changes to the overall anomalous sea surface temperatures. We show that salt advection at the surface drives the boreal spring stratification variability, rather than the propagating coastally trapped waves, and that anomalous salt advection is an important factor in boosting these coastal events of extreme sea surface temperatures.

The manuscript was submitted to *Geophysical Research Letters*.

Citation: **Aroucha, L. C.**, Hummels, R., & Lübbecke, J. F.: Turbulent Heat Flux Responses to Sea Surface Salinity Variability during Benguela Niños and Niñas, *submitted to Geophysical Research Letters.*

The candidate designed the original study, carried out all the analyses, produced all the figures, and authored the manuscript from the first draft to the final published version.

5.1 Abstract

Benguela Niño and Niña events are episodes of extreme warming and cooling off Angola with impacts on fisheries, ecosystems, and rainfall patterns over southwest Africa. They are typically forced remotely by variations in equatorial wind. We use an extensive in-situ dataset to show that sea surface salinity (SSS) changes act as a local forcing that amplifies these extreme warm and cold events by altering the water column stratification and consequently the impact of subsurface mixing. The mixed layer turbulent heat loss during an extreme warm episode with unusually low SSS in 1995 is nearly 3x lower than during a cold event with an anomalously high SSS in 1997. In addition, we demonstrate that interannual turbulent heat flux variability in early boreal spring off Angola is mainly driven by salt advection fluctuations, and that this turbulent mixing is a significant contributor to altering mixed layer temperatures and restoring mixed layer salinities.

5.2 Plain Language Summary

Benguela Niño and Niña events are periods in which the ocean off the coast of Angola becomes unusually warm or cold. These events are often triggered by wind changes at the equator and can affect fish populations, marine life, and rainfall in southwestern Africa. Using observational data, we find that changes in ocean salinity also play a key role in making these warm and cold events even stronger. When the ocean surface is less salty, it creates a separate layer that traps heat near the surface, amplifying the warm events. On the other hand, when the ocean is saltier, heat escapes more easily from the surface to deeper layers, making cold events even colder. In fact, during an extreme warm event with low salinity, the ocean surface layer loses three times less heat than during a cold event with high salinity. We also show that in early spring, year-to-year changes in surface salinity are the main driver of heat exchange between the ocean surface and subsurface layers. This mixing process significantly impacts ocean surface temperatures and salinities.

5.3 Introduction

Benguela Niños and Niñas are events of extremely warm and cold sea surface temperatures (SST), respectively, in the coastal region off Angola, usually peaking from February to May, governing the SST interannual variability in the region (Florenchie et al., 2003, 2004; Imbol Koungue et al., 2019; Imbol Koungue & Brandt, 2021; Lübbecke et al., 2010; Shannon et al., 1986). These events significantly impact the southeastern tropical Atlantic productivity, fisheries, and ecosystem management (Binet et al. 2001; Boyer & Hampton, 2001; Gammelsrød et al., 1998; Imbol Koungue et al., 2024; Jarre et al., 2015), as well as rainfall regimes and flooding in coastal Africa (Koseki & Imbol Koungue, 2020; Lutz et al., 2015; Rouault et al., 2003). Their forcing mechanism is mainly remotely via the relaxation or strengthening of the equatorial trade winds and the resulting eastward propagation of equatorial Kelvin waves, which then propagate southward as coastally trapped waves (CTWs) when reaching the African continent (e.g. Bachèlery et al., 2020; Lübbecke et al., 2010). However, in the last decades, local forcing (e.g. changes in meridional winds associated with

shifts in the South Atlantic Anticyclone) seems to play an increasingly important role in triggering these events (Imbol Koungue et al., 2021; Lübbecke et al., 2019; Prigent et al., 2020; Richter et al., 2010).

More recently, it has been shown that extreme warm events in the region can additionally be boosted by unusually low sea surface salinity (SSS) in the Angola-Benguela area (ABA, 10ºS – 20ºS, 10ºE to the coast), which strengthens the water column stratification, generates barrier layers, and likely reduces the surface cooling via turbulent mixing (Aroucha et al., 2024; Lübbecke et al., 2019; McPhaden et al., 2024). The Congo River is the primary source of low salinity anomalies, connecting the Indian Ocean Dipole to Benguela Niño events through increased precipitation over the African continent and subsequent higher river discharge (Jarugula & McPhaden, 2023; McPhaden et al., 2024). Turbulent mixing is indeed of major importance for cooling the SST and for the upward salt flux in this area (Awo et al., 2022; Körner et al., 2023), with the mixing strength depending mainly on the local background stratification (Zeng et al., 2021). Here we aim to quantify for the first time the magnitude of the SSS changes' impact on the turbulent heat fluxes and the subsequent impact on SST within the months of its maximum variability. We further discuss and analyze the hypothesis presented by McPhaden et al. (2024) of enhanced turbulent fluxes cooling the SST during a Benguela Niña event linked to anomalously low freshwater input. For that, we focus on the satellite-era most extreme Benguela Niño and Niña in 1995 and 1997, respectively (Figure 5.1 and Figure 5.4), but also discuss other similar events. By exploring these mechanisms, we attempt to show that the dynamics of freshwater input in the region are of major importance for understanding the local surface temperature variability, and potentially for improving Benguela Niño and Niña events prediction, which still poses a challenge (Bachèlery et al., 2025).

5.4 Data and Methods

5.4.1 Datasets

We use an extensive dataset of in-situ hydrographic measurements from the Nansen Programm of the Food and Agriculture Organization of the United Nations (FAO), where several research cruises were conducted on board the R/V Dr. Fridtjof Nansen (Tchipalanga et al., 2018). The cruises occurred twice a year, approximately during austral autumn (February – April, FMA) and austral winter (June-September, JAS) (Figure 5.5). Here, we use more than 5000 Conductivity-Temperature-Depth (CTD) profiles taken in the ABA (Figure 5.1) from 1995 to 2014 (Figure 5.5).

To estimate the turbulent heat fluxes (J_h), i.e. the mixed-layer (ML) turbulent heat loss, we use ocean turbulence data collected in Angolan waters during seven research cruises on board of R/V Meteor from 2013 to 2022 (Körner et al., 2023, 2024). This data was measured using a free-falling microstructure profiler equipped with two to three airfoil shear sensors from which the dissipation rates of turbulent kinetic energy (TKE, ε) were estimated. For more details, check Hummels et al. (2013, 2014) and Körner et al. (2023, 2024).

Monthly temperature, salinity, and ocean currents were obtained from the Global Ocean Eddy-resolving Reanalysis (GLORYS12, Lellouche et al., 2021), which has a horizontal resolution of 1/12º and 22 levels in the upper 100m. GLORYS12 is available from 1993 to 2021 and shows good agreement with the in-situ

temperature and salinity measurements from the Nansen Programme (Figure S2) and the velocity data from a moored acoustic Doppler current profiler (ADCP) off Angola (Aroucha et al., 2024).

Finally, monthly surface rates of evaporation and precipitation, shortwave radiation (SWR), longwave radiation (LWR), latent heat flux (LHF), sensible heat flux (SHF), and 10-m wind components were retrieved from the European Center for Medium-Range Weather Forecasts (ECMWF) reanalysis 5 (ERA5, Hersbach et al., 2020). ERA5 has a ¼° resolution, and is available from 1940 onwards. In the present study, we focus on the 20-year measurement period of the Nansen Programme, i.e., 1995 to 2014.

5.4.2 Methodology

5.4.2.1 Definitions

The mixed layer depth (MLD) is defined here as the depth at which the density is increased by 0.125kg/m^3 compared to the surface value, following Körner et al. (2024). The same criteria was applied to the CTD data and the vertical density profiles derived from GLORYS12 temperature and salinity fields. Thermocline depth is taken as the depth of the 26 kg/m^3 isopycnal, which represents the permanent thermocline depth in the region, that moves vertically with the passage of CTWs (Brandt et al., 2023; Kopte et al., 2017; Tchipalanga et al., 2018).

Following Imbol Koungue et al. (2017, 2019) we characterize an event as a Benguela Niño or Niña when detrended monthly anomalies of ABA-averaged SST exceed ± 1 STD for at least three consecutive months. When one of these months additionally features detrended monthly anomalies of ABA-averaged sea surface salinity (SSS) exceeding ± 1 STD, the event is also termed "fresh" or "salty". Based on this definition, we find 2 concomitant fresh and warm events (i.e. 1995, 2001) and 3 salty and cold events (i.e. 1997, 2010, 2012) between 1995 and 2014 (Figure 5.4).

5.4.2.2 Turbulent heat fluxes calculation and error estimates

ML turbulent heat loss (J_h) is estimated via a combination of the CTD profiles from the Nansen Programme with the microstructure shear measurements. This estimation is based on the previous works of Hummels et al. (2013, 2014), where a detailed description can be found.

Turbulent heat fluxes are calculated via the following equation:

$$J_h = -\rho c_p K_\rho \frac{\partial \mathrm{T}}{\partial \mathrm{z}} \quad (5.1)$$

where ρ is the seawater density and c_p is the specific heat capacity. $\frac{\partial \mathrm{T}}{\partial \mathrm{z}}$ is the vertical temperature gradient and K_ρ represents the eddy diffusivity of mass, which is calculated following Osborn (1980): $K_\rho = \Gamma\, \varepsilon\, N^{-2}$. Γ represents the mixing efficiency and is set as 0.2, based on Gregg et al. (2018). From the CTD profiles within the ABA, we calculate the Brunt-Väisäla frequency, N^2, and $\frac{\partial \mathrm{T}}{\partial \mathrm{z}}$. Vertical measurements in the upper 3m were discarded. To determine individually each profile's J_h, we converted the vertical coordinate from depth to

distance to MLD (i.e. MLD +ΔZ) by binning each profile into a grid with 5m vertical resolution. Measurements within the ML and 5m below it were disregarded to avoid ship turbulent effects, and because the mixing efficiency is unknown in weakly stratified waters (Gregg et al. 2018). Measurements were then averaged for each respective depth bin. From the binned profiles of ε and N^2, we estimate K_ρ, followed by the estimation of the J_h also considering the binned profiles of $\frac{\partial \mathrm{T}}{\partial \mathrm{z}}$. Similarly, turbulent salt fluxes (J_s) were calculated via $J_s = K_\rho \frac{\partial \mathrm{S}}{\partial \mathrm{z}}$ (5.2), where the vertical salinity gradient ($\frac{\partial \mathrm{S}}{\partial \mathrm{z}}$) was also taken from the CTD profiles.

From the shear sensors' measurements, we estimated ε by using the variance method assuming isotropy, as in Hummels et al. (2013, 2014), and Körner et al. (2023). ε from the 2-3 shear foils were averaged individually for each profile. Even though the microstructure measurements from the research cruises do not overlap temporally with the Nansen Programm campaigns, it is still reasonable to assume constant values of ε for the 1995-2014 period, since mixing in this region is driven mostly by internal tides and the tidal energy available is nearly constant throughout the year (Körner et al., 2023; Zeng et al., 2021). Indeed, from the analyzed microstructure measurements, we observed that TKE rates are rather similar in the region, and are not influenced by seasonal changes in stratification (not shown). The mean ε is thus assumed to be only a function of bathymetry (Körner et al., 2023, Figure 5.6). Hence, we separated both microstructure and CTD profiles in three subregions, following Körner et al. (2023): shallow waters (i.e. depth < 75m); shelf break (i.e. 175m >= depth >= 75m); deep waters (depth > 175m) (Figure 5.6). After estimating J_h and J_s individually for each profile, we calculated a weighted mean for the ABA, considering that shallow waters cover 4% of the region, while shelf break and deep waters represent 7% and 89%, respectively.

Finally, to compensate for the uneven number of CTD profiles taken in each season (i.e. FMA, JAS), we initially calculated the anomaly for each profile by subtracting the monthly climatological mean. Then, we added the seasonal climatology for each profile individually. Finally, we averaged the profiles for each year's season to get a mean seasonal profile for each of the 20 years analyzed.

Errors in J_h and J_s calculations are estimated based on the 95% confidence limits (CL95), following Hummels et al. (2013, 2014). For N^2, $\frac{\partial \mathrm{T}}{\partial \mathrm{z}}$, and $\frac{\partial \mathrm{S}}{\partial \mathrm{z}}$.we convert the standard error (SE) to CL95 via $CL95 = \bar{x} \pm 1.96\, SE$, where $\bar{x}$ is the monthly average of the term x. CL95 for K_ρ, J_h and J_s are derived via Gaussian error propagation. Finally, for ε, CL95 is obtained via boostrapping.

5.4.2.3 Mixed layer heat and salt budgets

To relate the changes in SST and SSS to changes in turbulent heat fluxes, we performed both an ML heat and salt budget analysis. For the ML heat budget, we used

$$\rho\, c_p\, h \frac{\partial \mathrm{T}}{\partial \mathrm{t}} = -\rho\, c_p\, h\, \boldsymbol{v}\, .\nabla \mathrm{T} + q_{net} + res_H \quad (5.3)$$

where T (in ºC) and $\boldsymbol{v}$ (in m/s) are the ML temperature and horizontal currents, respectively, and h (in meters) is the MLD. ρ represents the seawater density, here assumed as 1027 kg/m^3 and c_p is specific heat capacity

taken as 4000 J/kg ºC. q_{net} (in W/m^2) is the sum of LWR, SHF, LHF and SWR absorbed within the ML, defined by considering an albedo rate of 6% as in Aroucha et al. (2024) and Foltz et al. (2020). res_H is the heat budget residual, which includes the turbulent heat fluxes, vertical temperature covariance and advection, data uncertainty, and processes in temporal and spatial scales smaller than the dataset scales here used. Each term represents, from left to right: temperature tendency, horizontal advection, net surface heat flux, and residual.

For the ML salt balance, we consider the following:

$$\frac{\partial \mathrm{S}}{\partial \mathrm{t}} = -\boldsymbol{v} \,.\, \nabla \mathrm{S} + \frac{S}{h}(\mathrm{E} - \mathrm{P}) + res_S \quad (5.4)$$

where S (in psu) is the ML salinity (MLS), P and E are the precipitation and evaporation rates (m day^{-1}), respectively. res_S is the salt budget residual, which includes vertical advection, salinity covariance, turbulent salinity flux, data uncertainty, and computational errors. Each term represents, from left to right: salt tendency, horizontal advection, local freshwater forcing, and residual. Both heat and salt budgets were estimated for every grid point and then averaged for the ABA. J_h and J_s are not included in the calculation of res_H and res_S, respectively.

5.5 The contrasting 1995 and 1997 extreme events

The 1995 (1997) Benguela Niño (Niña) events have been extensively documented and discussed in the literature (e.g. Aroucha et al. (2024); Bachèlery et al. (2020); Florenchie et al. (2003, 2004); Gammelsrød et al. (1998); Imbol Koungue et al. (2019); Imbol Koungue & Brandt (2021); McPhaden et al. (2024)). They were predominantly remotely triggered via a relaxation (strengthening) of the equatorial trade winds and the subsequent propagation of equatorial Kelvin waves and CTWs. For the 1995 event, local meridional wind fluctuations also played a role (e.g. Richter et al., 2010). The events reached their peak in March (April) with an ABA-averaged FMA mean of +2.5 ºC (-2.0ºC) (Figure 5.1a, d and Figure 5.4a).

Strikingly, these events oppose each other in terms of SSS (Fig. 5.1b,e) and coastal meridional current anomalies at the surface (Fig. 5.1c,f). During the 1995 (1997) Benguela Niño (Niña), a plume of negative (positive) SSS anomalies is present in the region with an ABA-averaged FMA mean of -0.67 (+0.61). At the same time, there is an anomalous southward (northward) coastal current. The coastal current changes are likely related to CTW propagation (Bachèlery et al., 2016; Kopte et al., 2017) as indicated by the thermocline depth anomalies (Fig 5.1c,f) and shifts in the local wind stress and wind stress curl (Aroucha et al., 2024; Fennel et al., 2012; Junker et al., 2015, Fig. 5.7). Since salt advection is one of the dominant terms in altering the MLS during boreal late-winter and early-spring (Awo et al., 2022), the surface current anomalies likely drove the unusual SSS fields in the region throughout these months (see also Section 5.7). One effect of the opposite SSS anomalies is evident in the MLD (Figure 5.1c,f), with an apparent ML shoaling (deepening) compared to the FMA climatology during FMA 1995 (1997). This is already an indication of

increased (reduced) stratification during such events. Therefore, we further examine the impact of these contrasting SSS anomalies on both the stratification and turbulent heat flux during each event.

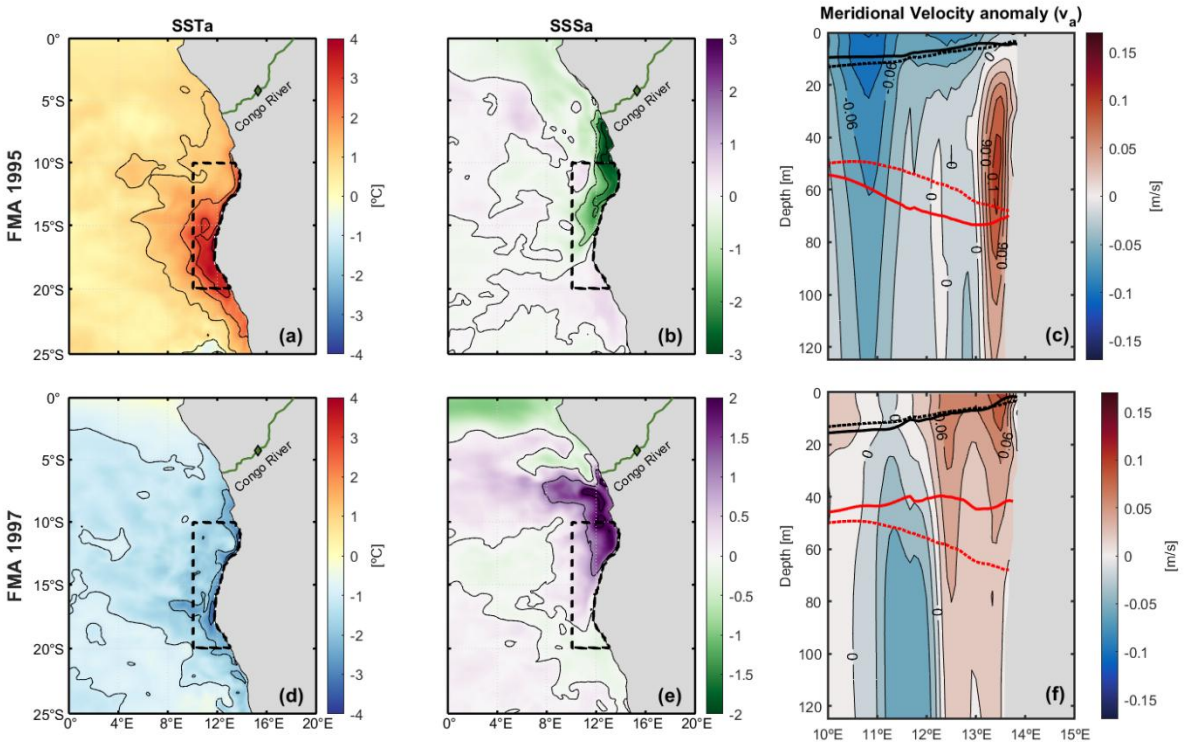

Figure 5.1. Mean February-March-April (FMA) anomalies of SST (a,d), SSS (b,e), and meridional currents (c,f) from GLORYS12 during 1995 Benguela Niño (a-c) and 1997 Benguela Niña (d-f). The dashed black box indicates Angola-Benguela Area (ABA, 10ºS-20ºS, 10ºE to coast). Black (red) lines in (c) and (f) show calculated mixed layer (thermocline) depths. Dotted (solid) lines in (c) and (f) indicate FMA mean climatological (FMA 1995 in (c) and FMA 1997 in (d)) values.

5.6 Turbulent heat fluxes

Calculated from 5.1, the mean ABA FMA turbulent heat loss immediately below the ML was approximately three times stronger during the 1997 Benguela Niña in comparison to the 1995 Benguela Niño (-120.0 [-227.5, -51.3] W/m^2 in 1997 vs -41.2 [-77.2, -16.3] W/m^2 in 1995) (Figure 5.2d). When averaging from 2m to 15m below the ML, a similar 3-fold factor in magnitude is observed (-62.3 [-109.5, -32.2] W/m^2 in 1997 vs -22.3 [-38.6, -11.0] W/m^2 in 1995) (Figure 5.8a). In both years, J_h was also significantly different from the FMA climatology, especially during FMA 1995. This result indicates that the ML cooling efficiency was much stronger (weaker) during the Benguela Niña (Niño) months with anomalously high (low) SSS. These differences in J_h can not be related to an increased/decreased vertical temperature gradient (Figure 5.2a), which shows only slight differences between years at 10m below the ML. Instead, it reflects the different K_ρ between these years (Figure 5.2c), explained here exclusively by the strong stratification differences (Figure 5.2b), as dissipation rates were assumed constant within the respective years. The mean FMA 1997 N^2 profile characterizes a weak water column stability (unusually reduced stratification down to 30m below the ML), which results in an elevated J_h. The opposite is true for the mean FMA 1995, when the N^2 peaks at 2.5m below the ML, being three times stronger than the FMA climatology and more than 4 times in comparison to 1997 (Figure 5.2b).

Zeng et al. (2021) showed that the cooling strength of the turbulent heat flux in the Angolan upwelling region depends mainly on the background stratification on which the tidal energy acts. Indeed, our results indicate that, when assuming the tidally driven dissipation rates as constant throughout the year, the different water column stratification creates hugely contrasting magnitudes of J_h in 1995 and 1997 (Figure 5.2). The same effect is also observed in other years of concomitant anomalous SSS and SST. In FMA 2001, during a weaker Benguela Niño event compared to 1995, but also characterized by unusually low SSS in the ABA (Figure 5.4), the increased stratification stands out, and resulted in reduced J_h (i.e. the second lowest mixing rate below the ML in the 20-years analyzed) (Figure 5.8 and 5.9). On the other hand, in similar Benguela Niña months coinciding with anomalous positive SSS but smaller in magnitude, J_h is also increased due to reduced water column stability, especially in 2010 (Figure 5.8 and 5.9). It seems likely that the main driver of these stratification changes is the varying SSS, as the vertical temperature gradients are similar. However, since the passage of CTWs triggering the episodes of extreme SSTs in the region is also related to a vertical displacement of the thermocline (e.g. Brandt et al., 2023; Figure 5.1), also impacting the water column stratification, we further investigate what drives the stratification and the consequent turbulent heat flux variability in the ABA.

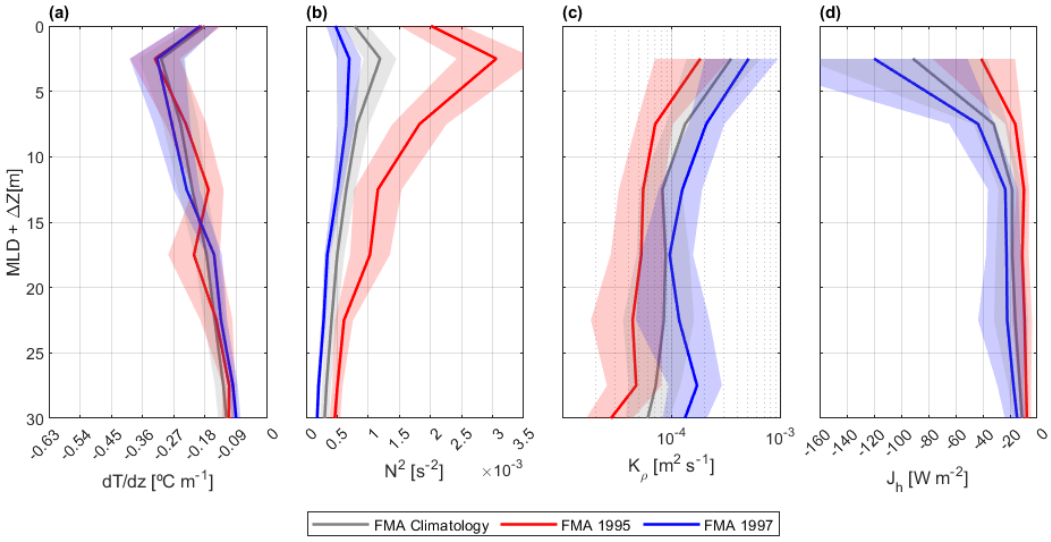

Figure 5.2. Averaged profiles of the turbulent heat flux terms. (a) vertical temperature gradient (ºC/m). (b) Squared Brunt-Väisäla frequency (s^{-2}). (c) Eddy diffusivity (m^2/s). (d) Turbulent heat flux (W/m^2). Grey, red, and blue lines indicate FMA climatological, 1995, and 1997 means, respectively. Shaded areas represent 95% confidence level.

5.7 Salt advection as the main driver of turbulent heat flux variability

The seasonal cycle of J_h off Angola is connected to seasonal variations in stratification, meaning that rather constant mixing by internal tides will be more efficient during the weaker stratification season, i.e. boreal summer (Körner et al., 2023). Indeed, Figure S5 shows that J_h averaged from 2m to 15m below the ML is higher during JAS than FMA, while its variability is more than two times lower (Figure 5.8). Since Benguela Niño/Niña events occur mainly from February to April, we here focus on explaining the J_h variability during FMA. These months also feature maximum SSS variability off Angola, linked to the timing of higher freshwater input by the Congo River north of the ABA (Jarugula & McPhaden, 2023; McPhaden et

al., 2024) and increased southward advection of low salinity waters, which climatologically reach as far south as 12ºS (Awo et al., 2022; Houdengnoto et al., 2021). This southward advection is likely related to a stronger and shallower Angola Current during these months (Kopte et al. 2017; Tchipalanga et al. 2018). At the same time, the passage of CTWs in the region also occurs in boreal spring months. Therefore, the two main mechanisms that would influence the stratification variability within these months, and consequently J_h, are: the passage of a CTW and/or changes in ABA SSS.

A ML salt budget analysis shows that anomalous salt advection, i.e. the second term in 5.4, is one of the main drivers of MLS interannual variability in the ABA during FMA (Figure 5.10b). The salinity advection variability itself is dominated by changes in the horizontal salinity gradient, with anomalous currents playing an apparent secondary role (Fig. 5.11). Vertical salinity flux across the base of the salt-stratified ML is as well as an important term for interannual ML salinity changes (J_s in Figures 5.12b), representing ~58% of the MLS rate of change, and explaining a great part of the calculated res_S FMA variability (r = 0.71, Figure 5.10b). In fact, during fresh (salty) events, due to stronger (weaker) vertical salinity gradients, the Js is higher (lower), acting to restore the MLS (Figures 5.12 and 5.13). Still, the anomalous salt advection explains more than 86% of MLS interannual changes (i.e. r=0.93). Hence, we focus on analyzing how the FMA mean J_h correlates with both thermocline and salt advection anomalies.

Anomalies of salt advection are significantly and highly correlated to turbulent heat flux changes in the ABA (r=-0.73, p-value <0.05), and explain more than half of the mean FMA J_h variability (53%) (Figure 5.3a,b). In fact, the year with the most negative (positive) salt advection anomaly is 1995 (1997). At the same time, even though thermocline depth anomalies also significantly correlate with J_h (r = 0.62, p-value < 0.05) (Figure 5.3c,d), they explain only 38% of its FMA variability in the ABA. Furthermore, we performed the same correlation analysis for ABA-averaged FMA mean MLD, Isothermal Layer Depth (ILD), and Barrier Layer Thickness (BLT, i.e. BLT = ILD – MLD) anomalies using the Nansen Programme CTD profiles. Similarly, J_h variability is more closely related to changes in MLD rather than in ILD (i.e. r = -0.69 and -0.41, respectively, not shown), agreeing with a ML shoaling (deepening) when there is a negative (positive) SSS anomaly, instead of a downward (upward) movement of the thermocline related to the passage of a downwelling (upwelling) CTW. The correlation is even stronger with the BLT anomalies (r = 0.77, not shown), with a thicker (thinner) barrier layer representing stronger (weaker) stratification and consequently less (more) turbulent heat flux, as shown in Aroucha et al. (2024) and McPhaden et al. (2024). Therefore, we can conclude that the anomalous salt advection into ABA is likely the main driver of the FMA stratification variability at the ML base, which results in anomalous J_h off Angola, with the propagating CTWs playing a secondary role in stratification changes.

It has been suggested that turbulent mixing across the base of the ML is an imperative cooling term for SST in this region (Körner et al. 2023). However, its representation in a ML heat budget assessment from observational products is challenging due to its complex calculation, dependent on TKE measurements and eddy dissipation rate estimations. Turbulent heat fluxes are then usually represented by the residual term in such budgets (e.g. Aroucha et al., 2024; Imbol Koungue et al., 2024; Körner et al., 2023). Here, by estimating J_h based on in-situ CTD profiles and microstructure measurements, we can compare how well the ML heat

budget residual (res_H) represents both the magnitude and variability of the turbulent heat fluxes, highlighting the importance of this mixing term for the overall ML temperature changes. Indeed, Figures 5.3e,f show that J_h explains 69% of the res_H interannual variability, which is a crucial term for the ML heat budget (Figure 5.10a). In terms of magnitude, FMA J_h anomalies represent 82% and 55% of the FMA residual anomaly in 1995 and 1997, respectively (Figure 5.10a).

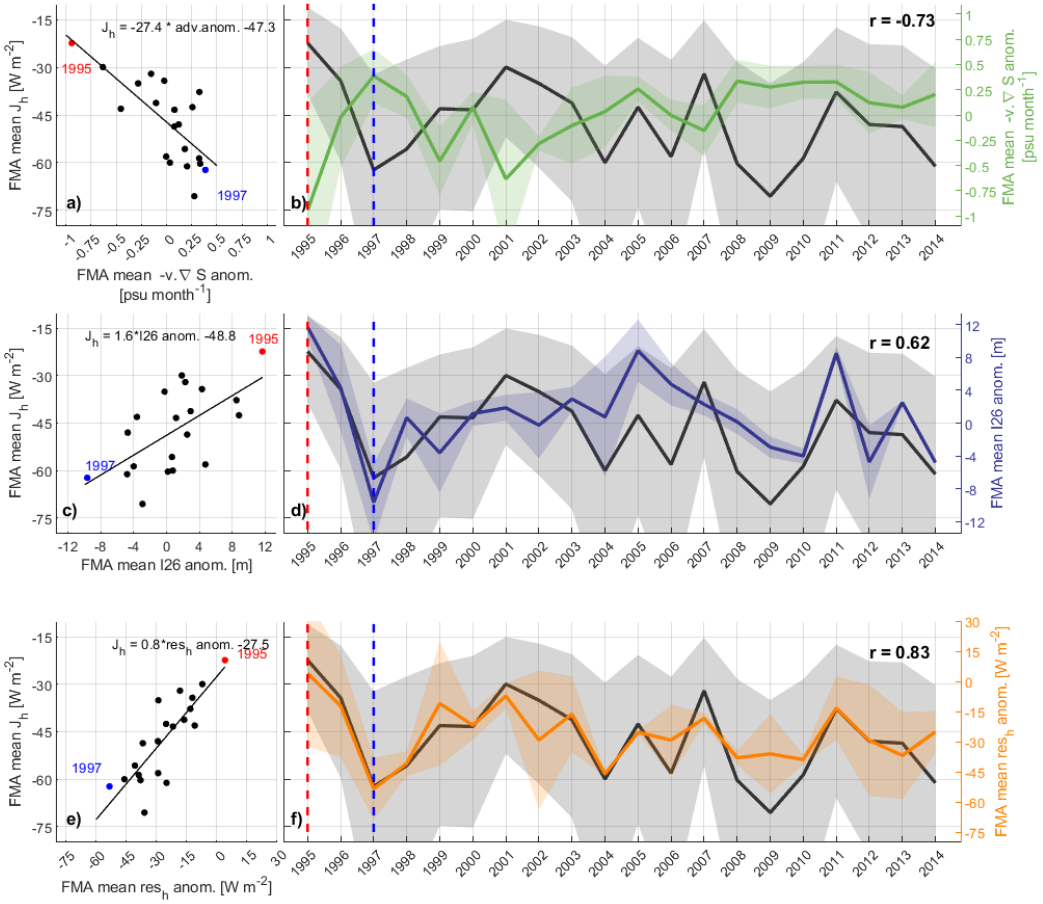

Figure 5.3. (a, c, e) Scatter diagram and linear regression fit between ABA FMA mean turbulent heat fluxes and: ABA FMA mean ML salt advection anomalies (a); ABA FMA mean thermocline depth anomalies (c); ABA FMA mean ML heat budget residual (e). (b, d, f) Time series of ABA FMA mean turbulent heat fluxes (black) and: ABA FMA mean ML salt advection anomalies (b); ABA FMA mean thermocline depth anomalies (d); ABA FMA mean ML heat budget residual (f). Red (blue) dots in (a, c, e) and dashed lines in (b, d, f) indicate 1995 (1997). Linear least squares regression fit equations are shown in (a), (c), and (e). Correlation coefficients are shown in (b), (d), and (f). Shaded areas represent 95% confidence level (for variables on right axis taken from SE).

5.8 Summary and Discussion

This study demonstrates the role of SSS anomalies in amplifying a Benguela Niño/Niña by modifying the water column stratification and consequently the efficiency of ocean mixing. It also confirms the hypothesis from McPhaden et al. (2024) that this effect is likewise acting during extreme cold and salty episodes. By quantifying, for the first time, the turbulent heat fluxes during these extreme warm and cold events, we highlight the role of the SSS change forcing mechanism, showing its key importance in driving turbulent heat loss variability during boreal spring months.

We emphasize that the stratification changes and the subsequent changes in the mixed layer heat loss in the ABA are more strongly associated with ML salt advection anomalies than with the vertical displacement of the thermocline. CTW propagation, however, can also impact the salt advection, since the variability of the Angola current is influenced by these coastal propagating waves (Bachèlery et al., 2016; Tchipalanga et al., 2018). Martins and Stammer (2022) actually suggested the need for a combined propagating CTW with an increased Congo River freshwater discharge for the low-salinity plume to reach far enough south to impact the ABA.

The effects of stratification changes, barrier layer formation, and subsurface mixing on extreme warm and cold events, also related to the El Niño Southern Oscillation in the tropical Pacific, have recently garnered increasing attention in the scientific community (Guan et al., 2025; Liu et al., 2025; Tozuka, 2025). Such impacts on extreme episodes are even more crucial to comprehend in a region with high mixing rates and freshwater input variability like off Angola. Furthermore, regions off the Congo mouth have been pointed out as hotspot areas for Benguela Niño/Niña predictability (Bachèlery et al., 2025), highlighting the importance of further understanding the impact of SSS variability in boosting SST anomalies. In conclusion, our study quantitatively supports the importance of this mechanism, highlighting at the same time the crucial role of stratification changes in driving turbulent heat loss variability during extreme events.

Acknowledgments. The authors declare no relevant conflicts of interest regarding this study. This study was supported by the German Academic Exchange Service Doctoral Research Grant (57552340). We thank the captains, crews, scientists, and technicians involved in several research cruises in the Angola-Namibian waters.

Open Research. The hydrographic data from the Nansen Programme are available at https://doi.org/10.1594/PANGAEA.886492, while the microstructure data from the research cruises are available at https://doi.pangaea.de/10.1594/PANGAEA.953869 and https://doi.org/10.5281/zenodo.10062790. GLORYS12 product is available at https://data.marine.copernicus.eu/product/GLOBAL_MULTIYEAR_PHY_001_030/download; ECMWF ERA5 surface heat fluxes and wind data are available at: https://cds.climate.copernicus.eu/datasets/reanalysis-era5-single-levels-monthly-means?tab=download.

5.9 Supplementary Material

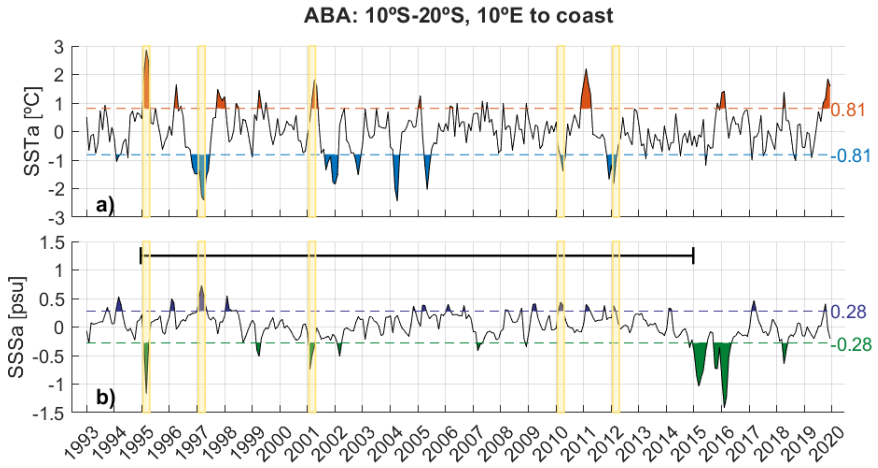

Figure 5.4. Time series of ABA averaged detrended SST (a) and SSS (b) anomalies from GLORYS12. Dashed lines indicate ±1STD, and their values are shown on the right side of each line. The horizontal solid black line shows the 20-year period of the Nansen Program. Yellow shading indicates FMA months of events with concomitant SST and SSS anomalies extremes (i.e. warm and fresh: 1995, 2001; cold and salty: 1997, 2010, 2012).

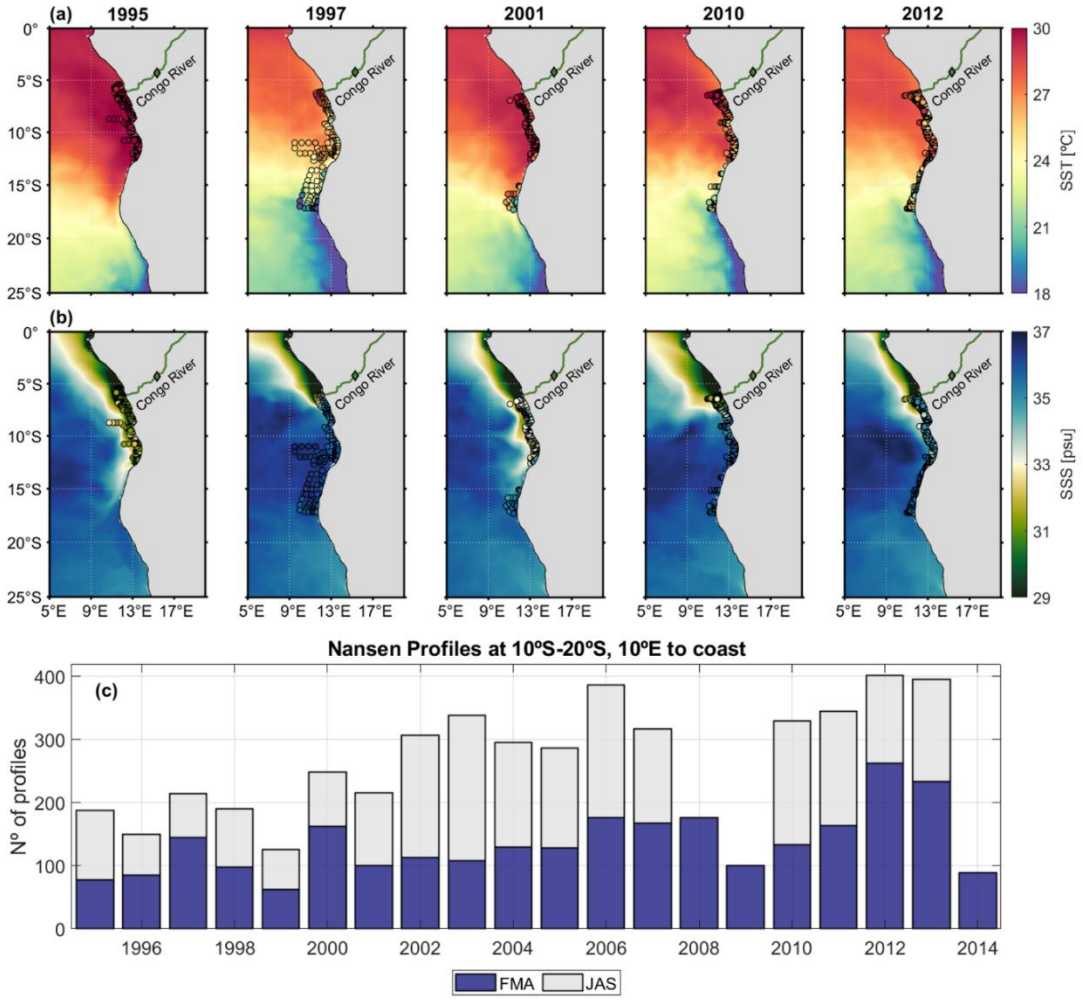

Figure 5.5. FMA averaged SST (a) and SSS (b) for selected years (yellow shading in S1) from GLORYS12 (shading) and 4m temperature (a) and salinity (b) from Nansen Program during FMA (circles). (c) Number of Nansen Program CTD profiles in ABA during FMA and JAS from 1995-2014.

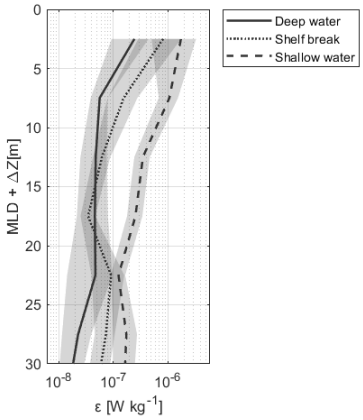

Figure 5.6. FMA averaged profiles of the dissipation rate of turbulent kinetic energy (W/kg). Solid, pointed, and dashed lines respectively represent the three profiles groups according to depth: deep water, shelf break and shallow water. Shaded areas represent 95% confidence level.

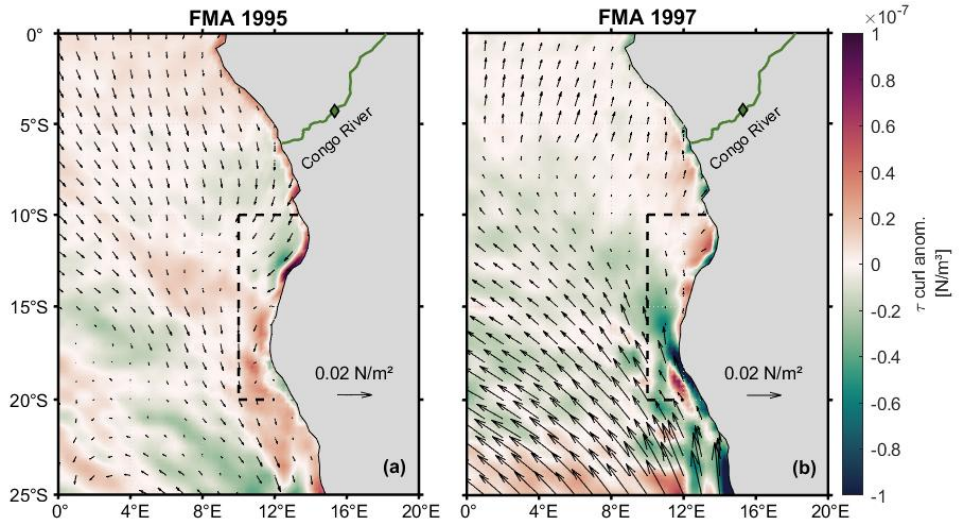

Figure 5.7. Mean FMA anomalies of wind stress curl (shading) and wind stress (arrows) during 1995 Benguela Niño (a) and 1997 Benguela Niña (b). The dashed black box indicates Angola-Benguela Area (ABA, 10ºS-20ºS, 10ºE to coast).

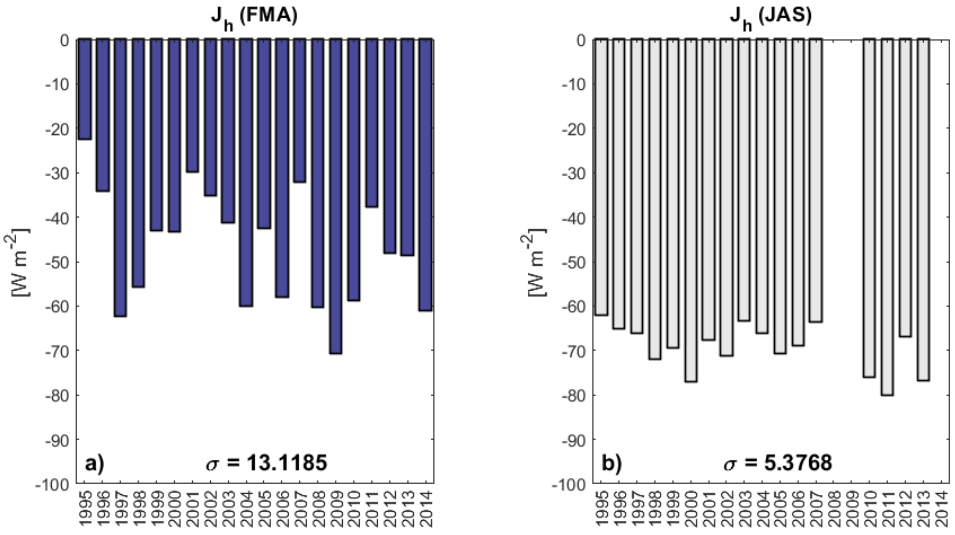

Figure 5.8. ABA mean turbulent heat fluxes averaged from 2m to 15m depth for each year. (a) FMA. (b) JAS. STD for the respective season is shown in each plot.

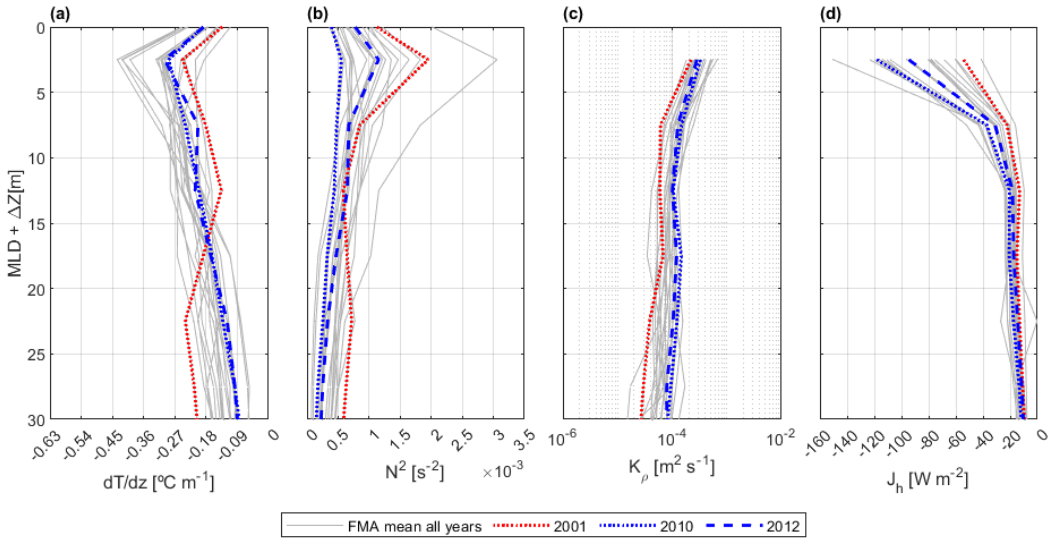

Figure 5.9. Averaged profiles of the turbulent heat flux terms. (a) vertical temperature gradient (ºC/m). (b) Squared brunt-Väisäla frequency (s^{-2}). (c) Eddy diffusivity (m^2/s). (d) Turbulent heat flux (W/m^2). Red and blue lines indicate FMA warm and fresh, and cold and salty event years, respectively. Grey lines represent other years. 2001 and 2010 are shown as dotted lines, while 2012 is shown as a dashed line.

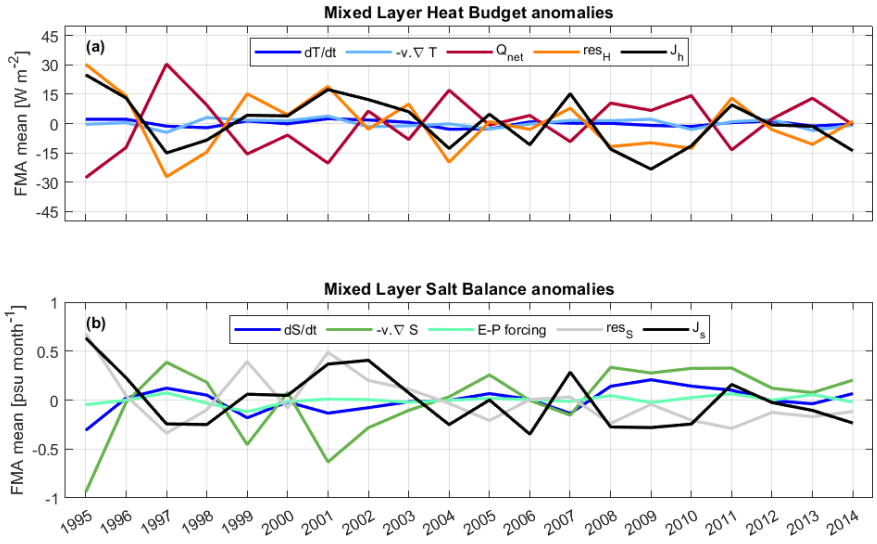

Figure 5.10. ABA averaged FMA mean anomalies of the mixed layer heat (a) and salt (b) budget terms calculated from 1993-2020 from ERA5 and GLORYS12. Heat (salt) budget residual is represented by orange (grey) line in the upper (lower) plot. The estimated turbulent heat (J_h) and salt fluxes (J_S) (black line in (a) and (b), respectively) are not included in the calculation of heat (res_H) and salt residual (res_S) terms (see 5.1 and 5.2).

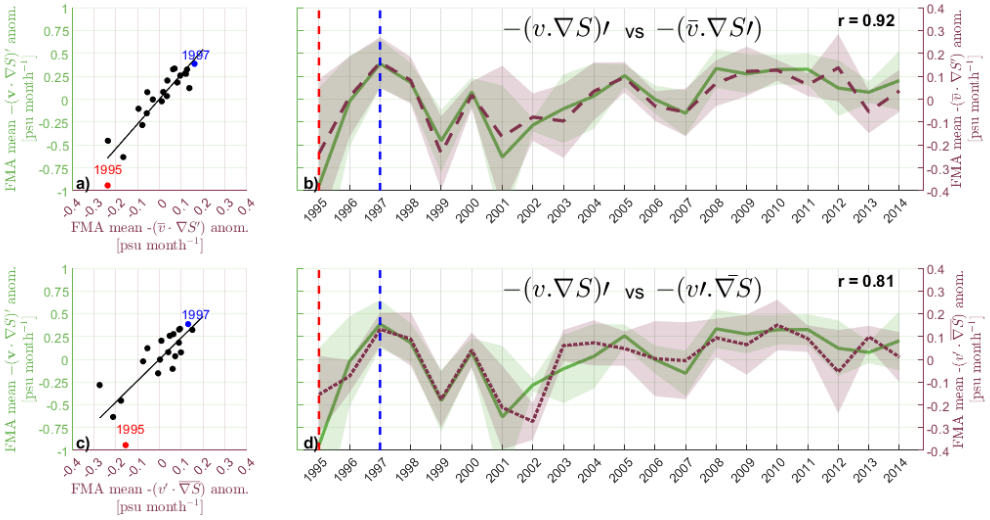

Figure 5.11. (a, c) Scatter diagram and linear regression fit between ABA FMA ML salt advection anomalies and: ABA FMA ML salt advection anomalies by only varying horizontal salinity gradient (a); ABA FMA ML salt advection anomalies by only varying horizontal velocities (c). (b, d) Time series of ABA FMA ML salt advection anomalies (solid green) and: ABA FMA ML salt advection anomalies by only varying horizontal salinity gradient (dashed brown) (b); ABA FMA ML salt advection anomalies by only varying horizontal velocities (pointed brown) (d). Red (blue) dots in (a, c) and dashed lines in (b, d) indicate 1995 (1997). Correlation coefficients are shown in (b) and (d). Shaded areas represent 95% confidence level (taken from SE).

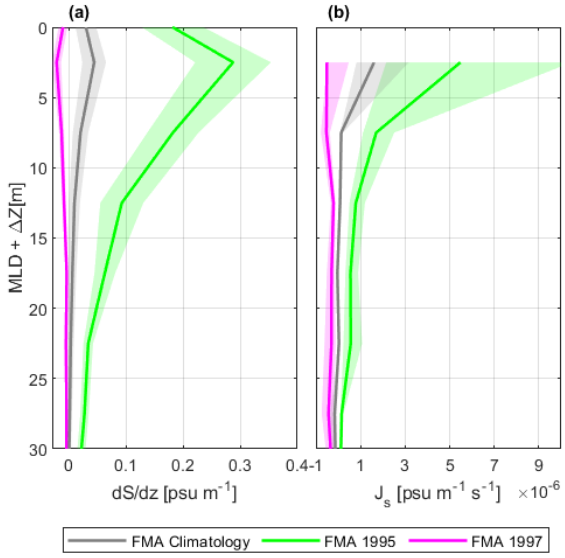

Figure 5.12. Averaged profiles of the turbulent salt flux terms. (a) vertical salinity gradient (psu/m). (b) turbulent salt flux (psu/m^{-1} s^{-1}). Grey, green, and magenta lines indicate FMA climatological, 1995, and 1997 means, respectively. Shaded areas represent 95% confidence level.

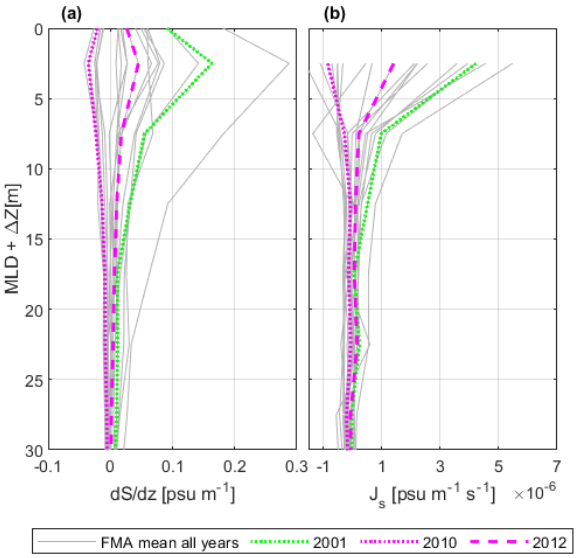

Figure 5.13. Averaged profiles of the turbulent salt flux terms. (a) vertical salinity gradient (psu/m). (b) Turbulent salt flux (psu/m^{-1} s^{-1}). Green and magenta lines indicate FMA warm and fresh, and cold and salty event years, respectively. Grey lines represent other years. 2001 and 2010 are shown as dotted lines, while 2012 is shown as a dashed line.

Chapter 6

The Indian Ocean Dipole intensifies Benguela Niño through Congo River discharge

The following chapter highlights the connection between the IOD, the strongest SST variability mode in the Indian Ocean, to Benguela Niño events, via atmospheric changes over the Congo River's basin, which lead to increased discharge in the Southeastern Tropical Atlantic. The mechanism and events presented in Chapters 4 and 5 are explored, indicating a land bridge between the two different ocean basins. Here a potential new source of predictability for Benguela Niños is suggested, since IOD events lag Benguela Niños by 3-4 months.

The manuscript was published in *Communications Earth & Environment* in December 2024.

Citation: McPhaden, M.J., Jarugula, S., **Aroucha, L.C.,** & Lübbecke, J. Indian Ocean Dipole intensifies Benguela Niño through Congo River discharge. *Communications Earth & Environment* 5, 779, https://doi.org/10.1038/s43247-024-01955-x, 2024.

The candidate contributed to all the analyses, produced Figure 6.7, and participated in the drafting of the manuscript.

6.1 Abstract

Benguela Niños are episodes of unusual El Niño-like warming in the upwelling zone off the coast of southwest Africa, with consequential impacts on marine ecosystems, coastal fisheries and regional weather. The strongest Benguela Niño in the past 40 years occurred in February–April 1995 with local sea surface temperature anomalies up to 4 °C off the coast of Angola and Namibia. Here, we show that a strong Indian Ocean Dipole in September–November 1994 helped boost the amplitude of the 1995 Benguela Niño through a land bridge involving Congo River discharge. We use atmospheric, oceanic, and hydrological data to demonstrate the sequential linkage between Indian Ocean Dipole development, unusually high rainfall in the Congo River basin, high Congo River discharge, low salinity near the Congo River mouth, and southward advection of this low salinity water into the Benguela upwelling region. The low salinity water isolated the surface mixed layer from the thermocline, which limited vertical mixing with colder subsurface waters and led to enhanced sea surface temperature warming. We also discuss how other Indian Ocean Dipole events may have similarly affected subsequent Benguela Niños and the possibility that Indian Ocean Dipole impacts on Benguela Niños may become more prominent in the future.

6.2 Introduction

Benguela Niños are episodes of unusual warming that develop every few years in the upwelling zone off the coast of southwest Africa with consequential impacts on regional marine ecosystems, coastal fisheries and weather variability (Boyer et al., 2001; Rouault et al., 2003; Lübbecke et al., 2018; Illig et al., 2020). These events typically occur in late boreal winter-early spring (February–April) and are generated through wind-forced dynamical processes originating in the Atlantic basin involving either a weakening of the trade winds along the equator (Florenchie et al., 2004; Lübbecke et al., 2010; Imbol Koungue et al., 2017) a local weakening of the alongshore winds off of west Africa (Richter et al., 2010; Lübbecke et al., 2019), or a combination of the two (Imbol Koungue & Brandt, 2021; Imbol Koungue et al., 2019). The strongest Benguela Niño in the past 40 years occurred in February–April 1995 (Gammelsrød et al., 1998; Aroucha et al., 2024), with temperature anomalies in early 1995 reaching 2 °C above normal on average off the coast of Angola and Namibia and up to 4 °C in localized areas (Fig. 6.1a, d). This extreme warming was associated with increased mortality and southward migration of fish stocks such as sardines, horse mackerel, and kob off the coast of Angola (Gammelsrød et al., 1998).

While dynamical processes internal to the Atlantic basin generate Benguela Niños, it has recently been argued that the extraordinary warming in early 1995 was boosted by southward advection of unusually high freshwater discharge from the Congo River and precipitation over the western African coast (Aroucha et al., 2024). Anomalous alongshore flow advected Congo River discharge southward to the Benguela upwelling region where it led to the formation of shallow freshwater mixed layers above thick salt stratified barrier layers that limited vertical turbulent mixing with colder thermocline waters below. The reduction in vertical mixing then caused SSTs to sharply rise in the surface mixed layer (Aroucha et al., 2024).

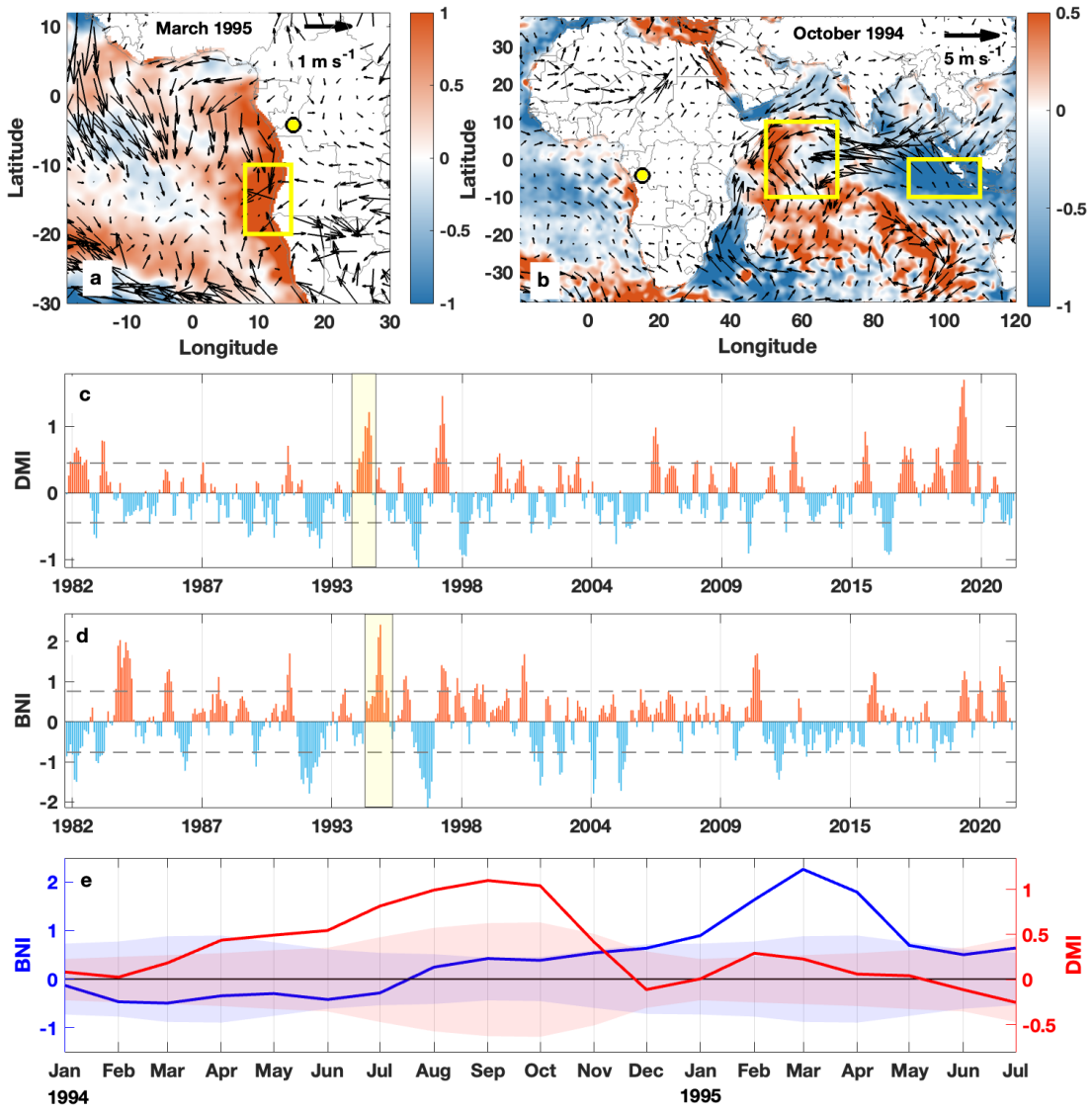

Figure 6.1. Indian Ocean Dipole and Benguela Niño Indices. Monthly sea surface temperature (SST) anomaly (shading, °C) in (a) March 1995 and (b) October 1994 relative to a monthly climatology for 1991–2020. Wind anomalies from the European Centre for Medium-Range Weather Forecasts Reanalysis v5 (ERA5) relative to a 1987–2020 climatology (vectors, in m s−1) are overplotted. c Monthly Dipole Mode Index (DMI, °C) and (d) Benguela Nino Index (BNI, °C) estimated from SST for 1982–2021 with the 1994 and 1995 events outlined in yellow shading. Horizontal dashed lines are drawn for ±1 standard deviation which is often used as a threshold for defining significant events. e The DMI and BNI during January 1994–June 1995 with ±1 monthly standard deviation (shaded area) computed based on the period 1991–2020. The monthly time series in (e) are slightly smoothed with a 1–2-1 digital filter for clarity. BNI is calculated as the SST anomaly over the Angola-Benguela Area (10°S–20°S, 8°E–14°E; yellow box in a). The DMI is calculated as the SST anomaly difference between the eastern (10°S–0°N, 90°E–110°E) and western (10°S–10°N, 50°E–70°E) equatorial Indian Ocean (yellow boxes in b).

Why the Congo River discharge was high in early 1995 is an open question. Here, we will identify the cause of that high discharge as an Indian Ocean Dipole (IOD) event, one of the strongest of the past 40 years, that occurred in late 1994 (Fig. 6.1b, c). The IOD (Saji et al., 1999; Webster et al., 1999), which is similar to the Pacific El Niño that develops every few years through coupled ocean-atmosphere interactions involving surface wind and sea surface temperature (SST) variations, is a major source of year-to-year variability in Congo River basin rainfall (Moihamette et al., 2022; Jarugula & McPhaden, 2023), and Congo River discharge (Jarugula & McPhaden, 2023). It has further been shown, by highlighting two recent extreme IOD events of opposite sign in 2016 and 2019 and by analyzing historical data over the last 40–60 years, that

there is a direct link between the IOD, Congo River rainfall, Congo River discharge, and eastern tropical Atlantic sea surface salinity (SSS) (Jarugula & McPhaden, 2023). There is a delay of several months between the peak of an IOD event, which typically occurs in boreal fall (September–November), and the peak eastern tropical Atlantic SSS anomaly because of intrinsic lags between changes in Indian Ocean SSTs, changes in atmospheric circulation and rainfall, Congo river basin hydrology, and river discharge.

We will demonstrate that linkages previously described (Jarugula & McPhaden, 2023), involving oceanic, atmospheric, and hydrological processes connecting the Indian and Atlantic Oceans, were clearly at work in late 1994 to early 1995. We will also show that the resultant eastern tropical Atlantic SSS anomalies that were generated in early 1995 by the 1994 IOD event are the same as those identified as having intensified the 1995 Benguela Niño (Aroucha et al., 2024). Finally, we will argue that the IOD may have been a factor in amplifying other Benguela Niño events through its impacts on eastern tropical Atlantic salinity such as in early 2016 (Lübbecke et al., 2019), a moderate amplitude Benguela Niño that was preceded by a moderate IOD event in late 2015 (Utari et al., 2019).

6.3 Results and Discussion

6.3.1 Development of the 1994 Indian Ocean Dipole

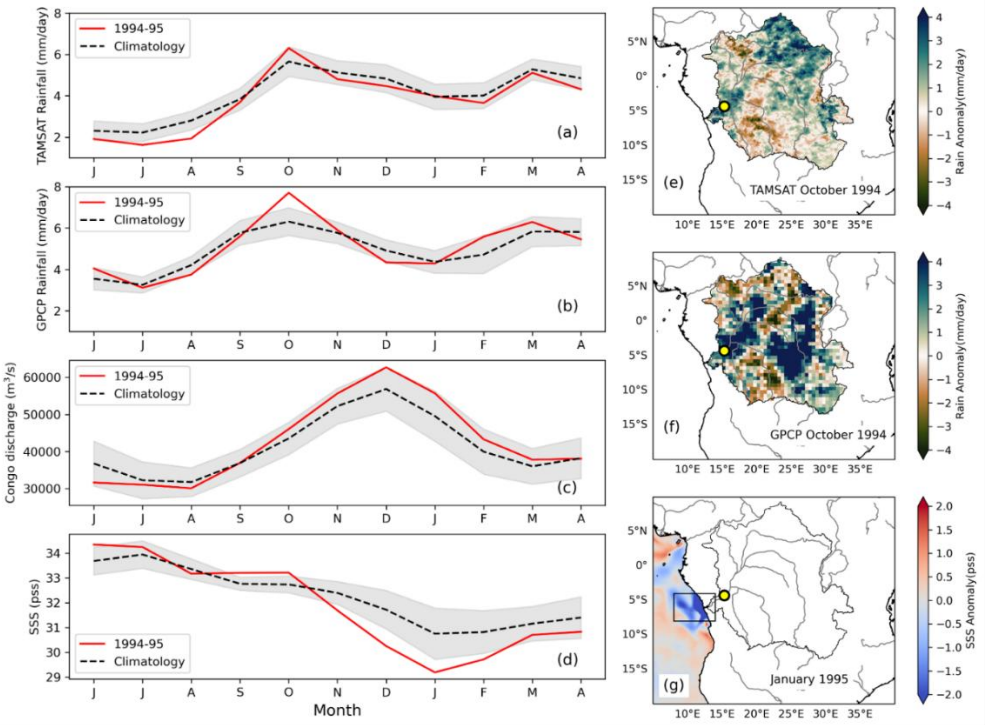

Figure 6.2. Congo basin rainfall, Congo River discharge, and sea surface salinity near the Congo River mouth from July 1994 to April 1995. Monthly mean values of (a) Tropical Applications of Meteorology using SATellite (TAMSAT) rainfall (mm day^{-1}) and (b) Global Precipitation Climatology Project (GPCP) rainfall (mm day^{-1}) averaged over the Congo basin, c Congo River discharge (m^3 s^{-1}) measured at the Kinshasa-Brazzaville station (yellow dot in e–g) and (d) Global Ocean Eddy resolving Reanalysis (GLORYS12) sea surface salinity (SSS; pss) averaged over coastal ocean near the Congo River mouth (4°S–8°S, 8°E–14°E; black box marked in g) during June 1994 to March 1995 (red lines). Monthly climatologies (black dotted lines) and ±1 standard deviation (gray shading) are shown in (a–d). Spatial distribution of monthly rainfall anomalies (mm day^{-1}) over Congo basin in October 1994 from (e) TAMSAT and (f) GPCP. g Spatial map of monthly GLORYS12 reanalysis SSS anomaly (pss) in January 1995. The anomalies are estimated using monthly climatology during the period 1983–2020 for TAMSAT and GPCP rainfall, 1950–2019 for Congo River discharge and 1994–2020 for reanalysis SSS.

As is typical of most IOD events, the 1994 IOD began to develop in boreal spring, peaked in September to November, and then rapidly decayed by early 1995 (Fig. 6.1). During the peak phase in October 1994, rainfall was anomalously high in the Congo River basin (Fig. 6.2a, b) with a broad consistency in the spatial structure of rainfall within the basin exhibited by two different rainfall products (Fig. 6.2e, f). This rainfall was associated with a low-level wind convergence mainly driven by strong easterly wind anomalies from the western Indian Ocean (Fig. 6.3). We can quantify the relationship of the large-scale wind field to Congo River basin rainfall through an analysis of the column integrated moisture budget (see "Data and Methods"), which indicates that the excess of precipitation over evaporation in the Congo River basin in October 1994 was the result of moisture convergence into the region with little contribution from changes in the column integrated moisture content (Fig. 6.4a–c). Moreover, focusing on October, which is typically in the peak season of IOD development, a decomposition of the moisture balance into contributions related to dynamic changes in atmosphere circulation vs thermodynamic contributions related to changes in atmospheric humidity (see "Data and Methods") indicates that in general it is predominantly changes in atmospheric circulation that control the moisture convergence and rainfall in the Congo River basin rather than changes in humidity (Fig. 6.4d).

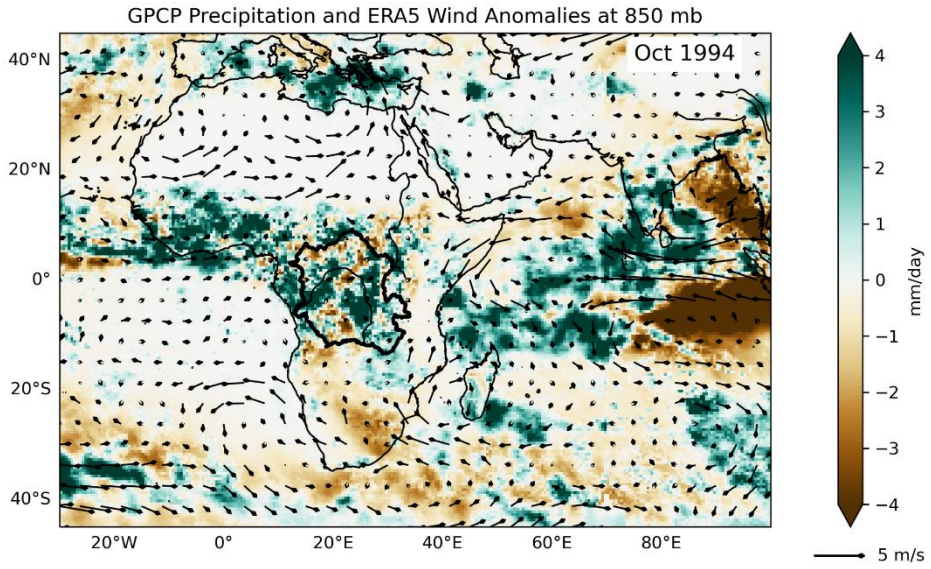

Figure 6.3. Anomalous low-level winds and rainfall around Africa in October 1994. Global Precipitation Climatology Project (GPCP) precipitation anomalies (shading, mm day^{-1}) are overplotted on 850 mb wind anomalies relative to a 1987–2020 climatology (vectors, in ms^{-1}) based on the European Centre for Medium-Range Weather Forecasts Reanalysis v5 (ERA5).

6.3.1 Effects on Congo discharge and coastal zone salinity

Congo River discharge measured at the Kinshasa-Brazzaville station, about 500 km upstream of the river mouth, provides an estimate of the outflow for over 98% of the Congo River Basin (Alsdorf et al., 2016). Peak Congo River discharge occurs typically during December–January and was significantly higher than normal during November 1994 to January 1995 (by ~1 standard deviation) following the peak IOD and associated Congo basin rainfall anomaly (Fig. 6.2c). The delay of a few months from the peak Dipole Mode Index (DMI) results from the time it takes for the atmospheric circulation to adjust to coupled ocean-atmosphere interactions in the Indian Ocean, for the circulation to converge the moisture over the Congo

basin, and for the tributaries of the Congo River to funnel the runoff to the river mouth (Jarugula & McPhaden, 2023). SSS began to drop in the coastal zone of the eastern tropical Atlantic as the anomalously large volume of Congo River water was discharged into the eastern Atlantic (Figs. 6.2c, d and 6.5). SSS anomalies lag Congo River discharge anomalies by about 1 month (Fig. 6.5) and the peak DMI by 3–5 months (Fig. 6.9), consistent with previous analysis (Jarugula & McPhaden, 2023). Thus, the largest SSS anomalies near the mouth of the Congo occurred from December 1994 to February 1995 (Figs. 6.2d, g and 6.6b, c). There was a small contribution of local freshwater forcing to the accumulation of low salinity water near the Congo River mouth in November and December 1994 (Fig. 6.5) because this is the time of year when the Intertropical Convergence Zone is shifted to the south of the equator in the eastern tropical Atlantic (Alsdorf et al., 2016). However, that contribution, even though enhanced relative to normal years (Fig. 6.5), was small relative to Congo River discharge.

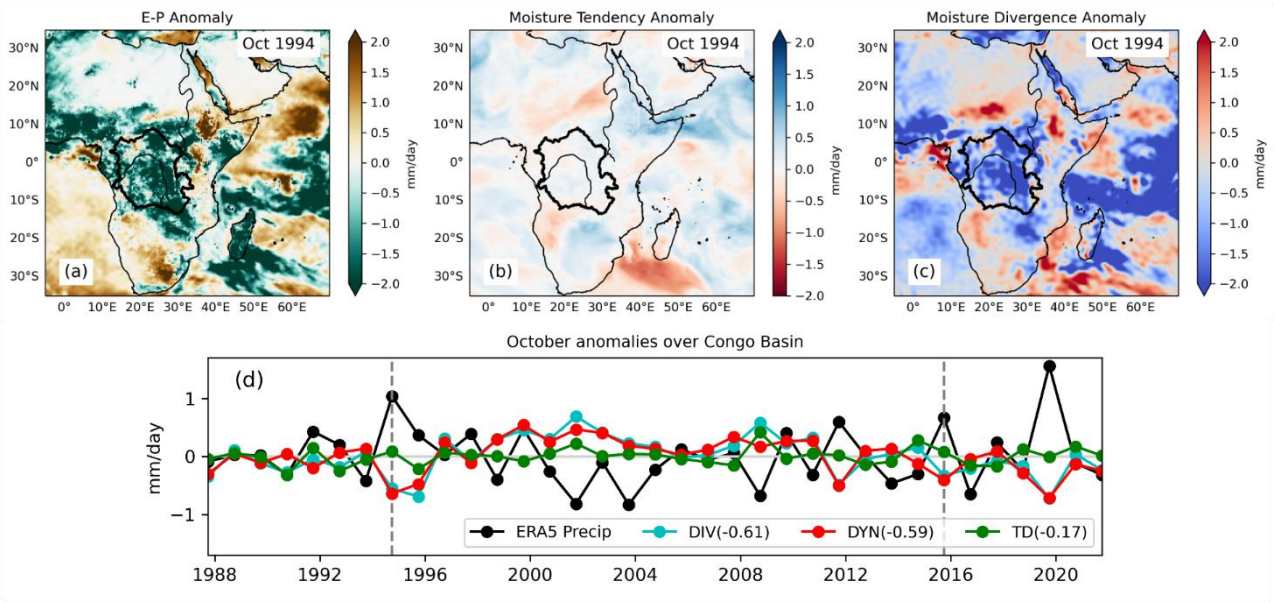

Figure 6.4. Atmospheric moisture budget anomalies for the Congo River basin. October 1994 anomalies relative to a 1987–2020 climatology for (a) Evaporation minus precipitation (E − P), b column integrated moisture time tendency ($\partial q/\partial t$) and (c) moisture divergence flux ($\nabla.(qV)$) based on the European Centre for Medium-Range Weather Forecasts Reanalysis v5 (ERA5). The Congo River basin is outlined in each panel. d Detrended monthly anomalies for October precipitation (black), moisture divergence (DIV; blue), and dynamic (DYN; red) and thermodynamic (TD; green) components of moisture divergence averaged over the Congo basin based on the ERA5 reanalysis, with October 1994 and October 2015 marked by a dashed line. Correlation coefficients between DIV, DYN, TD, and the corresponding precipitation anomaly are indicated in parentheses. Standard deviations of DIV, DYN, and TD for October 1987–2020 are 0.33, 0.30, and 0.14, respectively. The correlations and standard deviations indicate the dominance of year-to-year variations in atmospheric circulation in determining the moisture divergence and rainfall over the Congo basin. All units in mm day−1.

6.3.1 Impact of freshwater on 1995 Benguela Niño development

The anomalous surface freshwater pool near the Congo River mouth was very thin, only 5–15 m deep (Aroucha et al., 2024). Once established in January 1995, the freshwater pool was advected southward to the Angola-Benguela Area (ABA, defined as 10°–20°S, 8°E–14°E) by very strong surface southward flows near the African coast most notably in February 1995 (Fig. 6.6c, e). This anomalous southward flow resulted from a downwelling coastal Kelvin wave remotely forced by weakening of the easterly trade winds near the equator (Imbol Koungue & Brandt, 2021) reinforced by a weakening of the alongshore local winds that also favored

anomalous southward flow (Aroucha et al., 2024; Fennel et al., 2012). Some freshwater was advected offshore via eddies generated by the plume itself (Palma & Matano, 2017; Vic et al., 2014) (Fig. 6.6d) but the bulk remained trapped to the coast of Angola and Namibia resulting in thin (5–15 m deep) surface mixed layers resting above thick salt-stratified barrier layers (Fig. 6.7) (Aroucha et al., 2024). These barrier layers were thickest in March–April 1995 coincident with the highest SSTs during the event. The strong shallow vertical density stratification due to low surface salinities limited vertical turbulent mixing with colder thermocline water below, which amplified warm mixed-layer temperature anomalies as shown in the surface layer temperature balance analysis conducted by Aroucha et al. (2024). Local precipitation contributed to some surface freshening in the ABA particularly in March 1995 as coastal SSTs reached their peak, resulting in anomalous deep convection and rainfall over the warm SSTs (Fig. 6.6e) (Aroucha et al., 2024). Overall however, the largest source of freshening in the ABA in early 1995 was by far southward advection of Congo River discharge (Fig. 6.5).

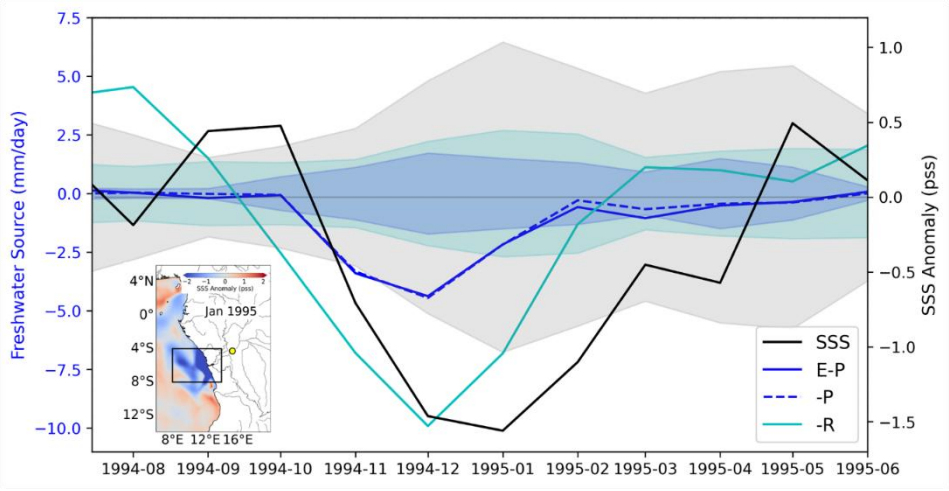

Figure 6.5. Congo River discharge is the dominant source of freshwater in the area surrounding the Congo River mouth in late 1994-early 1995. Monthly anomaly time series of sea surface salinity (SSS), evaporation minus precipitation (E − P) and river discharge per unit area (−R, with the negative sign to indicate a freshening effect on SSS) near the mouth of the Congo River (the oceanic area within 4°S–8°S, 8°E–14°E highlighted in the lower left inset) for July 1994–June 1995. E − P based on the European Centre for Medium-Range Weather Forecasts Reanalysis v5 (ERA5) and SSS is from the Global Ocean Eddy-resolving Reanalysis (GLORYS12). For reference, −P (which dominates E − P) is also plotted. Anomalies are computed relative to a 1994–2020 climatology with ±1 standard deviation for each term (shading) estimated from these anomalies. The standard deviation for −P is not shown for clarity; it is nearly equivalent to the standard deviation of E − P. Consistent with Aroucha et al. (2024), Congo River discharge is larger in magnitude than E − P and −P in the vicinity of the Congo River mouth in late 1994-early 1995 and primarily responsible for the observed drop in SSS at that time.

In summary, as previously reported (Aroucha et al., 2024), the amplitude of the extraordinarily strong Benguela Niño in early 1995 (Fig. 6.1e) was boosted by anomalously high freshwater discharge from the Congo River that was advected southward in early 1995 (Fig. 6.6). The precise mechanism by which Congo River discharge amplified ABA warm SST anomalies was through the formation of thin, salt-stratified mixed layers overlying thick barrier layers that limited vertical mixing with colder temperatures in the thermocline (Fig. 6.7) (Aroucha et al., 2024). The results of this study identify the ultimate cause of the anomalously high Congo River discharge as the 1994 Indian Ocean Dipole which peaked several months before the onset of the 1995 Benguela Niño (Fig. 6.1e). The IOD altered the atmospheric circulation to enhance moisture convergence and rainfall over the Congo River basin in late 1994 (Figs. 6.3, 6.4). Rain water runoff was then

shunted by the Congo River into the eastern tropical Atlantic where it significantly lowered coastal salinity (Fig. 6.2), after which this fresh water mass was swept southward into the ABA. We emphasize that based on the evidence we have presented, the 1994 IOD helped to boost the amplitude of the 1995 Benguela Niño, but was not the ultimate cause for it. Warm anomalies were already developing in the ABA in January 1995 (Fig. 6.1e) before the major southward pulse of Congo River discharge in February 1995 (Fig. 6.6c,e).

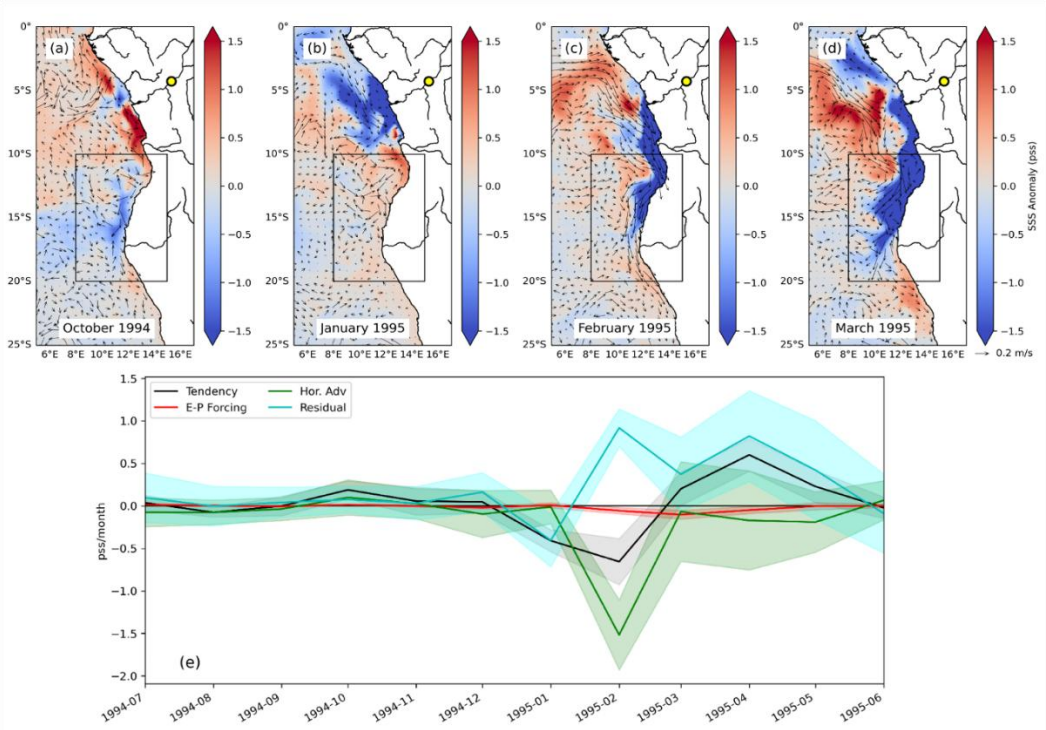

Figure 6.6. Surface salinity, surface currents, and mixed-layer salt balance in the eastern tropical Atlantic in late 1994-early 1995. Spatial maps of monthly Global Ocean Eddy-resolving Reanalysis (GLORYS12) SSS anomaly (pss; color) overlaid by surface velocity vector anomalies during (a) October 1994 (b) January 1995 (c) February 1995 and (d) March 1995 off the southwest coast of Africa. The Angola-Benguela Area (ABA; 10°S–20°S, 8°E–14°E) is indicated by the black box. Monthly anomalies are constructed relative to a 1994–2020 climatology. A reference vector of 0.2 m s-1 is shown in the bottom right. e Salt balance averaged over the ABA based on (6.1) in "Data and Methods", showing the time tendency for SSS anomalies (black curve), the anomalous local freshwater forcing term related to evaporation minus precipitation (E − P, red curve) and horizontal advection (green curve). Also shown is the residual (light blue curve) which includes terms that cannot be explicitly computed, such as vertical advection, entrainment, and diffusion, plus any computational errors. The ±1 standard deviation for each term (shading) is computed from monthly anomalies over the period 1994–2020. The large negative value of advection in February 1995 is mostly due to freshwater advection from the north. The large positive residual in February–April 1995 is consistent with an upward flux of high salinity water across the base of the salt-stratified mixed layer due to turbulent vertical mixing. Since there is no vertical temperature gradient at the base of the mixed layer (Fig. 6.7) this vertical mixing does not also lead to an upward flux of cold thermocline water (Aroucha et al., 2024).

Most previous wind-forced ocean model simulations of the 1995 Benguela Niño have tended to underestimate the amplitude of the event compared with observations (Illig et al., 2020; Florenchie et al., 2004; Lübbecke et al., 2010; Imbol Koungue et al., 2019). In every case, these modeling studies failed to include the effect of Congo River discharge on barrier layer formation and the mixed layer heat balance. Our analysis suggests that including anomalous Congo River discharge in model simulations of Benguela Niños may help to reconcile this discrepancy. A previous idealized modeling study has suggested that Congo River discharge had little impact on SST in the region to the north of the ABA (Martins & Stammer, 2022). However, no similar modeling studies have been conducted in the ABA during the developing phase of

Benguela Niños. Such studies would be a valuable contribution to further quantify the effects of barrier layer formation on Benguela Niño amplitudes in general and for the 1995 Benguela Niño in particular.

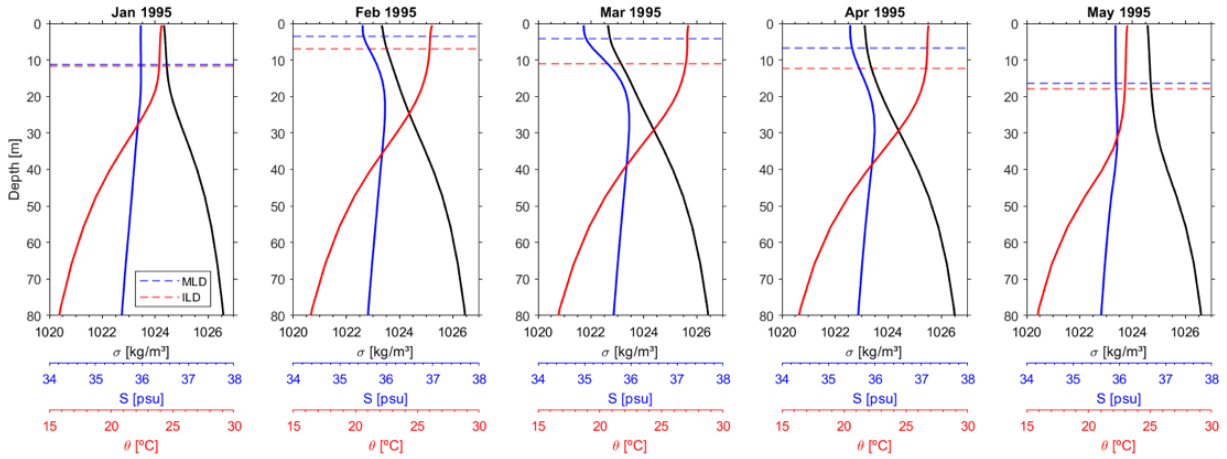

Figure 6.7. Vertical hydrographic structure in the Angola-Benguela Area. Monthly averaged vertical profiles of temperature (red), salinity (blue), and potential density (black) in the Angola Benguela Area (ABA; 10°S–20°S, 8°E–14°E) for January-May 1995 from the Global Ocean Eddy-resolving Reanalysis (GLORYS12). The mixed layer depth (MLD) and isothermal layer depth (ILD) for each month are indicated by horizontal blue and red lines, respectively. The barrier layer is defined as the region between these two layers.

6.3.2 Indian Ocean Dipole effects on other Benguela Niños

The series of inter-basin events described in this paper appear to happen coincidentally, so one might not expect a systematic relationship between the IOD and Benguela Niños. There are, however, other Benguela Niños that appear to have been influenced by the IOD in a similar fashion, one of which occurred in 2016. This Benguela Niño was weaker than the 1995 event but as in 1995, enhanced freshwater input to the region from Congo River discharge helped to boost its amplitude (Lübbecke et al., 2019) . This event was preceded in the boreal fall of 2015 by a moderate amplitude IOD event (Fig. 6.1c,d) (Utari et al., 2019) that altered the atmospheric circulation around Africa to converge moisture over the Congo River basin (Fig. 6.4d). While the various rainfall estimates (TAMSAT, GPCP, ERA5) are less in agreement on the overall magnitude of the Congo River basin rainfall anomaly in late 2015 (cf. Figs. 6.4d and 6.10a, b), there were regions in the basin that experienced excess rainfall (Fig. 6.10e, f) and these regions likely contributed to the substantial increase in Congo River discharge in late 2015-early 2016 (Fig. 6.11c). Similar to what happened in early 1995, this river discharge and its southward advection along the coast of Angola and Namibia (Fig. 6.11) contributed to the formation of thin surface mixed layers, thick subsurface barrier layers and warmer coastal SSTs (Lübbecke et al., 2019).

Previous research based on satellite observations has suggested that the salinity impacts of anomalous Congo River discharge on Benguela Niño development would only rarely occur and be difficult to observe (Martins & Stammer, 2022). However, recognizing the IOD's impact on Congo River discharge (Jarugula & McPhaden, 2023) facilitates identification of such events. Over the 40 year-long (1982–2021) DMI and Benguela Niño time series (Fig. 6.1), the events discussed in this article, namely 1994–95 and 2015–16, clearly stand out. However, there are other related events as well that appear in the record. For example, there was also a strong negative IOD event in late 1996 that was followed by a Benguela Niña in early 1997.We

hypothesize that the mechanisms by which a positive IOD amplifies a Benguela Niño work equivalently but in an opposite sense for negative IOD events and Benguela Niñas like in 1996–97. For such events, reduced Congo River discharge would lead to elevated SSS and the absence of barrier layers in the ABA, facilitating enhanced vertical mixing and lower SSTs.

We also note that for the period 1993–2020, there is an inverse relationship between monthly SSS from the GLORYS12 reanalysis and the monthly BNI (Fig. 6.8) with a zero-lag crosscorrelation of −0.41 (significantly nonzero with 90% confidence). A regression fit to the data suggests that a 1 pss freshening of surface salinity would be associated with a 1 °C increase in Benguela Niño SST, while a 1 pss increase in salinity would be associated with anomalous surface cooling of 1 °C. The years 1995 and 2016 (Benguela Niños following positive IOD events) and 1997 (a Benguela Niña following a negative IOD event) stand out in the BNI and SSS scatterplot (Fig. 6.8). Correlation does not imply causality and there is ambiguity about cause and effect with BNI and SSS most highly correlated at zero lag. Rainfall does increase slightly in March 1995 associated with higher SSTs in the ABA as noted above (Fig. 6.5), but in general local rainfall is a small contributor to SSS variability during the development of Benguela Niños. The variations in mixed layer salt storage are more affected by horizontal advection and vertical exchanges (Fig. 6.6e). That suggests that low SSS is leading to higher SSTs more than the other way around. As evident from Fig. 6.7, advection of low salinity from the Congo discharge causes the mixed layer to shoal to only 5 m depth in February–March 1995. With such low heat capacity, the shallow mixed layer responds within a few days to heat exchanges across the air-sea interface. For example, a 20 W m−2 surface heat flux into a 5 m deep mixed layer would warm the mixed layer by about 1 °C in 10 days. Thus, a monthly time average does not resolve the detailed SST adjustment to surface heat flux trapped in such a shallow layer, which would explain the zero-lag correlation. Thus, we conclude that salinity changing the depth of the mixed layer so as to trap heat and raise SST is a more plausible first-order explanation for the SSS/BNI relationship than enhanced rainfall linked to unusually warm SST causing the salinity to drop.

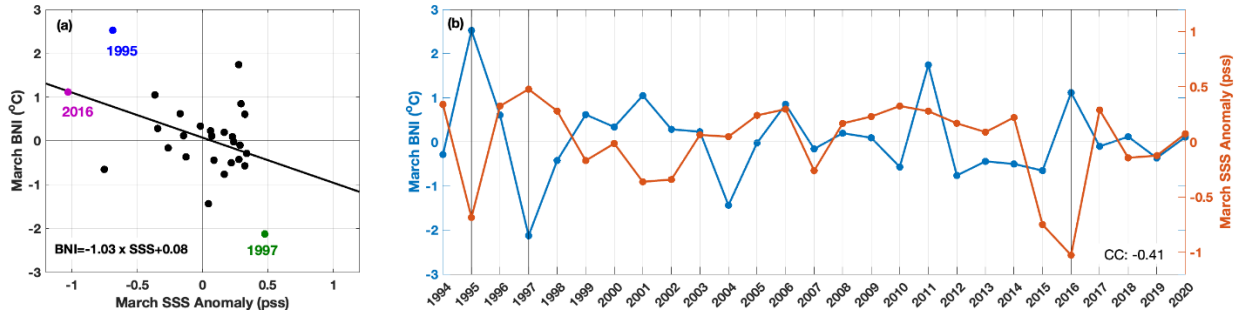

Figure 6.8. Low surface salinity in the Angola-Benguela Area is associated with stronger Benguela Niños. a Scatter diagram and linear regression fit between the BNI and ABA SSS in March when Benguela Niños and Niñas typically peak from the GLORYS12 reanalysis for the period 1993–2019. The years 1995 and 2016 (Benguela Niños following positive IOD events) and 1997 (Benguela Niña following a negative IOD event) are highlighted. b Time series of March BNI and SSS values with 1995, 1997, and 2016 indicated by vertical lines. The crosscorrelation (CC) of the two time series shown in the lower right of panel (b) is −0.41, which is significantly nonzero with 90% confidence. The linear least squares regression fit equation is shown in (a).

It is interesting to note that associated with the easterly wind anomalies in the Indian Ocean linked to the development of the IOD in October 1994, there are low-level westerly wind anomalies evident in the equatorial Atlantic (Figs. 6.1b and 6.3). That is also true for the 2019 IOD (Jarugula & McPhaden, 2023).

These low-level westerly anomalies in the Atlantic are consistent with the atmospheric mass and moisture balance that require inflow to supply ascending air in the convective center over the Congo basin. Thus, it may be more than coincidence that the IOD is sometimes followed by a Benguela Niño event, in that the IOD-driven rainfall over the Congo may also result in low-level westerly wind anomalies along the equator in the Atlantic that contribute to the initiation of a subsequent Benguela Niño. Indeed, it has been noted that the IOD-related convection over Africa can weaken the Atlantic trade winds near the equator, thereby triggering Atlantic Niño events (Zhang & Han, 2021; Fan & Meng, 2023). Weakened trade winds constitute remote forcing for Benguela Niños, which is why Atlantic Niños and Benguela Niños often occur together in the same year (Illig et al., 2020; Lübbecke et al., 2010). Our study has focused on Indian Ocean forcing of the Atlantic via a land bridge involving Congo River discharge. However, it is very plausible that IOD forcing of the Atlantic may occur simultaneously through both land and atmospheric bridges, a hypothesis that warrants further testing in a modeling framework that can incorporate both pathways.

6.4 Conclusion

Given the substantial environmental and economic impacts of Benguela Niños, there is tremendous societal value in developing skillful prediction models for these events. However, seasonal forecast skill for Atlantic SSTs in general and Benguela Niños in particular is limited to a few months at most (Li et al., 2020, 2023; Oettli et al., 2021). This study suggests one potential new source of predictability for Benguela Niños, namely the IOD through both a land bridge involving the Congo River basin hydrology and possibly an atmospheric route involving convection over Africa. There is predictability built into the phase lags between IOD development, atmospheric circulation changes, Congo basin rainfall, Congo River discharge, and eastern tropical Atlantic SSS, with SSS lagging the DMI by 3–5 months (Figure 6.9). Thus, for a Benguela Niño that develops early in the calendar year following an IOD event, we might anticipate that its amplitude and impacts will be more pronounced than they would have otherwise been had there been no antecedent IOD. We can moreover gauge the likelihood for such an amplification by monitoring Congo River basin rainfall, river discharge, and eastern tropical Atlantic surface salinity anomalies. Ensuring that these processes are properly represented in Benguela Niño forecast models should be a priority.

Finally, there is a diversity of IOD events in terms of their amplitude, spatial structure, and temporal evolution (Cai et al., 2021). It has been suggested from climate model simulations under high greenhouse gas emission scenarios that the frequency of extreme IOD events, like the 1994 event which boosted the amplitude of the 1995 Benguela Niño, will increase by almost a factor of three over the course of the twenty-first century (Cai et al., 2014). This represents an increase from one extreme IOD event every 17 years during the twentieth century to one extreme event every 6 years by the end of the 21st century. If this increase in frequency is realized, it is likely that future IOD events will exert much more influence than today on Benguela Niño development through both the land bridge which has been the focus of this study, and possibly also through an atmospheric bridge as suggested in Zhang & Han (2021) and Fan & Meng (2023).

6.5 Data and Methods

6.5.1 Data sources and Indices

We used monthly mean SST data from the high-resolution NOAA Optimum Interpolation SST (OISST) data set, consisting of blended satellite and in-situ measurements from 1981 to present, with spatial resolution of 0.25° (Huang et al., 2021; Reynolds et al., 2007).

We define the Dipole Mode Index (DMI), a measure of IOD strength, as the SST anomaly difference between the eastern (90°E–110°E, 10°S–0°N) and western (50°E–70°E, 10°S–10°N) equatorial Indian ocean. We define the Benguela Niño Index (BNI) as the average of SST anomalies in the ABA (10°S–20°S, 8°E–14°E). Anomalies are based on a 30-year climatology for 1991–2020. A long-term linear trend has been removed from the BNI time series.

IOD events occur with both positive and negative polarity. Positive events like 1995 (DMI > 1 standard deviation) are associated with unusually cold SSTs in the eastern Indian Ocean, unusually warm SSTs in the western Indian Ocean, and anomalous easterly surface winds (Fig. 6.1b). Negative events (DMI < −1 standard deviation) are associated with anomalies of opposite sign. Similarly, there is a cold counterpart to Benguela Niños (BNI > 1 standard deviation), referred to as Benguela Niñas (BNI < −1 standard deviation), that occur when SSTs in the ABA are significantly colder than climatology.

Congo River discharge is based on daily data measured at Kinshasa-Brazzaville station 500 km upstream from the river mouth, for January 1954 to February 2020, available from the Global Runoff Data Centre. We use two different monthly rainfall data sets, one of which is from the Global Precipitation Climatology Project (GPCP) at 0.5° spatial resolution from 1979 to 2021 (Adler et al., 2003). The second is the Tropical Applications of Meteorology using SATellite (TAMSAT) data, available from the University of Reading for 1983–2020, which are based on ground-based observations at 0.0375° spatial resolution from land areas only. Comparison of these two data sets (Jarugula & McPhaden, 2023) indicates that they provide complementary and consistent views of rainfall variability in the region.

Monthly temperature, salinity, ocean currents, sea level, and mixed layer depth are taken from the Global Ocean Eddy-resolving Reanalysis (GLORYS12) (Lellouche et al., 2021), with 1/12º horizontal resolution and 50 vertical levels, of which 22 are in the upper 100 m. The reanalysis is based on the Nucleus for European Modelling of the Ocean (NEMO) with atmospheric forcing by the European Centre for Medium-Range Weather Forecasts (ECMWF) Interim Reanalysis (ERA-Interim) and the ECMWF Reanalysis v5 (ERA5) in recent years. Assimilated observations include Reynolds 0.25° AVHRR only SST, delayed mode sea level anomaly from all altimetric satellites, in situ temperature/salinity profiles from Copernicus Marine CORAv4.1 database, and IFREMER/CERSAT sea ice concentration. GLORYS12 only incorporates climatological monthly mean river runoff but the effects of interannual variations in runoff are included though data assimilation in the model. The reanalysis is available from 1993 onward and we use output for the period 1993-2020.

Temperature and salinity data in upper 200 m of the reanalysis product in the southeastern tropical Atlantic were previously validated against independent in-situ measurements from the Nansen Programme

(Aroucha et al., 2024), which comprises more than 8000 Conductivity-Depth-Temperature (CTD) profiles taken off the Angola and Namibia coasts from 1994–2014 (Tchipalanga et al., 2018). Although the GLORYS12 reanalysis is forced with climatological river runoff, validation against the CTD profiles showed correlation and root-mean square deviation of 0.68 (0.96) and 0.55 pss (1.3 °C), respectively, for the salinity (temperature) values in the coastal zone (Aroucha et al., 2024).

Monthly specific humidity, atmospheric winds at several pressure levels ranging from 1000 – 1 hPa, surface rate of evaporation, surface rate of precipitation, and the vertically integrated atmospheric moisture budget terms at 0.25º spatial resolution during 1987–2021 are obtained from the ERA5 (Hersbach et al., 2023; Mayer et al., 2021).

6.5.2 Ocean mixed layer balance

We use a mixed-layer salt balance equation in the ABA to relate the change in mixed-layer salinity to local surface forcing and horizontal advection. This equation can be written as:

$$\frac{\partial \mathrm{S}}{\partial \mathrm{t}} = -\boldsymbol{u}.\nabla \mathrm{S} + FW_{forc} + Res. \quad (6.1)$$

where $\frac{\partial \mathrm{S}}{\partial \mathrm{t}}$ is the time rate of mixed layer salinity (S). Horizontal advection is the first term on the right side of the equation, with $\boldsymbol{u}$ as the horizontal vector velocity in the mixed layer and ∇S is the two-dimensional horizontal salinity gradient. The local freshwater forcing term is computed using:

$$FW_{forc} = \frac{S_o}{h}\,(E - P) \quad (6.2)$$

where E is the rate of evaporation (in m day^{-1}), P is the rate of precipitation (in m day^{-1}), S_o is the surface salinity (in pss) and h is the mixed layer depth (in m). The residual term (Res) includes terms that cannot be explicitly computed (such as vertical advection, entrainment, and diffusion) and any computational errors.

6.5.3 Atmospheric moisture budget

We use ERA5 monthly evaporation and precipitation, monthly sea surface salinity, horizontal velocities, and mixed layer depth from the GLORYS12 reanalysis to estimate terms in (6.1). E − P estimates in this calculation are essentially the same when the ERA5 precipitation is replaced by GPCP precipitation.

The atmospheric moisture budget equation can be written as:

$$\mathrm{E} - \mathrm{P} = \frac{1}{\mathrm{g}}\nabla.\int_{\mathrm{pt}}^{\mathrm{ps}} \mathrm{qVdp} + \frac{1}{\mathrm{g}}\frac{\partial}{\partial \mathrm{t}}\int_{\mathrm{pt}}^{\mathrm{ps}} \mathrm{qdp} \quad (6.3)$$

where P and E are rates of precipitation and evaporation (in kgm^{-2} s $^{-1}$), g is acceleration due to gravity (m^2 s^{-1}), q is specific humidity (kg/kg), v is the horizontal wind vector (m/s), ps is surface pressure 1000 hPa and

pt is pressure at the uppermost level of the atmosphere, chosen to be 100 hPa. The first and second terms on the right-hand side of the equation denote the divergence field of moisture flux and the moisture tendency, respectively. In order to determine the relative contribution of dynamic and thermodynamic processes to the moisture divergence term, we decompose the wind and specific humidity as $V = \overline{V} + V'$ and $q = \bar{q} + q'$, where $\overline{V}, \bar{q}$ are the climatological means over the period 1987–2020 and V', q' are the deviations from the 34-year climatology (Seager et al., 2010; Wang et al., 2017). Moisture divergence can then be written as the sum of dynamic (DYN), thermodynamic (TD) and transient eddy (TE) components estimated using:

$$\mathrm{DYN} = \frac{1}{g}\nabla . \int_{pt}^{ps} \bar{q}V' \, dp \quad (6.4)$$

$$\mathrm{TD} = \frac{1}{g}\nabla . \int_{pt}^{ps} q'\overline{V} \, dp \quad (6.5)$$

$$\mathrm{TE} = \frac{1}{g}\nabla . \int_{pt}^{ps} q'V' \, dp \quad (6.6)$$

All units in kg m^{-2} s^{-1}. We find that the TE component is negligible compared to the DYN and TD components of moisture divergence as the deviations of q and V from the climatology are quite small. Thus, we do not consider it further in our analysis.

Open research. All the datasets are freely available in the public domain. OISST data are available at National Centers for Environmental Information (www.ncei.noaa.gov). Daily in situ measurements of river discharge measured at Kinshasa-Brazzaville station were obtained from the Global Runoff Data Centre (https://www.bafg.de/GRDC/EN/Home/homepage_node.html). TAMSAT data are available at https://www.tamsat.org.uk/ and GPCP data are available at (https://data.nasa.gov/dataset/GPCPPrecipitation-Level-3-Monthly-0-5-Degree-V3-2/2kyxn57r/data). The GLORYS12 reanalysis is distributed by the EU Copernicus Marine Service Information (http://marine.copernicus.eu/) and monthly ERA5 data can be accessed at https:// www.ecmwf.int/en/forecasts/dataset/ecmwf-reanalysis-v5. We use basic statistics packages and plotting methods in MATLAB and Python for the analysis. We do not use any specific code for data processing. The codes used in this study are available upon request to the second author S.J.

Acknowledgements. The authors wish to thank three anonymous reviewers for their thoughtful and constructive comments on an earlier version of this manuscript. M.J.M. is funded by NOAA. L.C.A. is funded by the German Academic Exchange Service Doctoral Research Grant (57552340). Part of this research was carried out by S.J. at the Jet Propulsion Laboratory, California Institute of Technology, under a contract with the National Aeronautics and Space Administration (80NM0018D0004). PMEL contribution no. 5661. M.J.M. conceived of the study and wrote the first draft. S.J. and L.C.A. contributed analyses and graphics. All authors (M.J.M, S.J., L.C.A., and J.F.L.) contributed to the interpretation of the results and to writing and editing the final manuscript. The authors declare no competing interests.

6.6 Supplementary Material

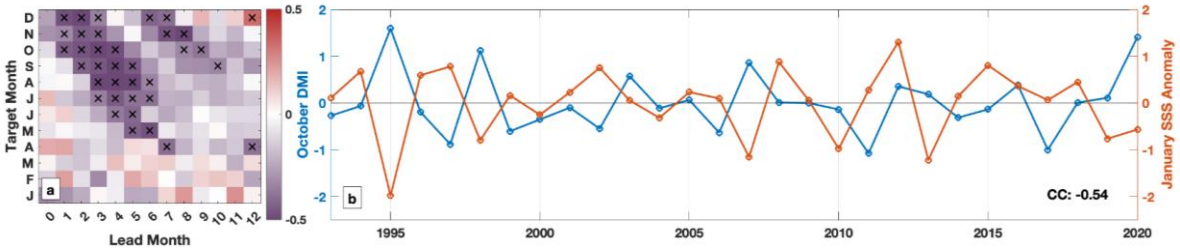

Figure 6.9. Relationship between Indian Ocean Dipole and sea surface salinity near the mouth of the Congo River. (a) Cross-correlation of the Dipole Mode Index (DMI) and Global Ocean Eddy-resolving Reanalysis (GLORYS12) sea surface salinity (SSS; pss) anomalies in the Congo River discharge region (4°S–8°S, 8°E–14°E) as a function of target (or start) month for the DMI (y-axis) and SSS at lead times of 0-12 months (x-axis). Purple (red) values indicate negative (positive) cross-correlation. Cross-correlation coefficients significant at a 90% confidence level are marked with a black cross. (b) an illustration of the relationship between DMI and SSS showing the time series of October DMI (blue line) and the following January SSS anomalies (red line). The October DMI time series is shifted 3 months forward to align with January SSS anomalies; the year on the x-axis refers to the year of the SSS anomalies (e.g., January 1995 SSS anomalies plotted with corresponding October 1994 DMI). The cross-correlation (CC) between the two time series is shown in the lower right.

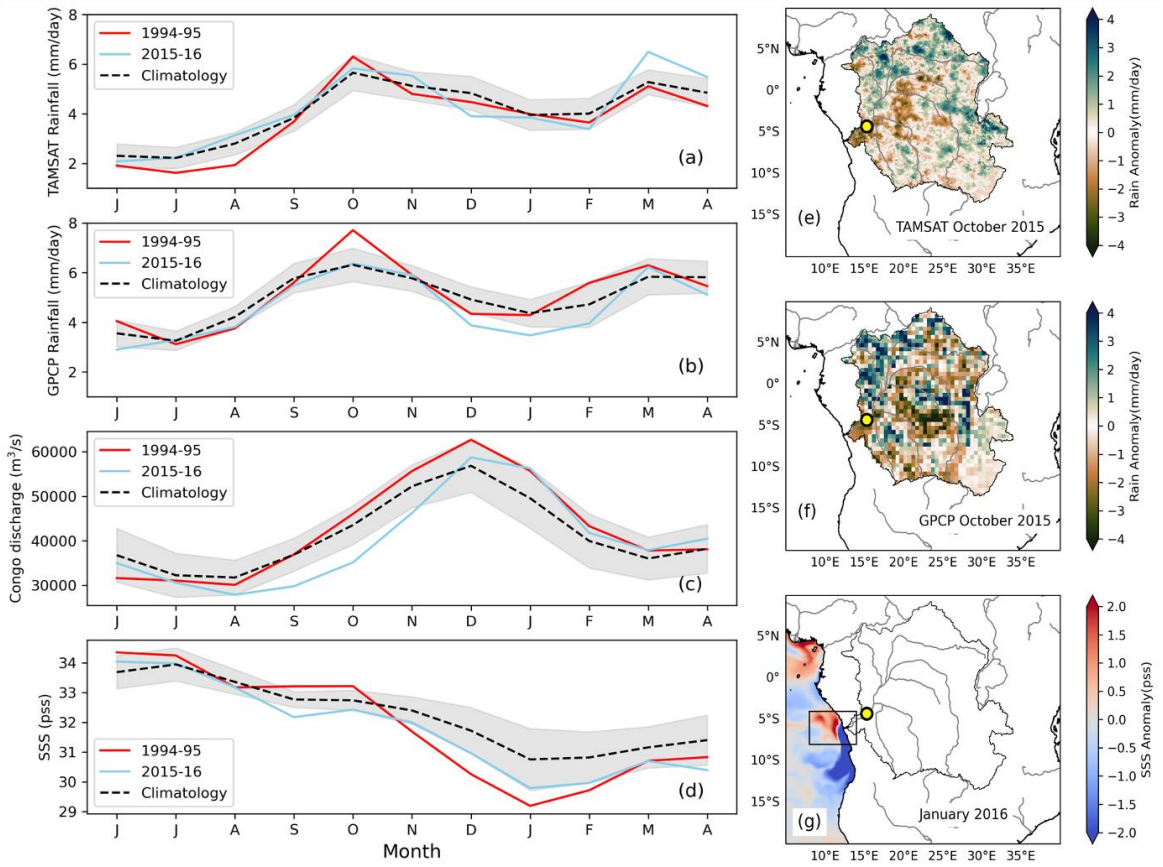

Figure 6.10. Congo basin rainfall, Congo River discharge, and sea surface salinity near the Congo River mouth from June 1994 to April 1995 and from June 2015 to April 2016. Monthly mean values of a) Tropical Applications of Meteorology using SATellite (TAMSAT) rainfall (mm day^{-1}) and b) Global Precipitation Climatology Project (GPCP) rainfall (mm day^{-1}) averaged over the Congo basin, (c) Congo River discharge (m^3 s^{-1}) measured at the Kinshasa-Brazzaville station (yellow dot in panels e-g) and (d) Global Ocean Eddy-resolving Reanalysis (GLORYS12) sea surface salinity (SSS; pss) averaged over coastal ocean close to the Congo River mouth (4°S–8°S, 8°E–14°E; black box marked in g) during June 1994 to April 1995 (red lines) and June 2015 to April 2016 (blue lines). Monthly climatologies (black dotted lines) and ±1 standard deviation (gray shading) are shown in panels (a-d). Spatial distribution of monthly rainfall anomalies (mm day^{-1}) over Congo basin in October 2015 from (e) TAMSAT and (f) GPCP. (g) Spatial map of monthly GLORYS12 reanalysis SSS anomaly (pss) in January 2016. The anomalies are estimated using a monthly climatology based on the period 1983-2020 for TAMSAT and GPCP rainfall, 1950-2019 for Congo River discharge and 1994-2020 for reanalysis SSS.

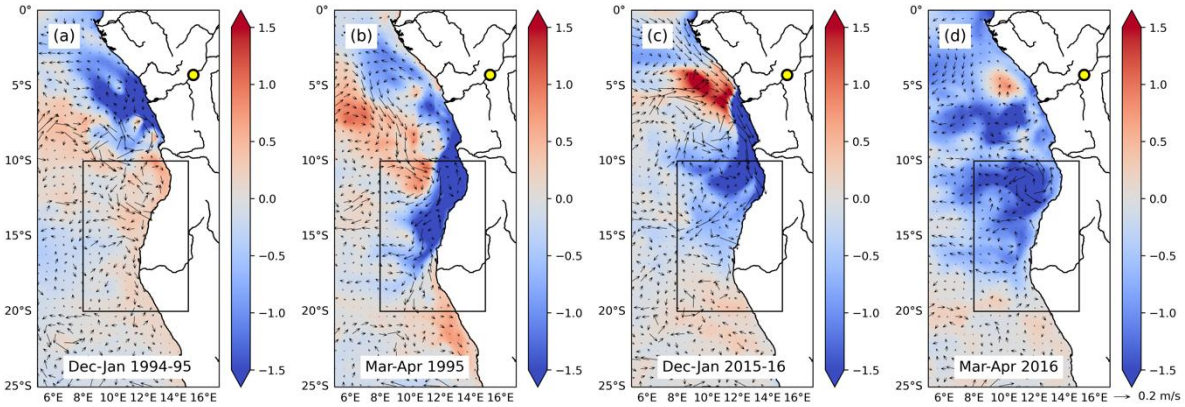

Figure 6.11. Sea surface salinity (shading, pss) and surface currents (vectors) in the eastern tropical Atlantic for the 1995 and 2016 Benguela Niños. Global Ocean Eddy-resolving Reanalysis (GLORYS12) sea surface salinity (SSS; pss) for (a) December 1994-January 1995, (b) Mar-April 1995, (c) December 2015-January 2016 and (d) March-April 2016. The box indicates the Angola-Benguela Area. The yellow circle indicates the location of the Kinshasa–Brazzaville station.

Chapter 7

Summary, Discussion and Outlook

7.1 Summary

The present thesis aimed to understand the impact of freshwater input on both mean-state and interannual variability of SST in the Southeastern Tropical Atlantic. To this end, a broad range of datasets were used, from *in-situ* data to modelling experiments, exploring the different mechanisms responsible for such influence. First, based on model simulations, an evaluation of how the presence of a land-to-ocean freshwater discharge, mainly from the Congo River, affects the mean-state SST and the coastal dynamics of the SETA was performed (Chapter 3). Further, the focus was on understanding the influence of freshwater input variability on the extreme warm and cold events off Angola, which modulates SST variability in this region. To do that, reanalysis data and observations, such as satellite products and *in-situ* measurements were analyzed, attempting to answer how the waters subject to the anomalously high freshwater input from the Congo River were transported to the Angola-Benguela Area during the satellite-era's most extreme warm event in the region, the 1995 Benguela Niño, and also by which mechanism these anomalously low SSS waters amplified the surface warming from this acute episode (Chapter 4). Furthermore, this analysis was extended to other similar and contrasting events, such as the 1997 Benguela Niña. By leveraging extensive *in-situ* measurements from previous research cruises, the contribution of the anomalous SSS waters to changes in water column stratification and their subsequent impact on turbulent heat fluxes was quantified, indicating how much of the turbulent flux variability is explained by anomalous salt advection at the oceans' surface (Chapter 5). Finally, the connection between the IOD and Benguela Niños via the Congo River basin hydrology was explored, pointing also to a possible new source of predictability for the southeastern tropical Atlantic warm events (Chapter 6). Below, the answers to the main questions addressed within this thesis, raised in Chapter 1, are summarized.

- **Does the freshwater input in the SETA impact the mean-state SST? What are the mechanisms involved in this influence?**

  In Chapter 3, the impact of land-to-ocean outflow, primarily from the Congo River, on the SETA coastal dynamics and SST mean-state was evaluated (Aroucha et al., 2025). From sensitivity experiments performed with a high-resolution ocean model (INALT20, 1/20º resolution), the differences between the 19-years long (2000-2018) simulations with a climatological discharge (CLIMA) and without any discharge (NORIV) were assessed. By including freshwater, the mean-state SETA coastal region is significantly warmed on average by 0.26ºC, up to 0.9ºC in the region of

the ABF (Figure 3.3). At the same time, a cooling signature of up to -1.9ºC in the coastal region north of the Congo River's mouth was generated by the presence of a river outflow. The effects of freshwater input on SST are explained by coastal dynamics changes associated with such discharges (Figure 3.6). Initially, freshwater discharge reduces the SSS around the River's mouth, with differences reaching -6 psu, accompanied by a similar spatial pattern of SSH increase up to 7cm (Figure 3.3). This SSS and SSH relation is explained by the halosteric effect, i.e. a volumetric expansion of the water column due to a reduction in SSS and consequently, in density. The surface signature of this expansion generates meridional pressure gradients, where pressure within the River's plume is higher than both north and south of it. This primary meridional pressure gradient is associated with a geostrophic flow moving from high to low pressure and deflecting to the left due to the Coriolis effect (Figure 3.6). The primary cross-shore geostrophic currents generate upwelling north of 6ºS and downwelling south of it (Figure 3.5). Concomitantly, this cross-shore flow creates a secondary zonal pressure gradient north and south of the River's mouth, which is then balanced by an alongshore geostrophic current, flowing northward and southward north and south of 6ºS, respectively. This secondary geostrophic flow advects warmer tropical waters further south (Figure 3.3 and 3.4). At the same time, the strengthening of this southward coastal flow likely contributes to shifting the ABF position further south (Figure 3.14). Finally, even though a ML shoaling and a BL generation by including freshwater discharge into the ocean were observed, the region where BLs were formed does not correspond to the location of the SST changes (Figure 3.14). One explanation might be the counteracting cooling effect of a very shallow ML, at which the penetrating solar radiation is lost to the layers below the ML (White & Toumi, 2014). Hence, the final effects of freshwater input on the SST mean-state in the SETA are a result of the combination of changes in upwelling, downwelling, and coastal advection by geostrophic currents, north and south of the Congo's mouth.

- **What is the impact of the freshwater outflow on the SST variability within the SETA? Does it amplify or counteract the extreme warm and cold events in this region? Can this contribution be quantified?**

  In Chapters 4 and 5, the impact of freshwater input and the resulting changes in SSS off Angola-Namibia during extreme warm and cold events, the Benguela Niños and Niñas, respectively, that influence SST variability in this region, were evaluated from observational and reanalysis data (Aroucha et al., 2024; Aroucha et al., *submitted*). It was demonstrated that a combination of higher (lower) than normal CRD, weakened (strengthened) southerly winds, and anomalously strong (weak) southward coastal currents contributed to decreasing (increasing) SSS in the ABA during the 1995 (1997) Benguela Niño (Niña) event (Figures 4.4, 4.5, 4.6, 5.1). The propagation of downwelling (upwelling) CTWs may have also supported salt advection shifts at the ocean surface (Figure 5.1). Salt advection, along with turbulent salt fluxes, primarily drives SSS changes during FMA, with horizontal salinity gradients playing a seemingly dominant role in salt advection over changes in

coastal currents, though both factors are important (Figure 5.11). The quantification of the freshwater input's impact on SST was attempted by calculating the residual term from a mixed-layer heat budget analysis (Chapter 4) and by estimating the turbulent heat flux and its variability's relationship with SSS changes (Chapter 5). During the peak of the 1995 Benguela Niño in March 1995, the residual accounted for 92% of the total warming terms in the heat budget (Figure 4.8). This residual is known to be a key factor in overall SST variations in the region (Körner et al., 2023). In fact, turbulent heat flux variability in FMA accounts for 85% of this residual within the ABA (Figure 5.3), and during the extremely warm 1995 event, turbulent heat fluxes below the ML were three times lower than during the 1997 Benguela Niña, with higher-salinity waters being advected into the region. Overall, variations in SSS in the ABA caused by both anomalous Congo outflow and shifts in alongshore currents were demonstrated to be an overlooked local forcing that amplifies the extreme SST events off Angola.

- **What are the mechanisms responsible for such an impact on SST variability?**

  The mechanism by which a freshwater input impacts the SST variability within the SETA was explored in Chapters 4 to 6 with reanalysis and observational data, as well as *in-situ* measurements (Aroucha et al., 2024, *submitted*; McPhaden et al., 2024). The increased or decreased Congo discharge combined with changes in the alongshore currents in the SETA can generate negative and positive SSS anomalies within the ABA, respectively. This change in SSS is associated with a shift in vertical stratification in the water column, with a lower-than-normal SSS shoaling the MLD and increasing the water column stability (Figures 4.1, 4.2, 4.3, 5.2, 6.7). Conversely, a higher-than-normal SSS deepens the MLD and reduces the stratification and the stability between ocean layers (Figure 5.2). In addition, the MLD shoaling associated with a freshening in SSS can create a BL with the ML situated within the IL, weakening at the same time the vertical temperature gradient between ML temperatures and temperature below its base. The BLs reduce the vertical mixing between surface and thermocline waters, hence contributing to increasing the SST. The effect of BLs generation in reducing the vertical temperature gradient was also observed during the 1995 warm event (Figure 4.8, 5.2). However, it seems that changing this vertical gradient played a secondary role in the turbulent fluxes, with the stratification changes dominating the variability of the effects of mixing (Figure 5.2). Further, stratification variability is strongly correlated with SSS changes rather than a thermocline vertical displacement consequence of propagating CTWs (i.e. $r = -0.73$ vs $r = 0.62$) (Figure 5.3). An increase in turbulent heat fluxes was observed in years of climatologically higher SSS due to a weaker stratification (Figure 5.3). Finally, the conclusion is that the change in the vertical stratification of the water column, mainly associated with SSS shifts, is the main mechanism by which a freshwater input can impact SST variability within the ABA, via reducing the turbulent heat fluxes from mixing by a factor of up to 3-fold (Figure 5.2). It is suggested from a regression fit to the data that a 1 psu reduction (increase) of SSS would be associated with a 1°C warming (cooling) in Benguela Niño SSTs.

- **Do other ocean basins influence the freshwater input variability in the SETA? Can a connection be established between Benguela Niño and Niña events and SST variability modes from other oceans?**

  In Chapter 6, observational and reanalysis data are explored to understand the interbasin connection between the September-October 1994 positive IOD event and the 1995 Benguela Niño peaking in March (McPhaden et al., 2024). It is shown that the 1994 IOD, with anomalously warm SSTs in the western Indian Ocean and cooler-than-normal SSTs at the eastern part, generated a low-level wind and moisture convergence over the Congo River basin, which led to increased precipitation in this region (Figures 6.3 and 6.4). This intensified precipitation was then translated into an anomalously high freshwater input into the SETA via an increased CRD. A similar picture was observed for the 2015 IOD and the 2016 warm event in the ABA. From this, it is suggested that the IOD development is one potential new source of predictability for amplified Benguela Niños through both a land bridge involving the Congo River basin hydrology and an atmospheric route involving convection over Africa, with the IOD lagging Benguela Niños by 3-5 months (Figure 6.9). Moreover, the likelihood of such boosting can be gauged by an extensive monitoring of rainfall over the Congo River basin, the CRD, and the SETA SSS anomalies. The SST variability teleconnection between the Indian and the Atlantic Oceans was assessed here via a local forcing effect on the development of Benguela Niños. However, this connection might be even stronger when considering that IOD events have been linked to weakening of the equatorial trade winds in the Atlantic, and the subsequent propagation of EKWs (Fei & Meng, 2023; Zhang & Han, 2021). Hence, the IOD might contribute to the development of Benguela Niño events by impacting both the local forcing of changing the CRD and the consequent turbulent heat fluxes in the ABA, and the remote forcing by triggering EKWs, which propagates to the ABA as CTWs.

7.2 Discussion and Outlook

Overall, the importance of the Congo River discharge and freshwater input for both mean-state and interannual variability of SST within the ABA is demonstrated throughout this thesis. Further, the impacts of this input on coastal salinity, stratification, and dynamics within the SETA are discussed, highlighting their role in changing SST, especially off Angola. The up-until-now unnoticed mechanism of freshwater input as a local forcing for Benguela Niño and Niña events is brought to light, pointing out its interbasin connection to the IOD and possibly contributing to improving the forecast of these extreme events in the SETA. In this section, the main findings of this thesis are further discussed, at the same time that the potential future works that could investigate the caveats of this study are explored.

On the contribution of Coastally Trapped Waves propagation, Congo River discharge anomalies, and wind variations for salt advection anomalies into the ABA

The crucial role of the salt advection term in developing the SSS anomalies in the ABA, and consequently triggering the impact of freshwater input on SST variability within the Benguela Niño and Niña extreme events, was demonstrated in Chapters 4, 5, and 6 (Aroucha et al., 2024, *submitted*; McPhaden et al., 2024). This term is proportional to both surface salinity horizontal gradients and the strength of the surface current (i.e. the AC). It appears that the variability of salt advection into the ABA in FMA is strongly related to changes in the horizontal SSS gradient rather than with anomalous alongshore surface currents, even though the latter seems to also exert a significant influence on such advection (Figure 5.11, Aroucha et al. *submitted*). In fact, Sena Martins & Stammer (2022) argue for the contribution of both terms, stating that the advection of low-salinity waters into the ABA is only possible when there is a combination of stronger-than-normal CRD and CTW propagation impacting the alongshore currents. The two most extreme events that were extensively analyzed in this thesis, both of them with profound salt advection anomalies at the surface, occurred under the remote influence of a propagating CTW. Imbol Koungue & Brandt (2021) showed from observations that two weeks before the peak of both the 1995 warm and the 1997 cold event, a downwelling wave with a 2.9 cm amplitude and an upwelling wave with a -1.5 cm, respectively, were present in the region.

Indeed, it has been previously shown that the AC variability is directly linked to the passage of southward propagating CTWs (Tchipalanga et al., 2018; Kopte et al., 2017; Bachèlery et al., 2016a; Rouault, 2012). The passage of a downwelling (upwelling) CTW deepens (shoals) the thermocline and increases (decreases) the poleward flow, which leads to a stronger (weaker) seasonal leakage of Angolan tropical waters into the ABF (Rouault, 2012). Additionally, wind stress and its curl modulate the AC core position and strength (Junker et al., 2015; Fennel et al., 2012), and during the above-cited extreme events, shifts in both wind stress and curl were observed (Figures 4.7 and 5.7). Fennel et al. (2012) argue that the role of CTWs versus the effect of Ekman pumping driven by the wind curl is crucial for shaping the coastal current system. Furthermore, the increased CRD could also contribute to increasing the geostrophic component of the AC via the same mechanism discussed in Section 1.2.1 and in Chapter 3 (Aroucha et al., 2025), even though the halosteric effect on SSH anomalies appears to be of much smaller magnitude than the SSH signature of a propagating wave.

Therefore, separating the direct effects from a propagating CTW, from wind changes, and CRD on the strength of the alongshore coastal currents is a challenging task. Future work could explore the different contributions of each of these factors to the overall change in surface currents. With that, one could understand whether the remote forcing from EKWs overlaps with the local forcing from the changes in wind and freshwater input in triggering and amplifying Benguela Niño events, comprehending if the low-SSS waters inflow into the ABA should be treated uniquely as a local forcing or as another consequence of the remote equatorial trigger.

On the limitations and potential improvements of model, reanalysis, and satellite datasets

Ocean surface salinity measurements by the SMAP and SMOS satellite missions to an accuracy of 0.2 psu provided a more consistent and uniform sampling of SSS as compared to the observing platforms during the last decade (Jarugula et al., 2025). Still, even though both satellite missions increased the observation resolution to approximately 40km away from the coast, systematic errors remain in such products, especially in the regions with high SSS variability, strong vertical gradients, and low sampling rates as regions affected by river discharge (Martins and Stammer, 2022; Nyadjro et al., 2022; Boutin et al., 2021). Additionally, SSS satellite measurements only started in 2010 (Boutin et al., 2021), leaving a substantial gap in observational salinity measurements from the start of the altimetry era (i.e. from 1993). Hence, the use of salinity datasets from reanalysis implies both a temporal and spatial limitation, especially when focusing on coastal regions and in years before the SSS satellite era. Further, only a few episodes of strong SSS anomalies were observed in the ABA since 1993 (e.g. 1995, 1997, 2001, 2016, Figure 5.4). Therefore, the establishment of significant statistical correlations between SSS changes and SST extreme events in the ABA remains difficult and not robust, especially considering the wide range of forcing mechanisms that can trigger Benguela Niños. To overcome this, the analysis focused on exploring only the few Benguela Niño and Niña events occurring concomitantly with SSS anomalies. There is an uprising need to improve such ocean salinity measurements to allow higher-confidence analysis of SSS changes impacting oceanic SST.

From the modelling sensitivity experiments presented in Chapter 3, it was expected to observe impacts on SST and on its variability from using an interannually varying river discharge in CTRL when compared to the climatological runoff from CLIMA. However, some model limitations and the complexity of the SETA dynamics could explain why these differences were not observed. It is known that representing the SETA eastern boundary upwelling system is a challenging task. The struggle lies in the systematically observed SST bias when compared to observations, which likely comes from the poor representation of upwelling velocities and equatorward surface flow, shallow clouds and shortwave radiation, the convergence of distinct water masses, and the unique structure of the wind field (Small et al., 2024; Kurian et al., 2021; Bonino et al., 2019; Koseki et al., 2018; Richter, 2015; Huang et al., 2007). In addition, the mean-state and the variability of the MLD, a crucial term to understand the freshwater input impacts on SST, are commonly not well-depicted in climate models (Fox-Kemper et al., 2023; Treguier et al., 2023).

Specifically, for the INALT20 CTRL and CLIMA experiments, low-SSS were hardly ever inflowing into the ABA, contradicting, for instance, observations of extreme negative SSS anomalies in the region during 2016 (McPhaden et al., 2024; Lübbecke et al., 2019). It was shown that the alongshore southward current is underestimated from January to May in CTRL when compared to mooring measurements (Figure 3.11), and the stronger northward jet depicted by CTRL did not allow the southward transport of low-SSS waters. Further, the Congo plume spreading is directly related to the geomorphology and the coastline bathymetry of the River's estuary (Vic et al., 2014; Denamiel et al., 2013), and a poor model representation of these geological aspects might also impact the unobserved differences. Finally, and likely most importantly, the JRA55-do atmospheric forcing, even though its use has been linked to a reduction in the warm bias in the

SETA when compared to using coarser resolution atmospheric reanalysis (Prigent & Farneti, 2024), presents a substantial uncertainty in depicting the CRD, mainly due to the complex hydrology of the River's basin (Chandanpurkar et al., 2022; Hua et al., 2019). The observed discrepancies when comparing the atmospheric forcing CRD to the Kinshasha-Brazzaville measurements, both seasonally and interannually (Aroucha et al., 2025, Figure 3.7), might lead to strong SSS biases (Chandanpurkar et al., 2022). Therefore, it is believed that the uncertainty involved in the discharge from the atmospheric reanalysis added to the complexity of the coastal currents system within the SETA could likely not well represent the expected differences of using either a climatological or interannual varying runoff in the model simulations.

On the impact of Congo River discharge on the SETA SST in a warming climate

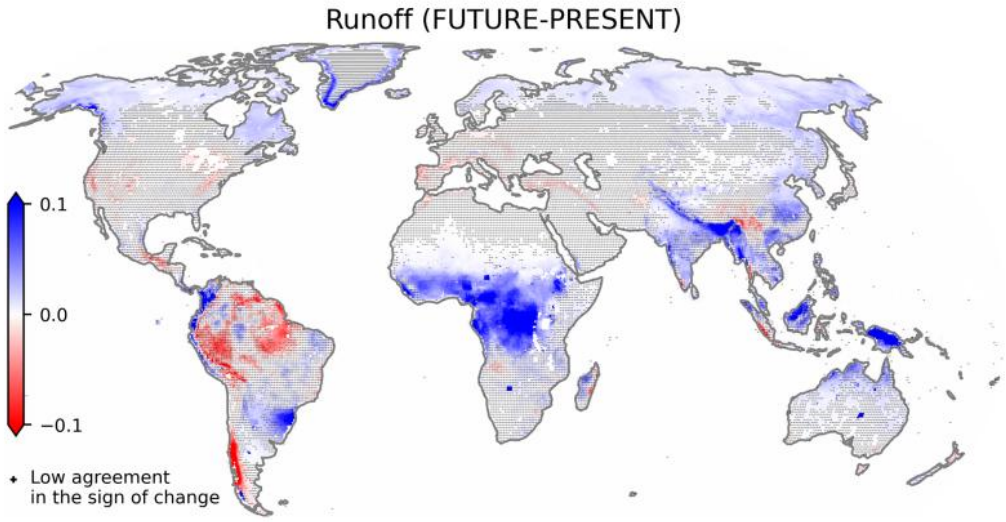

Figure 7.1. Multi-model ensemble means differences in runoff (10^3 km^3 yr^{-1}) between FUTURE (2015–2050) and PRESENT (1950–2014). The crosses indicate that at least 3 out of 18 GCMs disagree in terms of the sign of change. From: Müller et al. (2024).

Land-to-ocean discharge, especially from the Congo River, has been shown to be able to impact the coastal dynamics and mean-state SST in the SETA, and also to push the ABF further south. At a time when the latest climate projections suggest a significant change in the global water cycle and the consequent increase in the Congo river discharge in the future warming scenario (Figure 7.1) (Müller et al., 2024; Aloysius and Saiers, 2017), the impact of the Congo discharge to the SETA dynamics are also expected to be stronger. An increase in the Congo discharge due to global warming could lead to an enhanced southward geostrophic current, shifting the SST mean-state in the ABA to even more tropical conditions. In fact, a recent trend of warming off Angola, with warmer and fresher tropical waters moving poleward via an intensification of the AC has been recently observed (Tomety et al., 2024; Roch et al., 2021). Whether this trend already reflects the increase in freshwater discharge remains uncertain. Additionally, the intensification in discharge rates from the Congo could also increase the likelihood of amplified Benguela Niño events due to a more usual presence of low SSS in the ABA region. Additionally, it is also expected an increase in the IOD events frequency by a factor of 3 under high greenhouse gas emission scenarios over the twenty-first century (Cai et

al., 2014). With this, future IOD events will likely influence Benguela Niño events even more via the increase in precipitation over the Congo Basin.

Finally, climate change will also likely impact upwelling at the southwestern African coast due to wind-related geostrophic changes (Ayissi et al., 2024; Jing et al., 2023). Considering the prominent role of geostrophic flows in the Atlantic eastern boundary upwelling system mean-state and long-term changes (Jing et al., 2023), understanding potential sources that could shift these geostrophic currents within the SETA is of major importance. An enhanced Congo discharge might increase both the water column stratification off Angola and the southward geostrophic flow component. This could then lead to more extreme Benguela Niño events, and an even stronger shift of the BUS to tropical conditions. Monitoring how the processes and mechanisms related to freshwater input in the SETA will change with climate warming is crucial for an improved comprehension of the expected dynamical changes within the region in a warmer world.

On the Indian Ocean teleconnection potentially improving the predictability of Benguela Niños

Benguela Niños and Niñas play a substantial role in coastal oxygen availability, fish habitat, and marine ecosystem management and resources for western African countries (e.g. Bachèlery et al., 2016b; Blamey et al., 2015; Rouault, 2012). Hence, improving the forecast of these events would be of great benefit to the local ecosystem and management strategies. Along with Atlantic Niños, the predictability of these events has been only partially successful through dynamic forecasting systems, leading to a growing consensus that these events are inherently unpredictable (Keenlyside et al., 2020; Dippe et al., 2018; Richter et al., 2018). More recently, Bachèlery et al. (2025) demonstrated by using a deep learning approach with a convolutional neural network architecture that Atlantic and Benguela Niño can be predicted up to 3-4 months in advance, with forecast skill correlation of around 0.9 for the first lead month. The authors highlight the central south tropical basin, i.e. the location of the SAA, as a hotspot region for the prediction of these events, and that understanding the dynamics and variability of this South Atlantic high-pressure system might play a key role in improving the accuracy of such forecasts (Bachèlery et al., 2025). In addition, they also observed a hotspot forecast area for the 2001 and 2016 warm events near the Congo mouth (Bachèlery et al., 2025), indicating that the Congo plume dynamics might also impact the forecast of such extreme events, especially in years of low-SSS waters reaching the ABA, as in 1995, 2001, and 2016 (Aroucha et al., 2024).

Low-level westerly wind anomalies along the equatorial Atlantic, in connection with the SAA, have been linked to the occurrence of IOD events (Fei & Meng, 2023; Zhang & Han, 2021). These wind anomalies result from the IOD-driven rainfall over the Congo Basin, also exerting influence on the SETA SSS variability (Jarugula & McPhaden, 2023; McPhaden et al., 2024). The connection between an IOD event, the equatorial trade winds, and precipitation over the Congo basin, and the subsequent Benguela Niño events may not be accidental. When the IOD triggers increased rainfall over the Congo, and generates westerly wind anomalies along the equatorial Atlantic, it potentially supports the start of a Benguela Niño. Since SSS changes in the ABA lag IOD by 3-5 months, and SAA shifts are related to the IOD, it might be possible to anticipate how extreme the Benguela Niño events would be. Determining whether these extreme events would be amplified

by an IOD occurrence is critical for developing adaptive management strategies, such as early warning systems and anticipation of socioeconomic impacts. For that, there is an ongoing need to monitor the occurrence of IOD events, the precipitation over the Congo basin, and the Congo discharge rates as an attempt to improve the forecast of Benguela Niños.

On the effects of freshwater input and turbulent heat fluxes changes in Atlantic Niños and Niñas

Freshwater input has been shown to generate BLs and impact SST during El Niño and La Niña events (Liu et al., 2025, 2022; Zheng & Zhang, 2012; Zhang & Busalacchi, 2009). The main source of freshwater within this region is via enhanced rainfall within the ITCZ. A positive ocean-atmosphere feedback is observed within these events, with the warm SST anomalies leading to stronger convection and consequently precipitation, impacting the BL generation and amplifying the surface warming. A similar study within the ITCZ was performed in the tropical North Atlantic (Foltz & McPhaden, 2009). More recently, the effects of stratification changes and the subsequent impact on turbulent mixing by turbulent heat fluxes have been assessed and related to the development mostly of Central Pacific El Niños (Guan et al., 2025; Liu et al., 2025; Tozuka, 2025). Bearing in mind the similarities in both the mean-stated dynamics and the forcing driving both ENSO and Atlantic Niños, as well as the precipitation rates in the equatorial region in the two ocean basins, and the fact that Central Atlantic Niños are emerging in the last decades (Zhang et al., 2023), it is likely that SSS and turbulent mixing changes in the equatorial Atlantic might similarly impact Atlantic Niño events.

References

Adler, R. F., Huffman, G. J., Chang, A., Ferraro, R., Xie, P.-P., Janowiak, J., et al. The version-2 global precipitation climatology project (GPCP) monthly precipitation analysis (1979–present). *J. Hydrometeor*. **4**, 1147–1167. https://doi.org/10.1175/1525-7541(2003)004%3C1147:TVGPCP%3E2.0.CO;2, 2003.

Alizadeh, O. A review of ENSO teleconnections at present and under future global warming. WIREs Climate Change, 15(1), e861. https://doi.org/10.1002/wcc.861, 2024.

Alory, G., Da-Allada, C. Y., Djakouré, S., Dadou, I., Jouanno, J., & Loemba, D. P.: Coastal Upwelling Limitation by Onshore Geostrophic Flow in the Gulf of Guinea Around the Niger River Plume, Front. Mar. Sci., 7, 607216, https://doi.org/10.3389/fmars.2020.607216, 2021.

Aloysius, N. & Saiers, J.: Simulated hydrologic response to projected changes in precipitation and temperature in the Congo River basin, Hydrol. Earth Syst. Sci., 21, 4115–4130, https://doi.org/10.5194/hess-21-4115-2017, 2017.

Alsdorf, D., Beighley, E., Laraque, A., Lee, H., Tshimanga, R., O'Loughlin, F., Mahé, G., Dinga, B., Moukandi, G., & Spencer, R. G. M.: Opportunities for hydrologic research in the Congo Basin, Rev. Geophys., 54, 378–409, https://doi.org/10.1002/2016RG000517, 2016.

Aroucha, L. C. & Schwarzkopf, F. U. Supplementary Data to: River discharge impacts coastal Southeastern Tropical Atlantic sea surface temperature and circulation: a model-based analysis [dataset]. GEOMAR Helmholtz Centre for Ocean Research Kiel [distributor]. https://hdl.handle.net/20.500.12085/2b927bcd-afab-4bc6-ba97-634d09435daa, 2024.

Aroucha, L. C., Hummels, R., & Lübbecke, J. F. Turbulent Heat Flux Responses to Sea Surface Salinity Variability during Benguela Niños and Niñas, submitted to *Geophysical Research Letters*.

Aroucha, L. C., Lübbecke, J. F., Körner, M., Imbol Koungue, R. A., & Awo, F. M.: The Influence of Freshwater Input on the Evolution of the 1995 Benguela Niño, JGR Oceans, 129, e2023JC020241, https://doi.org/10.1029/2023JC020241, 2024.

Atlas, R., R. N. Hoffman, J. Ardizzone, S. M. Leidner, J. C. Jusem, D. K. Smith, D. Gombos. A cross-calibrated, multiplatform ocean surface wind velocity product for meteorological and oceanographic applications. Bull. Amer. Meteor. Soc., 92, 157-174. https://doi.org/10.1175/2010BAMS2946.1, 2011.

Awo, F. M., Rouault, M., Ostrowski, M., Tomety, F. S., Da-Allada, C. Y., & Jouanno, J.: Seasonal Cycle of Sea Surface Salinity in the Angola Upwelling System, JGR Oceans, 127, e2022JC018518, https://doi.org/10.1029/2022JC018518, 2022.

Ayissi, F. F. B. K., Da-Allada, C. Y., Baloïtcha, E., Worou, L. O., & Tilmes, S.: Changes in coastal upwelling in the northern Gulf of Guinea under Stratospheric Aerosol Injection, Regional Studies in Marine Science, 76, 103607, https://doi.org/10.1016/j.rsma.2024.103607, 2024.

Bachèlery, M. L., Illig, S., & Dadou, I. Interannual variability in the South-East Atlantic Ocean, focusing on the Benguela Upwelling System: remote versus local forcing. Journal of Geophysical Research Oceans 121, 284–310. https://doi.org/10.1002/2015JC011168, 2016a.

Bachèlery, M. L., Illig, S., & Rouault, M. Interannual coastal trapped waves in the Angola-Benguela upwelling system and Benguela Niño and Niña events. Journal of Marine Systems, 203, 103262. https://doi.org/10.1016/j.jmarsys.2019.103262, 2020.

Bachèlery, M.-L., Brajard, J., Patacchiola, M., Illig, S., & Keenlyside, N. Predicting Atlantic and Benguela Niño events with deep learning. Science Advances, 11(14), eads5185. https://doi.org/10.1126/sciadv.ads5185, 2025.

Bachèlery, M.-L., Illig, S., & Dadou, I. Forcings of nutrient, oxygen, and primary production interannual variability in the southeast Atlantic Ocean. Geophysical Research Letters 43, 8617–8625. https://doi.org/10.1002/2016GL070288, 2016b.

Bakun, A., Black, B. A., Bograd, S. J., García-Reyes, M., Miller, A.J., Rykaczewski, R.R., Sydeman, W.J. Anticipated effects of climate change on coastal upwelling ecosystems. Current Climate Change Reports 1(2):85–93, https://doi.org/10.1007/s40641-015-0008-4, 2015.

Balaguru, K., Chang, P., Saravanan, R., Jang, C. J. The barrier layer of the Atlantic warmpool: formation mechanism and infuence on the mean climate. Tellus A Dyn Meteorol Oceanogr 64(1):18162. https://doi.org/10.3402/tellusa.v64i0.18162, 2012a.

Balaguru, K., Chang, P., Saravanan, R., Leung, L. R., Xu, Z., Li, M. & Hsieh, J. Ocean barrier layers' effect on tropical cyclone intensification, *Proc. Natl. Acad. Sci*. U.S.A. 109 (36) 14343-14347, https://doi.org/10.1073/pnas.1201364109, 2012b.

Barnier, B., Madec, G., Penduff, T., Molines, J.-M., Treguier, A.- M., Le Sommer, J., Beckmann, A., Biastoch, A., Böning, C., Dengg, J., Derval, C., Durand, E., Gulev, S., Remy, E., Talandier, C., Theetten, S., Maltrud, M., McClean, J., & De Cuevas, B. Impact of partial steps and momentum advection schemes in a global ocean circulation model at eddy-permitting resolution, Ocean Dynam., 56, 543–567, https://doi.org/10.1007/s10236- 006-0082-1, 2006.

Bastin, S., Koldunov, A., Schütte, F., Gutjahr, O., Mrozowska, M. A., Fischer, T., Shevchenko, R., Kumar, A., Koldunov, N., Haak, H., Brüggemann, N., Hummels, R., Specht, M. S., Jungclaus, J., Danilov, S., Dengler, M., & Jochum, M. Sensitivity of the tropical Atlantic to vertical mixing in two ocean models (ICON-O v2.6.6 and FESOM v2.5), Geosci. Model Dev., 18, 1189–1220, https://doi.org/10.5194/gmd-18-1189-2025, 2025.

Behara, A. & P. N. Vinayachandran. An OGCM study of the impact of rain and river water forcing on the Bay of Bengal, *J. Geophys. Res. Oceans,* 121, 2425–2446, https://doi.org/10.1002/2015JC011325, 2016.

Behrens, E., Våge, K., Harden, B., Biastoch, A., & Böning, C. W. Composition and variability of the Denmark Strait Overflow Water in a high-resolution numerical model hindcast simulation, J. Geophys. Res., 122, 2830–2846, https://doi.org/10.1002/2016JC012158, 2017.

Biastoch, A., Durgadoo, J. V., Morrison, A., van Sebille, E., Weijer, W., & Griffies, S. Atlantic multi-decadal oscillation covaries with Agulhas leakage, Nat. Commun., 6, 10082, https://doi.org/10.1038/ncomms10082, 2015.

Biastoch, A., Schwarzkopf, F. U., Getzlaff, K., Rühs, S., Martin, T., Scheinert, M., Schulzki, T., Handmann, P., Hummels, R., & Böning, C. W.: Regional imprints of changes in the Atlantic Meridional Overturning Circulation in the eddy-rich ocean model VIKING20X, Ocean Sci., 17, 1177–1211, https://doi.org/10.5194/os-17-1177-2021, 2021.

Binet D., Gobert B., Maloueki L. El Niño-like warm events in the Eastern Atlantic (6°N and 20°S) and fish availability from Congo to Angola (1964–1999). Aquat. Living. Resour. 14, 99–113. https://doi.org/10.1016/S0990-7440(01)01105-6, 2001.

Blamey, L. K., Shannon, L. J., Bolton, J. J., Crawford, R. J. M., Dufois, F., Evers-King, H., et al. Ecosystem change in the southern Benguela and the underlying processes. J. Mar. Syst. 144, 9–29. https://doi.org/10.1016/j.jmarsys.2014.11.006, 2015.

Böning, C., Behrens, E., Biastoch, A., & Bamber, J. Emerging impact of Greenland meltwater on deepwater formation in the North Atlantic Ocean, Nat. Geosci., 9, 523–527, https://doi.org/10.1038/ngeo2740, 2016.

Bonino, G., Masina, S., Iovino, D., Storto, A., & Tsujino, H.: Eastern Boundary Upwelling Systems response to different atmospheric forcing in a global eddy-permitting ocean model, Journal of Marine Systems, 197, 103178, https://doi.org/10.1016/j.jmarsys.2019.05.004, 2019.

Bordbar, M. H., Mohrholz, V., & Schmidt, M.: The relation of wind-driven coastal and offshore upwelling in the Benguela Upwelling System, Journal of Physical Oceanography, https://doi.org/10.1175/JPO-D-20-0297.1, 2021.

Boutin, J., Reul, N., Koehler, J., Martin, A., Catany, R., Guimbard, S., Rouffi, F., Vergely, J. L., Arias, M., Chakroun, M., Corato, G., Estella-Perez, V., Hasson, A., Josey, S., Khvorostyanov, D., Kolodziejczyk, N., Mignot, J., Olivier, L., Reverdin, G., Stammer, D., Supply, A., Thouvenin-Masson, C., Turiel, A., Vialard, J., Cipollini, P., Donlon, C., Sabia, R., & Mecklenburg, S.: Satellite-Based Sea Surface Salinity Designed for Ocean and Climate Studies, JGR Oceans, 126, e2021JC017676, https://doi.org/10.1029/2021JC017676, 2021.

Bove, M. C., J. B. Elsner, C. W. Landsea, X. Niu, & J. J. O'Brien: Effect of El Niño on U.S. Landfalling Hurricanes, Revisited. Bull. Amer. Meteor. Soc., 79, 2477–2482, https://doi.org/10.1175/1520-0477(1998)079<2477:EOENOO>2.0.CO;2, 1998.

Boyer, D. C., & Hampton, I. An overview of the living marine resources of Namibia. South African Journal of Marine Science, 23(1), 5–35. https://doi.org/10.2989/025776101784528953, 2001.

Boyer, D. C., Boyer, H. J., Fossen, I. & Kreiner, A. Changes in abundance of the northern Benguela sardine stock during the decade 1990 - 2000, with comments on the relative importance of fishing and the environment. Afr. J. Mar. Sci. **23,** 67–84, 2001.

Brandt, P., Alory, G., Awo, F. M., Dengler, M., Djakouré, S., Imbol Koungue, R. A., Jouanno, J., Körner, M., Roch, M., & Rouault, M. Physical processes and biological productivity in the upwelling regions of the tropical Atlantic, Ocean Sci., 19, 581–601, https://doi.org/10.5194/os-19-581-2023, 2023.

Brandt, P., Bordbar, M. H., Coelho, P., Koungue, R. A. I., Körner, M., Lamont, T., Lübbecke, J. F., Mohrholz, V., Prigent, A., Roch, M., Schmidt, M., Van Der Plas, A. K., & Veitch, J.: Physical Drivers of Southwest African Coastal Upwelling and Its Response to Climate Variability and Change, in: Sustainability of Southern African Ecosystems under Global Change, vol. 248, edited by: Von Maltitz, G. P., Midgley, G. F., Veitch, J., Brümmer, C., Rötter, R. P., Viehberg, F. A., & Veste, M., Springer International Publishing, Cham, 221–257, https://doi.org/10.1007/978-3-031-10948-5_9, 2024.

Brandt, P.; Kopte, R.; Krahmann, G. Physical oceanography (CTD) during METEOR cruise M131. PANGAEA, https://doi.org/10.1594/PANGAEA.910994, 2020. [Dataset]

Brandt, P.; Subramaniam, A.; Schmidtko, S.; Krahmann, G. Physical oceanography (CTD) during METEOR cruise M158. PANGAEA, https://doi.org/10.1594/PANGAEA.952354, 2022. [Dataset]

Cai, W., McPhaden, M. J., Grimm, A. M. et al. Climate impacts of the El Niño–Southern Oscillation on South America. Nat Rev Earth Environ 1, 215–231, https://doi.org/10.1038/s43017-020-0040-3, 2020.

Cai, W., Santoso, A., Wang, G. et al. Increased frequency of extreme Indian Ocean Dipole events due to greenhouse warming. *Nature* 510, 254–258, https://doi.org/10.1038/nature13327, 2014.

Cai, W., Yang, K., Wu, L. et al. Opposite response of strong and moderate positive Indian Ocean Dipole to global warming. *Nat. Clim. Chang.* 11, 27–32, https://doi.org/10.1038/s41558-020-00943-1, 2021.

Campbell, D.: The Congo River basin, in: The World's Largest Wetlands: Ecology and Conservation, edited by: Fraser, L. H. & Keddy, P. A., Cambridge University Press, Cambridge, 149–165, https://doi.org/10.1017/CBO9780511542091.006, 2005.

Chandanpurkar, H. A., Lee, T., Wang, X., Zhang, H., Fournier, S., Fenty, I., Fukumori, I., Menemenlis, D., Piecuch, C. G., Reager, J. T., Wang, O., & Worden, J.: Influence of Nonseasonal River Discharge on Sea Surface Salinity and Height, J Adv Model Earth Syst, 14, e2021MS002715, https://doi.org/10.1029/2021MS002715, 2022.

Chao, S. River-Forced Estuarine Plumes. *J. Phys. Oceanogr*., 18, 72–88, https://doi.org/10.1175/1520-0485(1988)018<0072:RFEP>2.0.CO;2, 1988.

Chao, Y., Farrara, J. D., Schumann, G., Andreadis, K. M., & Moller, D.: Sea surface salinity variability in response to the Congo river discharge, Continental Shelf Research, 99, 35–45, https://doi.org/10.1016/j.csr.2015.03.005, 2015.

Chassignet, E. P., Le Sommer, J., & Wallcraft, A. J. General Circulation Models, 3rd Edn. Elsevier. 4560. ISBN: 978-0-12-813081-0, https://doi.org/10.1016/B978-0-12-409548-9.11410-1, 2019.

Chelton, D. B., deSzoeke, R. A., Schlax, M. G., El Naggar, K., & Siwertz, N.: Geographical Variability of the First Baroclinic Rossby Radius of Deformation. J. Phys. Oceanogr., 28, 433–460, https://doi.org/10.1175/1520-0485(1998)028<0433:GVOTFB>2.0.CO;2, 1998.

Clarke, A. J. The Reflection of Equatorial Waves from Oceanic Boundaries. Journal of Physical Oceanography 13(7): 1193–1207, https://doi.org/10.1175/1520-0485(1983)013%3C1193:TROEWF%3E2.0.CO;2. 1983.

Dagg, M., Benner, R., Lohrenz, S., & Lawrence, D. Transformation of dissolved and particulate materials on continental shelves influenced by large rivers: Plume processes. *Continental Shelf Research*, 24, 833–858. https://doi.org/10.1016/j.csr.2004.02.003, 2004.

Dai, A. & Trenberth, K. E.: Estimates of Freshwater Discharge from Continents: Latitudinal and Seasonal Variations, Journal of Hydrometeorology, 3, 660–687, https://doi.org/10.1175/1525-7541(2002)003<0660:EOFDFC>2.0.CO;2, 2002.

de Boyer Montégut, C., Madec, G., Fischer, A. S., Lazar, A., & Iudicone, D. Mixed layer depth over the global ocean: An examination of profile data and a profile-based climatology. Journal of Geophysical Research, 109(C12). https://doi.org/10.1029/2004JC002378, 2004.

de Boyer Montégut, C., Mignot, J., Lazar, A., & Cravatte, S. Control of salinity on the mixed layer depth in the world ocean: 1. General description. Journal of Geophysical Research, 112(C6). https://doi.org/10.1029/2006JC003953, 2007.

De La Vara, A., Cabos, W., Sein, D. V., Sidorenko, D., Koldunov, N. V., Koseki, S., Soares, P. M. M., & Danilov, S.: On the impact of atmospheric vs oceanic resolutions on the representation of the sea surface temperature in the South Eastern Tropical Atlantic, Clim Dyn, 54, 4733–4757, https://doi.org/10.1007/s00382-020-05256-9, 2020.

Denamiel, C., Budgell, W. P., & Toumi, R.: The Congo River plume: Impact of the forcing on the far-field and near-field dynamics, *JGR Oceans*, 118, 964–989, https://doi.org/10.1002/jgrc.20062, 2013.

Dengler, M.; Brandt, P.; Herrford, J.; Krahmann, G. Physical oceanography (CTD) during METEOR cruise M148. PANGAEA, https://doi.org/10.1594/PANGAEA.928997, 2021. [Dataset]

DeVries, T., Holzer, M., & Primeau, F. Recent increase in oceanic carbon uptake driven by weaker upper-ocean overturning. *Nature*, 542(7640):215–218, https://doi.org/10.1038/nature21068, 2017.

Dippe, T., Greatbatch, R.J. & Ding, H. On the relationship between Atlantic Niño variability and ocean dynamics. *Clim Dyn* 51, 597–612. https://doi.org/10.1007/s00382-017-3943-z, 2018.

Durand, F., Piecuch, C., Becker, M., Papa, F., Raju, S. Khan, J., & Ponte, R. Impact of Continental Freshwater Runoff on Coastal Sea Level. *Surveys in Geophysics*, https://doi.org/10.1007/s10712-019-09536-w, 2019.

Durgadoo, J., Loveday, B., Reason, C., Penven, P., & Biastoch, A. Agulhas Leakage Predominantly Responds to the Southern Hemisphere Westerlies, J. Phys. Oceanogr., 43, 2113–2131, https://doi.org/10.1175/JPO-D-13-047.1, 2013.

Echols, R., & Riser, S. C. The impact of barrier layers on Arabian Sea surface temperature variability. Geophysical Research Letters, 47, e2019GL085290. https://doi.org/10.1029/2019GL085290, 2020.

Fan, L., & Meng, X. The Asymmetric predictive power of Indian Ocean Dipole for subsequent year's ENSO: Role of Atlantic Ocean as an intermediary. Geophys. Res. Lett. **50**, e2023GL105525. https://agupubs.onlinelibrary.wiley.com/doi/10.1029/2023GL105525, 2023.

FAO: Fishery and Aquaculture Country Profiles, Angola, 2020, Country Profile Fact Sheets, Fisheries and Aquaculture Division [online], Rome, https://www.fao.org/fishery/en/facp/ago?lang=%20en, 2020. (last access: 22 July 2024), updated 7 February 2022.

Farneti, R., Stiz, A., & Ssebandeke, J. B.: Improvements and persistent biases in the southeast tropical Atlantic in CMIP models, npj Clim Atmos Sci, 5, 42, https://doi.org/10.1038/s41612-022-00264-4, 2022.

Fennel, W., Junker, T., Schmidt, M., & Mohrholz, V. Response of the Benguela upwelling systems to spatial variations in the wind stress. Continent. Shelf Res. **45**, 65–77, https://doi.org/10.1016/j.csr.2012.06.004, 2012.

Fennel, W.: Theory of the Benguela Upwelling System, Journal of Physical Oceanography, 177–190, https://doi.org/10.1175/1520-0485(1999)029%3C0177:TOTBUS%3E2.0.CO;2, 1999.

Florenchie, P., Lutjeharms, J. R. E., Reason, C. J. C., Masson, S., & Rouault, M. The source of Benguela Niños in the South Atlantic Ocean. Geophysical Research Letters, 30(10), 2003GL017172. https://doi.org/10.1029/2003GL017172, 2003.

Florenchie, P., Reason, C. J. C., Lutjeharms, J. R. E., Rouault, M., Roy, C., & Masson, S.: Evolution of Interannual Warm and Cold Events in the Southeast Atlantic Ocean, Journal of Climate, 17, 2318–2334, https://doi.org/10.1175/1520-0442(2004)017<2318:EOIWAC>2.0.CO;2, 2004.

Foltz, G. R. & McPhaden, M. J. Impact of barrier layer thickness on SST in the central tropical North Atlantic. J Clim 22(2):285–299. https://doi.org/10.1175/2008JCLI2308.1, 2009.

Foltz, G. R., Eddebbar, Y. A., Sprintall, J., Capotondi, A., Cravatte, S., Brandt, P., Sutton, A. J., Morris, T., Hermes, J., McMahon, C. R., McPhaden, M. J., Looney, L. B., Tuchen, F. P., Roxy, M. K., Wang, F., Chai. F., Rodrigues, R. R., Rodriguez-Fonseca, B., Subramanian, A. C., Dengler, M., Stienbarger, C., Bailey, K. & Yu, W. Toward an integrated pantropical ocean observing system. Front. Mar. Sci. 12:1539183. https://doi.org/10.3389/fmars.2025.1539183, 2025.

Foltz, G. R., Grodsky, S. A., Carton, J. A., & McPhaden, M. J. Seasonal mixed layer heat budget of the tropical Atlantic Ocean, *Journal of Geophysical Research*, 108, 3146, https://doi.org/10.1029/2002jc001584, 2003.

Foltz, G. R., Hummels, R., Dengler, M., Perez, R. C., & de Araujo, M. Vertical turbulent cooling of the mixed layer in the Atlantic ITCZ and trade wind regions. *Journal of Geophysical Research: Oceans*, 125, e2019JC015529. https://doi.org/10.1029/2019JC015529, 2020.

Fong, D. A. & Geyer, W. R. Response of a river plume during an upwelling favorable wind event. *Journal of Geophysical Research: Oceans*, 106, 1067-1084, https://doi.org/10.1029/2000JC900134, 2001.

Fong, D. A. & Geyer, W. R. The Alongshore Transport of Freshwater in a Surface-Trapped River Plume, *Journal of Physical Oceanography*, 32, 957–972, https://doi.org/10.1175/1520-0485(2002)032%3C0957:TATOFI%3E2.0.CO;2, 2002.

Fox-Kemper, B., Adcroft, A., Böning, C. W., Chassignet, E. P., Curchitser, E., Danabasoglu, G., Eden, C., England, M. H., Gerdes, R., Greatbatch, R. J., Griffies, S. M., Hallberg, R. W., Hanert, E., Heimbach, P., Hewitt, H. T., Hill, C. N., Komuro, Y., Legg, S., Le Sommer, J., Masina, S., Marsland, S. J.,

Penny, S. G., Qiao, F., Ringler, T. D., Treguier, A-M., Tsujino, H., Uotila, P. & Yeager, S. G. Challenges and Prospects in Ocean Circulation Models. Front. Mar. Sci. 6:65. https://doi.org/10.3389/fmars.2019.00065, 2019.

Fox-Kemper, B., Hewitt, H. T., Xiao, C., Adalgeirsdottir, G., Drijfhout, S. S., Edwards, T. L., Golledge, N. R., Hemer, M., Kopp, R. E., Krinner, G., Mix, A., Notz, D., Nowicki, S., Nurhati, I. S., Ruiz, L., Sallee, J.-B., Slangen, A. B. A., and Yu, Y. Ocean, Cryosphere and Sea Level Change. Climate Change 2021: The Physical Science Basis. Contribution of Working Group I to the Sixth Assessment Report of the Intergovernmental Panel on Climate Change, pages 1211–1362, ISBN: 9781009157896, https://doi.org/10.1017/9781009157896.011, 2023.

Gammelsrød, T., Bartholomae, C. H., Boyer, D. C., Filipe, V. L. L., & O'Toole, M. J.: Intrusion of warm surface water along the Angolan-Namibian coast in February–March 1995: the 1995 Benguela *Nino*, South African Journal of Marine Science, 19, 41–56, https://doi.org/10.2989/025776198784126719, 1998.

Gévaudan, M., Jouanno, J., Durand, F., Morvan, G., Renault, L., & Samson, G.: Influence of ocean salinity stratification on the tropical Atlantic Ocean surface, Clim Dyn, 57, 321–340, https://doi.org/10.1007/s00382-021-05713-z, 2021.

Goubanova, K., Illig, S., Machu, E., Garçon, V., Dewitte, B. SST subseasonal variability in the central Benguela upwelling system as inferred from satellite observations (1999–2009), J. Geophys. Res. Oceans, 118, 4092–4110, https://doi.org/10.1002/jgrc.20287, 2013.

Gregg, M. C., D'Asaro, E. A., Riley, J. J., & Kunze, E. Mixing Efficiency in the Ocean. Annual Review of Marine Science, 10(1), 443–473. https://doi.org/10.1146/annurev-marine-121916-063643, 2018.

Guan, C. McPhaden, M. J, Hu, S., Wang, F., Li, Y. & Cui, M. Barrier layer variability in the central equatorial Pacific associated with ENSO development. Geophysical Research Letters, 52, e2024GL113396. https://doi.org/10.1029/2024GL113396, 2025.

Hansingo, K., & Reason, C. J. C. Modelling the atmospheric response over southern Africa to SST forcing in the southeast tropical Atlantic and southwest subtropical Indian Oceans. Int. J. Climatol. 29, 1001–1012. https://doi.org/10.1002/joc.1919, 2009.

Hassoun, A. E. R., Tanhua, T., Lips, I., Heslop, E., Petihakis, G & Karstensen, J. The European Ocean Observing Community: urgent gaps and recommendations to implement during the UN Ocean Decade. Front. Mar. Sci. 11:1394984. https://doi.org/10.3389/fmars.2024.1394984, 2024.

Hatin, T., Crosta, X., Le Hérissé, A., Droz, L., Marsset, T. Diatom response to oceanographic and climatic changes in the Congo fan area, equatorial Atlantic Ocean, during the last 190ka BP, Palaeogeography,

Palaeoclimatology, Palaeoecology, 469, 47-59, ISSN 0031-0182, https://doi.org/10.1016/j.palaeo.2016.12.037, 2017.

Hernandez, O., Jouanno, J., Durand, F. Do the Amazon and Orinoco freshwater plumes really matter for hurricane-induced ocean surface cooling? J Geophys Res Oceans 121(4):2119–2141. https://doi.org/10.1002/2015JC011021, 2016.

Hersbach, H., Bell, B., Berrisford, P., Biavati, G., Horányi, A., Muñoz Sabater, J., Nicolas, J., Peubey, C., Radu, R., Rozum, I., Schepers, D., Simmons, A., Soci, C., Dee, D., Thépaut, J.-N. ERA5 monthly averaged data on pressure levels from 1940 to present. Copernicus Climate Change Service (C3S) Climate Data Store (CDS). [Dataset]. https://doi.org/10.24381/cds.6860a573, 2023.

Hersbach, H., Bell, B., Berrisford, P., Hirahara, S., Horányi, A., Muñoz-Sabater, J., et al. (2020). The ERA5 global reanalysis. Q. J. R. Meteorol. Soc. 146, 1999–2049. https://doi.org/10.1002/qj.3803, 2020.

Holte, J. & Talley, L. A new algorithm for finding mixed layer depths with applications to Argo data and subantarctic mode water formation. *Journal of Atmospheric and Oceanic Technology*, 26(9):1920–1939, http://journals.ametsoc.org/doi/pdf/10.1175/2009JTECHO543.1, 2009.

Hopkins, J., Lucas, M., Dufau, C., Sutton, M., Stum, J., Lauret, O., & Channelliere, C.: Detection and variability of the Congo River plume from satellite derived sea surface temperature, salinity, ocean colour and sea level, Remote Sensing of Environment, 139, 365–385, https://doi.org/10.1016/j.rse.2013.08.015, 2013.

Horner-Devine, A.R., Hetland, R.D. & MacDonald, D.G. Mixing and transport in coastal river plumes. *Annu Rev. Fluid. Mech.* 47, 569–594. https://doi.org/10.1146/annurev-fluid-010313-141408, 2015.

Houndegnonto, O. J., Kolodziejczyk, N., Maes, C., Bourlès, B., Da-Allada, C. Y., & Reul, N.: Seasonal Variability of Freshwater Plumes in the Eastern Gulf of Guinea as Inferred From Satellite Measurements, JGR Oceans, 126, e2020JC017041, https://doi.org/10.1029/2020JC017041, 2021.

Hu, Z., & B. Huang. Physical Processes Associated with the Tropical Atlantic SST Gradient during the Anomalous Evolution in the Southeastern Ocean. J. Climate, 20, 3366–3378, https://doi.org/10.1175/JCLI4189.1, 2007.

Hua, W., Zhou, L., Nicholson, S. E., Chen, H., & Qin, M.: Assessing reanalysis data for understanding rainfall climatology and variability over Central Equatorial Africa, Clim Dyn, 53, 651–669, https://doi.org/10.1007/s00382-018-04604-0, 2019.

Huang, B., Hu, Z. Z., & Jha, B. Evolution of model systematic errors in the tropical Atlantic basin from coupled climate hindcasts, Clim. Dynam., 28, 661–682. https://doi.org/10.1007/s00382-006-0223-8, 2007.

Huang, B., Liu, C., Banzon, V., Freeman, E., Graham, G., Hankins, B., Smith, T., & Zhang, H.-M.: Improvements of the Daily Optimum Interpolation Sea Surface Temperature (DOISST) Version 2.1, Journal of Climate, 34, 2923–2939, https://doi.org/10.1175/JCLI-D-20-0166.1, 2021.

Hummels, R., Dengler, M., & Bourlès, B. Seasonal and regional variability of upper ocean diapycnal heat flux in the Atlantic cold tongue. Progress in Oceanography, 111, 52–74. https://doi.org/10.1016/j.pocean.2012.11.001, 2013.

Hummels, R., Dengler, M., Brandt, P., & Schlundt, M. Diapycnal heat flux and mixed layer heat budget within the Atlantic Cold Tongue, Clim. Dynam., 43, 3179–3199. https://doi.org/10.1007/s00382-014-2339-6, 2014.

Hummels, R., Dengler, M., Rath, W; Foltz, G.; Schütte, F.; Fischer, T.; Brandt, P. Surface cooling caused by rare but intense near-inertial wave induced mixing in the tropical Atlantic. Nat Commun 11, 3829. https://doi.org/10.1038/s41467-020-17601-x, 2020.

Hummels, R.; Imbol Koungue, R. A.; Brandt, P.; Krahmann, G Physical oceanography from mooring KPO_1215. PANGAEA, https://doi.org/10.1594/PANGAEA.939249, 2021. [Dataset]

Illig, S., Bachèlery, M.-L., Lübbecke, J. F. Why do Benguela Niños lead Atlantic Niños? Journal of Geophysical Research: Oceans, 125, e2019JC016003. https://doi.org/10.1029/2019JC016003, 2020.

Imbol Koungue R. A., Brandt P., Lübbecke J., Prigent A., Martins M. S. & Rodrigues R. R. The 2019 Benguela Niño. Front. Mar. Sci. 8:800103. https://doi.org/10.3389/fmars.2021.800103, 2021.

Imbol Koungue, R. A., & Brandt, P. Impact of intraseasonal waves on Angolan warm and cold events. Journal of Geophysical Research: Oceans, 126, e2020JC017088. https://doi.org/10.1029/2020JC017088, 2021.

Imbol Koungue, R. A., Brandt, P., Prigent, A., Aroucha, L. C., Lübbecke, J., Imbol Nkwinkwa, A. S. N., Dengler, M. & Keenlyside, N. Drivers and impact of the 2021 extreme warm event in the tropical Angolan upwelling system. Scientific Reports, 14(1), 16824. https://doi.org/10.1038/s41598-024-67569-7, 2024.

Imbol Koungue, R. A., Illig, S., Rouault, M. Role of interannual Kelvin wave propagations in the equatorial Atlantic on the Angola Benguela Current system. J. Geophys. Res. Oceans 122, 4685–4703. https://doi.org/10.1002/2016JC012463, 2017.

Imbol Koungue, R. A., Rouault, M., Illig, S., Brandt, P., & Jouanno, J. Benguela Niños and Benguela Niñas in forced ocean simulation from 1958 to 2015. Journal of Geophysical Research: Oceans, 124(8), 5923–5951. https://doi.org/10.1029/2019JC015013, 2019.

IOC, SCOR, & IAPSO. The International Thermodynamic Equation of Seawater-2010: Calculation and Use of Thermodynamic Properties. Intergovernmental Oceanographic Commission, Manuals and Guides No. 56, UNESCO. 196, 2010.

Jarre, A., Hutchings, L., Kirkman, S. P., Kreiner, A., Tchipalanga, P. C. M., Kainge, P., Uanivi, U., Van Der Plas, A. K., Blamey, L. K., Coetzee, J. C., Lamont, T., Samaai, T., Verheye, H. M., Yemane, D. G., Axelsen, B. E., Ostrowski, M., Stenevik, E. K., & Loeng, H.: Synthesis: climate effects on biodiversity, abundance and distribution of marine organisms in the Benguela, Fisheries Oceanography, 24, 122–149, https://doi.org/10.1111/fog.12086, 2015.

Jarugula, S. & McPhaden, M. J.: Indian Ocean Dipole affects eastern tropical Atlantic salinity through Congo River Basin hydrology, Commun Earth Environ, 4, 366, https://doi.org/10.1038/s43247-023-01027-6, 2023.

Jarugula, S., Fournier, S., Reager J. T., & Pascolini-Campbell, M. Intercomparison of In Situ and Satellite Sea Surface Salinity Products for Global Coastal Ocean Studies. *J. Atmos. Oceanic Technol*., 42, 3–16, https://doi.org/10.1175/JTECH-D-23-0168.1, 2025.

Jing, Z., Wang, S., Wu, L., Wang, H., Zhou, S., Sun, B., Chen, Z., Ma, X., Gan, B., & Yang, H.: Geostrophic flows control future changes of oceanic eastern boundary upwelling, Nat. Clim. Chang., https://doi.org/10.1038/s41558-022-01588-y, 2023.

Junker, T., Schmidt, M., Mohrholz, V. The relation of wind stress curl and meridional transport in the Benguela upwelling system. J. Mar. Syst., 143, 1–6, https://doi.org/10.1016/j.jmarsys.2014.10.006, 2015.

Kako, S., Nakagawa, T., Takayama, K., Hirose, N. & Isobe, A. Impact of Changjiang River Discharge on Sea Surface Temperature in the East China Sea. *J. Phys. Oceanogr*., 46, 1735–1750, https://doi.org/10.1175/JPO-D-15-0167.1, 2016.

Keeling, R. F., Körtzinger, A., & Gruber, N. Ocean deoxygenation in a warming world. *Annual Review of Marine Science*, 2(1):199–229, https://doi.org/10.1146/annurev.marine.010908.163855, 2010.

Keenlyside, N., Kosaka, Y., Vigaud, N., Robertson, A. W., Wang, Y., Dommenget, D., Luo, J-J., Matei, D., "Basin interactions and predictability," in Interacting Climates of Ocean Basins: Observations, Mechanisms, Predictability, and Impacts (Cambridge Univ. Press, 2020), pp. 258–292., https://doi.org/10.1017/9781108610995.009, 2020.

Kirkman, S., Blamey, L., Lamont, T., Field, J., Bianchi, G., Huggett, J., Hutchings, L., Jackson-Veitch, J., Jarre, A., Lett, C., Lipiński, M., Mafwila, S., Pfaff, M., Samaai, T., Shannon, L., Shin, Y.-J., Van Der Lingen, C., and Yemane, D.: Spatial characterisation of the Benguela ecosystem for ecosystem-based

management, African Journal of Marine Science, 38, 7–22, https://doi.org/10.2989/1814232X.2015.1125390, 2016.

Kopte, R. & Dengler, M. Physical oceanography during METEOR cruise M120. PANGAEA, https://doi.org/10.1594/PANGAEA.868654, 2016 [Dataset]

Kopte, R., Brandt, P., Claus, M., Greatbatch, R. J., & Dengler, M. Role of Equatorial Basin-Mode Resonance for the Seasonal Variability of the Angola Current at 11°S. Journal of Physical Oceanography, 48(2):261–281, ISSN: 0022-3670, https://doi.org/10.1175/JPO-D-17-0111.1, 2018.

Kopte, R., Brandt, P., Dengler, M., Tchipalanga, P. C. M., Macuéria, M., & Ostrowski, M.: The Angola Current: Flow and hydrographic characteristics as observed at 11°S: THE ANGOLA CURRENT AS OBSERVED AT 11°S, J. Geophys. Res. Oceans, 122, 1177–1189, https://doi.org/10.1002/2016JC012374, 2017.

Körner, M., Brandt, P., & Dengler, M.: Seasonal cycle of sea surface temperature in the tropical Angolan Upwelling System, Ocean Sci., 19, 121–139, https://doi.org/10.5194/os-19-121-2023, 2023.

Körner, M., Brandt, P., Illig, S., Dengler, M., Subramaniam, A., Bachèlery, M.-L., & Krahmann, G.: Coastal trapped waves and tidal mixing control primary production in the tropical Angolan upwelling system, Sci. Adv., 10, eadj6686, https://doi.org/10.1126/sciadv.adj6686, 2024.

Koseki, S., & Imbol Koungue, R. A. Regional atmospheric response to the Benguela Niñas. International Journal of Climatology, 41(S1). https://doi.org/10.1002/joc.6782, 2020.

Koseki, S., Giordani, H., & Goubanova, K.: Frontogenesis of the Angola–Benguela Frontal Zone, Ocean Sci., 15, 83–96, https://doi.org/10.5194/os-15-83-2019, 2019.

Koseki, S., Keenlyside, N., Demissie, T., Toniazzo, T., Counillon, F., Bethke, I., Ilicak, M., & Shen, M.-L.: Causes of the large warm bias in the Angola–Benguela Frontal Zone in the Norwegian Earth System Model, Clim Dyn, 50, 4651–4670, https://doi.org/10.1007/s00382-017-3896-2, 2018.

Krahmann, G. & Brandt, P. Physical oceanography during METEOR cruise M98. PANGAEA, https://doi.org/10.1594/PANGAEA.868640, 2016 [Dataset]

Kurian, J., Li, P., Chang, P., Patricola, C. M., & Small, J.: Impact of the Benguela coastal low-level jet on the southeast tropical Atlantic SST bias in a regional ocean model, Clim Dyn, 56, 2773–2800, https://doi.org/10.1007/s00382-020-05616-5, 2021.

Laplace, P. S., Bowditch, N., and Bowditch, N. I. Mécanique céleste. Boston, MA: Hillard, Gray, Little, and Wilkins, 1829.

Lellouche, J.-M., Greiner, E., Bourdallé Badie, R., Garric, G., Melet, A., Drévillon, M., Bricaud, C., Hamon, M., Le Galloudec, O., Regnier, C., Candela, T., Testut, C-E., Gasparin, F., Ruggiero, G., Benkiran, M., Drillet, Y. & Le Traon, P-Y.: The copernicus global 1/12 oceanic and sea ice GLORYS12 reanalysis. Frontiers in Earth Science, 9, 1–27. https://doi.org/10.3389/feart.2021.698876, 2021.

Levitus, S., Boyer, T. P., Conkright, M. E., Brien, T. O., Antonov, J., Stephens, C., Stathoplos, L., Johnson, D., & Gelfeld, R.: NOAA Atlas NESDIS 18, World Ocean Database 1998: Volume 1: Introduction, U.S. Gov. Printing Office, Wash., D.C., 1998.

Li, G., Cheng, L., Zhu, J., Trenberth, K. E., Mann, M. E., & Abraham, J. P. Increasing ocean stratification over the past half-century. *Nature Climate Change*, 10(12):1116–1123, http://dx.doi.org/10.1038/s41558-020-00918-2, 2020.

Li, X., Bordbar, M. H., Latif, M., Park, W. & Harlaß, J. Monthly to seasonal prediction of tropical Atlantic sea surface temperature with statistical models constructed from observations and data from the Kiel Climate Model. *Clim. Dyn.* **54**, 1829–1850, https://doi.org/10.1007/s00382-020-05140-6, 2020.

Li, X., Tan, W., Hu, Z.-Z. & Johnson, N. C. Evolution and Prediction of Two Extremely Strong Atlantic Niños in 2019–2021: Impact of Benguela Warming. *Geophys. Res. Lett*. **50**, https://doi.org/10.1029/2023GL104215, 2023.

Liu, C., Huo, D., Liu, Z., Wang, X., Guan, C., Qi, J., & Wang, F. Turbulent mixing in the barrier layer of the equatorial Pacific Ocean. *Geophysical Research Letters*, 49(5), e2021GL097690. https://doi.org/10.1029/2021GL097690, 2022.

Liu, C., Wang, F., Köhl, A. et al. Subsurface ocean turbulent mixing enhances central Pacific ENSO. Nat Commun 16, 2315. https://doi.org/10.1038/s41467-025-57058-4, 2025.

Llort, J., Lévy, M., Sallée, J. B., & Tagliabue, A. Nonmonotonic Response of Primary Production and Export to Changes in Mixed-Layer Depth in the Southern Ocean. *Geophysical Research Letters*, 46(6):3368–3377, https://doi.org/10.1029/2018GL081788, 2019.

Lübbecke, J. F., Böning, C. W., Keenlyside, N. S., & Xie, S.: On the connection between Benguela and equatorial Atlantic Niños and the role of the South Atlantic Anticyclone, J. Geophys. Res., 115, 2009JC005964, https://doi.org/10.1029/2009JC005964, 2010.

Lübbecke, J. F., Brandt, P., Dengler, M., Kopte, R., Lüdke, J., Richter, I., Sena Martins, M., & Tchipalanga, P. C. M.: Causes and evolution of the southeastern tropical Atlantic warm event in early 2016, Clim Dyn, 53, 261–274, https://doi.org/10.1007/s00382-018-4582-8, 2019.

Lübbecke, J. F., Durgadoo, J., & Biastoch, A. Contribution of Increased Agulhas Leakage to Tropical Atlantic Warming, J. Climate, 28, 9697–9706, https://doi.org/10.1175/JCLI-D-15- 0258.1, 2015

Lübbecke, J. F., Rodríguez-Fonseca, B., Richter, I., Martín-Rey, M., Losada, T., Polo, I., & Keenlyside, N. S. Equatorial Atlantic variability—Modes, mechanisms, and global teleconnections. *WIREs Climate Change* **9**, e527. https://doi.org/10.1002/wcc.527.S2CID, 2018.

Lumpkin, R., & Garzoli, S. L. Interannual to decadal changes in the Western South Atlantic's surface circulation. Journal of Geophysical Research, 116(C1), C01014. https://doi.org/10.1029/2010JC006285, 2011.

Lutz K., Jacobeit J., Rathmann J Atlantic warm and cold water events and impact on African west coast precipitation. Int. J. Clim., 35:128–141. https://doi.org/10.1002/joc3969, 2015.

Ma, X., Liu, H., Wang, X. Interannual Variability of Barrier Layer in the Tropical Atlantic and Its Relationship with the Tropical Atlantic Modes. Journal of Physical Oceanography, 53, https://doi.org/10.1175/JPO-D-21-0235.1, 2023.

Madec G, & the NEMO team: NEMO ocean engine—version 3.6, Note du Pôle de modélisation, Institut Pierre-Simon Laplace (IPSL), France, p 406, 2016.

Maes, C. & O'Kane, T. J. Seasonal variations of the upper ocean salinity stratification in the tropics. J Geophys Res Oceans 119(3):1706–1722. https://doi.org/10.1002/2013JC009366, 2014.

Malan, N., Backeberg, B., Biastoch, A., Durgadoo, J. V., Samuelsen, A., Reason, C., & Hermes, J. Agulhas Current Meanders Facilitate Shelf-Slope Exchange on the Eastern Agulhas Bank, J. Geophys. Res., 123, 4762–4778, https://doi.org/10.1029/2017JC013602, 2018.

Marchesiello, P. & Estrade, P.: Upwelling limitation by onshore geostrophic flow, J Mar Res, 68, 37–62, https://doi.org/10.1357/002224010793079004, 2010.

Martins, M. S. & Stammer, D.: Interannual Variability of the Congo River Plume-Induced Sea Surface Salinity, Remote Sensing, 14, 1013, https://doi.org/10.3390/rs14041013, 2022.

Materia, S., Gualdi, S., Navarra, A., & Terray, L.: The effect of Congo River freshwater discharge on Eastern Equatorial Atlantic climate variability, Clim Dyn, 39, 2109–2125, https://doi.org/10.1007/s00382-012-1514-x, 2012.

Mayer, J., Mayer, M., Haimberger, L., Mass-consistent atmospheric energy and moisture budget monthly data from 1979 to present derived from ERA5 reanalysis. Copernicus Climate Change Service (C3S) Climate Data Store (CDS). [Dataset]. https://doi.org/10.24381/cds.c2451f6b, 2021.

McPhaden, M.J., Jarugula, S., Aroucha, L.C., & Lübbecke, J. Indian Ocean Dipole intensifies Benguela Niño through Congo River discharge. Commun Earth Environ 5, 779, https://doi.org/10.1038/s43247-024-01955-x , 2024.

Meade, R. H. & Emery, K. O.: Sea Level as Affected by River Runoff, Eastern United States, Science, 173, 425–428, https://doi.org/10.1126/science.173.3995.425, 1971.

Mears, C.; Lee, T.; Ricciardulli, L.; Wang, X.; Wentz, F. Improving the Accuracy of the Cross-Calibrated Multi-Platform (CCMP) Ocean Vector Winds. Remote Sens., 14, 4230. https://doi.org/10.3390/rs14174230, 2022.

Mercier, H., Arhan, M., Lutjeharms, J. R. E. Upper-layer circulation in the eastern Equatorial and South Atlantic Ocean in January–March 1995. Deep-Sea Res. I, 50, 863–887, https://doi.org/10.1016/S0967-0637(03)00071-2, 2003.

Mignot, J., Lazar, A., & Lacarra, M. On the formation of barrier layers and associated vertical temperature inversions: A focus on the northwestern tropical Atlantic. Journal of Geophysical Research, 117(C2). https://doi.org/10.1029/2011JC007435, 2012.

Moihamette, F., Pokam, W. M., Diallo, I. & Washington, R. Extreme Indian Ocean dipole and rainfall variability over Central Africa. *Int. J. Climatol.* **42**, 5255–5272, https://doi.org/10.1002/joc.7531, 2022.

Moisan, J. R. & Niiler, P. P. The seasonal heat budget of the North Pacific: Net heat flux and heat storage rates (1950–1990), J. Phys. Oceanogr., 28, 401–421, https://doi.org/10.1175/1520-0485(1998)028<0401:TSHBOT>2.0.CO;2, 1998.

Mrozowska, M. A., Jochum, M., Bastin, S., Hummels, R., Koldunov, A., Dengler, M., Fischer, T., Nuterman, R., & Hansen, R. R.. Using NIW Observations to Assess Mixed Layer Parameterizations: A Case Study in the Tropical Atlantic, J. Geophys. Res.-Oceans, 129, e2024JC020985, https://doi.org/10.1029/2024JC020985, 2024.

Müller, O. V., McGuire, P. C., Vidale, P. L., & Hawkins, E.: River flow in the near future: a global perspective in the context of a high-emission climate change scenario, Hydrol. Earth Syst. Sci., 28, 2179–2201, https://doi.org/10.5194/hess-28-2179-2024, 2024.

Munzimi, Y. A., Hansen, M. C., & Asante, K. O.: Estimating daily streamflow in the Congo Basin using satellite-derived data and a semi-distributed hydrological model, Hydrological Sciences Journal, 64, 1472–1487, https://doi.org/10.1080/02626667.2019.1647342, 2019.

Navier, C.-L. Mémoire sur les lois du mouvement des fluides. Mem. de l'Acad. des Sci. 389, 234–245, 1822.

Ngakala, R. D., Alory, G., Da-Allada, C. Y., Kom, O. E., Jouanno, J., Rath, W., & Baloïtcha, E.: Joint observation–model mixed-layer heat and salt budgets in the eastern tropical Atlantic, Ocean Sci., 19, 535–558, https://doi.org/10.5194/os-19-535-2023, 2023.

Nyadjro, E. S., Foli, B. A. K., Agyekum, K. A., Wiafe, G., & Tsei, S.: Seasonal Variability of Sea Surface Salinity in the NW Gulf of Guinea from SMAP Satellite, Remote Sens Earth Syst Sci, 5, 83–94, https://doi.org/10.1007/s41976-021-00061-2, 2022.

Oettli, P., Yuan, C. & Richter, I. The other coastal Niño/Niña—the Benguela, California, and Dakar Niños/Niñas. in Tropical and Extratropical Air-Sea Interactions (ed. Behera, S. K.) 237–266 *Elsevier*. https://doi.org/10.1016/B978-0-12-818156-0.00010-1, 2021.

Osborn, T. R. Estimates of the Local Rate of Vertical Diffusion from Dissipation Measurements. Journal of Physical Oceanography, 10, 83–89. https://doi.org/10.1175/1520-0485(1980)010<0083:EOTLRO>2.0.CO;2, 1980.

Ostrowski, M., da Silva, J. C. B., Bazik-Sangolay, B. The response of sound scatterers to El Niño and La Niña-like oceanographic regimes in the southeastern Atlantic. Ices J Mar Sci 66: 1063 – 1072. https://doi.org/10.1093/icesjms/fsp102, 2009.

Pailler, K., Bourlès, B., Gouriou, Y. The barrier layer in the western tropical Atlantic Ocean. Geophys Res Lett 26(14):2069–2072. https://doi.org/10.1029/1999GL900492, 1999.

Palma, E. D., & Matano, R. P. An idealized study of near equatorial river plumes, *J. Geophys. Res.* **122**, 3599–3620, https://doi.org/10.1002/2016JC012554, 2017.

Patricola, M. C., & Chang, P. Structure and dynamics of the Benguela low-level coastal jet. Climate Dyn., 49, 2765–2788, https://doi.org/10.1007/s00382-016-3479-7, 2017.

Perez, R. C., Foltz, G. R., Lumpkin, R., & Schmid, C. Direct measurements of upper ocean horizontal velocity and vertical shear in the tropical North Atlantic at 4°N, 23°W. Journal of Geophysical Research: Oceans, 124(6), 4133–4151. https://doi.org/10.1029/2019JC015064, 2019

Peterson R. G. & Stramma, L. Upper-level circulation in the South Atlantic Ocean. Progress in Oceanography 26(1):1–73, https://doi.org/10.1016/0079-6611(91)90006-8, 2019.

Philander, S. G (editor). El Niño, La Niña, and the Southern Oscillation. International Geophysics, Academic Press, https://doi.org/10.1016/S0074-6142(08)60171-0, 1990.

Piecuch, C. G., Bittermann, K., Kemp, A. C., Ponte, R. M., Little, C. M., Engelhart, S. E., & Lentz, S. J.: River-discharge effects on United States Atlantic and Gulf coast sea-level changes, Proc. Natl. Acad. Sci. U.S.A., 115, 7729–7734, https://doi.org/10.1073/pnas.1805428115, 2018.

Polo, I., Lazar, A., Rodriguez-Fonseca, B., & Arnault, S. Oceanic Kelvin waves and tropical Atlantic intraseasonal variability: 1. Kelvin wave characterization. J. Geophys. Res. 113:C07009. https://doi.org/10.1029/2007JC004495, 2008.

Prigent, A. & Farneti, R.: An assessment of equatorial Atlantic interannual variability in Ocean Model Intercomparison Project (OMIP) simulations, Ocean Sci., 20, 1067–1086, https://doi.org/10.5194/os-20-1067-2024, 2024.

Prigent, A., Imbol Koungue, R. A., Lübbecke, J. F., Brandt, P., & Latif, M. Origin of Weakened Interannual Sea Surface Temperature Variability in the Southeastern Tropical Atlantic Ocean. Geophysical Research Letters, 47(20), e2020GL089348. https://doi.org/10.1029/2020GL089348, 2020.

Reynolds, R. W., Smith, T. M., Liu, C., Chelton, D. B., Casey, K. S., & Schlax, M. G.: Daily High-Resolution-Blended Analyses for Sea Surface Temperature, Journal of Climate, 20, 5473–5496, https://doi.org/10.1175/2007JCLI1824.1, 2007.

Richter, I., Behera, S. K., Masumoto, Y., Taguchi, B., Komori, N., & Yamagata, T. On the triggering of Benguela Niños: remote equatorial versus local influences. Geophys. Res. Lett. 37 L20604. https://doi.org/10.1029/2010GL044461, 2010.

Richter, I., Doi, T., Behera, S.K. & Keenlyside, N. On the link between mean state biases and prediction skill in the tropics: an atmospheric perspective. *Clim Dyn* 50, 3355–3374. https://doi.org/10.1007/s00382-017-3809-4, 2018.

Richter, I.: Climate model biases in the eastern tropical oceans: causes, impacts and ways forward, WIREs Climate Change, 6, 345–358, https://doi.org/10.1002/wcc.338, 2015.

Rio, M. -H., Mulet, S., & Picot, N.: Beyond GOCE for the ocean circulation estimate: Synergetic use of altimetry, gravimetry, and in situ data provides new insight into geostrophic and Ekman currents, Geophysical Research Letters, 41, 8918–8925, https://doi.org/10.1002/2014GL061773, 2014.

Roch, M., Brandt, P., Schmidtko, S., Vaz Velho, F., & Ostrowski, M.: Southeastern Tropical Atlantic Changing From Subtropical to Tropical Conditions, Front. Mar. Sci., 8, 748383, https://doi.org/10.3389/fmars.2021.748383, 2021.

Ropelewski, C. F., & Halpert, M. S. Global and Regional Scale Precipitation Patterns Associated with the El Niño/Southern Oscillation. Mon. Wea. Rev., 115, 1606–1626, https://doi.org/10.1175/1520-0493(1987)115%3C1606:GARSPP%3E2.0.CO;2, 1987.

Rouault, M. Bi-annual intrusion of tropical water in the northern Benguela upwelling. Geophysical Research Letters, 39, L12606. https://doi.org/10.1029/2012GL052099, 2012.

Rouault, M., & Tomety, F. S. Impact of El Niño–Southern Oscillation on the Benguela Upwelling. *J. Phys. Oceanogr*., 52, 2573–2587, https://doi.org/10.1175/JPO-D-21-0219.1, 2022.

Rouault, M., Florenchie, P., Fauchereau, N., & Reason, C. J. C. South East tropical Atlantic warm events and southern African rainfall. Geophys. Res. Lett. 30. 8009. https://doi.org/10.1029/2002GL014840, 2003.

Rouault, M., Illig, S., Bartholomae, C., Reason, C. J. C., & Bentamy, A.: Propagation and origin of warm anomalies in the Angola Benguela upwelling system in 2001, Journal of Marine Systems, 68, 473–488, https://doi.org/10.1016/j.jmarsys.2006.11.010, 2007.

Rouault, M., Illig, S., Lübbecke, J., & Koungue, R. A. I.: Origin, development and demise of the 2010–2011 Benguela Niño, Journal of Marine Systems, 188, 39–48, https://doi.org/10.1016/j.jmarsys.2017.07.007, 2018.

Rühs, S., Schmidt, C., Schubert, R., Schulzki, T., Schwarzkop, F., U., Le Bars, D., & Biastoch, A.: Robust estimates for the decadal evolution of Agulhas leakage from the 1960s to the 2010s. Commun Earth Environ 3, 318. https://doi.org/10.1038/s43247-022-00643-y, 2022.

Rühs, S., Zhurbas, V., Koszalka, I. M., Durgadoo, J. V., & Biastoch, A. Eddy diffusivity estimates from Lagrangian trajectories simulated with ocean models and surface drifter data – a case study for the greater Agulhas system, J. Phys. Oceanogr., 48, 175–196, https://doi.org/10.1175/JPO-D-17-0048.1, 2017.

Saha, A., Serra, N., & Stammer, D.: Growth and Decay of Northwestern Tropical Atlantic Barrier Layers, JGR Oceans, 126, e2020JC016956, https://doi.org/10.1029/2020JC016956, 2021.

Saji, N. H., Goswami, B. N., Vinayachandran, P. N. & Yamagata, T. A dipole mode in the tropical Indian Ocean. *Nature* **401**, 360–363, https://doi.org/10.1038/43854, 1999.

Schmidt, C., Schwarzkopf, F. U., Rühs, S., & Biastoch, A.: Characteristics and robustness of Agulhas leakage estimates: an inter-comparison study of Lagrangian methods, Ocean Sci., 17, 1067–1080, https://doi.org/10.5194/os-17-1067-2021, 2021.

Schwarzkopf, F. U., Biastoch, A., Böning, C. W., Chanut, J., Durgadoo, J. V., Getzlaff, K., Harlaß, J., Rieck, J. K., Roth, C., Scheinert, M. M., & Schubert, R.: The INALT family – a set of high-resolution nests for the Agulhas Current system within global NEMO ocean/sea-ice configurations, Geosci. Model Dev., 12, 3329–3355, https://doi.org/10.5194/gmd-12-3329-2019, 2019.

Seager, R., Naik, N., & Vecchi, G. A. Thermodynamic and dynamic mechanisms for large-scale changes in the hydrological cycle in response to global warming. *Journal of Climate*, *23*(17), 4651-4668, https://doi.org/10.1175/2010JCLI3655.1, 2010.

Shannon, L. V., Boyd, A. J., Brundrit, G. B., & Taunton-Clark, J.: On the existence of an El Niño-type phenomenon in the Benguela System, J Mar Res, 44, 495–520, https://doi.org/10.1357/002224086788403105, 1986.

Siegfried, L., Schmidt, M., Mohrholz, V., Pogrzeba, H., Nardini, P., Böttinger, M., et al. The tropical-subtropical coupling in the Southeast Atlantic from the perspective of the northern Benguela upwelling system. PLoS ONE 14(1): e0210083. https://doi.org/10.1371/journal.pone.0210083, 2019.

Small, R. J., Kurian, J., Chang, P., Xu, G., Tsujino, H., Yeager, S., Danabasoglu, G., Kim, W. M., Altuntas, A., and Castruccio, F.: Eastern Boundary Upwelling Systems in Ocean–Sea Ice Simulations Forced by CORE and JRA55-do: Mean State and Variability at the Surface, Journal of Climate, 37, 2821–2848, https://doi.org/10.1175/JCLI-D-23-0511.1, 2024.

Song, Q., Aiki, H., & Tang, Y. The role of equatorially forced waves in triggering Benguela Niño/Niña as investigated by an energy flux diagnosis. Journal of Geophysical Research: Oceans, 128, e2022JC019272. https://doi.org/10.1029/2022JC019272, 2023.

Sorí, R., Nieto, R., Vicente-Serrano, S. M., Drumond, A., & Gimeno, L.: A Lagrangian perspective of the hydrological cycle in the Congo River basin, Earth Syst. Dynam., 8, 653–675, https://doi.org/10.5194/esd-8-653-2017, 2017.

Sowman, M. & Cardoso, P.: Small-scale fisheries and food security strategies in countries in the Benguela Current Large Marine Ecosystem (BCLME) region: Angola, Namibia and South Africa, Marine Policy, 34, 1163–1170, https://doi.org/10.1016/j.marpol.2010.03.016, 2010.

Stevenson, J. W. & Niiler, P. P. Upper Ocean Heat Budget During the Hawaii-to-Tahiti Schuttle Experiment, J. Phys. Oceanogr., 13, 1894–1907, https://doi.org/10.1175/1520-0485(1983)013%3C1894:UOHBDT%3E2.0.CO;2, 1983.

Stewart, K., Hogg, A. M., Griffies, S., Heerdegen, A., Ward, M., Spence, P., & England, M. Vertical resolution of baroclinic modes in global ocean models, Ocean Modell., 113, 50–65, https://doi.org/10.1016/j.ocemod.2017.03.012, 2017.

Stewart, R. H. Introduction to Physical Oceanography. Texas A&M University, 2008.

Stewart, R. H. Seasat: Results of the Mission. Bull. Amer. Meteor. Soc., 69, 1441–1447, https://doi.org/10.1175/1520-0477(1988)069<1441:SROTM>2.0.CO;2, 1988.

Stokes, G. G. On the theories of the internal friction of fluids in motion, etc. Trans. Camb. Philos. Soc. 8, 287–319, 1845.

Sun, Q., Whitney, M. M., Bryan, F. O., & Tseng, Y. H. A box model for representing estuarine physical processes in Earth system models. Ocean Modell. 112, 139–153. https://doi.org/10.1016/j.ocemod.2017.03.004, 2017.

Talley, L. D., Pickard, G. L., Emery, W. J., & Swift, J. H. Descriptive Physical Oceanography - An Introduction. Elsevier, 6 edition, 2011.

Tchipalanga, P., Dengler, M., Brandt, P., Kopte, R., Macuéria, M., Coelho, P., Ostrowski, M., Keenlyside, N. S. Eastern boundary circulation and hydrography off Angola: Building Angolan oceanographic capacities. Bulletin of the American Meteorological Society, 99(8), 1589–1605. https://doi.org/10.1175/BAMS-D-17-0197.1, 2018.

Tchipalanga, P., Ostrowski, M., & Dengler, M. Physical oceanography on the Angolan continental shelf and Cabinda. PANGAEA. [Dataset]. https://doi.org/10.1594/PANGAEA.886492, 2018.

Tim, N., Zorita, E., & Hunicke, B. Decadal variability and trends of the Benguela upwelling system as simulated in a high-resolution ocean simulation. *Ocean Sci*., 11, 483–502, https://doi.org/10.5194/os-11-483-2015, 2015.

Tomety, F. S., Illig, S., Ostrowski, M., Awo, F. M., Bachèlery, M.-L., Keenlyside, N., & Rouault, M.: Long-term climatological trends driving the recent warming along the Angolan and Namibian coasts, Clim Dyn, https://doi.org/10.1007/s00382-024-07305-z, 2024.

Topé, G. D. A., Alory, G., Djakouré, S., Da-Allada, C. Y., Jouanno, J., & Morvan, G.: How does the Niger river warm coastal waters in the northern Gulf of Guinea?, Front. Mar. Sci., 10, 1187202, https://doi.org/10.3389/fmars.2023.1187202, 2023.

Tozuka, T. Importance of the vertical mixing process in the development of El Niño Modoki. npj Clim Atmos Sci 8(76). https://doi.org/10.1038/s41612-025-00973-6, 2025.

Treguier, A. M., De Boyer Montégut, C., Bozec, A., Chassignet, E. P., Fox-Kemper, B., McC Hogg, A., Iovino, D., Kiss, A. E., Le Sommer, J., Li, Y., Lin, P., Lique, C., Liu, H., Serazin, G., Sidorenko, D., Wang, Q., Xu, X., and Yeager, S. The mixed-layer depth in the Ocean Model Intercomparison Project (OMIP): impact of resolving mesoscale eddies. *Geoscientific Model Development*, 16(13):3849–3872, ISSN: 19919603, https://doi.org/10.5194/gmd-16-3849-2023, 2023.

Trenberth, K. E., Smith, L., Qian, T., Dai, A., & Fasullo, J. Estimates of the Global Water Budget and Its Annual Cycle Using Observational and Model Data. *J. Hydrometeor*., 8, 758–769, https://doi.org/10.1175/JHM600.1, 2007.

Tsujino, H., Urakawa, S., Nakano, H., Small, R. J., Kim, W. M., Yeager, S. G., Danabasoglu, G., Suzuki, T., Bamber, J. L., Bentsen, M., Böning, C. W., Bozec, A., Chassignet, E. P., Curchitser, E., Boeira Dias,

F., Durack, P. J., Griffies, S. M., Harada, Y., Ilicak, M., Josey, S. A., Kobayashi, C., Kobayashi, S., Komuro, Y., Large, W. G., Le Sommer, J., Marsland, S. J., Masina, S., Scheinert, M., Tomita, H., Valdivieso, M., & Yamazaki, D.: JRA-55 based surface dataset for driving ocean–sea-ice models (JRA55-do), Ocean Modelling, 130, 79–139, https://doi.org/10.1016/j.ocemod.2018.07.002, 2018.

Utari, P. A., Khakim, M. Y. H., Setiabudidaya, D., & Iskandar, I. Dynamics of 2015 positive Indian Ocean Dipole. *J. So. Hemisph. Earth Sys. Science* **69**, 75-83. https://doi.org/10.1071/ES19002, 2019.

Veitch, J., Penven, P., Shillington, F. The Benguela: a laboratory for comparative modeling studies. Prog Oceanogr 83:296–302. https://doi.org/10.1016/j.pocean.2009.07.008, 2009.

Verri, G., Pinardi, N., Bryan, F., Tseng, Y., Coppini, G., Clementi, E. A box model to represent estuarine dynamics in mesoscale resolution ocean models. *Ocean Modelling*, 148, ISSN 1463-5003, https://doi.org/10.1016/j.ocemod.2020.101587, 2020.

Vialard, J., & P. Delecluse. An OGCM Study for the TOGA Decade. Part I: Role of Salinity in the Physics of the Western Pacific Fresh Pool. J. Phys. Oceanogr., 28, 1071–1088, https://doi.org/10.1175/1520-0485(1998)028<1071:AOSFTT>2.0.CO;2, 1998.

Vic, C., Berger, H., Tréguier, A. & Couvelard, X. Dynamics of an equatorial river plume: theory and numerical experiments applied to the Congo Plume case. *J. Phys. Oceanogr*., 44, 980–994, https://doi.org/10.1175/JPO-D-13-0132.1, 2014.

Vieira, L.H., Krisch, S., Hopwood, M.J. et al. Unprecedented Fe delivery from the Congo River margin to the South Atlantic Gyre. *Nat Commun* 11, 556, https://doi.org/10.1038/s41467-019-14255-2, 2020.

Vinayachandran, P. N., Jahfer, S., Nanjundiah, R. S. Impact of river runoff into the ocean on Indian summer monsoon, *Environ. Res. Lett*, 10, 054008, http://dx.doi.org/10.1088/1748-9326/10/5/054008, 2015.

Wang, R., Chen, L., Li, T. & Luo, J.-J. Atlantic Niño/Niña Prediction Skills in NMME Models. *Atmosphere* **12**, 803, https://doi.org/10.3390/atmos12070803, 2021.

Wang, Z., Duan, A., Yang, S., & Ullah, K. Atmospheric moisture budget and its regulation on the variability of summer precipitation over the Tibetan Plateau. *Journal of Geophysical Research: Atmospheres*, *122*(2), 614-630, https://doi.org/10.1002/2016JD025515, 2017.

Webster, P. J., Moore, A. M., Loschnigg, J. P. & Leben, R. R. Coupled ocean–atmosphere dynamics in the Indian Ocean during 1997–98. *Nature* **401**, 356–360, https://doi.org/10.1038/43848, 1999.

White, R. H. & Toumi, R.: River flow and ocean temperatures: The Congo River, J. Geophys. Res. Oceans, 119, 2501–2517, https://doi.org/10.1002/2014JC009836, 2014.

Yankovsky, A. E. & Chapman, D. C. A Simple Theory for the Fate of Buoyant Coastal Discharges. *J. Phys. Oceanogr.*, 27, 1386–1401, https://doi.org/10.1175/1520-0485(1997)027<1386:ASTFTF>2.0.CO;2, 1997.

Zeng, Z., Brandt, P., Lamb, K. G., Greatbatch, R. J., Dengler, M., Claus, M., & Chen, X. Three-Dimensional Numerical Simulations of Internal Tides in the Angolan Upwelling Region, J. Geophys. Res.-Oceans, 126, e2020JC016460, https://doi.org/10.1029/2020JC016460, 2021.

Zhang, L. & Han, W. Indian Ocean Dipole leads to Atlantic Niño. *Nature Communications* **12**, 5952. https://doi.org/10.1038/s41467-021-26223-w , 2021.

Zhang, L., Wang, C., Han, W., McPhaden, M. J., Hu, A. & Xing, W. Emergence of the Central Atlantic Niño. *Sci. Adv.* 9, eadi5507, https://doi.org/10.1126/sciadv.adi5507, 2023.

Zhang, R.-H. & Busalacchi, A. J.: Freshwater Flux (FWF)-Induced Oceanic Feedback in a Hybrid Coupled Model of the Tropical Pacific, Journal of Climate, 22, 853–879, https://doi.org/10.1175/2008JCLI2543.1, 2009.

Zheng, F. & Zhang, R-H. Effects of interannual salinity variability and freshwater flux forcing on the development of the 2007/08 La Niña event diagnosed from Argo and satellite data, *Dynamics of Atmospheres and Oceans*, V. 57, 45-57, https://doi.org/10.1016/j.dynatmoce.2012.06.002, 2012.

Acknowledgments

First, I would like to thank my supervisor, Joke Lübbecke, for the opportunity to conduct this PhD. Your support, guidance, and reliability kept me on track during the last four years. I greatly appreciate all the shared knowledge, constant feedback, and generosity you showed me throughout this time. For the coming years, your dedicated supervision will remain a role model in my career. Thank you for everything.

To the Professors who also oversaw the development of this thesis: thanks to Arne Biastoch for examining, and again to Arne and Peter Brandt for being part of the Advisory Committee. Thank you to Stephan Juricke and Christian Berndt for agreeing to be part of my Examination Committee. For the discussions and go-to source of help: thank you again to Peter and Marcus Dengler.

My gratitude and acknowledgment to all coauthors I've had the honor of working with: Arne Biastoch, Franziska Schwarzkopf, Joke Lübbecke, Mareike Körner, Mesmin Awo, Michael McPhaden, Peter Brandt, Rebecca Hummels, Rodrigue Imbol Koungue, and Sreelekha Jarugula.

To all my peers from the Physical Oceanography department at GEOMAR: fellow researchers, technicians, and professors. To the staff, a special thanks to the secretaries Nadira Mahmud, Christin Jahr, Juliane Barth, Silke Gesinn for their countless support. Special thanks to Daniel Rudloff, Tina Hans, Rodrigue, Fehmi Dilmahamod, Marco Schulz, Mareike, Marisa Roch, Arthur Prigent, Federico Scarscelli, Ruirui Wang, Jinghong Wang, Clara McKellar, Zhendong Hu, Hao Huang, Qingwen Zhong, Hannes Sandberg for the long discussions, shared inspiration, good company, lunch breaks and overall support.

A special mention and gratitude to Prof. Dóris Veleda, who has accompanied me from my early studies and laid the foundation for the researcher I have become. Without her encouragement to come to Kiel and pursue this PhD, none of it would likely have happened.

I also want to thank all the friends from Kiel, Hamburg, and Berlin for making life on this side of the Atlantic less cold. To all the climate-related sciences friends I've made along the way during conferences and cruises, especially to Marta Mrozowska: my biggest thank you.

This research was subsidized by the DAAD, so I wish to thank the institution for the scholarship that made it possible and to Maria Salgado for the attentive help.

Agradeço também a Marcelo Agra, pelo acompanhamento durante esses anos. Aos amigos do Brasil que, apesar da distância, se fizeram presentes. A toda minha família no Brasil, e aos que se tornaram família no percurso: Fábio, Andreia, Cecília, Sofia.

A Davi, Debi e Guma pelo alicerce. Especialmente pro Galego: não te acompanhar crescendo foi um dos mais duros sacrifícios dessa escolha. Que o nosso amor e conexão não mudem nunca. Finalmente, aos meus pais, Doda e Coca, que colocaram tudo de si na construção do que somos hoje, e assim abriram ainda mais caminhos do que parecia possível. Essa conquista é, acima de tudo, uma conquista nossa. Obrigado por tudo, sempre. Amo muito vocês.

Por fim, a Júlia, por todos os dias passados, presentes e futuros. Por segurar minha mão. Por ser quem é. Conseguimos, meu amor.

Own Publications

Aroucha, L. C., Hummels, R., Lübbecke, J. Turbulent Heat Flux Responses to Sea Surface Salinity Variability during Benguela Niños and Niñas (*submitted*), Geophysical Research Letters.

Aroucha, L. C., Lübbecke, J., Brandt, P., Schwarzkopf, F. U., & Biastoch, A. River discharge impacts coastal Southeastern Tropical Atlantic sea surface temperature and circulation: a model-based analysis, Ocean Sci., 21, 661–678, https://doi.org/10.5194/os-21-661-2025, 2025.

Aroucha, L. C., Lübbecke, J. F., Körner, M., Imbol Koungue, R. A., & Awo, F. M. The Influence of Freshwater Input on the Evolution of the 1995 Benguela Niño. Journal of Geophysical Research: Oceans, 129, e2023JC020241. https://doi.org/10.1029/2023JC020241, 2024.

Aroucha, L. C., Veleda, D., Lopes, F. S., Tyaquiçã, P., Lefèvre, N., & Araujo, M. Intra- and inter-annual variability of North Brazil Current rings using angular momentum eddy detection and tracking algorithm: observations from 1993 to 2016. Journal of Geophysical Research: Oceans, 125, e2019JC015921. https://doi.org/10.1029/2019JC015921, 2020.

Aroucha, L. C.; Duarte, H. O.; Droguett, E. L.; Veleda, D. Practical aspects of meteorology and oceanography for mariners: A guide for the perplexed. Cogent Engineering, v.5, p.1-23. https://doi.org/10.1080/23311916.2018.1492314, 2018.

Imbol Koungue, R.A., Brandt, P., Prigent, A., **Aroucha, L. C.**, Lübbecke, J., Imbol Nkwinkwa, A. S. N., Dengler, M., & Keenlyside, N. Drivers and impact of the 2021 extreme warm event in the tropical Angolan upwelling system. Scientific Reports, 14, 16824. https://doi.org/10.1038/s41598-024-67569-7, 2024.

McPhaden, M., Jarugula, S., **Aroucha, L. C.**, Lübbecke, J. Indian Ocean Dipole Intensifies Benguela Niño Through Congo River Discharge, Commun Earth Environ 5, 779. https://doi.org/10.1038/s43247-024-01955-x, 2024.

Declaration

I hereby declare that - apart from my supervisor's guidance and acknowledged assistance - the content and design of this thesis is my own work. This thesis has not been submitted either partially or wholly as part of a doctoral degree to another examining body and has not been published or submitted for publication except for the chapters where this is explicitly stated. This thesis has been prepared in accordance with the Rules of Good Scientific Practice of the German Research Foundation. An academic degree has never been withdrawn from me.

Kiel, 10.07.2025, _____

(Léo Costa Aroucha)